CRANFIELD UNIVERSITY
LIBRARY

CRANFIELD UNIVERSITY

P C AUGOOD

LOW-TEMPERATURE THERMAL-ENERGY STORAGE AND TRANSMISSION SYSTEMS EMPLOYING HYDROPHILIC POLYMERIC MATERIALS

SCHOOL OF MECHANICAL ENGINEERING

PhD THESIS

CRANFIELD UNIVERSITY
LIBRARY

CRANFIELD UNIVERSITY

P C AUGOOD

LOW-TEMPERATURE THERMAL-ENERGY STORAGE AND TRANSMISSION SYSTEMS EMPLOYING HYDROPHILIC POLYMERIC MATERIALS

SCHOOL OF MECHANICAL ENGINEERING

PhD THESIS

CRANFIELD UNIVERSITY

SCHOOL OF MECHANICAL ENGINEERING

PhD THESIS

Academic Year 1996-7

P C AUGOOD

Low-Temperature Thermal-Energy Storage and Transmission Systems Employing Hydrophilic Polymeric Materials

Supervisors: Dr M Newborough
Dr D J Highgate

April 1997

Abstract

The wide fluctuations that occur in the aggregate electrical demand of a generating utility are punitive with respect to total system efficiency. Demand side management techniques have been applied to reduce such fluctuations including the conversion of electrical energy to thermal energy during periods of low demand for use during peak demand periods. For thermal processes requiring energy above ambient temperature it is feasible to use sensible heat due to the existence of stable storage mediums and efficient methods of heating at the high temperatures required. However where energy is required below ambient temperatures, efficiency of cooling limits the use of sensible heat, hence latent heat storage has been adopted. Conventional cold storage systems use ice banks to store cooling energy at 0°C in order to capture the high latent heat of fusion of water. The rate of discharge for such stores is limited by thermal resistance in the store and the thermal capacity of secondary coolants (such as glycol solutions).

This investigated the use of hydrophilic materials to overcome the limitations of current cold-storage technology. Such materials have the capacity to absorb and retain up to 95% by mass of water (or other aqueous solutions) regardless of how the materials is subdivided. Furthermore the thermal properties of the polymers in their hydrated state resemble those of the free hydration fluid, including any phase transitions. By supporting the hydrated materials in a non-freeing, non-aqueous fluid the resultant mixture provides a medium for cold storage that can be pumped and used at the point of load, and is not limited by the thermal resistance of an encapsulating material.

Three aspects concerning the utilisation of hydrophilic materials for thermal engineering applications have been investigated; (i) the physical properties of the materials in their hydrated state, (ii) methods of fluidising material in a high density store, and (iii) the heat transfer properties of hydrophilic based slurries while undergoing phase transition.

Material tests have shown that currently available hydrophilic materials have thermo-physical properties that depend principally upon the hydrating fluid, regardless of particle size, and are stable over long periods (>3years). Suitable hydration fluids can lower the temperature of the phase transition thus extending their potential as storage mediums beyond those of ice-based technologies. Novel materials, of very high water content (95%) have been produced and investigated. These appear to be very suitable for thermal storage because they increase the maximum achievable energy densities of a fluidised storage system and potentially reduce cost.

A number of thermal storage devices to utilise hydrophilic based slurries have been designed and evaluated. The resultant devices has been shown to provide a means of taking hydrophilic materials to, and from, a packed bed and feeding them at a controlled rate into a fluid stream. The thermal charge/discharge rates of such a device are limited only by the choice of external heat exchange systems.

An experimental apparatus has been designed to investigate the effects of phase change particles on the heat transfer properties of flowing mixtures. The results have shown that (i) at temperatures above the phase transition temperature the presence of the particles causes an increase in the measured heat transfer coefficient for concentrations above 10% by volume, (ii) there is a significant interaction of particles at the heat transfer surface, and (iii) that under high flow rate conditions, with phase change occurring, heat transfer coefficients are considerably enhanced (ie 80%) above those of the support fluid when used alone or with non-active particles.

Further work is recommended to extend this study to produce an engineering prototype storage system for trial evaluation.

For

Ros, Amy and Jasmin

Thankyou

Acknowledgements

I would like to thank my supervisors *Dr. Marcus Newborough* and *Dr. Don Highgate* for their encouragement and valuable assistance throughout the course of this project.

My sincere thanks to *Mr. Charles Knight* for his help with many of the practical problems encountered, and for *Mr. Richard Dewar* and *Mr. Derik Brown* for their help in the design of test apparatus.

I would like to thank all my *family* and *friends* for their support and encouragement.

Thanks are due to the Science and Engineering Research Council for providing financial support.

Finally I must thank my partner, *Ros*, and my two daughters, *Amy* and *Jasmin*, for there lasting patience, kind encouragement and continued support over the years.

Contents

Chapter 1 Current Energy Problems

1.1	Introduction	1
1.1.1	CO2 Production, Greenhouse Gasses and Global Warming	2
1.1.2	CFC Release and the Depletion of Stratospheric Ozone	5
1.3	Energy Conservation	9
1.3.1	Load Management	9
1.3.2	Energy Storage	13
1.4	Thermal Energy Storage	14
1.4.1	Conventional Cold Storage Methods and Applications	15
1.5	Secondary Refrigerants	19
1.6	Conclusions	20

Chapter 2 The Physical properties of Slurries

2.1	Introduction	21
2.2	Newtonian Fluids and Fluid Mechanics	21
2.2.1	The Reynolds Number and Flow Regimes	23
2.2.2	The Velocity Boundary Layer	24
2.2.3	Thermal Boundary Layer	26
2.2.4	Single Phase Convective Heat Transfer	28
2.2.5	Analogy Between Heat and Momentum Transfer	29
2.2.6	Empirical Correlations For Heat Transfer (Turbulent Flow In Tubes)	34
2.3	Classification of Solid-Liquid Mixtures	35
2.3.1	Terminal Velocity and Settling Behaviour	36
2.3.2	Rheological Classification of Non-Newtonian Fluids	39
2.4	Physical Properties of Slurries	41
2.4.1	Slurry Density	41
2.4.2	Slurry Heat Capacity	42
2.4.3	Slurry Viscosity and Newtonian Slurries	42
2.4.4	Thermal Conductivity of Slurries	43
2.5	Convective Heat Transfer to Slurries Under Turbulent Flow	45
2.5.1	Convective Heat Transfer to Slurries with Phase Change Particles	49
2.6	Discussion	52

Chapter 3 Hydrophilic Materials

3.1	Introduction	54
3.2	Phase Transition Behaviour	54

3.2.1	Experimental Method	55
3.2.1.1	Heat Transfer Mechanisms	57
3.2.2	The Effects of Ageing	60
3.2.3	Alternative Hydration Fluids	64
3.2.4	Novel Hydrophilic Materials	70
3.2.5	Miscellaneous Tests	74
3.3	The Thermal Conductivity Of Hydrophilic Materials	75
3.4	Discussion	78

Chapter 4 Cold Storage Device

4.1	Introduction	79
4.2	Previous Work and Relevant Literature	79
4.3	Preliminary Tests	81
4.4	The Fluidised Bed Cold Storage Device	82
4.4.1	Perspex Test Unit	82
4.4.2	Cold Storage Device MK I	86
4.4.3	Perspex Rig Modifications	93
4.4.4	Cold Storage Device MK II	93
4.4.5	The Cold Storage Device MK III (A Feed Based System)	99
4.4.6	Modifications to MK III	103
4.5	Discussion	107

Chapter 5 The Heat Transfer Test Rig

5.1	Introduction	109
5.2	Total System Design	110
5.2.1	The Heat Exchanger Test Section (HETS)	110
5.2.2	Thermocouple Selection and Calibration	115
5.2.3	Mass Flow Rate Measurement of the Slurry	118
5.2.4	General Components of the Slurry Circuit	122
5.2.5	The Primary Cooling System	122
5.3	Performance Verification	123
5.3.1	Water Heat Transfer Tests	125
5.4	Computer Data Acquisition	125
5.4.1	Addition and Calibration of Glycol Brine Flow Meter	125
5.4.2	Thermocouple Voltage Measuremnt Using Data Logger	130
5.5	Summary	132

Chapter 6 The Slurry Heat Transfer Tests

6.1	Introduction	133
6.2	Data Acquisition and Analysis	133

6.3.2 Modelling of the Effects of Particles 138
6.3 Phase-Change Slurry Heat Transfer Test 139
6.3.1 Overview of Heat Transfer Results 139
6.3.2 The Heat Transfer Model 141
6.3.3 The Effects of Phase Change 146
6.3.4 High Concentration Slurry Tests 149
6.4 Conclusions 151

Chapter 7 Discussion and Recommendations

7.1 General Discussion 153
7.2 Materials Tests 153
7.3 Cold Storage Device 154
7.4 Heat Transfer Test 154

References 157

Appendices

Appendix A Dimesionless Groups Used 165
Appendix B Engineering Drawings 166
Appendix C Physical Properties of Fusus Oil 172
Appendix D Experimental Codes as referred to in Chapter 6 173

List of Figures

Chapter 1

1.1 The growth in CO_2 Levels and Global Temperatures Since the Industrial Revolution.
1.2 Daily Load Curves.
1.3 Schematic Diagrams of Load Management Strategies.

Chapter 2

2.1 Mechanisms of Viscosity.
2.2 Development of Velocity Profile - Laminar.
2.3 Development of Velocity Profile - Laminar, Transition and Turbulent.
2.4 Development of thermal Boundary Layer Over a Flat Plate.
2.5 Convection Over an Arbitrary Shape.
2.6 The Exchange of "Fluid Lumps" During Turbulent Flow.
2.7 General Classification of Mixtures.
2.8 Rheograms for some Non-Newtonian Fluids.
2.9 Comparison of Viscosity Equations.
2.10 Mechanism of Micro-Convection.

Chapter 3

3.1 Schematic Layout of Phase Transition Test Apparatus.
3.2 Comparison of Predicted Heat Flux with Linear Function.
3.3 Energy Curve for Phase Transition of Water - Freezing.
3.4 Energy Curve for Phase Transition of Water - Thawing.
3.5 Example Energy Curves for the Freezing of Old (3 Years) Pre-Cycled Hydrophilic Samples.
3.6 Comparison of Freezing Curves for New and Old (3 years) Hydrophilic Samples.
3.7 Typical Phase Diagram of a Solution.
3.8 Initial and 20th Freeze-Thaw Cycle of Hydrophilic Sample Hydrated in 10% Calcium Chloride Solution.
3.9 Phase Transition Curves for Hydrophilic Blanks Hydrated in NaCl Solutions - 20th Freeze.
3.10 Extrapolated Data for NaCl Results.
3.11 First Freeze of Hydrophilic Materials Formed from Acrylamide Solutions.
3.12 The Effect of Thermally Cycling a Hydrated Hydrophilic Polymer Produced from an Irradiated Solution of Acrylamide (10%).
3.13 Thermal Conductivity Test Apparatus.
3.14 The Measured Thermal Conductivity of Hydrophilic Materials.

Chapter 4

4.1 Cross Section of Cold Storage Unit Used by Kay (1990).
4.2 Channelling in Perspex Test Unit.
4.3 Flow Pattern for Single Plate.
4.4 Effect of Using Four Three-Quarter Circle Distributor Plates.
4.5 Schematic Diagram of Distributor showing Placement of Thermocouples.
4.6 Mean Mixture Temperature of 10% Charge During Complete Cycle of Cold Storage Device (MK I).
4.7 Details of the Modified Baffle System for the Cold Storage Tank.
4.8 Plan View Showing Increase in Agglomerations of Baffled Zones as Temperature Decreased.
4.9 Mean Temperature of 30% Charge in the Cold Storage Device (MK II) During Cooling Period.
4.10 Energy Change of 30% Charge in the Cold Storage Device (MK II) During Cooling Period.
4.11 Schematic Layout of Feeder Based Cold Storage Device.
4.12 The Flow Pattern (a) Initially, (b) After the addition of Inserts.
4.13 Channelling Occurring in Cold Storage Device MK III.
4.14 Schematic Diagram of the Final Design of the Feed-Based Cold Storage Device.

Chapter 5

5.1 Schematic Layout of Slurry Flow in Thermo-Rheological Test Rig.
5.2 Schematic Cross Section of the Assembled Heat Exchanger.
5.3 Detailed Cross Section of End of Assembled Heat Exchanger.
5.4 Schematic Layout of Thermo-couple Measuring System (Manual).
5.5 Type E Thermocouple 1 - Calibration Results.
5.6 Detail of Slurry Discharge chute.
5.7 Layout of Glycol Cooling Circuit.
5.8 Comparison of Predicted Values of The Nulselt Number, Nu, from Equation 2.36 (Sieder, 1935) with that Derived from Measured Data.
5.9 Comparison of Predicted Values of The Nulselt Number, Nu, from Equation 2.37 (Petukhov, 1970) with that Derived from Measured Data.
5.10 Schematic Layout of Modified Glycol Circuit Including Turbine, Flow Meter, Frequency to Voltage Converted and Data Logger.
5.11 Flow Meter System Output (with error bars).

Chapter 6

6.1 Rate of Change of the Test Fluid Temperature at the Heat Exchanger Inlet.
6.2 Measured and Predicted Heat Transfer Coefficients for Fusus Oil.

6.3 Comparison of the Measure Heat Transfer Coefficient for Fusus Oil with that Predicted by Gnielinski (1979).
6.4 The Effect of Solids Concentration on the Heat Transfer Coefficient.
6.5 Comparison of Heat Transfer Coefficients for test Run05a04.
6.6 Comparison of Heat Transfer Coefficients for test Run05a05.
6.7 Comparison of Heat Transfer Coefficients for test Run05a06.
6.8 Comparison of Heat Transfer Coefficients for test Run05a08.
6.9 Comparison of Heat Transfer Coefficients for test Run05a07.
6.10 Comparison of Re against $Nu \cdot Pr^{-1/3}(\mu_f/\mu_w)^{-0.14}$ for Different Flow Conditions of 5% Slurry Heat Transfer Tests.
6.11 Comparison of Heat Transfer Coefficients for test Run10a04.
6.12 Comparison of Heat Transfer Coefficients for test Run10a05.
6.13 Comparison of Heat Transfer Coefficients for test Run10a06.
6.14 Comparison of Re against $Nu \cdot Pr^{-1/3}(\mu_f/\mu_w)^{-0.14}$ for Different Flow Conditions of 10% Slurry Heat Transfer Tests.
6.15 Distribution Of flow Rates during Equivalent Flow Conditions.
6.16 Measured Heat Transfer Coefficient for High Flow Rates at Concentrations of 10%.
6.17 Measured Heat Transfer Coefficient for Low Flow Rates at Concentrations of 10%.
6.18 Heat Transfer Coefficient Measured for 25% Concentration.

Chapter 7
7.1 Typical Layout of Cold Storage System.

Notation

Normal Letters

A	Area, m^2
A_s	Surface Area, m^2
a	Linear dimention, m
a,b,c,d..	Coefficients in equations
C_p	Specific Heat Capacity, $kJ \cdot kg^{-1} \cdot K^{-1}$
C_f	Friction coefficient
D	Diameter of Duct, m
D_e	Hydraulic Diameter of Rectangular Duct, m
d	Diameter of Particle, m
e	Realative roughness
F_D	Force due to drag, N
F_g	Force due to gravity, N
F_w	Settling velocity factor
f	Friction factor
g	Gravitational acceleration, $m \cdot s^{-2}$
h	Convective heat transfer coefficient, $W \cdot m^{-2} \cdot K^{-1}$
K	Consistency index
k	Thermal Conductivity, $W \cdot m^{-1} \cdot K^{-1}$
L	Latent Heat, $J \cdot kg^{-1}$; Characteristic length, m
l	Length, m
m	Mass, kg; Coefficient used for Equation 3.3, $W \cdot m^{-2} \cdot K^{-1}$; Coefficient used for Equation 5.4; $V \cdot K^{-1}$
$\dot{m}$	Mass flow rate, $kg \cdot s^{-1}$
Nu	Nusselt Number
Pe	Peclet Number
Pr	Prandlt Number
p	Pressure, $N \cdot m^{-2}$
Q	Energy change, J
q	Heat transfer rate, W
q''	Heat flux, $W \cdot m^{-2}$
Re	Reynolds Number
Re_c	Critical reynolds number
St	Stanton Number
Ste	Stephan Number
T	Temperature, K or °C
U	Velocity of flow, $m \cdot s^{-1}$
U_{mf}	Minimum fluidisation velocity, $m \cdot s^{-1}$
u	Velocity component, $m \cdot s^{-1}$
V	Velocity, $m \cdot s^{-1}$
V_M	Minimal velocity to reach homogeneous mixture, $m \cdot s^{-1}$
V_0	Terminal velocity, $m \cdot s^{-1}$

v	Velocity component, $m \cdot s^{-1}$
x	Length, m
X	General length in dimensionless number, m

Greek Letters

α	Thermal diffusivity, $m^2 \cdot s$
β	Coefficient, (Equation 2.60)
Δ	Small change or differential
δ	Hydrodynamic boundry layer thickness, m
δ_T	Thermal boundary layer thickness, m
δ_c	Critical boundry layer thickness, m
ε	Emmisivity, (0 to 1); Eddy viscosity, $m^2 \cdot s^{-1}$
ε_H	Eddy thermal diffusivity, $m^2 \cdot s$
ϕ	Solids Concentration. %,or 0 to 1
ϕ_{max}	Maximum solids concentration. %,or 0 to 1
γ	Rate of Shear, s^{-1}
λ	Void Fraction (Equation 2.50)
μ	Dynamic Viscosity, $kg \cdot s^{-1} \cdot m^{-1}$
θ	Fluid Film Coefficient (Equation 2.60)
ρ	Density, $kg \cdot m^{-3}$
σ	Stephan - Boltzmann consant, $W \cdot m^{-2} \cdot K^{-4}$
τ	Shear stress, $N \cdot m^{-2}$
τ_y	Yield stress, $N \cdot m^{-2}$
ν	KinematicViscosity, $m^2 \cdot s^{-1}$

Subscript

con	Convective component
D	Pertaining to characteristic diameter *D*
f	Pertaining to a single phase fluid
i	Inlet condition
L	Pertaining to Phase Transition, or characteristic length
l	Pertaining to laminar flow
lm	Log mean value
m	Pertaining to a solid-liquid mixture or slurry
new	Conditions at new temperature
o	Outlet condition
p	Pertaining to a particle
rad	Radiative component
ref	Property of reference material
s	Pertaining to solid or surface.
sample	Property of sample
set	Conditions at charging tank

surroundings	Property surrounding sample
t	Pertaining to turbulent flow
total	Combined convective and radiative component
w	Pertaining to conditions at heat transfer surface
1	Initial Conditions
2	Final Conditions

Superscript

'	Varring component
-	Average component
n	Power index
B	Power index

Abreviations

ac	Alternating Current
CFC	Chloro-Fluoro-Carbon
CFD	Computational Fluid Dynamic
CRO	Cathode Ray Oscilloscope
DSM	Demand Side Management
dc	Direct Current
e.m.f.	Electromotive Force
HDPE	High Density Polyethylene
HVAC	Heating, Ventilation and Air Conditioning
HETS	Heat Exchanger Test Section
ID	Internal Diameter
MMA	Methyl Methacrylate
OD	Outer Diameter
PVC	Poly-Vinyl Chloride
PVA	Poly-Vinyl Alcohol
rpm	Revolutions per Minute
TES	Thermal Energy Storage
VP	Vinyl Pyrollidone
X-HDPE	Partially cross linked High Density Polyethylene

Chapter 1

Current Energy Problems

1.1 Introduction

This work is concerned with the application of slurries containing phase change materials for both the storage and the transmission of thermal energy at temperatures below ambient. The active materials in the slurries are hydrated hydrophilic polymers (Chapter 3) which have the ability to absorb and retain water. The thermal properties of these materials when hydrated, although slightly modified, resemble that of water in its free state. Of particular interest is the water to ice transition occurring at 0°C which has a high heat of fusion (333 $kJ \cdot kg^{-1}$). The subdivision of the materials into particles does not reduce its water holding capacity or modify the thermal behaviour of the hydrated materials, but eliminates the dependence of heat transfer upon thermal conduction. As particles these materials can form a pumpable slurry with the use of a non-freezing (at 0°C) support fluid.

A system of mobilised particles could be employed as a high thermal density cold storage system yielding rapid rates of charge/discharge. Furthermore the ability to pump the slurries to (and back from) the thermal load removes the need for intermediate heat exchangers, and hence improves system performance. In the extreme, the bulk storage capacity could be bypassed to provide a highly effective thermal transfer fluid or secondary refrigerant. The use of rapid charge/discharge thermal storage systems is increasingly desirable due to the use of time-of-use electricity tariffs (Section 1.3.1). High efficiency thermal transfer fluids will aid the introduction of alternative primary refrigerants requiring remote siting from the thermal loads. Both applications could provide energy efficiency benefits, which in turn will lead to reduced CO_2 emissions. The second (transport) application would aid the application of non-CFC based refrigerants leading to a reduction in the use of ozone depleting gases.

This chapter starts by introducing two environmental problems resulting from the use of fossil fuels, and in particular thermal processes used for cooling below ambient temperatures. Following this load management is discussed, as a technique of improving the efficiency of electrical generation. To achieve optimal efficiency, flat electrical demands are desired, and the technique of energy storage is frequently employed. Current methods are presented, together with their limitations. The penultimate section explores the need for secondary coolants in the refrigeration industry. The final section outlines the aims of this investigation and the way in which the work undertaken is presented.

1.1.1 CO_2 Production, Greenhouse Gasses and Global Warming

The Earth is surrounded by a layer of gases comprising of roughly 80% nitrogen, 20% oxygen, with traces of other gaseous molecules including carbon dioxide (CO_2), and water vapour (H_2O). This layer of gas provides many functions that regulate the earths climate, one of which is to regulate the thermal balance of the Earth by a process known as the *Greenhouse Effect*. Human activity has increased some of these trace gasses, mainly CO_2, and it is expected that the scale of these increases may be causing the mean global atmospheric temperature to rise (Bolin, 1986; Gribbin, 1994).

The combustion of fossil fuels has been in evidence since the Iron Age, although the scale of utilisation was not significant until the mid 18th century, the start of the industrial revolution. Virtually all fossil fuel employed was in the form of coal which was used in its raw form or processed to form *Town Gas*. The development of the internal combustion engine during the early part of the 20th century catalysed the growth in the utilisation of oil. The exploration and drilling activities for oil revealed a new form of fossil fuel, namely natural gas, the growth of which has increased steadily over the last forty years. In the UK this has totally replaced the production and use of town gas. The global growth in fossil fuel usage over the last 250 years has increased at an almost exponential rate.

Thermal processes requiring temperatures above ambient can employ fossil fuels for direct heating, and high efficiencies (>60%) can be achieved. Cooling below ambient, on the other hand, requires the employment of heat pumps. These often require motive power, virtually all of which is supplied in the form of electricity. In an industrialized nation refrigeration can account for 20-25% of electrical energy use (Frivik, 1996). This in turn can account for 5-10% (Frivik, 1996) of fossil fuels used for the generation of electricity.

Common to the combustion of all fossil fuels is the production of CO_2 in the reaction

$$C + O_2 \Rightarrow CO_2 \qquad (1.1)$$

In a similar reaction carbon dioxide is formed as part of a natural carbon cycle driven by the respiration of all animals and plants. The rate of absorption of CO_2 by plants is driven by the level of solar radiation at the Earths surface. This varies throughout the year which in turn leads to a natural variation in atmospheric CO_2 concentrations. When averaged out the effects of mans activities become apparent, and evidence suggests that an increase of around 80ppm has occurred from 1750 to the present (Figure 1.1). This is not only a result of the combustion of fossil fuels but also results from deforestation, reducing the natural sinks for CO_2.

Until the late 1980's it was generally considered that CO_2 was a harmless byproduct of combustion, and any environmental concerns about the use of fossil fuels focused on the production of environmental toxins (These being the sulphur oxides, nitrogen oxides and liberated of heavy metals). Several studies had shown that CO_2 levels were rising and suggested the possible effect being a rise in global temperature due to an

increase in the greenhouse effect. This concern only became serious in 1988 once political interests were stirred. This happened at the conference "The Changing Atmosphere", held in Toronto at the end of May 1988. During this conference evidence was presented showing a rise in the mean global temperature (Figure 1.1). Such a change in the temperature suggested the thermal balance of the earth was changing due to man's activities increasing the greenhouse effect.

Shortwave radiation (optical) from the sun penetrates the Earth's atmosphere and is absorbed by the Earth's land masses and oceans. This energy is re-emitted at longer wavelengths (infrared) some of which is absorbed by radiatively-active gasses in the atmosphere causing it to warm. This warmed part of the atmosphere again radiates in all directions, some of this energy is lost to space while the rest is trapped in an effective thermal blanket. (The process is much more complex than summarised here - a full account can be found in Bolin (1986)). The main greenhouse gas is water vapour, although carbon dioxide, methane, nitrous oxide, and the chloro-fluro-carbons (CFCs) play an important role.

All but the CFC's occur naturally, though the concern here is about anthropogenic sources and how they are changing the natural equilibrium levels in the atmosphere, known as the enhanced greenhouse effect, or *Global Warming*. The contributions from the man made sources are estimated at being (IPCC, 1992) CO_2: 61.2%, CH_4: 17.1%, N_20: 4.1% CFC's and HCFC: 11.7% (remaining 5.9% is due to changes in stratospheric water vapour coming about as an indirect effect of changes in methane concentration). The production of CO_2 from energy related sources is 80%. The net effect on these man made greenhouse gases has been estimated to have forced a net increase in mean global temperature of 0.5°C to 0.8°C from 1750 to 1980 (Schneider, 1984).

This seems a small temperature rise on its own but inspection of Figure 1.1 shows that there is a time lag between CO_2 increase and temperature rise. This is mainly due to the thermal inertia of the oceans, but is also perturbed by a variety of solar cycles. With these taken into account a variety of climate models predict rises in the mean global temperature to that of pre-industrial periods of between 2.3°C and 3.5°C by the year 2030 (Gribbin, 1990) . Such temperature rises seem small compared to those experienced in a daily or seasonal time frame, but their implications for the general global environment are significant. Predictions based on such temperature rises have indicated that:

a) A general rise in sea level of 8.8cm to 28.9cm will occur over the next 20 - 30 years. This is in part due to melting of polar ice caps but mainly due to thermal expansion of the oceans (Houghton, 1990).

b) An increase in hurricane activity by at least a factor of two due to the increase in energy levels in the atmosphere (Gribbin, 1990).

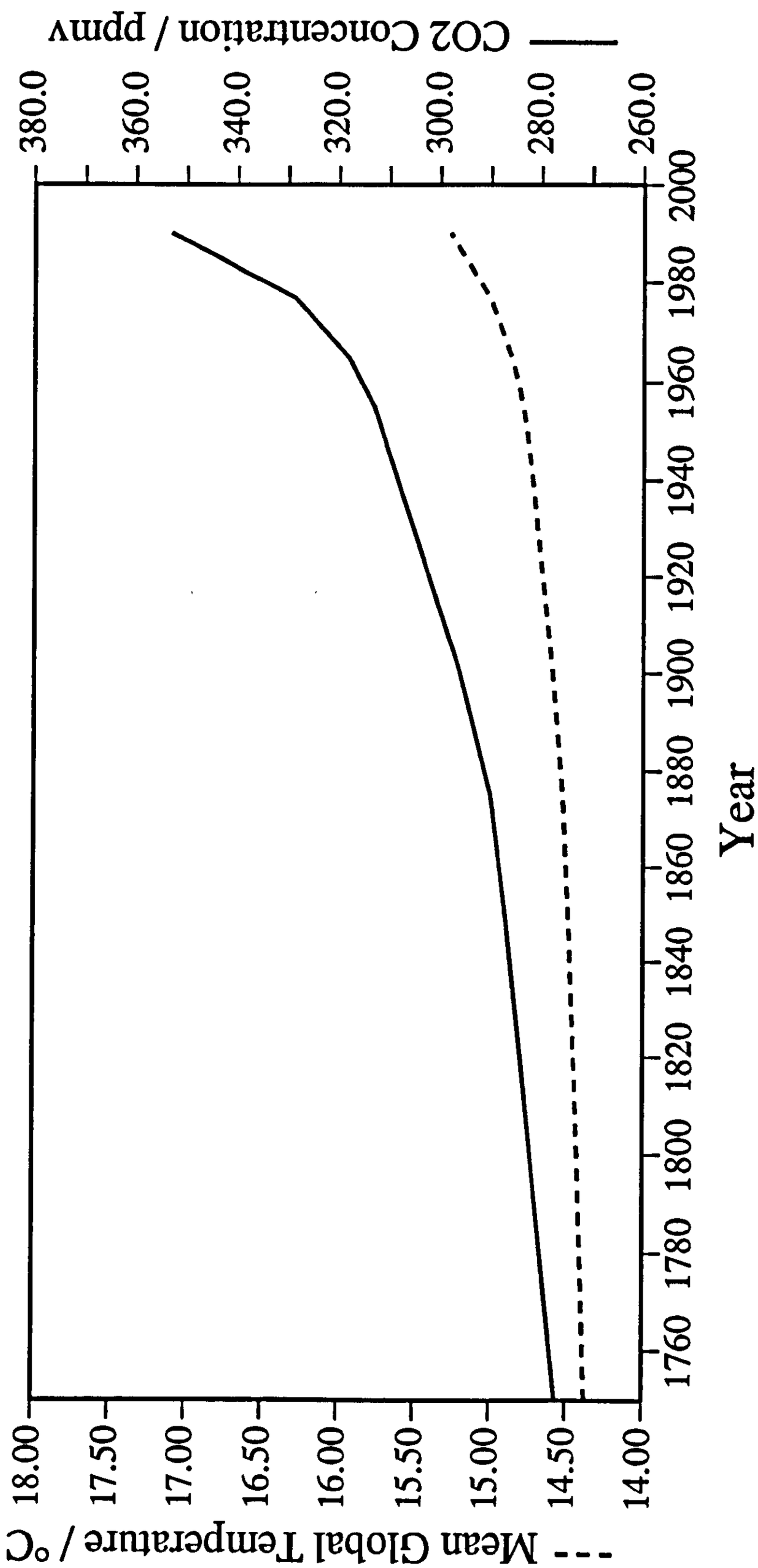

Figure 1.1: The growth in CO_2 Levels and Global Temperatures Since the Industrial Revolution (Data from Ridgwell (1994)).

c) An increase in droughts throughout the world as precipitation patterns change, particularly in the southern states of the regions of USA and southern Europe (Bolin, 1986; Wellburn, 1994).

d) More extreme winter and summer conditions throughout the northern hemisphere, again as a result of the higher energetics of the atmosphere (Bolin, 1986).

Generally any increase in the efficiency of utilisation of fossil fuels as energy sources will reduce the rate at which CO_2 is placed into the atmosphere, and extend the life of these sources, especially for common electrically driven processes such as refrigeration. Furthermore other environmental toxins from combustion processes will be reduced.

1.1.2 CFC Release and the Depletion of Stratospheric Ozone

In the 1930's chemical engineers working for the Dow chemical company were presented with the challenge of finding a new refrigerant (to replace ammonia) that was chemically inert, non-toxic, non-flammable, and had good thermodynamic refrigeration properties. Their success yielded fluorinated hydrocarbons, more commonly known as CFC's, which have to date been widely used not only as refrigerants, but as blowing agents, aerosol propellants, medical sterilization fluids, and cleaning agents for the electronics industry. Unchecked, the versatility of CFC's caused an exponential growth in their production and application until 1974, when evidence showed that CFC's were reaching the upper atmosphere. At these altitudes the intensity of shortwave radiation is sufficient to liberate chlorine atoms from the CFC's, and these atoms tip the equilibrium of ozone (O_3) production back towards oxygen. As ozone concentration is decreased the intensity of UV radiation striking the earths surface increases. Fears of the effects of increased UV radiation levels have caused international agreement and legislation towards completely phasing out the production and application of CFC's over the next decade (Hibberd, 1992; Wellburn, 1994).

The reactivity of the halogens (fluorine,chlorine and bromine) is such that their covalent bonding with carbon is very strong. It is the strength of this bonding that makes the halocarbons both chemically inert and non-toxic, two of the requirements for an ideal refrigerant. The molecules of CFC's are only broken up when they interact with short wave radiation, normally filtered out by the ozone layer. For this reason the CFC molecules survive until they reach the stratosphere where the halogens are liberated and cause maximum damage by reducing the equilibrium concentration of ozone.

The current state of the Earths atmosphere has evolved over millions of years through a complex web of biological, chemical and geophysical interactions. One of the main products of this system is oxygen, which is comfortably maintained at a concentration of 23% (by mass). Most of this oxygen is in the form of diatomic oxygen (O_2), but a small concentration is found in its triatomic form ozone (O_3). This is a pale blue gas that is poisonous to most forms of life even at very low concentrations (Wellburn, 1994). It is produced from the reaction of O_2,with a monatomic oxygen. These single

oxygen atoms are produced by electrical discharge, photolysis of nitrogen oxides and the photodissociation of O_2. The latter is the prime source of monatomic oxygen, and hence ozone, in the stratosphere. The reactions are as follows:

$$O_2 + \gamma_{UV} \Rightarrow O + O \qquad (1.2)$$

$$O_2 + O + M \Rightarrow O_3 + M \qquad (1.3)$$

Where γ_{UV} represents a photon of 242 nm or less and M represents a catalyst to act as a momentum absorber, typically nitrogen.

Not all of the monatomic oxygen will react with O_2 to form ozone, some will recombine to form O_2, or even destroy O_3 to form $2O_2$. Other, more rapid, natural processes exist for the destruction of ozone. The most dominant occurs because of the formation of highly reactive *OH radicals. These are formed in the reaction of water and monatomic oxygen as follows:

$$H_2O + O \Rightarrow 2^{\cdot}OH \qquad (1.4)$$

$$O_3 + {}^{\cdot}OH \Rightarrow H_2O^{\cdot} + O_2 \qquad (1.5)$$

The concentration of ozone will depend on the rates of these, and many other, chemical reactions. These are affected by the density of oxygen and the spectral distribution of incident solar radiation. This leads to a predominant variation with altitude. Further variations with latitude occur due to local air temperatures and ozone distribution by prevailing wind patterns. Finally variations with time occur, due to changes in the solar flux, on a daily and seasonal basis, and with solar activity (Gribbin 1990).

The mean concentration of ozone is low, if condensed into a single layer at atmospheric pressure it would make a film typically only 3.6mm thick. Despite this our atmospheric ozone is extremely effective at filtering out unwanted UV-B radiation (280-315nm). It is possible that the small quantity of beneficial UV-B that does reach the Earth's surface is, and has been, regulated by bio-feedback mechanisms (Lovelock, 1988). These mechanisms inject nitrogen oxides (NO_x) into the atmosphere. These compounds destroy ozone through a series of chemical reactions and return to the Earth's surface as nitric acid. Increased rates of NO_x production due to mans activities are causing concentrations of ozone to drop. This artificial NO_x comes from soil denitrification, caused by unused artificial fertilizers, and oxidation of nitrogen during combustion processes.

The production of NO_x through combustion processes increases as combustion temperatures increase. Higher temperatures are sought in the electrical generating industry to increase the total efficiency of the system. To counteract the higher production of NO_x, catalytic converters are often applied. Although these are effective at design throughputs, turn down of generating plant causes a decrease in the quantity

of NO_x they can remove. The application of energy storage for load management (Section 1.3.1) allows generating plants to be operated at a more constant level, thus improving the total performance of fitted flue gas cleaning devices.

Chlorine and bromine atoms liberated from CFC's by high frequency photons in the stratosphere have a much higher ozone depleting effect than NO_x. This is due to the fact that the ozone destroying reactions that take place return the original chlorine, or bromine, atom thus allowing the reactions to take place again.

$$Cl + O_3 \Rightarrow ClO + O_2 \tag{1.6}$$

$$ClO + O \Rightarrow Cl + O_2 \tag{1.7}$$

This means that one chlorine atom has the potential to destroy several thousand ozone molecules before a reaction with NO_2 is likely to remove it by forming hydrochloric acid (HCl).

$$ClO + NO_2 + M \Rightarrow ClNO_3 + M \tag{1.8}$$

$$ClNO_3 + 2H_2O \Rightarrow 2HNO_3 + 2HCl + O_2 \tag{1.9}$$

Because of different reaction rates, bromine has the potential to destroy 40 times as many ozone molecules as chlorine.

The damage to the ozone layer was first observed over Antarctica in the 1980's, and linked directly to the increase in levels of chlorine monoxide. It is now generally accepted that these compounds are reducing the levels of ozone in the stratosphere, allowing a higher flux of UV radiation to reach the Earth's surface. There are many predicted effects of increased levels of UV radiation, effecting both human life and all life in general. Potential hazards to human health include increased rates of skin cancer, eye damage and a general decrease in the skin's immune system leading to increased rates of infections. Other life will also be adversely affected, the higher plants are known to show retardation in growth when exposed to high levels of UV, microbe activity can be imbalanced (eg nitrogen fixers such as the cyanobacteria), and low level marine such as phytoplankton, one of the primary producers in the oceans, could be severely diminished (Such an effect would further reduce CO_2 sinks, further enhancing global warming).

These concerns led to the *Vienna Convention* in 1986 and the subsequent signing of the *Montreal Protocol*. This agreement limited the production of CFC's towards an eventual phase out in the year 2000. The initial agreement has had subsequent revisions (London 1990 and Copenhagen 1992). The agreement, signed by over 50 nations, has several steps. The first was reduced production of CFC's to 50% of 1986 levels by 1995. This was followed by a goal of 85% by 1997, and 100%by the year 2000. Table 1.1 shows the materials covered by this agreement.

Further to the reduction of CFC's, the Montreal Protocol lists the HCFC's as compounds

Table 1.1: Controlled Compounds for the Purpose of the Montreal Protocol (Adapted form Table 7.2, Wellburn (1994)).

Substance	Common Code	O_3 Depleting Potential
$CFCl_3$	CFC-11	1.0
CF_2Cl_2	CFC-12	0.8
$CF_2ClCFCl_2$	CFC-113	1.1
CF_2ClCF_2Cl	CFC-114	0.8
CF_3CF_2Cl	CFC-115	0.4
CF_2ClBr	Halon-1211	4.1
CF_3Br	Halon-1301	12.5
CF_3CFBr_2	Halon-2402	5.9
CF_3Cl	CFC-13	1.0
$CFCl_2CCl_3$	CFC-111	1.0
$CFCl_2CFCl_2$	CFC-112	1.0
C_3FCl_7	CFC-211	1.0
to	to	
C_3F_7Cl	CFC-217	1.0
CCl_4	Carbontetrachloride	1.08
CH_3CCl_3	Methylchloroform	0.12

[a] O_3 Depleting potential based upon CFC-11 set to 1.0 (source Wellburn (1994)).

to be monitored (their use as transitional alternatives). These have weaker bonding than the CFC's and tend to break down in the lower atmosphere, hence do not liberate chlorine into the stratosphere. This does bring its own set of problems in the form of HCl production, leading to acid rain and soil denitrification.

There are other alternatives including water, air, ammonia, carbon dioxide and hydrocarbons, which are considered safe as refrigerants in the long term (Turiel, 1989; Lizardos, 1992). The term safe here refers to the potential environmental damage, particularly stratospheric ozone. To humans some pose hazards, such as ammonia which is toxic and explosive, or the hydrocarbons which are also flammable. The use of these compounds will require the re-adoption of secondary refrigerants (Section 1.5).

1.3 Energy Conservation

In Section 1.1.1 the effects of rising global CO_2 levels in the atmosphere were discussed. The main method of reducing the rate at which this increase occurs is to reduce fossil fuel usage. This can be done by (a) an increase in the use of renewable energy sources such as wind, tidal and solar power, and (b) increased efficiency in the way fossil fuel are currently used.

In the long term renewable energy sources provide the only sustainable solution to avoid a continual build up of CO_2 in the atmosphere. The rate at which these are being adopted is far too low to meet the reductions in CO_2 release required. This is a result of their variable nature, relative high costs and development periods. Improvements in the efficiency of fossil fuel utilisation is the best short term option for reducing CO_2 emission rates. One method of improving the efficiency of electricity generation is the adoption of *load management.* Such techniques aim at allowing generating plants to work at optimum levels and hence improve overall efficiency. (Similar methods will also have to be applied to meet the variability in renewable energy sources).

1.3.1 Load Management

Our complex society does not function at the same rate continuously, and demands energy at a variable rate throughout the day. This demand for energy is further complicated by weekly behaviour patterns, seasonal climate changes and national holidays. Because fossil fuels are relatively easy to store their use as direct energy sources can be easily met with correctly employed management strategies. Electricity, on the other hand, can not be stored directly, so production must always meet or exceed demand to avoid supply failure. Generation methods that use low cost fuels are not flexible enough to follow daily demand, so methods that employ high grade fuels must be used to avoid gross inefficiencies, although this is at a cost penalty. Load management is the process that reduces fuel costs, or increases efficiency, by matching electricity demand to optimum production.

The variability of daily electricity demand is shown in Figure 1.2, and although variation occurs throughout the week the general shape remains the same. To meet this type of curve, generating utilities use three types of generating plant:

a) *Base Load* These plants are large and are rated at 800-1200 MW. They use cheap fuels, such as coal or nuclear, but have high capital costs. They are run at constant levels for 50% to 80% of the year.

b) *Intermediate Load* These plants burn oil, gas, or in some cases coal, and are typically rated at 200-800 MW. They are operated in a flexible manner to match the daily demand but have time constants of hours, hence some predictive methods have to be employed. Because of their flexible generating capacity these plants tend to be more inefficient than equivalent base load plants.

c) *Peak Load* These are usually small plants of 100 MW or less. They use high cost fuels, such as gas or diesel fuel, in combustion turbines. These are capable of rapid start and are used to meet peaks that other plants can not match. Despite the low capital costs of such plants the frequency of use, less than 10%, makes rates of return very low.

Generally a combination of these types of plant has been used to meet the electricity demand for a generating utility. Costs of fuel types, or more specifically the differential costs of fuel types, will govern the utilities approach to load management strategies. The general aims of these are to reduce generating costs and increase the profits of a utility. Recently government legislation in the US has caused a financial penalty to a utility to be made if it has not reduced its electricity production by a certain amount for a particular year. This has further increased the interest in load management.

The required changes to the load-profile shape must be decided before a load management program is implemented. This depends on factors such as (i) projected fuel cost, (ii) future plant output, (iii) market share of demand and (iv) legislation penalties. Load shape changes can be classified into six types, these are shown in Figure 1.3 and are as follows:

a) *Peak Clipping.* This is the reduction of load during peak periods. Appliances causing peaks must be targeted for either replacement with higher efficiency variants or direct control by the generating utility.

b) *Valley Filling.* To level the demand curve, increased use is desirable during off-peak periods. This is typically achieved through off-peak water heating or thermal storage (space heating, cold storage).

c) *Load Shifting.* This is a combination of (a) and (b) and requires either a change in operating periods (eg curing paint in automotive industries at night), or storing energy for use during some other period (eg ice thermal storage, Section 1.4.1).

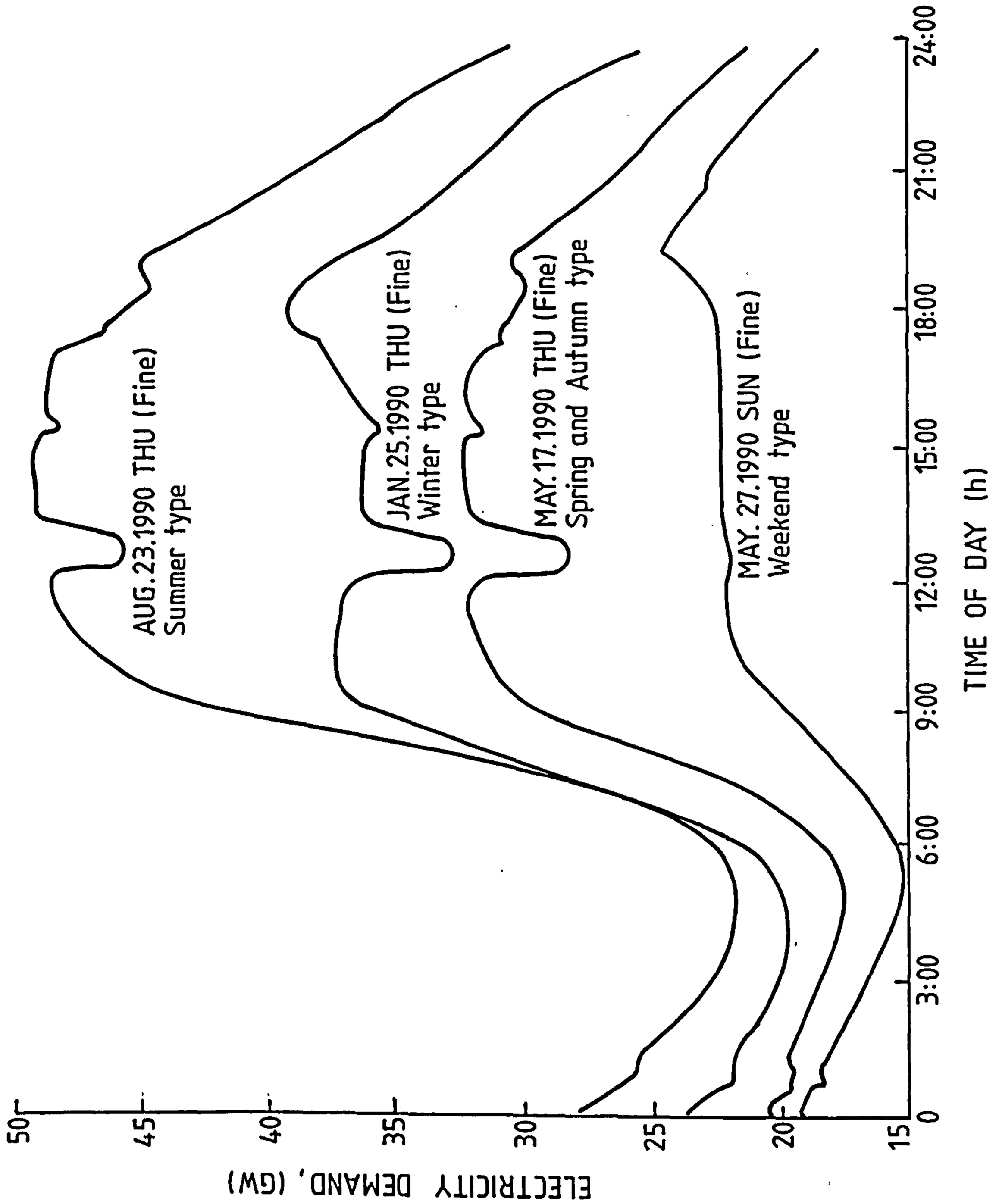

Figure 1.2: Daily Load Curves. (Adapted from Itoh (1990) - showing typical daily profiles for the Tokyo Electric Power Company).

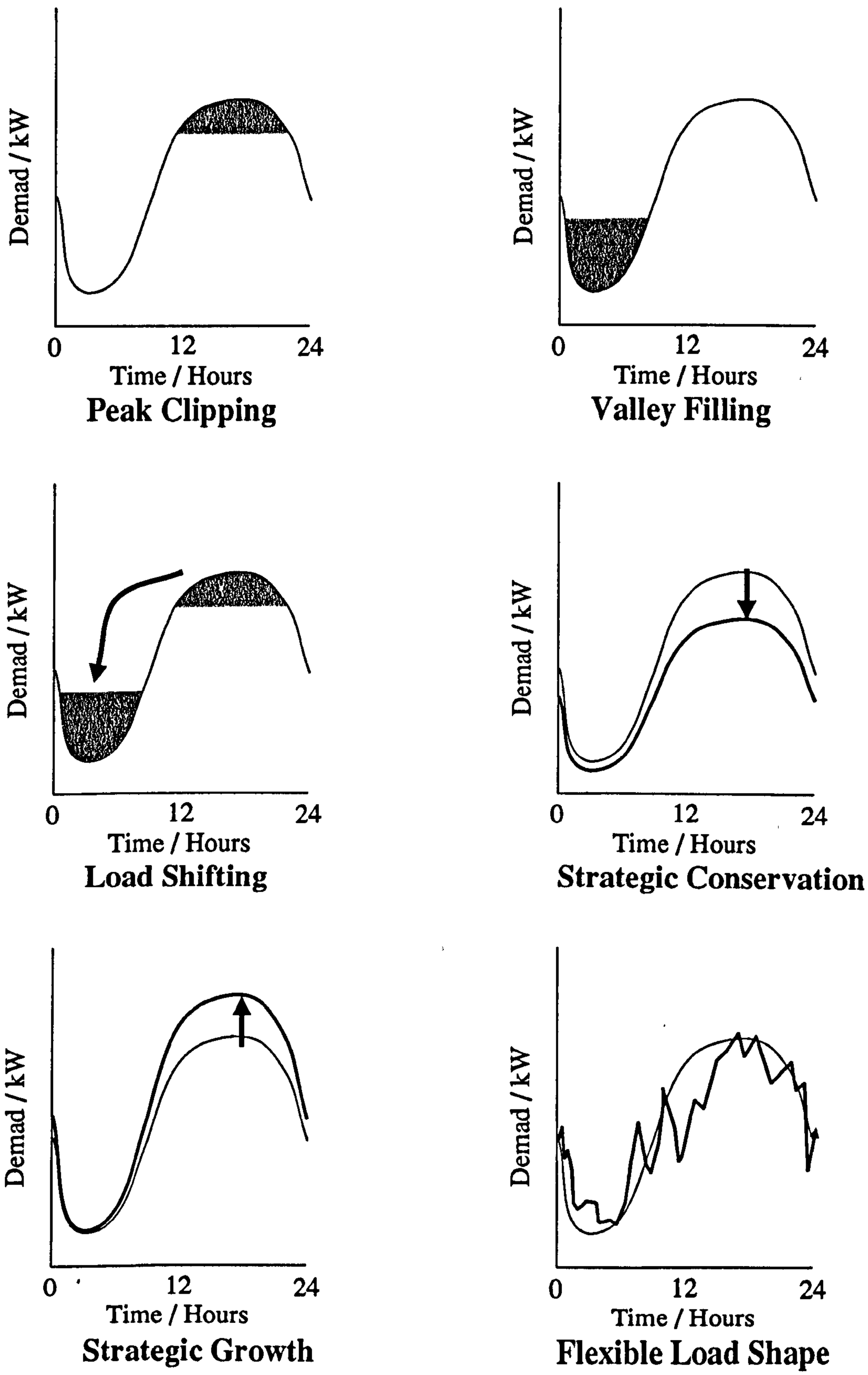

Figure 1.3: Schematic Diagrams of Load Management Strategies.

d) *Strategic Conservation.* This method is applied when generating capacity is likely to diminish due to de-commissioning of generating plants.

e) *Strategic Growth.* Similar to (d) this process is applied to increase general demand where new generating capacity becomes available, or the supply network is upgraded.

f) *Flexible load shape:* This process is in its infancy, although growth is occurring. It is where the utility controls points of demand either directly or via spot pricing. In these ways the individual loads making up the total demand can be influenced to a state most beneficial to the utility.

The method of load shifting is of particular interest to this project. Its principal gains for an electricity utility are firstly the reduction in peak load. The utility gains from this in two ways by the reduced need to use high-cost rapid response generating plants, and by avoiding or postponing the need to reinforce the distribution network. Secondly the increase in demand during the valley enables the utility to make greater utilisation of more efficient slow response generating equipment (eg nuclear or coal fired generating plants). The principal method of load shifting is to employ some form of energy storage.

1.3.2 Energy Storage

The preceding sections have shown that the storage of energy can achieve both a financial gain as well as environmental benefits. The concept of energy storage is far more common than it first appears, and many of our daily activities would not be possible without it. All fossil fuels are forms of long term stored solar energy, a battery is stored chemical energy, and an alarm clock contains a mechanical energy store in the form of a coiled spring. The success of these storage systems in everyday life is a result of their ability to meet certain criterion (Jenson, 1984), these are listed below.

a) *High Rate of Energy Supply and Removal.* This is the quantity of energy that can be removed or added per unit time (measured in Watts).

b) *High Transfer Efficiency.* Do we lose energy in the transfer processes? An example is the internal heating of a battery. With some systems the transfer efficiency can be 100%, such as pumping petrol to a carburettor. In a thermal energy storage *(TES)* system the transfer efficiency will be a function of the temperature differential available, and the heat transfer mechanism involved. Rates are typically improved by using large heat transfer surfaces.

c) *Long and Low-Loss Storage.* The application of a storage system will depend on the rate at which energy is lost in relation to the period required for storage. Thermal storage system losses are related to the external environmental temperatures and the degree of insulation applied.

d) *High Energy Content.* The energy density of a store, by mass or by volume, is significant. High energy densities reduce both storage material costs and, to a lesser extent, minimise containment costs (for TES systems this includes insulation costs). The surface area of a thermal storage system (related to its volume) will also determine the rate of energy loss.

e) *Minimal Change in Energy Quality.* Energy quality is typically measured as the ratio of free energy *(F)* to actual energy *(E)* in the system. It is a measure of how the energy can be used. A volume of warm water may contain the same energy as a battery, but it uses are far more limited. A phase change TES system that showed a differential melting to solidifying transition temperature would result in a loss of quality of the energy stored.

f) *Modest Containment and Transfer Requirements.* This statement mainly reflects the economics of providing an energy storage system. It should be cheap, both financially and environmentally. The use of glycol brines to store sensible heat is effective but the size of the store results in high costs, both for containment materials and floor space. The use of phase change systems employing ice (with a high latent heat) can substantially reduce volumes and hence costs.

1.4 Thermal Energy Storage

There are two specific methods for thermal energy storage, one employs the specific heat of a medium, while the other uses the latent heat of a phase transition (usually solid to liquid). The amount of energy *(Q)* stored in a medium is a function of its change in temperature. For a solid to liquid transition at constant pressure (eg an open system) Equation 1.10 applies (Guyer, 1988).

$$Q = m[L + C_{ps}(T_L - T_1) + C_{pl}(T_2 - T_L)] \qquad (1.10)$$

Here C_{ps} and C_{pf} relate to the mean specific heats of the solid and fluid phases respectfully. Furthermore, Equation 1.10 assumes the system has moved from one steady state to another and all phase transition has been completed.

Sensible heat storage of thermal energy works well when the energy stored is for heating purposes. This is possible because dense materials and efficient methods exist which allow a large ΔT between the store and its application temperature. When sensible heat storage methods for cooling are examined the case is very different. Low temperature mediums exist, but the efficiency of cooling them decreases rapidly once temperatures are 10 to 20 K below ambient (because the coefficient of performance (COP) of the heat-pump falls with increasing ΔT). So to avoid the need for low temperatures in the store a large mass is required. This raises containment and insulation costs and requires, where fluids are used, some form of chemical treatment. Latent heat stores are much more common for cooling applications. The medium used is water which is cheap and has a high latent heat of fusion, 333kJ/kg (cf C_p water 4.2 $kJ \cdot kg^{-1} \cdot K$). The containment costs are lower, and other benefits such as smaller

ducting and lower flow rates, cause costs to be reduced even further.

Systems used for cold storage work in a variety of modes, namely full storage, partial storage or cascading. The first two are more frequently employed because only one compressor is required in the refrigeration system, thus having a lower cost. Full storage works by cooling the store during the off peak periods, to give it enough cooling capacity to meet the full cooling load during peak demand periods. This system requires a large storage capacity and a heavy duty compressor. The second method uses a compressor continuously. During non-cooling periods the cooling capacity is used to charge the store. During peak periods the cooling load is met by a combination of the compressor and thermal store. The third method cools a store during off peak periods with one compressor. In peak demand cooling is provided by a second refrigeration system. The store is used to cool the condensing side of this, system thus increasing its efficiency.

1.4.1 Conventional Cold Storage Methods and Applications

There are several technologies used for cold storage, these are employed in both HVAC (Heating, Ventilation and Air Conditioning) applications and industrial cooling applications. These technologies can essentially be split into two, those using sensible heat for storage and those that employ latent heat. The principal difference between the two being the energy density (kJ/kg) of the stores (Table 1.2). Both technologies charge in either of two modes; (a) at low continuous rates to meet short lived peak demands, or (b) during specific off peak periods to supply cooling energy during higher unit-cost periods (combinations of these modes often exist).

Table 1.2: Principle Cold Storage Methods and their Relative Space Requirements (Adapted from Kemp (1990)).

Method	Relative Space Requirements
Chilled Water Storage[a]	5
Eutectic Systems[b]	4
Internal Melt[b]	3
External Melt[b]	2
Ice Harvesting[b]	1

notes
a - sensible heat storage
b - latent heat storage

Sensible-heat cold-storage devices employ large tanks of either water or an antifreeze solution that is cooled during appropriate periods. During discharge the solution is pumped to the load and returned at an elevated temperature. To maintain consistent supply conditions, designs have aimed at separating the returned fluid from that stored. This has been achieved by either using a separate tank, a selection of baffles or recently by taking advantage of stratification. Such systems have a low capital and maintenance

cost compared with those employing phase change (Natgun, 1991), although the maximum energy densities are nearly two orders of magnitude lower than possible with ice storage systems. One advantage, if using antifreeze solutions, is being able to store at temperatures below 0°C, although this causes a reduction in energy density and can be achieved better with eutectic based phase change systems, yielding higher energy densities.

Eutectic systems are based around the use of an encapsulated solution with phase change properties suited to the application. The active materials are typically enclosed in spheres, or blocks, made of polythene. This has to be thick enough to withstand the internal pressure changes that take place during phase change, and which increases the capsule's thermal resistance. The spheres are packed in large tanks through which an antifreeze solution is circulated during both charge and discharge modes. Two competing factors effecting performance are present in the system, namely the rate of discharge and the achievable energy density. To increase the rate at which thermal energy passes to the spheres, limited by their surface area, requires smaller diameters, yet as this is reduced the maximum volume of phase change material that can be packed into a given space is decreased. Hence only slight improvements over sensible heat storage methods are achievable. Despite this many HVAC systems have employed these types of store because of their ability to operate at temperatures other than 0°C (Kostyum, 1987; Ames, 1989).

Despite the limited storage temperature there are numerous examples of the successful application of ice-based thermal storage throughout the buildings service industry due to the high latent heat of fusion of ice. Success has been achieved for both new and retro-fitted systems, where partial or total storage was the implementation goal. In the application of ice thermal storage there are principally three methods, or designs, used. These are (a) internal melting (ice-on-coil), (b) external melting (ice-on-coil) or (c) harvesters (ice shuckers). All produce ice at selected periods of the day and return chilled water (or brine) to the required load at temperatures at or above 0°C (McCullough, 1988).

The internal melting design typically consists of a polythene coil submerged in a water tank constructed of a similar material (able to withstand deformation between freezing and thawing of the ice). An ethylene glycol solution, cooled by a packaged chiller, is circulated around this coil at temperatures of -4°C during charge period (ice formation) until virtually all the water has frozen. During the discharge, or melt-out mode, the ethylene glycol is circulated to the load (air handling units). The warmed glycol solution is returned to the coils where it is re-cooled. During the early part of discharge the rate of cooling is high due to the direct contact of the ice with the coils. As melting continues the performance of the system decreases due to the ring of water (having a lower thermal conductivity) that forms between the coil and the ice. The net effect is that the temperature of the glycol supplied to the load rises with time. Furthermore, the maximum rate of charging/discharging the system is limited by the thermal conductivity of the coil.

The second method, external melting, also consists of a coil which is submerged in water, and cooling is again supplied via chilled glycol solutions flowing through coils. The principal difference being that air is used to agitate the freezing water around the coils and the thickness of ice formed is limited to a maximum of 4cm. The discharge differs in that water from the tank is used to cool the load, the main advantage of this being that the water leaves the system within 2°C of freezing throughout the operation (air-agitation is employed during discharge too). The disadvantages of this method compared with internal melting are firstly that other simultaneous chilling from a compressor cannot be applied due to the possibility of freezing within the unit. Secondly because of the ice-thickness limitations, greater coil lengths and larger tanks are required to achieve the same stored energy as internal melting.

Ice harvesters can also be used in parallel with chiller operation. In these systems water is passed over the evaporators and allowed to freeze until a thickness of about 6mm of ice has formed. Once this has occurred (20 to 30 minutes) hot refrigeration gases are passed through the tubes for 20 to 40 seconds to melt the bond between the heat exchanger and the ice. This allows the ice to fall into a collection tank where non-frozen water also collects and is re-circulated. The heat exchanger tubes are controlled in batches so that the whole process is continuous (ie one set is warmed while the others are chilled). Discharge is similar to external melt without the air agitation. This system also supplies water close to 0°C, although returned water can be chilled during discharge by passing it over the evaporator upon its return to the storage tank. Another advantage of this system's design is the removal of the glycol brine from the primary cooling circuit, instead direct refrigeration fluid is used raising the overall thermodynamic efficiency.

Whatever method of ice-storage system is applied there are numerous financial gains to be made. Operational savings will come from the ability of the system to switch electrical usage from periods with high tariffs, to lower cost off-peak electricity tariffs. Furthermore maximum demand charges will be reduced. (Cost relating to the peak demand a user makes on the electrical distribution system). In the USA this can actually be a rebate from the electrical utilities. Less obvious savings are also present, particularly for new constructions:

a) *Utility Rebate.* In the USA utilities pay financial incentives to users for any reductions made in their demand during peak periods. This can be a major incentive both in the design of a new, or a retro-fitted, HVAC system. Wendland (1987) reported that over 15 electricity utilities were paying incentives of $115 to $550 for every kW shifted from peak periods.

b) *Peak to Off-Peak Demand Differential.* The utilities charge users for the peak electrical demand they make on a system. The rate of this charge will depend on the time of day, rates for off-peak periods being 25% of that for peak periods (Wendland, 1987). It reflects the need of the utility to postpone the construction of new plant or up grade the distribution network. Demand charges can account for up to 50% of total electricity bills (Peters, 1986).

c) *Peak to Off-Peak Rate Differential.* The cost of electrical energy used depends on the time of day. Typically peak rates can be 2 to 4 times higher than off-peak rates. Such differentials are applied as incentives for valley filling, and peak lopping.

d) *Reduced Air Handling Costs.* The lower temperature of the chilled water (1 to 4°C compared to conventional 15°C) supplied to air handling units increases the heat transfer rate to the supply air, and reduces its delivered temperature, requiring lower flow rates. This results in smaller heat exchangers, smaller fans, smaller ducts and air distribution terminals. All reduce the capital cost of the air handling equipment, but less obvious is the reduction in ceiling height that can be achieved due to small duct work. In a new building this can give a major saving in construction costs (Kemp, 1990). The lower flow rates of air required in the ducts can reduce pumping cost.

e) *Reduced Duct Noise.* Noise from air supply ducts will result from turbulence. At the lower flow rates achievable with reduced air temperatures this can be significantly reduced. This in turn allows a greater flexibility in the routing of ducts at the design stage.

f) *Reduced or Absent Compressor Noise.* Ice thermal storage systems reduce compressor noise during building occupancy. In a partial system this results from a reduction in the compressor capacity. For full storage systems the operation of the compressor is performed while the building is unoccupied. This can also allow greater flexibility in locating the compressor. Other noise problems can be reduced, such as noise from cooling towers (Grumman, 1988).

g) *Improved Air Quality.* The lower temperature of the air in the ducts in known to eliminate fungus and algae growth. The existence of these biological materials are believed to be significant factors contributing to sick building syndrome (Landry, 1991).

Over the last 10-15 years the application of ice-based TES has had much success for HVAC applications. In the industrial sector the growth in the use of cold storage has been minimal (Timm, 1990). There are many applications in industrial processes that use chilled water at ~4°C or anti-freeze solutions at lower temperatures. These include the cooling of jacketed storage tanks, jacketed reactors, jacketed size reduction equipment, dehumidification equipment and vacuum system coolers. One factor that has prevented cold storage application has been that cooling energy being a small fraction of the total process cost, hence it has had a low priority. More critically some processes require rates that can only be achieved through the direct evaporation of the refrigerant at the point of load. The pumping of chilled water, on account of its thermal capacity, would require excessive pumping rates.

The success of applying ice based TES systems in HVAC applications is the fairly fixed time period for both charge and discharge, typically 8 hours of off-peak tariffs for charge and 12 hours of peak pricing for discharge. The introduction of half hourly

tariffs in the UK after April 1998, will dramatically change the best operational methods of energy storage systems. The ability of a user to vary their electrical demand throughout the day, according to the requirements of a supply utility, will be in a situation to make maximum cost savings. To achieve this through TES a user will require a thermal store, capable of achieving much higher charge and discharge rates, than currently available. The same limitations of using a heat transfer fluid limited by sensible heat capacity applies here, as it does in time varying industrial process applications.

This project addresses these requirements by using a combination of novel materials (hydrophilic co-polymers) and the process of solid-liquid fluidisation, to achieve a pumpable mixture with latent heat energy densities. Such a flowing mixture has both a very high thermal capacity and enhanced rates of heat transfer.

1.5 Secondary Refrigerants

The use of CFC's in refrigeration applications has grown since the 1930's. Their application in large installations (retail stores, food processing industries) has been adopted because of (a) their safe application, due to non-toxicity, at the point of load, (b) to eliminate an intermediate heat exchanger, hence reduce to required system temperature differential (this in turn improved efficiency of the prime mover), and (c) the high thermal capacity/ rate of transfer due to direct evaporation of the refrigerant at the load end (this reduced pumping energy and delivery line size). The networks of piping required to carry the CFC's around the systems are long, and can result in annual leakage rates as high as 10% (Bael, 1996).

The international agreements of the industrial nations on the phasing out of the halo-carbons will give the refrigeration industry many problems. Many of these will be linked to the redesign and performance of refrigeration plants when used with alternative refrigerants (Lizardos, 1992). Many of the long term replacements (non-HCFC's) are either of a toxic nature (eg ammonia), or explosive (hydrocarbons), and pose a further problem in that they can not be used as *secondary refrigerants*. These, also known as heat transferring liquids, are often the means of transporting the cooling energy of the refrigeration unit to the load.

Two emerging technologies, flo-ice (Bael, 1996; Paul, 1993) and CO_2 in a transitional liquid-vapour state (Reiner, 1996), address this problem. Flo-ice, or binary ice, employs a mixture of water, ethanol and small quantities of other compounds. The mixture is cooled to -3.8°C at which point tiny ice crystals start to form on the surface of the evaporator. These are removed by a rotating scraper and the mixture pumped to the load. Binary ice has a potential for storage and this can result in modelled energy savings of 17%. This is a result of taking advantage of lower ambient temperatures causing a better coefficient of performance (COP) (Bael, 1996) from the compressor. Bael does not indicate if system losses are accounted for, or if the energy required for agitating the buffer store and evaporator scraper are included in the model.

The use of CO_2 in a liquid-vapour transitional state is a safe secondary coolant for systems that require temperature of -33°C. This method can employ the existing network with the addition of safety valves (to avoid dangerous pressure build up during shut down periods). The compressor end has to be modified to separate the working refrigerant (ammonia) from the CO_2 secondary refrigerant. The disadvantage of using this fluid is its limit on operational temperatures (-33(±1)°C) and its inability to provide storage capacity.

1.6 Conclusions

This chapter aimed to give the reader an overview of the need for energy conservation and the need for cold storage systems. The rest of this work is concerned with an investigation into the use of hydrophilic materials, in a non-freezing support fluid, for thermal storage at 0°C. Chapter 2 reviews relevant literature pertaining to the flow and heat transfer properties of solid liquid mixtures. It discusses the possible enhancements in heat transfer that can be gained form flowing slurries with phase change occurring. Chapter 3 summarises the tests performed on hydrophilic materials for suitable thermal properties at 0°C. It also shows that by using a suitable hydration fluid the phase transition temperature can be changed to below 0°C, extending the range of their application as storage mediums, beyond those of similar technologies (binary ice).

Systems for the bulk storage and distribution of the materials were investigated, these designs aimed at a low operational power demand, avoiding the high loads associated with the buffer agitators and scrapers required in binary ice systems. The findings from these tests are reported in Chapter 4. The final design detailed in this chapter proved capable of storing the phase change materials at very high densities, and supplying these at variable concentrations to the flowing heat transfer circuit.

To investigate the heat transfer mechanisms involved with the flowing mixtures a heat transfer test apparatus was constructed and calibrated. The differential temperatures involved with such measurements were small, hence the rig had to achieve a high sensitivity. Details of the design and calibration of the rig are presented in Chapter 5. The results from the test apparatus when using hydrophilic slurries having concentrations of 1%, 5%, 10% and 25% (by volume) are presented in Chapter 6.

The novelty of this project, combined with the wide range of variables involved, has limited the extent to which the study was undertaken. The employment of hydrophilic base phase-change slurries as thermal storage and transmission fluids was achieved under laboratory conditions. Chapter 7 details the routes required to (a) investigate further the enhancement in heat transfer properties of the slurries (due to the presence of phase change particles) and, (b) collect specific engineering data for the design and operation of thermal energy storage systems employing hydrophilic based slurries.

Chapter 2

The Physical Properties of Slurries

2.1 Introduction

This chapter of the work draws upon the literature for information regarding the flow and heat transfer properties of slurries. An understanding of both is essential to the application of hydrophilic phase change slurries for thermal storage and transmission applications. The first part of the chapter will look at some basic properties of single phase fluids, including the viscosity, the concept of turbulence, and correlations used to predict heat transfer coefficients.

The second part defines different categories of solid-liquid mixtures and the different behaviour of non-newtonian fluids. Specific correlations relating to the viscosity, thermal conductivity, and heat transfer to slurries are given.

2.2 Newtonian Fluids and Fluid Mechanics

The terms fluid and viscosity are used every day in engineering disciplines to describe the behaviour of many liquids that flow. Rheologically these terms are reserved and refer to the Newtonian fluid, the simplest form of flowing matter to characterise. These fluids have a property called viscosity, μ defined by the expression:-

$$\mu = \frac{\tau}{\gamma} \tag{2.1}$$

Where τ is the shear stress and γ is the rate of shear. The viscosity of a Newtonian fluid is constant under constant temperature and pressure. These concepts can be understood better if the one dimensional case, as shown in Figure 2.1, is considered. This shows two parallel layers of a fluid flowing over each other with a relative velocity Δu, and separated by a distance Δy. Each will experience a retarding force due to interactions between the two fluid layers . The specific value of this force is the shear stress.

The following expression can be written:-

$$\mu = \tau \frac{\Delta u}{\Delta y} \tag{2.2}$$

With many such layers a velocity gradient or rate of shear exists, and in the limit $\Delta y \rightarrow 0$

the viscosity becomes:-

$$\mu = \tau \frac{du}{dy} \tag{2.3}$$

In three dimensions du/dy is replaced by γ.

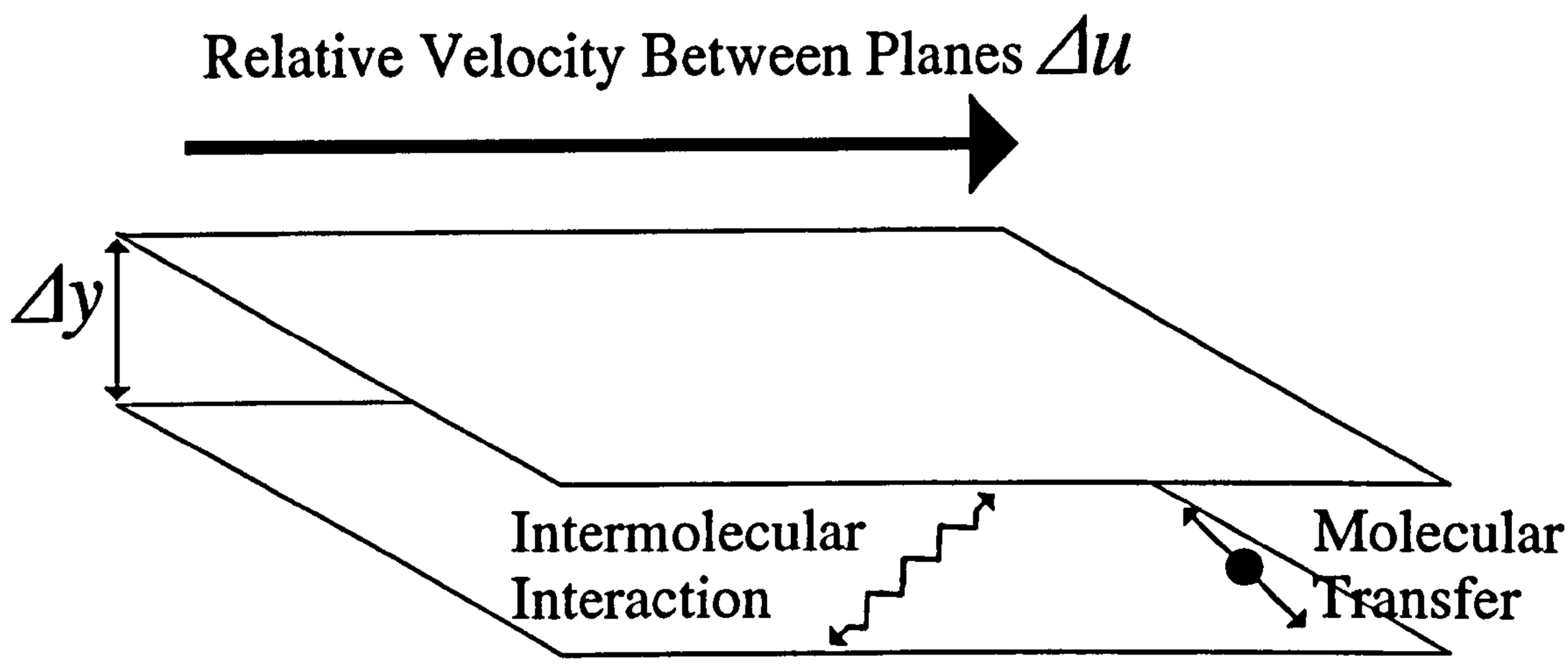

Figure 2.1: Mechanisms of Viscosity.

There are two main mechanisms of viscosity, and their relative importance determines how the viscosity of a fluid varies with temperature and pressure. The first mechanism is caused by the migration of the fluid molecules between the fluid layers. This leads to a transfer of momentum causing the two interacting layers to decelerate their relative velocities. The second mechanism exists due to intermolecular forces between the layers, again causing a decrease in the relative velocity. The origin of these intermolecular forces is primarily electrostatic (Harris, 1977; Tanner 1985).

If the inter-molecular spacing increases, as is the case when the fluid temperature rises, there will be a reduction in the strength of the inter-molecular force which in turn will lead to a reduction in viscosity. The rise in temperature will increase the random motion of the molecules and thereby increase the migration of molecules between layers (ie increase momentum transfer). This mechanism serves to increase viscosity. Nearly all liquids show a decrease in viscosity with temperature where the inter-molecular forces are dominant but gases exhibit an increase in viscosity with temperature indicating that momentum transfer dominates viscosity.

Most single phase liquids can be treated as Newtonian fluids, particularly those that contain small molecules. For those liquids that have large molecules or strong inter-molecular forces (eg long chain hydrocarbons), Newtonian behaviour is assumed over certain limits such as a range of shear rates. The viscosity of a fluid is predominant in determining the type of flow that exists in a system.

2.2.1 The Reynolds Number and Flow Regimes

If the flow of a Newtonian fluid in a pipe is analysed by measuring the pressure drop between two points on that pipe, it is found that there are two distinct regions of behaviour. At low flow rates it is found that the pressure drop along the length is proportional to the flow rate. As this flow rate increases a point is reached where the linearity fails and a more rapid rise in pressure drop with flow rate is observed, it is evident that two flow regimes exist. At low flow rates, *laminar* flow conditions are present, a fluid can be considered to flow in parallel layers similar to Figure 2.1 (all flow is in one direction and parallel to the pipes axis). At a certain point natural fluctuations in the fluids motion become too strong to be damped by the fluids viscosity and the layers break up, leading to a chaotic motion. The fluid is now said to be under conditions of *turbulent* flow. The local velocity is random and only the average fluid velocity acts along the pipe's axis.

The conditions under which there is a transition from laminar flow to turbulent flow can be predicted using the non-dimensional *Reynolds number*, Re. This is a dimensionless number, named after Osborne Reynolds who demonstrated the existence of the two flow regimes in 1883. This constitutes the ratio of the inertial forces and the viscous forces (Bennett, 1982):-

$$Re_x = \frac{\rho u_x X}{\mu} \tag{2.4}$$

Here ρ is the fluid density, the subscript, x, is used to indicate the geometry it refers to. X and u_x refer to the characteristic dimension and velocity of the particular Reynolds number. For the internal flow of a fluid in a tube u_x refers to the mean velocity of the fluid in the tube, and X the diameter of the tube (for this case the subscript x and X are replaced by D).

For a fluid flowing in a tube it is generally accepted that the flow stops being laminar at the *critical Reynolds number*, $Re_c \geq 2{,}300$ (Rohsenow, 1985). Fully developed turbulent flow is considered to exist at $Re \geq 10{,}000$. The intermediate flow behaviour is called *transitional flow*. These values are used only as a guide, it is possible for the start of transitional flow to be extended to higher values of Re depending on the previous flow history and the local environment (Massey, 1983).

Reynolds numbers are not only used to predict the transition from laminar to turbulent flow. Many correlations in fluid mechanics use it as a parameter where the ratio of turbulent-to-viscous energy dissipation or mixing is a governing factor. (ie convective heat transfer under turbulent conditions, Section 2.2.3). Other dimensionless numbers have been developed and are used as a method of simplifying problems in fluid engineering (Pitts, 1977; Massey, 1983). These groups relate physical properties, hence simplify analysis and extend the application of resultant correlations. Common dimensionless numbers, together with their physical significance, are listed in Appendix A.

2.2.2 The Velocity Boundary Layer

The velocity profiles and the temperature profiles across any surface are very different for the two types of flow, and consequently the convective heat transfer rates are very different. Figure 2.2 shows the behaviour of a fluid as it flows in the x-direction across the start of a flat plate. Before the fluid interacts, at $x = 0$, it has a uniform velocity. Once the fluid meets the flat plate, the velocity of the fluid on the wall surface will become zero. The mechanism of viscosity will cause layers of the fluid further away from the wall surface to slow down, giving a velocity profile $U(y)$. At some distance from the wall's surface the effects of viscosity will be negligible and $U(y) \rightarrow U_\infty$. The effects of viscosity penetrate further into the fluid as it moves down stream from the start of the plate. The locus of the points $y = \delta$ where $U(\delta) = 0.99U_\infty$ encloses what is called the *hydrodynamic boundary layer.*

If conditions are such that $Re \geq Re_c$ turbulent flow starts to develop and the flow profile of Figure 2.2 will be modified to that in Figure 2.3. When the thickness of the hydrodynamic boundary is greater than δ_c the velocity profile is considered to be flat because of the high degree of mixing. The boundary layer itself will now contain several distinct layers, the *laminar sub-layer,* the *buffer layer*, and the *turbulent region.* A similar layer exists for temperature distributions (Section 2.2.3).

Under conditions of laminar flow the shear stresses outside the hydrodynamic boundary layer become negligible. Energy losses in such flow problems are considered from the point of view of surface frictional effects and make use of the concept of the local *friction coefficient* C_f, sometimes called the fanning friction factor. This is a dimensionless parameter defined as

$$C_f = \frac{2\tau_s}{\rho u_\infty^2} \tag{2.5}$$

The surface shear stress τ_s can be found from a knowledge of the velocity profile and by using Equation 2.3 (Incropera, 1990).

In internal flow problems it is preferential to use the *Moody* (or Darcy) *friction factor,* f. This is another dimensionless parameter defined by

$$f = \frac{-2(dp/dx)D}{\rho u_\infty^2} \tag{2.6}$$

Here dp/dx is the pressure drop along a duct length, D is the characteristic length (diameter for circular ducts), and u_∞ is the mean flow velocity, which is nearly always used in internal flow correlations. To find values of f, and determine the pressure drop, use is made of correlations, tables or graphs of f against Re. Such graphs are frequently referred to as *Moody diagrams*. For the turbulent flow conditions a family of lines exist, each of which corresponds to a relative roughness, e (Incropera, 1990). (This dimensionless parameter is the ratio of the surface roughness to tube diameter).

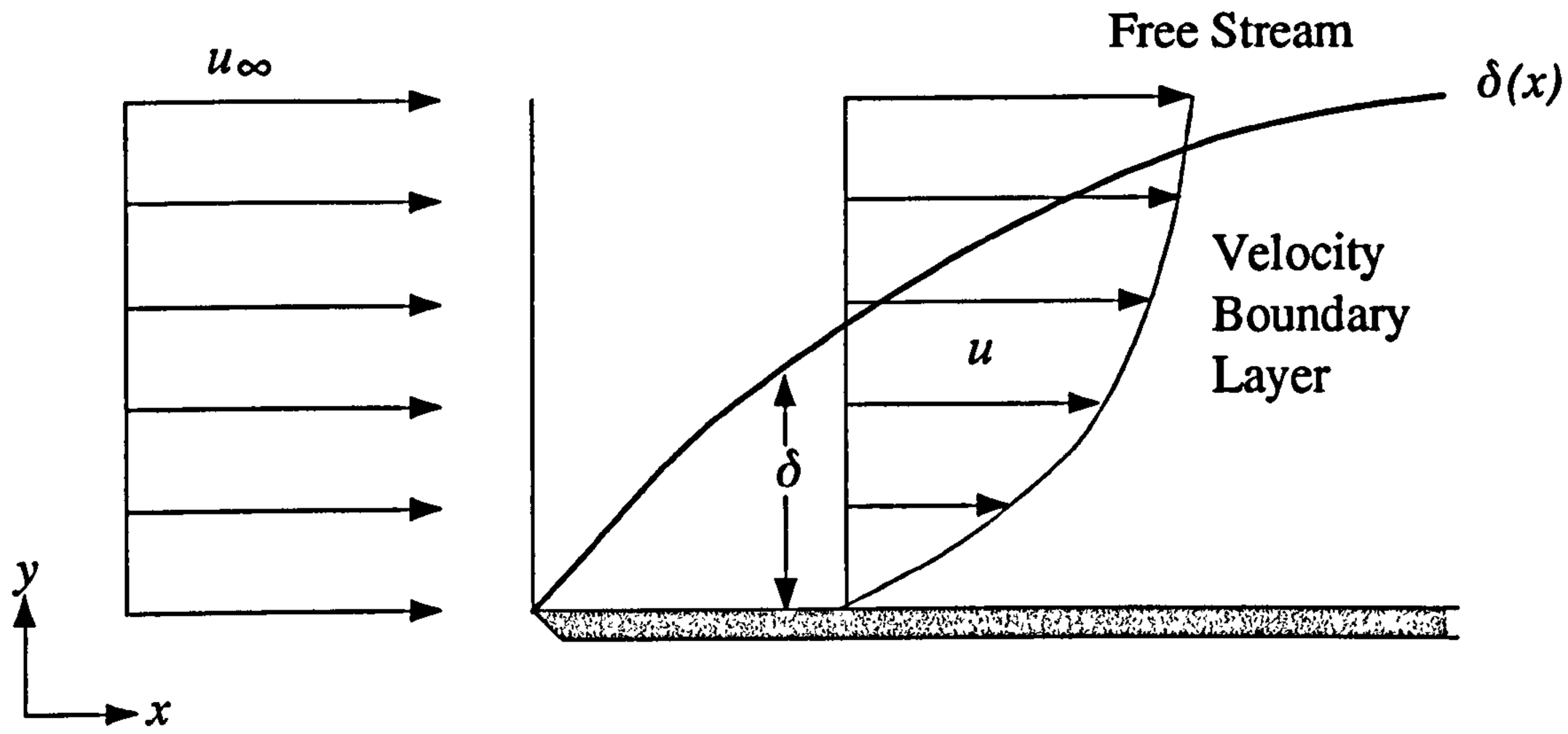

Figure 2.2 Development of Velocity Profile - Laminar.

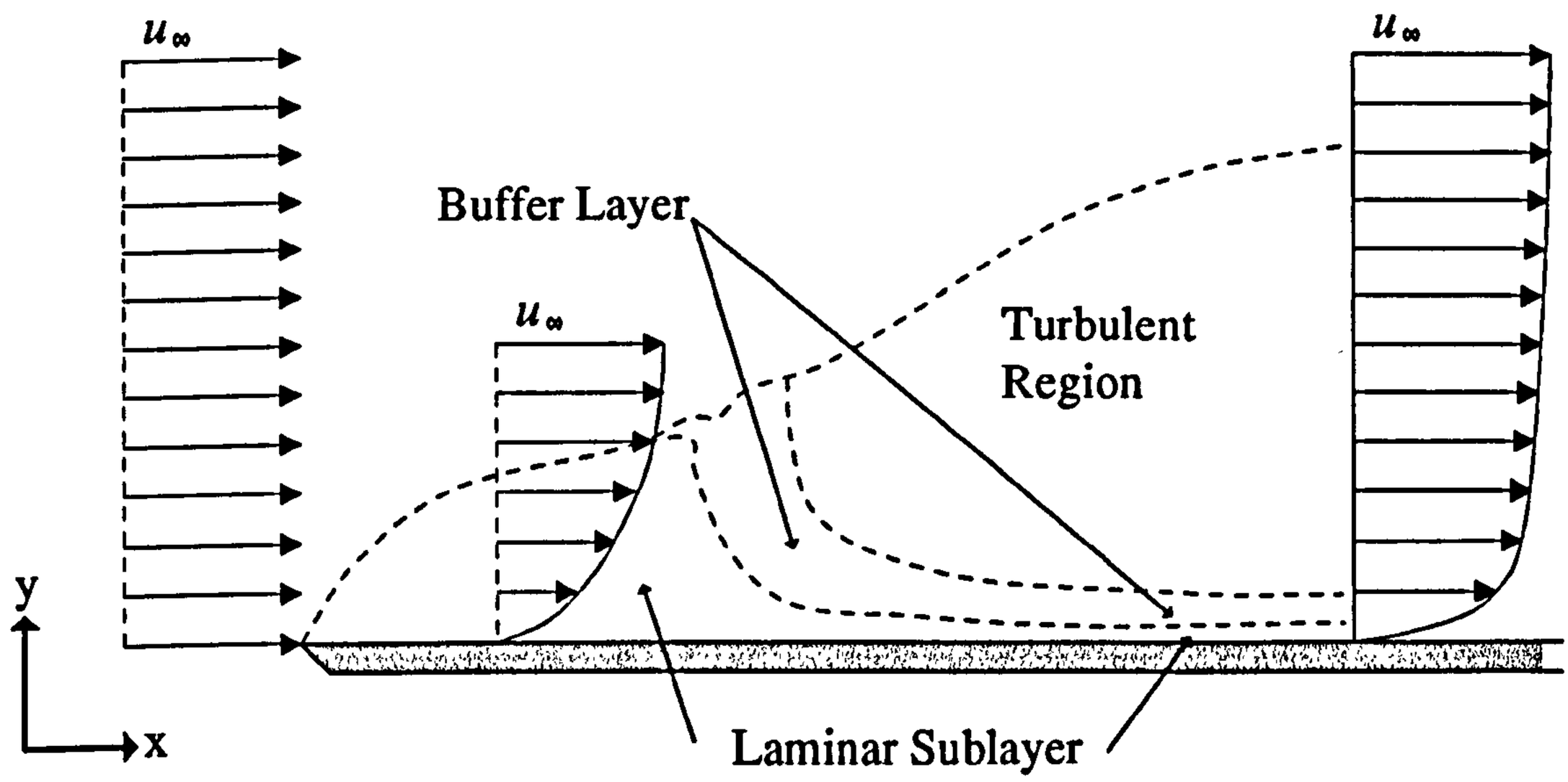

Figure 2.3 Development of Velocity Profile - Laminar, Transition and Turbulent.

Equations 2.5 and 2.6 are related by

$$C_f = \frac{f}{4} \tag{2.7}$$

There are several numerical methods to find the friction factor, f, although they are limited to certain flow regimes or conditions, for fully developed laminar flow in straight pipes use can be made of (Massey, 1983):-

$$f = \frac{64}{Re_D} \tag{2.8}$$

For smooth pipes where $e = 0$, the following correlations may be used to calculate Darcy friction factors for fully developed turbulent flow conditions (Massey, 1983; Incropera, 1990).

$$f = 0.316 Re_D^{-0.25} \tag{2.9}$$

for $Re_D \leq 20{,}000$, and

$$f = 0.184 Re_D^{-0.2} \tag{2.10}$$

for $Re_D \geq 20{,}000$.

So far only straight sections of pipes have been considered. When the geometry becomes more complex, such as bends, pipe entrances, or across valves, tables must be consulted (eg Rohsenow, 1985). These are usually produced by manufactures and are usually comprehensive giving values of f against Re.

2.2.3 Thermal Boundary Layer

If the surface temperature of the plate in Figure 2.4 differs from that of the fluid, a *thermal boundary layer* will develop similar to the velocity boundary layer in Section 2.2.2. This is denoted by δ_T, and is defined as the point where the fluid temperature satisfies $(T_s\text{-}T)/(T_s\text{-}T_\infty) = 0.99$ (Figure 2.4). As flow passes over the plate, δ_T will increase because of heat penetration into the fluid (Incropera, 1990). Because of the rapid mixing that occurs in turbulent zones of flow, most of the temperature differential will be across a laminar layer .

The only process allowing heat transfer under laminar flow conditions is conduction hence the thermal conductivity and the thickness of this layer will govern the overall local rate of heat flux from the surface by *Fourier's Law*:-

$$q'' = -k\frac{\partial T}{\partial y} \tag{2.11}$$

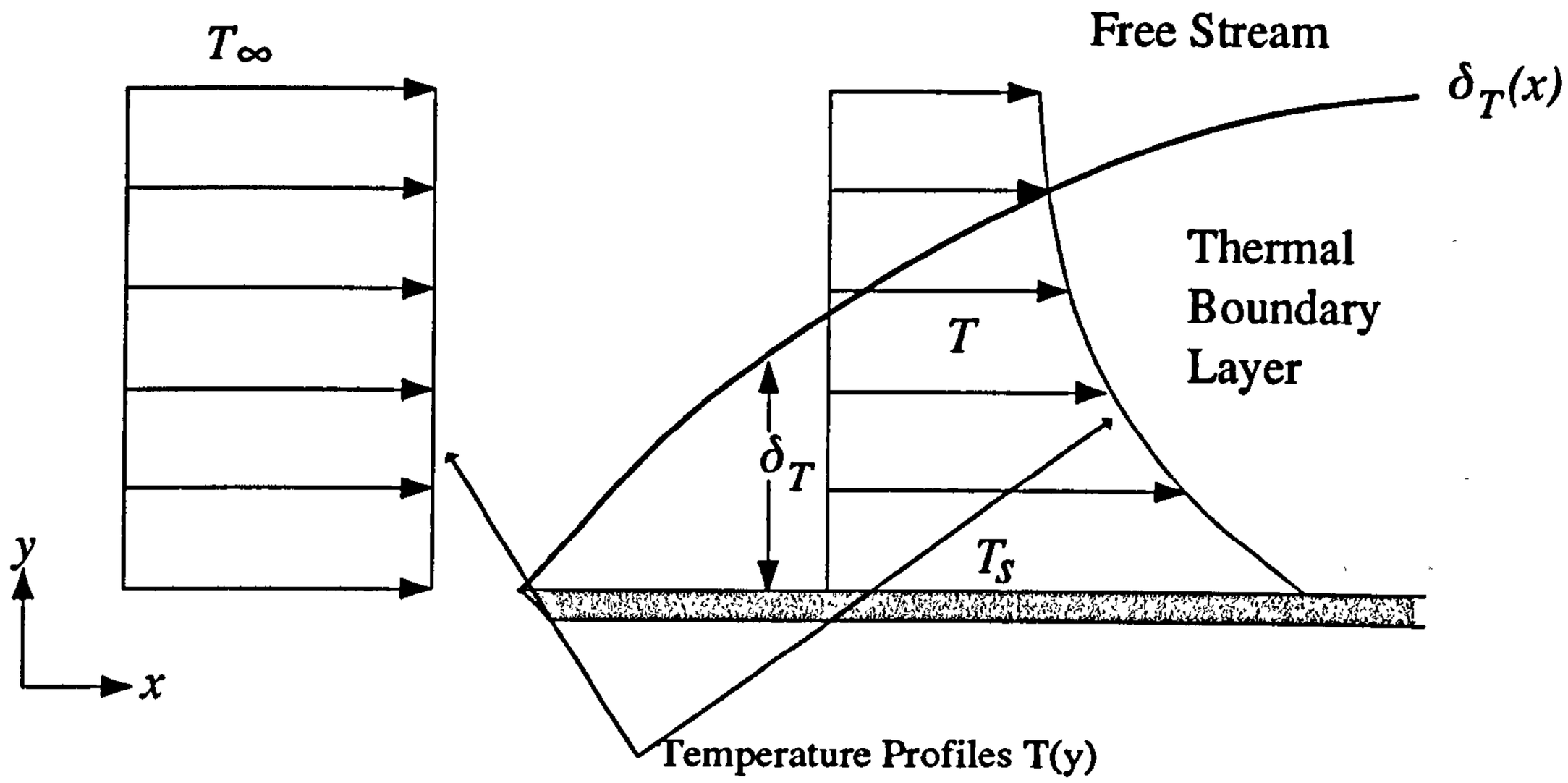

Figure 2.4: Development of Thermal Boundary Layer Over a Flat Plate.

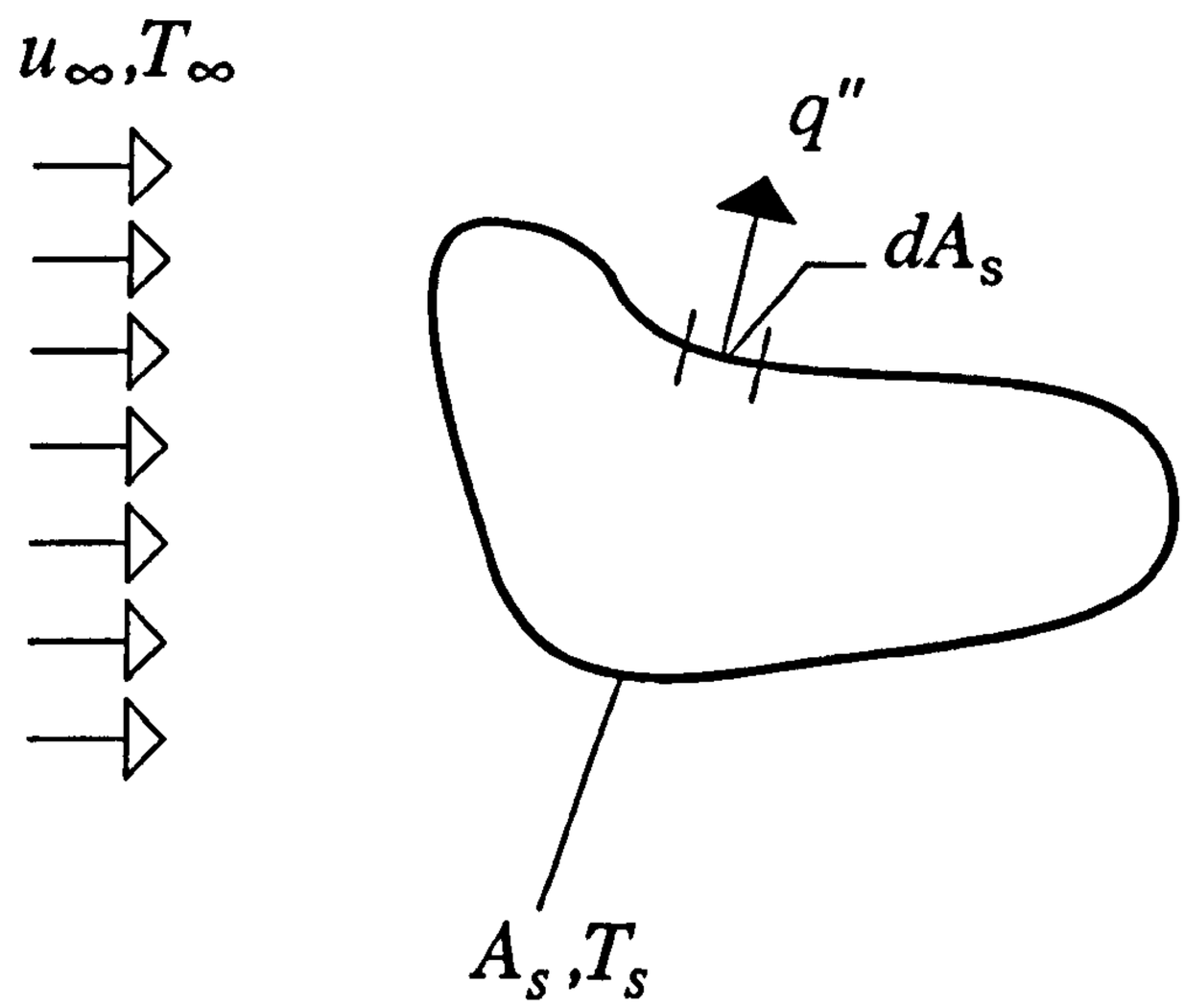

Figure 2.5: Convection Over an Arbitrary Shape.

2.2.4 Single Phase Convective Heat Transfer

In general when a fluid flows over a surface, area A_s (Figure 2.5), at a different temperature ($T_s \neq T_\infty$), convective heat transfer will occur .The fluid may be in motion because of (i) natural thermal effects (natural convection), or (ii) because of some form of pumping (forced convection). Whatever mechanism drives the fluid the local heat flux q'' can be expressed by:

$$q'' = h(T_s - T_\infty) \tag{2.12}$$

where h is the local convective heat transfer coefficient.

In the absence of forced motion (ie when no pumps or fans are employed) natural, or free, convective heat transfer may take place in the presence of both a temperature gradient and a body force (typically gravity). Although these conditions are essential, natural convection will only occur if the temperature gradient causes a density gradient that opposes the body force. A typical example is hot air rising from a domestic radiator. Here the negative temperature gradient in the vertical direction leads to a positive density gradient, which opposes the downward acting gravitational force. More simply, the hot air at the radiators surface is less dense than cooler air above it, hence the volumes of air exchange places, warmer air rises. Forced convection requires the fluid to be pumped over the surface. This action generally leads to higher rates of heat transfer than obtained under natural conditions, although at low flow rates natural convection heat transfer may be significant.

The local convection coefficient will be some function of the geometry of the system, its temperatures, and the fluid's properties and flow behaviour. In many convective heat transfer problems, the focus is on predicting the total heat transfer rate q, the integral of q'', which is given by:-

$$q_{convective} = \bar{h}A(T_{sample} - T_{surroundings}) \tag{2.13}$$

where the average convection coefficient $\bar{h}$ is given by:-

$$\bar{h} = \frac{1}{A}\int_{A_s} h \cdot dA_s \tag{2.14}$$

Table 2.1 shows ranges in values of $\bar{h}$ for a range of conditions.

For the purpose of dimensional analysis the *Nusselt number*, Nu is used. This is the ratio of convective to conductive heat transfer in a fluid. For a system with a characteristic length, L, the ratio is:-

$$Nu = \frac{hL}{k} \tag{2.15}$$

Historically much work has been undertaken to develop correlations for *Nu* for a wide variety of geometries and flow conditions (Dittus, 1930; Colburn, 1933; Sieder, 1936; Petukhov, 1970; Gnielinski, 1976). Generally these are found by one of a number of methods:-

i) the exact mathematical solutions of the equations describing the fluid flow and energy transport within the boundary layer (i.e. the boundary-layer equations);

ii) the approximate solution of the boundary-layer equations using integral analysis;

iii) by employing different analogies between heat and momentum transfers;

iv) dimensional analysis combined with experimental results, in order to obtain practical, empirical relationships;

v) computational fluid dynamics (CFD).

Historically methods (i) and (ii) are typically applied to laminar flow conditions with well defined geometries. The physical laws of conservation of momentum, mass and energy can be applied to generate differential equations. For example, by considering the laws of motion describing a fluid in a fixed volume of space leads to the Navier-Stokes equation (Pitts, 1977; Rohsenow, 1985; Incropera, 1990). Full solutions are often not possible and limitations are often imposed, such as neglecting viscosity effects (reduction of Navier-Stokes equation to Euler's equation). Once random effects of turbulence are involved, analytical methods fail, method (iii) or (iv) must be used. The recent developments in computer processors speeds, CFD techniques and turbulence theory have enabled the equations of motion to be computed, and growth in this area continues. Some workers have developed CFD models that include particles and have reached the stage of predicting both velocity profiles and solids concentrations in simple geometries (Hsu, 1989).

2.2.5 Analogy Between Heat and Momentum Transfer

For most practical applications flows in boundary layers are turbulent and, due to the complex nature of such motion, analytical solutions have not been achieved. To overcome this, use is made of analogies, in particular the *Eddy Diffusivity* leading to *Prandtl's Mixing Length.* In Section 2.2 the mechanism of momentum transfer and its effects on viscosity were introduced. Here a similar mechanism is considered where "lumps" of the fluid move between layers in turbulent flow. This concept is called eddy viscosity, and is introduced to explain the increased viscous dissipation of energy during turbulent flow. (Analogous to this is the effect of the addition of particles to a fluid to form a suspension or slurry, discussed in Section 2.6).

Figure 2.6 shows the flow of a fluid over a flat plate where the objects marked *A* and *B*

Table 2.1 Range of Values of $\bar{h}$ for Various Fluids (Pitts, 1977; Incropera, 1990).

Process		$\bar{h}$ / $W \cdot m^{-2} \cdot K^{-1}$
Free Convection:	air	5 to 25
Forced Convection:	gases	25 to 250
Forced Convection:	oils	50 to 1,500
Forced Convection:	water	250 to 10,000
Forced Convection:	boiling water	2,500 to 50,000
Forced Convection:	condensing steam	5,000 to 100,000

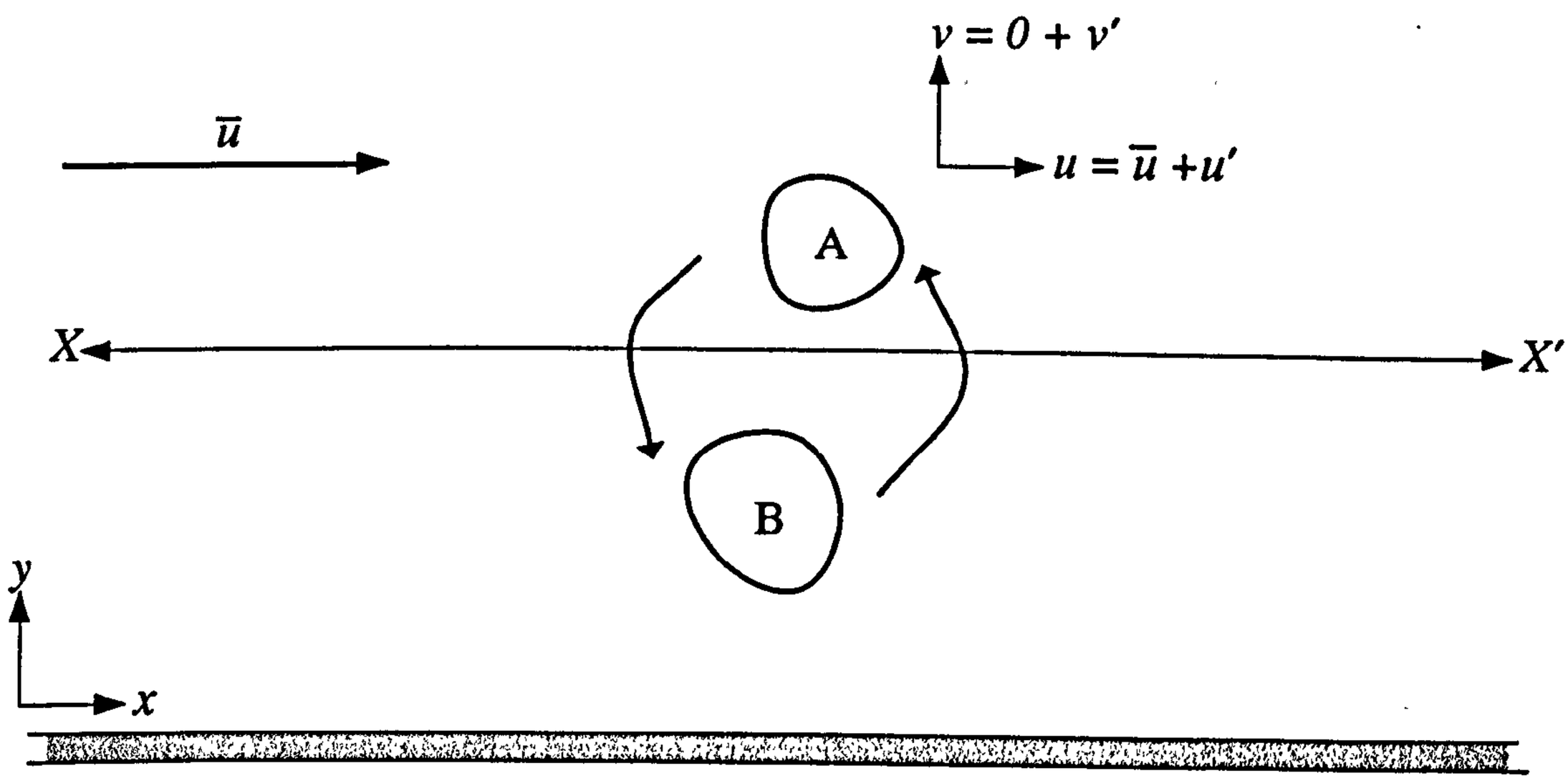

Figure 2.6: The Exchange of "Fluid Lumps" During Turbulent Flow.

are two lumps of the fluid set in motion by turbulent fluctuations. The lump A is shown moving to a region of increased velocity across a typical plane X-X'. To replace it the lump B moves across the plane into a region of lower velocity. Both lumps must undergo a change in momentum so that their time-average velocities equal those in their new regions. If the the velocity components are considered, then evaluation of the momentum change of the fluid lumps can be made in a quantitative manner (Pitts, 1977; Incropera, 1990). In the x and y direction:

$$u = \bar{u} + u', v = 0 + v' \tag{2.16}$$

The mass flow per unit area across the plane X-X' is given by the product $\rho v'$ since it is known that the mean velocity is zero because there is no mean flow in the y direction. If this is multiplied by u', the instantaneous velocity component in the x direction, an expression is obtained for the instantaneous momentum change, the average value of which is $\rho v'u'$.The force required to bring about this momentum change is parallel but opposite in direction to the average laminar flow, hence it adds to the laminar stress to produce:-

$$\tau = \tau_l + \tau_t \tag{2.17}$$

$$\tau = \left(\mu\frac{\partial \bar{u}}{\partial v} - \rho v'u'\right) \tag{2.18}$$

In this form the equation requires knowledge of the instantaneous velocity of each part of the fluid before it can be used. To overcome this, use is made of the *eddy viscosity*, ε, to give:-

$$\tau = (\mu + \rho\varepsilon)\frac{\partial \bar{u}}{\partial y} \tag{2.19}$$

or in terms of the kinematic viscosity, $\nu = \mu/\rho$:-

$$\frac{\tau}{\rho} = (\nu + \varepsilon)\frac{\partial \bar{u}}{\partial y} \tag{2.20}$$

Prandtl postulated that the migration of the microscopic lumps of the fluid is, on average, analogous to the motion of molecules in a gas. That is, they travel on average a distance l perpendicular to the direction of flow u before they lose their identities. It is this distance l that is known as *Prandtl's Mixing Length* (qualitatively equivalent to the mean free path in a gas)(Pitts, 1977; Incropera, 1990).

If two dimensional turbulent flow exists there will be extra terms coming into the above analysis, these will effectively lead to stresses normal to the plane of flow (one origin of vortices). During the turbulent flow of slurries solid particles may either move with the fluid 'lumps' or independently. The overall effect of this will depend on the relative

densities, fluid viscosity and rate of momentum change. For example, if the particles are more dense than the fluid but move with the eddy molecules the effective density will increase, reducing velocity fluctuations in the fluid and hence increasing the effective viscosity. Such effects are associated with the phenomena of shear thickening (Section 2.3.2).

The effects of turbulence on heat transfer can be approached in an analogous manner to the arguments used for the eddy viscosity. If the flow field of Figure 2.6 has temperature fluctuations given by:-

$$T = \bar{T} + T' \tag{2.21}$$

then the equation for the rate of heat transfer within the fluid will contain two parts. The first will be the same as the conductive equation in laminar flow heat transfer. The second will relate to the heat transferred via mass transfer. By defining the *eddy diffusivity for heat* as ε_H the equation can be reduced as follows:-

$$q' = q_l' + q_t' \tag{2.22}$$

$$= -k\frac{\partial T}{\partial y} + \rho C_p v T' \tag{2.23}$$

$$= -(k + \rho C_p \varepsilon_H)\frac{\partial \bar{T}}{\partial y} \tag{2.24}$$

and by using $\alpha = k/\rho C_p$ we obtain

$$\frac{q'/C_p}{\rho} = -(\alpha + \varepsilon_H)\frac{\partial \bar{T}}{\partial y} \tag{2.25}$$

Inspection shows that Equations 2.20 and 2.25 are of identical form, suggesting a strong analogy between momentum and heat transfer. In fact the ratio $\varepsilon/\varepsilon_H$ could be considered to be a turbulent Prandtl number Pr_t. Prandtl's mixing-length theory suggests that this ratio is unity since $\varepsilon = \varepsilon_H = v'l$.

The model of Prandtl's is very simplified although experimental evidence supports the approach, and Pr_t equal to unity serves most practical calculations. This assumption gives the turbulent heat flow:-

$$q_t = \tau_t C_p \frac{\partial T/\partial y}{\partial \bar{u}/\partial y} \tag{2.26}$$

This relationship was originally derived by Reynolds, and is called the *Reynolds analogy,* and is applicable to the turbulent boundary layer (it does not hold where the

Prandtl number is not unity(Incropera, 1990)). By considering turbulent flow over a flat plate (Figure 2.6) the shear stress in the laminar sub-layer is given by:-

$$\tau = \mu \frac{\partial u}{\partial y} \tag{2.27}$$

and the heat flux normal to the plane of the plate:-

$$q = -k \frac{\partial T}{\partial y} \tag{2.28}$$

These can be combined to form:-

$$q = -k\tau C_p \frac{\partial T/\partial y}{\partial u/\partial y} \tag{2.29}$$

Comparing 2.26 and 2.29 shows that the same equations for heat flux can apply if Pr = 1. Now if q and μ are considered to be constants (wrt y) then Equation 2.29 becomes:-

$$\frac{q_s}{\tau_s C_p} du = -dT \tag{2.30}$$

and integrating between the limits of $u = 0$, when $T = T_s$, and $u = u_\infty$ when $T = T_\infty$ gives:-

$$\frac{q_s}{\tau_s C_p} u_\infty = (T_s - T_\infty) \tag{2.31}$$

now replacing parameters with h (Equation 2.12) and C_f (Equation 2.5) yields:-

$$\frac{Nu}{RePr} = St = \frac{C_f}{2} \tag{2.32}$$

St, the Stanton number, is a modified Nusselt number and represents the ratio of heat transferred at the surface to that transported by the fluids thermal capacity. Equation 2.32 is valid for Pr = 1, Colburn (Colburn, 1933) modified this for $0.6 < Pr < 50$ to give:-

$$\frac{Nu}{RePr} Pr^{2/3} = St Pr^{2/3} = \frac{C_f}{2} \tag{2.33}$$

For all practical purposes Equation 2.33 requires the local friction factor obtainable from tables of f. Further refinement of this equation has since been achieved by Von Kármán (1939), and Coulson (1954), by incorporating the effects of the buffer layer.

2.2.6 Empirical Correlations For Heat Transfer (Turbulent Flow In Tubes)

One of the earliest correlations for the Nusselt number for fully developed turbulent flow is the *Colburn equation* (Equation 2.33). This uses the friction factor of Equation 2.10 substituted into Equation 2.33 yielding:-

$$Nu_D = 0.023 Re_D^{4/5} Pr^{1/3} \tag{2.34}$$

The *Dittus-Boelter equation* (Equation 2.35) is slightly different in that it is based upon a distinct power index for the Prandtl number depending on whether the fluid is hotter ($T_s > T_f$, $n = 0.4$), or cooler ($T_s < T_f$, $n = 0.3$), than the tube surface (Dittus 1930).

$$Nu_D = 0.023 Re_D^{4/5} Pr^{n} \tag{2.35}$$

This correlation is valid for the ranges $0.7 \leq Pr \leq 160$, $Re_D \gtrsim 10{,}000$, and $L/D \gtrsim 10$.

In any real situation there will exist a variation in fluid properties throughout the fluid due to the thermal gradient. If this is large, or the temperature coefficients of the fluid properties are large, Equation 2.35 will be invalid. The equation of Sieder and Tate (1936) overcomes these limitations by incorporating a factor to account for the viscosity difference of the fluid at the wall and at its mid stream. The work of Sieder and Tate (1936) was based upon the study of heat transfer correlations for a number of fluids, some having highly temperature dependent viscosities. Their correlation (Equation 2.36) includes the thermal entrance effects and has a reported error of ±25% (Incropera, 1990).

$$Nu_D = 0.027 Re_D^{0.8} Pr^{0.333} \left(\frac{\mu}{\mu_w}\right)^{0.14} \tag{2.36}$$

This is valid for $0.7 \leq Pr \leq 16{,}700$, $Re_D \gtrsim 10{,}000$, $L/D \gtrsim 10$, and may be applied for both constant wall heat flux or constant wall temperature.

For increased accuracy it is recommended (Incropera, 1990; ESDU, 1992) that the equation of Petukhov is used (Petukhov, 1970). This correlation (Equation 2.37) is reported to have errors within ±10% for a wide range of fluids.

$$Nu_D = \frac{(f/8) Re_D Pr}{1.07 + 12.7 (f/8)^{1/2} (Pr^{2/3} - 1)} \tag{2.37}$$

It is valid for the range $0.5 < Pr < 2000$ and $10^4 < Re_D < 5\times10^5$.The friction factor f can be found from the Moody diagram or for smooth tubes via the expression:-

$$f = (1.82 \log_{10} Re_D - 1.64)^{-2} \tag{2.38}$$

This is a more precise version of Equation 2.10 if used in the same range as Equation 2.37.

Where the Reynolds number indicates that transitional flow conditions exist, it is recommended (Incropera, 1990) that the modification to Equation 2.39 of Gnielinski (1976) is used (Equation 2.39).

$$Nu_D = \frac{(f/8)(Re_D - 1000)Pr}{1 + 12.7(f/8)^{1/2}(Pr^{2/3} - 1)} \tag{2.39}$$

This is valid for the range $0.5 < Pr < 2000$ and $2300 < Re_D < 5\times10^5$, and it is recommended that Equation 2.40 is used to determine the friction factor.

$$f = (0.79\ln Re_D - 1.64)^{-2} \tag{2.40}$$

Both Equations 2.36 and 2.37 relate only to single phase Newtonian fluids, as they stand, and are used in Chapter 5 as a means of testing the performance of the heat transfer test rig, when used with water. In Chapter 6, heat transfer under transitional flow conditions was examined and Equation 2.39 was used to verify the rig's performance for the single phase oil. Later, as solids were added to the system, Equation 2.39 was applied with appropriate account taken of the particles. This allowed a comparison to be made, highlighting the effects of phase change solids to the heat transfer coefficient.

2.3 Classification of Solid-Liquid Mixtures

The literature contains information on the behaviour of flowing systems (primarily for single phase fluids), and many works (Massey, 1983; Rohsenow, 1985; Incropera, 1990) contain useful correlations for calculating heat transfer coefficients or pressure drops along straight pipes and fittings. Typically the authors will limit the validity of these correlations to certain conditions, such as flow rates or particle sizes. Often these limitations will be of a dimensionless form such as Reynolds numbers, or particle diameters. This section deals with the way in which a mixture is categorised by its macroscopic properties.

The main classification to make is whether or not to treat the mixture as single or multi-phase. If the mixture is such that single phase correlations can be applied then it must be decided if the mixture is Newtonian or non-Newtonian in its behaviour (Section 2.2). Figure 2.7 shows schematically how the two classifications are related.

This work is interested in the fine and coarse dispersions, (the terms macro mixed and stratified apply to fluid-fluid mixtures only, eg oil-air, water-oil mixtures).When reference is made to slurries, the following definitions can be made:

i) *Fine Dispersion* - small solid particles more or less uniformly dispersed in a continuous phase;

ii) *Coarse Dispersion* - large solid particles dispersed in a continuous liquid phase where settling takes place.

It is found that some dispersions are stable under all conditions, even static, supported by Brownian motion or consistency properties of the fluid. Others are only found to be stable under conditions of flow, where the particles are continually dispersed by turbulence. It is these mixtures that must undergo some analysis to predict their behaviour with the flow conditions encountered in the system of interest.

The settling velocity of the particles contained in a slurry is an important factor in the classification of the mixture. The importance becomes more pronounced under laminar flow but has implications for turbulent conditions.

2.3.1 Terminal Velocity and Settling Behaviour

The effect of gravity on a solid-liquid mixture will cause the phases to separate. The rate at which this occurs depends on many factors which are discussed in this section, starting with the simplest case of a sphere falling (or rising) in a infinite fluid. The following factors all reduce the terminal velocity of the particle, these are in turn the effects of the fluid's boundary, the effects of irregularly shaped particles, and finally the effects of other particles. The simplest case to consider is that of a spherical particle falling through an infinite Newtonian fluid. After an initial acceleration a *terminal velocity*, V_0, will be reached where the gravitational force, F_g, will be balanced by the drag forces, F_D. The gravitational force is given by (Govier, 1977):

$$F_g = \frac{\pi d^3}{6}(\rho_s - \rho_f) \tag{2.41}$$

The particle will experience a drag force given by the equation :

$$F_D = C_D \frac{\rho_f V^2 \pi d^2}{8} \tag{2.42}$$

The term C_D is the *Drag Coefficient* which is a unique function of the particle Reynolds number. The form of this function has been approximated for various flow regimes, combined with Equations 2.41 and 2.42 so that functions for the terminal velocities are generated, see below (Shook, 1991). (A slight iteration must take place to see if the terminal velocity predicted matches the flow conditions assumed for that equation.)

Laminar motion, $Re < 1$

$$V_0 = \frac{g(\rho_s - \rho_f)d^2}{18\mu} \tag{2.43}$$

Transitional motion, $1 < Re < 1000$

$$V_0 = 0.2\left[g\frac{(\rho_s - \rho_f)}{\rho_f}\right]^{0.72} \frac{d^{1.18}}{(\mu/\rho)^{0.45}} \tag{2.44}$$

Turbulent motion, $800 < Re$

$$V_0 = 1.74\left[g\frac{(\rho_s - \rho_f)}{\rho_f}\right]^{0.5} d^{0.5} \tag{2.45}$$

These correlations have been developed from the ideal case of a spherical particle falling in an infinite fluid. In real engineering applications fluids must be contained and this tends to increase the drag force in turn leading to a lower terminal velocity. To correct for this the terminal velocity from the previous equations should be multiplied by a factor F_w (Govier, 1977). For laminar flow this is given by

$$F_w = 1 - \left(\frac{d}{D}\right)^{2.25} \tag{2.46}$$

and turbulent flow by

$$F_w = 1 - \left(\frac{d}{D}\right)^{1.5} \tag{2.47}$$

Account of the irregular shape of the particle must be made, and one method is to use an equivalent diameter (d_s), to replacing d in Equations 2.43, 2.44 and 2.45. This can be found from tabulated data (Table 2.2) relating d_s to the average screen size of the particle, d_{av} (Govier, 1977).

Finally the effects of solids concentration must be considered and this is found to be a function of the *volume fraction*, ϕ. Govier presents many correlations for calculating the hindered settling velocity, one of the most versatile being Equation 2.48 (Thomas, 1963), covering the range $1 > V_c/V_0 > 0.08$.

$$V_c = V_0 e^{-2.56\phi} \tag{2.48}$$

So far the settling velocity for particles has been given for particles falling in a vessel, or the fluid rising. Of interest is the settling velocity of particles flowing in horizontal tubes under turbulent conditions. Govier gives the empirical correlation (Spells, 1955) for the minimal velocity to achieve symmetric distribution of particles (V_M) in horizontal tubes with turbulent flow (Equation 2.49). Spells (1955) validated this for particles ranging in size from 50μ to 500μ.

$$V_M = 0.1196\left[gd\left(\frac{\rho_p - \rho_f}{\rho_f}\right)\right]^{0.816}\left(\frac{D\rho_m}{\mu_f}\right)^{0.633} \tag{2.49}$$

Single Phase	Multiphase (gas-liquid,liquid-liquid,solid-liquid,solid-gas)			
	Fine Dispersion	Coarse Dispersion	Macro Mixed	Stratified
True Homogeneous	Pseudo Homogeneous	Heterogeneous		

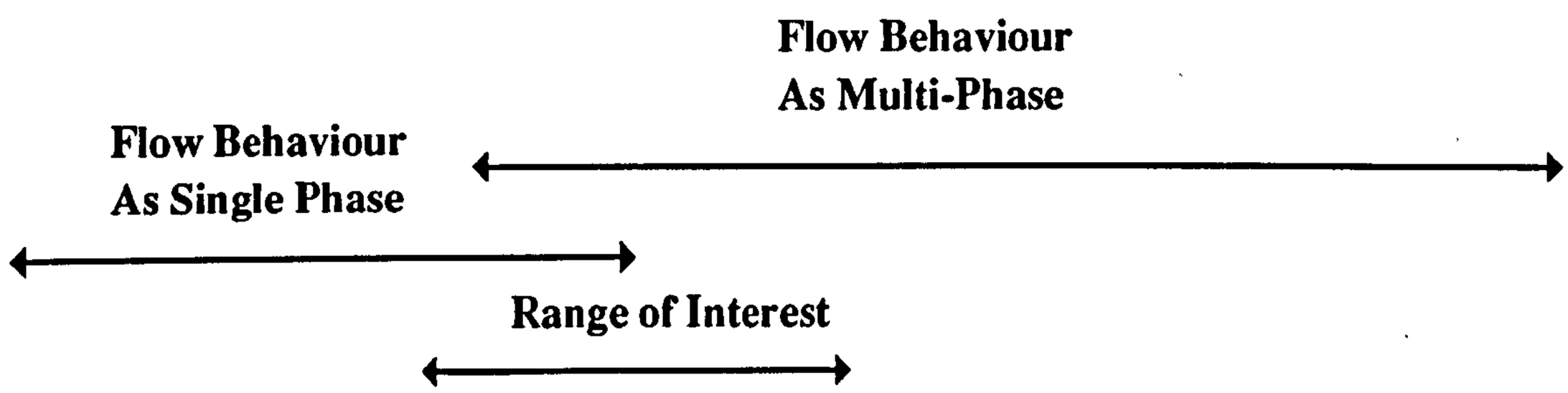

Figure 2.7: General Classification of Mixtures.

Table 2.2: Equivalent Diameters of Some Particles Shapes.

Shape	d_s/d_{av}
Sphere	1.00
Cube	1.24
Prism - a × a × 2a	1.564
Prism - a × 2a × 2a	0.985
Prism - a × 2a × 3a	1.127

2.3.2 Rheological Classification of Non-Newtonian Fluids

This section describes briefly the rheological classification used for continuous media that are capable of flow. The simple, but very specific case of the Newtonian fluid has been discussed in Section 2.2, which has a shear stress (τ) directly proportional to the rate of shear (γ) (Equation 2.1). The constant of proportionality is known as the viscosity and is independent of the rate of shear. Non-Newtonian fluids have more complex relationships between τ, and γ, the plot of this is known as a rheogram (Figure 2.8). The gradient of a tangent on one of the curves is known as the apparent viscosity μ_a, and this value is generally only valid for a particular rate of shear. How the apparent viscosity changes with rate of shear determines the classification of that fluid.

The first level of complexity are the *shear-thinning, or pseudoplastic fluids,* and *shear-thickening, or dilatant fluids.* As the names suggest, the apparent viscosity of these fluids decrease (shear-thinning) or increase (shear-thickening) with the rate of shear. Typically pseudoplastic fluids contain long molecules (Govier, 1977) which tend to align with the flow more, as shear rate is increased. Similar effects can occur as small particles group together and align to the flow direction. There are numerous models that relate apparent viscosity to the rate of shear, the simplest of these is the power law:

$$\tau = K\gamma^n \tag{2.50}$$

Where K is known as the *consistency index,* or *power law coefficient.* The exponent n is known as the *flow behaviour index,* or *power law exponent.* For a value of n=1 Equation 2.50 reduces to that of a Newtonian fluid (Equation 2.1). Values of n<1 describe pseudoplastic fluids where as n>1 describe dilatant fluids. The power law fluid is normally only valid over a certain range of γ, there are many other more complex models that describe both pseudoplastic and dilatant fluids better, but involve more constants (Govier, 1977). Despite its limitations many works have used Equation 2.50 for both flow (Metzner, 1955; Griskey, 1971; Green, 1968; Dodge 1959) and heat transfer (Quader, 198; Wilkinson 1960) investigations with non-Newtonian fluids.

Shear-thickening fluids have an apparent viscosity that increases with γ, and although this behaviour is less common than shear-thinning, it is frequently found to occur in high concentration suspensions between certain shear rates (Govier, 1977; Roscoe, 1953; Barnes, 1989). In his work, Barnes describes the phenomena occurring due to a transition from a two dimensional layered arrangement to a random three dimensional form. He showed that (a) the phenomena rarely occurred over more than order of magnitude of shear rate; (b) was strongly dependent on both particle size and shape; and (c) the magnitude was dependent on the solids concentration. The concentration dependency was found to be normalised by the maximum particle concentration possible, and hence with a wide distribution of particle sizes the level of shear-thickening was lowered.

The next complication in the classification of non-Newtonian fluids is one of the fluid exhibiting a *yield stress,* τ_y, (i.e. it will not flow below a certain finite shear stress). Once such fluids are flowing, they can behave as any of the previously mentioned

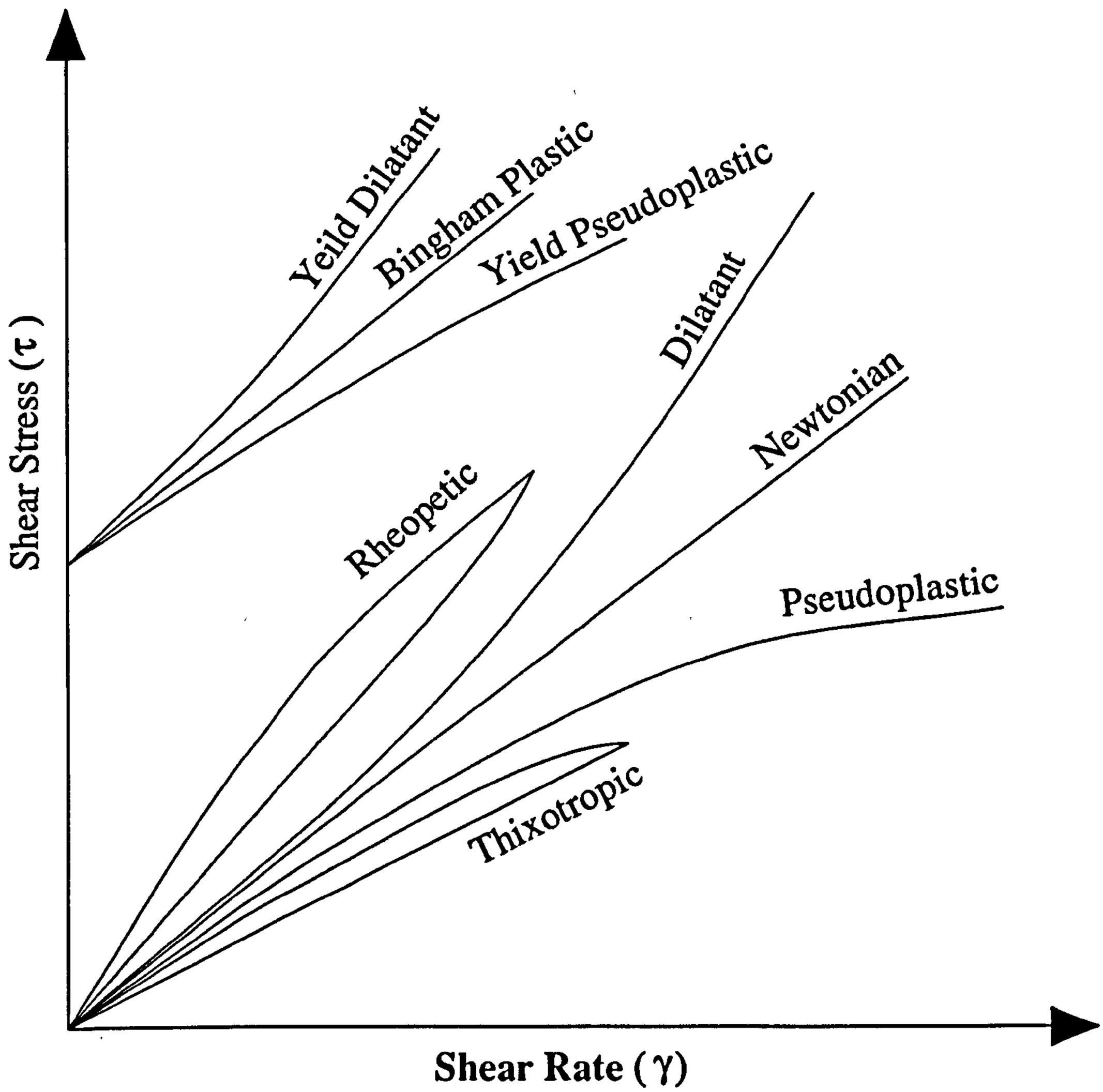

Figure 2.8: Rheograms for some Non-Newtonian Fluids.

fluids and can be typically described (Equation 2.51) in a similar form to Equation 2.50:

$$\tau - \tau_y = K\gamma^n \tag{2.51}$$

Where values of n=1 the fluid is termed a *Bingham Plastic*, for n<1 a *yield pseudoplastic*, and for n>1 a *yield dilatant*. Many high concentration slurries or suspensions (by volume) show a yield behaviour (Govier, 1977; Kawase, 1989).

The final degree of complexity is the time dependent fluids. These can have all the complexities of the past categories, but the exact behaviour will depend on the history of the fluid. *Thixotropic fluids* are defined as those that show a decrease in shear stress after a duration of shear. Fluids that exhibit the less common effect of shear stress increasing with time as a shear stress is applied, are called *Rheopetic Fluids*. Either type of behaviour is represented on a rheogram as two paths (Figure 2.8) but such diagrams are insufficient to fully describe these systems. Many solid-liquid mixtures show some degree of thixotropic behaviour (Govier, 1977) due to degradation of particles or structures, although for this work these effects will not be considered further.

2.4 Physical Properties of Slurries

In general the physical properties of a slurry are some function of the geometry of the system, the mixture temperature, and the individual physical properties of the constituent liquid and solid phases.

$$X_m = f\{l_m, T_m, \phi, a_s, a_f, b_s, b_f, c_s, c_f, \ldots\} \tag{2.52}$$

Here X_m is some physical property of the slurry, l_m a characteristic dimension such as a pipe diameter, T_m the temperature of the mixture, ϕ the volume fraction of the solids, and $a_f, b_f, c_f \ldots$ and $a_s, b_s, c_s \ldots$ are the individual physical properties of the liquid and solid phases respectively, such as thermal capacity (C_p). Some slurry properties, such as density, are linear functions of the individual properties and extend through the whole range of slurry parameters, whilst others, such as the viscosity, depend on non-linear functions or correlations and are only valid within certain limits. The rest of this section deals with the most important of the slurry properties, which will find some application in the understanding of the heat transfer processes.

2.4.1 Slurry Density

When we are considering a pseudo-homogeneous slurry the density is a linear function of the slurry constituents given by:-

$$\rho_m = \rho_f(1 - \phi) + \rho_s\phi \tag{2.53}$$

This is true if the slurry is isothermal and will otherwise be temperature dependent.

2.4.2 Slurry Heat Capacity

If the mixture is isothermal and the temperature is above or below the phase transition temperature of the supported particles a similar linear equation can be written for the heat capacity of the slurry:-

$$C_{p_m} = C_{p_l}\rho_l(1 - \phi) + C_{p_s}\rho_s\phi \qquad (2.54)$$

Both equations (2.53) and (2.54) are limited to well behaved mixtures where all constituents are at the same temperature. In this work we are faced with the fact that at certain temperatures we will have a discontinuous heat capacity during phase transition. To a lesser extent the phase transition will also cause a discontinuity in the density equation. Care must be taken in all correlations around these temperatures.

2.4.3 Slurry Viscosity and Newtonian Slurries

Slurries with large particles tend to be Newtonian (Shook, 1991), although at high volumetric concentrations the behaviour may tend toward a Bingham fluid, and a yield stress be evident. The Newtonian behaviour is frequently described as a function of the solids concentration ϕ_s, the simplest relation being that derived by Einstein (1906):

$$\mu_m = \mu_l(1 + 2.5\phi_s) \qquad (2.55)$$

where μ_m is the viscosity of the mixture. Equation 2.55 is valid for low concentrations where the interparticle distance is larger than the particles (typically ϕ_s<10%). For higher concentrations Equation 2.56 (Krieger, 1972) accounts for the rapid increase of viscosity as concentrations increase.

$$\mu_m = \mu_l\left(1 - \frac{\phi}{\phi_{max}}\right)^{-B\phi_{max}} \qquad (2.56)$$

Here ϕ_{max} is the maximum possible concentration of the solid possible with the particular size distribution. In limit of $\phi \rightarrow 0$ Equation 2.55 suggests that the constant B should have a value of 2.5 (Shook, 1991). (The value of $\phi_{max} = 0.63$ is typical of spherical particles of a single size.) The quadratic equation of Vand (1945) avoids the use of the maximum concentration:

$$\mu_m = \mu_l(1 - \phi - 1.16\phi^2)^{-2.5} \qquad (2.57)$$

This has been verified for concentrations up to $\phi = 0.2$, for particles ranging in size from 0.3μm to 400μm, and for duct-to-particle diameter ratios of 20 to 100 (Rutgers, 1962). Higher order polynomials describing the viscosity have been derived (Shook, 1991) although their predictions of viscosity deviate little from those of Equation 2.57, over solids concentrations ranging form $\phi = 0$ to $\phi = 0.6$. The equivalence of Equations 2.55, 2.56 and 2.57 are shown in Figure 2.9.

2.4.4 Thermal Conductivity Of Slurries

In the literature, several numerical relationships exist between the thermal conductivity of the slurry and the thermal conductivity of its constituent parts. This section reviews the most important of those found and indicates the limitations of each. Firstly the thermal conductivity of solid-liquid mixtures under static conditions are considered, this situation is encountered in the actual storage part of a cold storage device, when the system is passive. Next, expressions that refer to laminar flow conditions are discussed; these are quite complex and reflect the fact that the effective thermal conductivity includes micro-convection mechanisms that are encountered in slurry flow. Micro-convection serves to increase the effective thermal conductivity.

The thermal conductivity is generally the limiting physical property in both laminar flow heat transfer and turbulent conditions, where heat transfer is normally limited by the thermal resistance of the laminar boundary layer. Kasza (1985) suggested that during the turbulent flow of slurries, particle collisions with the laminar sub-layer will break it down and reduce its thickness. If this is the case then heat transfer will be generally increased. Furthermore direct thermal conduction between the particle and the heat transfer surface could occur during impact, again tending to increase the overall heat transfer rate.

The first and most commonly referenced work on the conductivity of a two component mixture is that of Maxwell (1954).This work actually considers the effective electrical conductivity of small spheres of one medium evenly dispersed in another continuous medium. The commonly used analogy between electrical and thermal conductivity suggests the use of this relation in thermal conductivity problems. Maxwell's discussion following his derivation, limits Equation 2.58 to mixtures where the inter-particle separation is much larger that the particle diameters. This in reality confines the validity to a maximum of 10% by volume of the particles, given by ϕ.

$$k_m = \frac{2k_c + k_f + \phi(k_c - k_f)}{2k_c + k_f - 2\phi(k_c - k_f)} k_f \qquad (2.58)$$

A further limitation on Equation 2.45 occurs when the relation:-

$$\frac{k_c - k_f}{2k_c - k_f} \gtrsim 1 \qquad (2.59)$$

If this is the case, as with the volume fraction, then Maxwell (1945) states that further terms are required in Equation 2.58 to make it valid.

For high-solids concentration packed beds, as encountered in a static cold storage tank, the work of Kunii (1960) is relevant. Kunii made a comparison of numerous data sets from previously published work, and based his arguments upon the analysis of spheres in a packed bed, to give correlations for the heat transfer characteristics of porous rock.

The thermal conductivity of such systems can be written as:

$$k_m = k_f \left\{ \lambda + \frac{\beta(1+\varepsilon)}{\theta + \gamma\left(\frac{k_f}{k_s}\right)} \right\} \tag{2.60}$$

Where β depends on the packing style of the bed and ranges from 0.9 for loose packing to 1.0 for close packing. In the systems considered in this work only natural settling will occur, it is anticipated that the particles will loosely pack, hence β will be 0.9. The λ represents the void fraction of the bed of solids and θ a measure of the effective thickness of the fluid film adjacent to the contact surface. From tables given in the work of Kunii (1960), and using typical values for the hydrophilic material used in this research project, θ will ranged between 0.2 and 0.5.

With Equations 2.58 and 2.60 it is important to stress that the relations are formulated for static mixtures. No effects associated with natural convection or turbulent mixing are included, the rest of this section considers the changes that take place when the mixture is in motion.

Leal (1973) used a numerical method to predict the thermal conductivity of dilute suspensions of spherical drops. His work was limited to fluid drops with low internal and external Reynolds numbers, the same limitation applied to the Peclet numbers for both the drop and the suspending fluid $Pe \ll 1$, this is given by:-

$$Pe_x = \frac{\rho C_{p_x} V L_x}{k_x} \tag{2.61}$$

Where the subscript x refers to properties of either the particle or the fluid. Other assumptions made were that the flow was purely shear and that both fluids were Newtonian in behaviour. No limitations were put upon the concentration of droplets but it is assumed the dilute in the title refers to suspensions of 10% or less. His numerical analysis lead to a complex equation involving many viscosity terms (Leal, 1973). However in this research only solid particles are used and the equation reduces to:-

$$k_m = k_f \left[1 + \phi \left\{ 3 + \frac{(4.636k_s^2 - 0.692k_s k_f - 3.944k_f^2)}{(k_s + 2k_f)^2} \right\} Pe_f^{2/3} \right] \tag{2.62}$$

From this it can be seen that there are two important conclusions. The first, and most important, is that the effective thermal conductivity is always enhanced by increasing the bulk shear rate (Pe is proportional to the shear rate). This is true regardless of the thermal conductivities, or viscous properties, of the constituents. Also the enhancement to k_m increases with larger particle concentrations. This is best shown by allowing the thermal conductivities to become equal, giving:-

$$k_m = k_f [1 + 3\phi Pe_f^{3/2}] \tag{2.63}$$

Equation 2.63 shows the contribution from micro-convective currents alone (Figure

2.10) (a mechanism caused by particles rotating due to differing shear rates influencing k_m). Analysis of Equation 2.62 also shows that as the difference in the thermal conductivities increases, whether $k_f>k_s$ or $k_s>k_f$, so does the effective thermal conductivity k_m. The origin of this process is linked to the promotion of a steeper particle to liquid thermal gradient, giving rise to higher surface convection on the particle.

Nir (1976) performed a similar numerical analysis to Leal (1973) for the limit of $Pe >> 1$, where the effects of the shear field are much higher. Again derivations were for systems where the system dimension was large compared to the inter-particle spacing, which in turn was large compared to the particle diameter; this again limited the volumetric concentration to <10%. The basic finding of Nir (1979) was that at high particle Peclet numbers, the effective thermal conductivity was a power law, Pe_s^n (n=1/11), and also a function of ϕ. The trend again was to enhance the thermal conductivity due to micro-convection.

The later work of Sohn (1981) experimentally investigated the enhancement to thermal conductivity during shear flow. These tests were performed for liquid-solid systems using high density polyethylene (HDPE) particles suspended in fluids giving neutrally buoyant mixtures. Particle Peclet numbers ranged from 0.2 to 2000 and volume particle concentrations at 15% and 30%. These results showed that for $Pe_s<50$ the enhancement to the thermal conductivity was small, although increased with rising Pe_s. At high values of the particle Peclet number, $Pe_s>300$, it was observed that the effective thermal conductivity followed a power law expression of the form:-

$$k_m = k_f f(\phi, \ldots) Pe_s^n \qquad (2.64)$$

where $n \cong 0.5$, a much higher value than that predicted by Nir. It was also observed that different ratios of k_f/k_s gave differing values of k_m, this was associated with other factors such as particle interactions, eg electrostatic.

2.5 Convective Heat Transfer to Slurries Under Turbulent Flow

One of the earliest investigations of the heat transfer characteristics of slurries is that of Salamone (1955). During the 1950s there was an interest in augmenting the heat transfer of the cooling gases in nuclear reactors by the addition of solid particles, spurred by the observation of the high rates of heat transfer in fluidised beds. The supporting fluid for all of Salamone's suspensions was water in which solid particles were dispersed. Solids used were copper, carbon, silica and chalk. The particle sizes used ranged from 1.5μm (silica) to 56μm (largest copper particles), and in solids concentrations from 2.3% to 10.7% (by volume). The rheological behaviour of the suspensions was found to be pseudoplastic.

The experimental results for heat transfer were obtained from a horizontal tube heat exchanger of internal diameter of 0.5 inch and heat was applied by the application of steam in an outer annulus (results for water were found to be in good agreement with

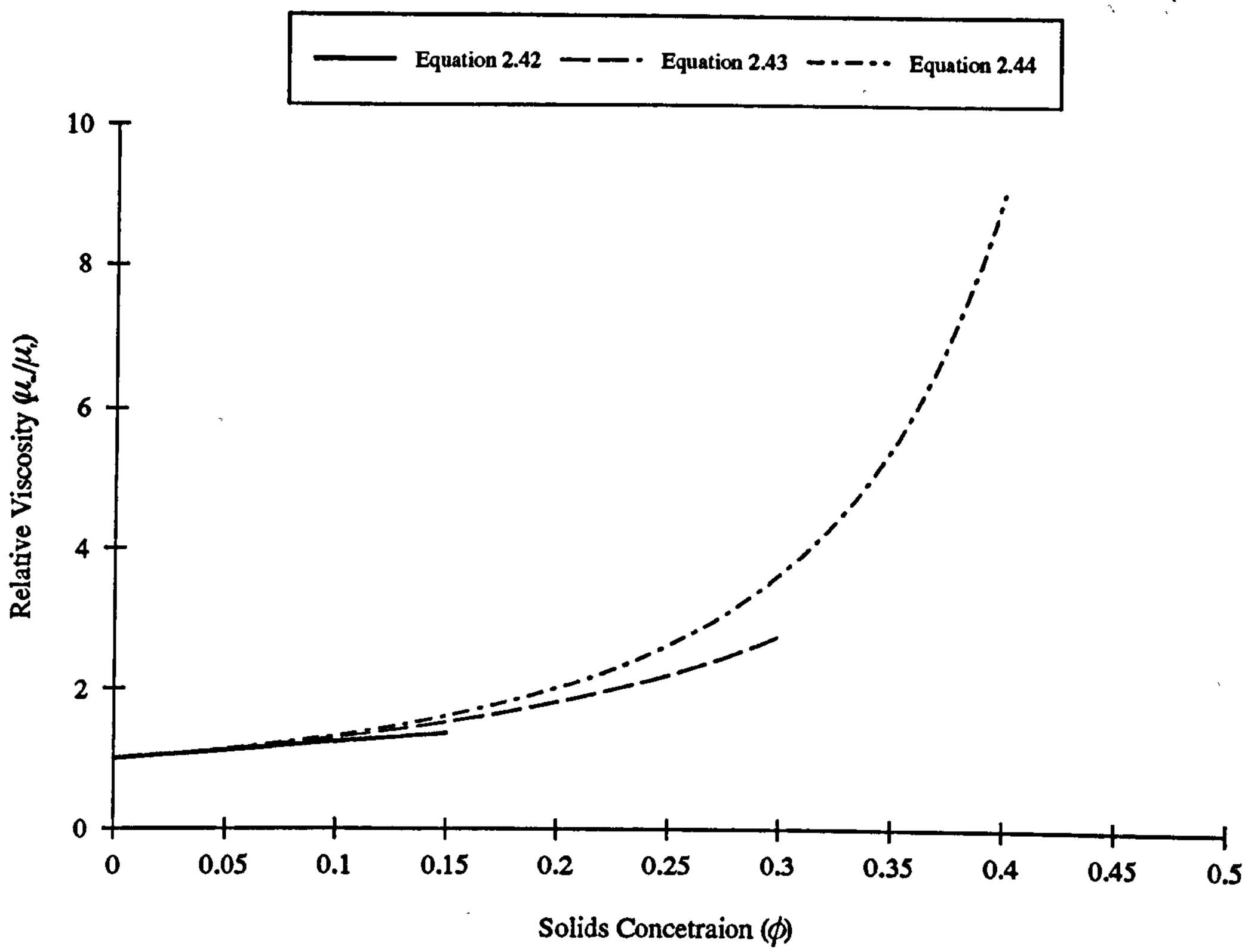

Figure 2.9: Comparison of Viscosity Equations.

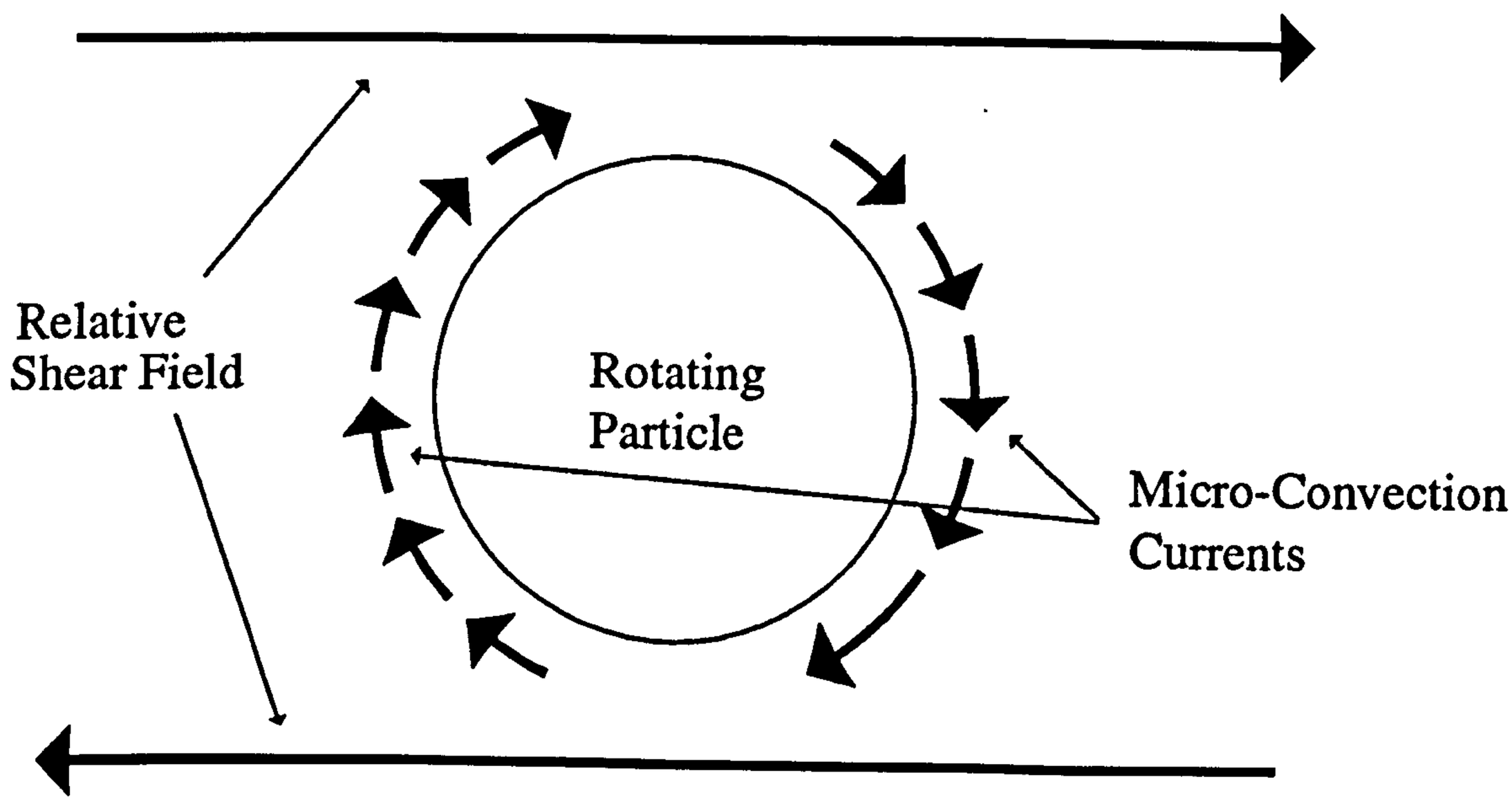

Figure 2.10: Mechanism of Micro-Convection.

standard correlations between Re = 60,000 to Re=150,000). By the application of dimensional analysis the correlation in Equation 2.65 was derived. The viscosity used in both Re_m and Pr_m, of the correlation, are that of the suspension as measured during each test run via an in-line tube viscometer.

$$Nu = 0.131 Re^{0.62} Pr^{0.72} \left(\frac{k_s}{k_f}\right)^{0.05} \left(\frac{D}{d}\right)^{0.05} \left(\frac{C_{ps}}{C_{pf}}\right)^{0.35} \tag{2.65}$$

for $14{,}000 \leqq Re \leqq 140{,}000$, $3.4 \leqq Pr \leqq 12.7$, $0.53 \leqq k_s/k_f \leqq 583$, $282 \leqq D/d \leqq 10{,}500$ and $0.09 \leqq C_{ps}/C_{pf} \leqq 0.22$.

Salamone (1955) applied this correlation to data sets from two independent investigations and found a close agreement. The small particle sizes involved with this work led to the rheological behaviour being pseudoplastic in nature. Harada (1985) looked at water suspension with particles of sizes between 0.06mm to 1.0mm with volumetric concentrations from 1% to 10%. Again their work looked at the heat transfer in horizontal tubes, although a range of diameters was used (14mm, 19mm and 25mm). The results deviated significantly from those of Salamone (1955) and an empirical correlation, based on that of Sieder-Tate (Equation 2.36), was proposed:-

$$Nu = 0.0161 Re^{0.88} Pr^{1/3} \left(\frac{\mu_f}{\mu_w}\right)^{-0.14} \tag{2.66}$$

valid for $8000 \leqq Re \leqq 50{,}000$, $0.01 \leqq \phi \leqq 0.1$ and $0.0024 \leqq d/D \leqq 0.071$.

The correlation (Equation 2.56) fitted the experimental data to within ±15%. Generally for particle diameters > 0.35mm the heat transfer coefficient was found to be always larger than that for water alone, and fairly independent of particle size, pipe diameter and the volume fraction of the solids. In contrast particles smaller than 0.15mm showed reductions in the heat transfer coefficient between Re = 6,000 and Re = 15,000. Temperature profiles were taken vertically and horizontally across the flow. These showed that while being symmetric in the horizontal direction, at all Reynolds numbers, they became increasing asymmetric vertically as Reynolds numbers decreased. At Re=7500 and Re=4500 it was observed that the temperature profiles were almost linear, which suggested that the particles had settled and formed a stationary bed, heat transfer through this part being by conduction alone. A correlation for h was developed for this case, and for simplicity, it was assumed that all heat transfer was by conduction alone (ie the remaining suspension moved as a plug and no fluid moved in the bed). The use of the effective thermal conductivity of Kunii et al (Equation 2.60) for each part of the system gave a result that correlated the data to ±20%.

Harada and co-workers published an extension to their work looking at the heat transfer of suspensions in rectangular ducts (Harada et al, 1989). In this study only suspensions consisting of glass beads of 0.35mm, 0.5mm and 1.0mm were investigated. It is not surprising that such a limited range of sizes were investigated, when it is noted that three modes of operation existed (top plate heated, bottom plate heated and both plates

heated). Heat transfer data was compared with the Sieder-Tate correlation again, and as with a circular duct, the coefficients were found to be 20% to 30% higher than with water alone. (In the calculations the Reynolds number used the equivalent diameter for rectangular ducts $D_e = 2H$ when single-plate heating applied, and $D_e = 4H$ when both plates were heated.) Similar to circular ducts, the correlation:-

$$Nu = 0.035Re^{0.8}Pr^{1/3}\left(\frac{\mu_f}{\mu_w}\right)^{-0.14} \tag{2.67}$$

can be used for $\Phi_s \leqq 0.05$ and $0.0058 \leqq d/D \leqq 0.017$ (Harada et al, 1989).

Again at low Reynolds numbers it was found that the vertical temperature profile was asymmetric and a two layer model was developed. This employed a correlation giving the thickness of the stationary bed based upon the system Reynolds number, and unlike the correlation for tubes, the flowing part was considered to be turbulent with heat transfer coefficient of that in Equation 2.67.

The previous works have all used particles with high settling velocities, making the detailed study of the enhancement to the heat transfer coefficient difficult at low flow rates. The work of Liu (1990) used mixtures of water and particles of partially cross-linked high-density polyethylene, X-HDPE. This was used for two reasons (i) it remains form-stable after a phase transition at 137°C with a high latent heat of 168kJ·kg^{-1}, and (ii) it is has a specific gravity of 0.96 giving it near neutral buoyancy. Under turbulent flow conditions, even at low flow rates, the solids distribution across the flow can be considered symmetrical.

The particle sizes used were 3.2mm and 1.3mm with solids concentrations from 0% to 45% volume. Flow rates ranged form 21.2 lt·s^{-1}- to 134.4 lt·s^{-1}, giving Reynolds numbers ranging from 28,000 to 200,000. Only one diameter (23.98mm) of tube was used, length 6m. All heat transfer tests were for heating of the fluid, heat provided by a electrical heater along the test sections length. The heater had voltage taps to provide power measurements for five equal sections. The results from these tests gave a number of interesting results.

The first was that for a particular particle size, volumetric concentration and flow rate reductions in the pressure drop could be achieved. For example, for all concentrations less than 30%, and at a flow rate of 65.6 kg/min, reductions in the pressure drop of a few percent was measured relative to water alone. With particle sizes of 3.2mm, reductions were only present below 5% loadings. In general larger particles always gave higher pressure drops. Dramatic reductions in pressure drop were measured if small quantities of Separan (slip additive) were added. At a flow rate of 65.5 kg/min with 65 wppm Separan, for example the reduction in pressure drop was observed be 73% less than that for water alone, 70% for 15% volumetric particle concentration (1.3mm) and reaching that of water only at particle concentrations above 40%.

The effect of particles on heat transfer coefficients was reported in terms of the Stanton number:-

$$St = \frac{Nu}{RePr} = \frac{h}{\rho C_p V} \tag{2.68}$$

For particles size of 3.2mm increases to the Stanton number were observed at all loadings up to ~35% for flow rates between 32kg/min and 86.4kg/min. The increase rose with particle concentrations, and for the same concentration, rose with flow rate. For 30% solids the gain in the Stanton number was 6% for a flow of 32 kg/min and rose to 12% for 86.4 kg/min. The 1.3 mm particle on the other hand, showed that above volumetric concentrations of 10% a decrease in the Stanton number occurred reaching a maximum of -15% (20% solids concentration, mass flow rate 63.6 kg/min).

The work of Lui (1990) attempted no correlations, although their results for water alone were compared to standard predicted values yielding errors of only ±0.1% for the pressure drop measurements, and 0.7% for the heat transfer coefficients. No phase transition took place within the X-HDPE; this work was reported to be in progress although no work has yet appeared in the published literature.

2.5.1 Convective Heat Transfer to Slurries with Phase Change Particles

In the literature, interest in the possible use of phase change slurries for thermal energy transmission and storage seems to have started in the early 1980's. An investigation carried out for the U.S. Department of Energy by Kasza (Kasza, 1982; Kasza, 1985), reported that the use of phase change slurries could improve thermal systems performances due to a number of factors. The first of these was the enhancement of the surface-to-fluid heat transfer coefficient, reducing the required heat exchange sizes and temperature difference between the fluid and the heat transfer surface. The mechanisms behind this were particle-boundary layer interactions, increased thermal conductivity and increased thermal capacity. The increase in thermal capacity could also have benefited the system by reducing the pumping energy and required pipe sizes, reducing initial cost, and thermal losses. By requiring lower temperature differences between the source and end use reduces the loss in energy quality. Finally such systems could incorporate high density (solids concentration) stores.

Despite the gains in thermal system performance suggested by Kasza (1982) little work has been published since. This is probably a reflection of the complexity, due to the number of parameters involved, of characterising heat transfer in slurries. Furthermore few suitable particle-fluid systems have been available for commercial applications. Of the works that have been published, only two (Goel, 1994; Choi 1884) have presented experimental data for the convective heat transfer properties of slurries with active phase change particles. The first of these is the work of Goel (1994). This paper presents the enhancement to heat transfer coefficients for laminar flow conditions. The particles used were *micocapsules* containing *n*-eicosane ($C_{20}H_{42}$), a phase change

material with a transition temperature of 42.5°C and a heat of transition of 240.4 kJ/kg (Roy, 1991). The support fluids used were water and an 80% aqueous ethanol solution. The second being chosen because of its similarity in density with that of the particles. This gave a final mixture that was neutrally buoyant, hence the rate of phase separation was be minimal. Two particle sizes were used, 100μm and 250μm, at solids concentrations of 5%, 10%, 15% and 20%.

The findings of Goel (1994) were all based upon the behaviour of the axial wall temperature of the heat transfer test section (all tests done in the heating mode). In all cases the rise in wall temperature, along the test sections length, was found to be reduced by the addition of phase change particles. The comparison for this was based upon a single phase fluid, with properties the same as the suspension Equation 2.53 for the density, 2.54 for the sensible heat, 2.58 for the thermal conductivity, and 2.57 for the viscosity. This indicated that the local heat transfer conditions were being enhanced along its length. The degree of enhancement was found to be fairly independent of solids concentration above 10%. Above these concentrations a reduction in wall temperature rise of ~50% was found along the whole length of the heat transfer test sections.

It must be stated that the solids concentrations of 15% and 20% were made for mixtures of 100μm and 250 μm particles, whereas the 5% and 10% test were for particles of only 100μm. This would clearly have an effect on the viscosity of the mixture due to the scaling effect of ϕ_{max}, which increases as the particle size distribution increases.

The work did find that the *bulk Stephan number* (Ste_m), defined as the ratio of sensible heat capacity to the latent heat capacity (Equation 2.68), was a critical factor.

$$Ste_m = \frac{C_{p_m}\left(\frac{q_w D}{k_m}\right)}{\phi L\left(\frac{\rho_s}{\rho_m}\right)} \tag{2.68}$$

As Ste_m increased, the rise in wall temperature decreased. Experimental data was compared to those predicted by Charunyakron (1991) and found to follow similar trends, but the enhancement was found to be lower. The reasons for this were postulated to be (i) the model assumed phase change to occur as soon as the suspension entered the test section, (ii) that phase change occurred at exactly one temperature in the model, (iii) that the particles were totally homogeneous (the particles in the test consisted of 30% by mass of $C_{20}H_{42}$), and (iv) no particle-particle interactions occurred. Such conditions would naturally be hard to totally reproduce experimentally, although Goel made modifications to his results to account for the entrance effects by considering a length of the test section for which the temperature was suitable for phase change. This only brought the model and experimental results to within 45% although the trends in the compared data were much closer.

Limited tests were performed to investigate the effects of the particle diameter, it was

found that for both concentrations tested (5% and 10%) larger (250μm) particles caused a reduction in wall temperature rise by 15%. Goel was unclear as to the origin of this effect, although believed it resulted from a phase separation effect due to the differential in densities between the particles, and the fluid. This was greatest with larger particles and the layer formed at the heat transfer surface would have been consequently larger.

Both the works of Goel and Charunyakron (1991), and a later paper by Zhang (1995), applied Equation 2.58 for the effective thermal conductivity. Zhang (1995) also made modifications to account for the encapsulating material of the particles. By applying such modifications Zhang was able to model the reduced rise in wall temperature measured by Goel (1994) to within 34%, compared to the previous models giving results within 45%. Further to this, Zhang reported that a broadening of the phase transition temperature would bring the experimental and modelled result even closer. This was not done in this paper due to a lack of data on the width of phase transition temperature of the particles used by Goel (1994).

The second work investigating convective heat transfer across the phase transition temperature was that of Choi (1994). The flow conditions were turbulent and again the slurry was heated from a temperature below that of transition to one above. The actual slurry consisted of particles of hexadecane supported in water (with an added emulsifier). To make the particles, liquid hexadecane was added to the water and emulsifier mixture, and stirred in a collection tank to below the transition temperature (16.5°C). The size of the particles was apparently controlled only by the concentration of the emulsifier, and for this work was always <0.1mm. The solids concentration was simply controlled by the volume of water and hexadecane used although only tests for ϕ=0.1 were reported. (The test section had a diameter of ~1cm giving d/D>100.) The mixture was maintained at 7°C in a stirred tank before being pumped through the heat transfer test section. Here electrical heaters were used to apply a constant heat flux for a number of regions along the length. Measurements of the mid-stream temperature and differential pressure drops were made along lengths of the test section.

The results of the work showed that three regions existed in the heat transfer test section, distinguished clearly by both the fluid temperature and the readings form the pressure transducers. The first region showed a fairly linear rise in temperature with axial distance from the inlet. Corresponding to this was a constant differential pressure drop. The second region showed a virtually constant temperature with a steady decrease in the pressure drop. Finally, the third region was the same as the first, a linear rise in temperature and a steady differential pressure drop.

The mechanisms underlying this were postulated to be that (i) in the first region the phase change occurred only in the laminar sub layer, (ii) when phase change started to extend into the turbulent zone, the rapid mixing forced a constant temperature in the bulk fluid of region 2, (iii) on completion of phase change across the diameter of the tube, a rise in temperature was again observed due to normal turbulent heat transfer mechanisms.

The behaviour of the pressure drop could also be explained by this mechanism. In the first region little change occurred in the majority of the fluid, hence no changes in the differential pressure drops were observed. In the third region the situation was similar although the phase change particles were now fluid, giving a lower pressure drop. The intermediate region, showing a pressure drop decrease, was associated with a transition between the fluid containing solid particles to containing fluid particles.

The mechanism was supported by the fact that at a higher wall heat flux the transition from region 1 to 2 occurred within a shorter distance from the inlet, also the duration of region 2 along the length was much shorter. Heat transfer coefficients based on the bulk temperature and the constant wall heat flux were developed. These showed that h rose from the start of region 1 to a maximum at its end. Region 2 then showed a steady decrease throughout its duration, reaching a minimum (for the whole length) at its end. Finally region 3 showed a very slight increase at distance increase. The peak of the increase at the end of region 1 was found to be lower for higher wall heat fluxes.

2.6 Discussion

It is evident from the limited number of published works on the heat transfer properties of slurries, that little is known about the effects of solids particles on the heat transfer coefficient. This is particularly evident of particles that have a phase change (with an associated latent heat capacity). With particles larger than 0.1mm no experimental results exist for phase change conditions. The work of Lui (1990) showed that with large particles (>1mm) the gains in the heat transfer coefficient are high, even at concentrations of around 5%. The true mechanisms of this gain are not understood, although Kasza (1982) suggested that disruption to the laminar sub-layer may take place due to particle collisions. This would effectively reduce the thickness of the sub-layer and increase the thermal gradient across that remaining.

The conditions under which this might occur are not clear, although they will qualitatively depend on the mean size of turbulent particle to the true particle in the system. If the mean size of fluid particles moving during turbulent flow is large, compared to the solid particle, then the solid will effectively move with the fluid lump. Under these conditions the energy transfer, both thermally and kineticly, will be a function of the relative densities and thermal capacities. If the thermal mass of the solid is high compared to that of the fluid, then turbulent mixing will increase the rate of heat transport across the fluid flow (c.f Section 2.2.5). A counteracting factor is the relative densities of the combined fluid-solid particle. If the particle density is higher, then momentum transfer will increase, hence an increase in the *Eddy Viscosity*, although the onset of turbulence will be extended to higher flow rates (c.f. Equation 2.4). Under such conditions the mixture will behave in a homogeneous manner.

When the movement of the solid particles is independent of the fluid particles (large particle, or high densities) impact with the laminar sub-layer is more likely as particles are *thrown* about. Under such conditions there will always be an increase in heat

transfer. Such conditions will result in higher energy dissipation, due to the increase in the size of the turbulent zone. These conditions will only be stable at high flow rates due to the degree of turbulence required. Some analysis of particle behaviour in vortices has been undertaken (Hetsroni, 1994), although this looked only at concentrations up to 0.006 for sizes of 0.92mm. The results were for $5100 < Re < 10150$ and it was shown that for each Re there existed a solids concentration for which heat enhancement was maximum. Furthermore the size of this enhancement increased with Re.

The effects of the latent heat in the boundary layer are also unclear, but it is evident form the work of Choi (1994) that the gains to the heat transfer coefficient are beneficial. It would seem that to gain a higher increase, the duration for which phase change in the sub-layer occurs should be maximised. This will be achieved at higher solids concentrations. Furthermore if the thermal conductivity is enhanced by particle rotation then a higher solids concentration is desirable.

Chapter 3

Hydrophilic Materials

3.1 Introduction

The purpose of this chapter is to introduce hydrophilic materials and explain why their physical behaviour has been of interest to this project. It starts with a brief introduction to the materials, then presents the results of a number of tests undertaken to determine the thermo-physical behaviour hydrated samples (ie phase transition temperatures and thermal conductivity).

Hydrophilic materials are a set of materials that absorb and retain water (Highgate, 1989). There are many such materials that behave in this way, some are natural, such as the starches, while others are man-made polymers that have found several applications in the biomedical industries. The ability of hydrophilic materials to absorb and retain a high mass of water provides a mechanism by which the high latent heat of fusion of water can be exploited for thermal energy storage and transmission systems. The hydrophilic materials of interest to this project are defined as crosslinked polymer networks that absorb a significant quantity of water (36% to 98% of the final mass of hydrated sample) without dissolving; hence it is limited to looking at man made co-polymers.

The technologies by which thermal energy storage and transmission systems can be achieved forms the core of later chapters in this work. The literature showed a very limited understanding of the thermal properties of hydrated hydrophilic materials. As such there was insufficient data to apply in the design of the thermal energy systems of interest. The work detailed in this chapter sought to address this lack of suitable data.

3.2 Phase Transition Behaviour

In earlier works looking at the thermal properties of hydrophilic polymers (Highgate, 1989) it had been observed that the expected phase change transition behaviour of the hydrated materials was not as expected from consideration of the constituent parts (ie water and polymer). During initial freezing it was apparent that some form of phase transition suppression was occurring. It was also found that after a number of freeze-thaw cycles the suppression was reduced. The number of cycles required to achieve this was shown to be dependent on the type of hydrophilic material used, and the quantity of water that it absorbed. Relatively high water uptake materials (78% water) achieved the improved freeze-thaw behaviour with 10 to 15 thermal cycles, while the lower water content materials (36% and 38% water) showed no observable phase transition

behaviour even after 20 cycles.

One model accounting for this behaviour is related to how water exists within the polymer matrix (Highgate, 1989). It is widely accepted that the water absorbed by a hydrophilic material can be considered as either *bound*, or *free* water. The bound water is effectively fixed to the polar sites on the polymer matrix, while the free water resides in the pores (or spaces) within the polymer matrix. Initially the bound water may perturb the freezing process of the free water. Subsequent rearrangement of both the bound and free water, as thermal cycling progresses, may allow more free water to freeze at 0°C. An alternative model is that the polymer matrix mechanically prevents freezing from occurring at 0°C. Microscopic degradation of the material after thermal cycling may increase the pore size thus allowing more water to freeze.

The work described in this section had three main goals (a) to extend the understanding of freezing suppression, (b) to observe the effects of hydration fluids other than water and (c) to investigate the synthesis behaviour of very high water uptake materials (90%-95%).

3.2.1 Experimental Method

To examine the phase transition temperatures of hydrated hydrophilic materials samples of suitable materials were prepared. In their dry state the materials were cylinders with 13 mm diameter and 5mm long (21mm diameter and 8mm long hydrated). The dry mass and dimensions of each sample was recorded before placing pairs of samples in their selected hydration fluid. Hydration was allowed to occur until full saturation had been reached, which was assessed by recording the mass at regular intervals until no further change was observed. The sample pairs were next arranged end to end, with a thermocouple trapped between them, forming a composite cylinder (21mm diameter, 16mm long). To prevent loss of water from the samples during repeated freezing and thawing, each composite was sealed within an impervious membrane. The free end of each thermocouple was connected to the temperature recording device. To prevent the conduction of heat to, and from, the sealed composites, each was suspended from a wire frame by a thread. The sealed samples were now repeatedly thermally cycled by placing them alternately in environments of different temperatures (20°C and -30°C), while temperatures were logged. The apparatus is shown in Figure 3.1.

The raw data collected from thermally cycling these samples gave a good indication of how the phase transition of the hydration fluid within the sample was behaving, and showed how the phase change properties of the materials changed with the number of thermal cycles. Detailed analysis was not possible because of the change in heating or cooling flux that occurred and a means of compensating for this had to be found. There were two possible methods of rectifying this problem. The first was to use a differential scanning calorimeter, and the second was to transform the collected data based on a thermal analysis of the test. Although a differential calorimeter was the preferred device, no such equipment was available for use in this project so the second method

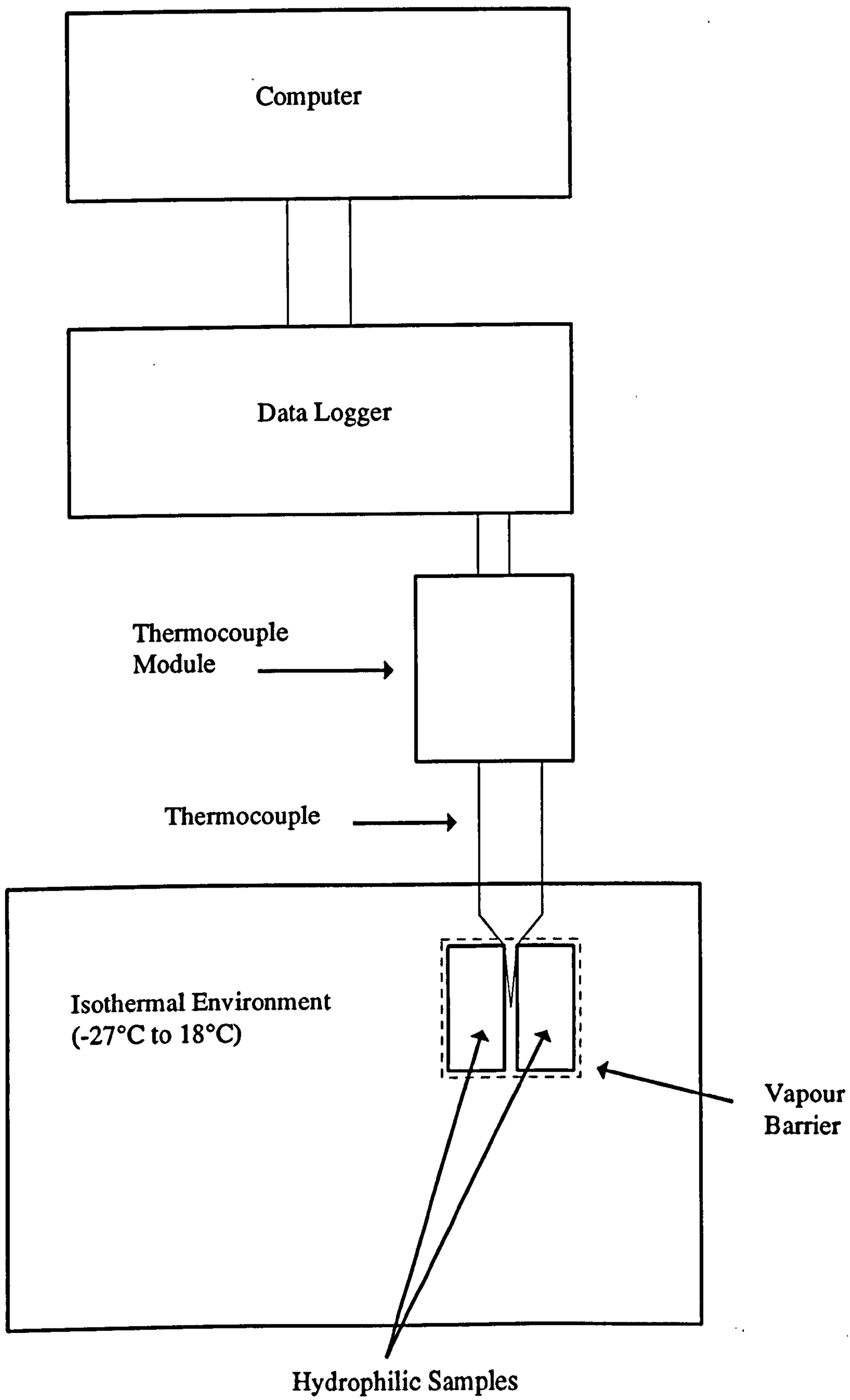

Figure 3.1: Schematic Layout of Phase Transition Test Apparatus.

of transforming the collected data was used.

This method extended the usefulness of the data collected by remodelling the time base of the logged data to give a term that related to the energy passing to or from the system (sample pairs). This in turn allowed a quantitative analysis of how the sensible heat capacities and latent heats developed during an individual thermal cycle, and with the number of thermal cycles. The rate of energy gain/loss was assumed to be a linear function of the temperature difference between that of the sample and the surroundings. Several assumptions or simplifications were made to do this, these are listed below.

i) The combined convective and radiative heat flux was assumed to be a linear function of the differential temperature between the sample and the surroundings. These processes are governed by the geometry of the sample, its surface temperature, physical properties, and the temperature and physical properties of the air (Section 3.2.1.1).

ii) The calculation of the mean convective heat transfer coefficient was based on the correlation for a spherical object because the cylindrical composites' length and diameter were similar (as opposed to an infinite rod).

iii) The emissivity of the sample (whether water or ice) was taken as $\varepsilon = 1$ (for ice at 273K, $\varepsilon = 0.95$-0.98; for water at 300°K, $\varepsilon = 0.96$ (Incropera, 1990)).

iv) The heat flux correlations were for the surface temperature of the sample. The temperature data was for the centre of the sample, so the analysis assumed that the sample was isothermal. This was not a bad approximation for the materials in their frozen state, where maximum temperatures of ~1°C could develop between the surface and the centre of the sample. In their unfrozen state this temperature differential could reach ~4°C (This was worse during cooling because of high rates heat transfer). The centre to surface temperature difference is believed to account for the failure of the method to determine the sensible heat capacities successfully (Section 3.2.1.1).

v) Finally, for the convective component it was assumed that each sample was surrounded by an infinite volume of air at a uniform temperature. The size of the freezer cabinet was 100 times the characterising length of the hydrated sample pair (diameter ≃21mm, length ≃16mm), and each sample was 10 diameters from another.

3.2.1.1 Heat Transfer Mechanisms

The combination of the heat transfer mechanisms can be satisfactorily represented by a single linear function of differential temperature between the system and its surroundings (the validity of this is shown below). The radiative component will be discussed first.

In the absence of any medium (solid, liquid or gas) heat transfer will take place via radiation alone. The rate at which heat is transferred is a function of the surface properties of the bodies involved and their absolute temperatures. If the surrounding surface of a sample are perfectly black ($\varepsilon = 1$) and the surface properties of the sample are uniform, then the heat flux is given by the *Stephan-Boltzmann law*:

$$q_{rad} = \varepsilon\sigma(T^4_{sample} - T^4_{surroundings}) \tag{3.1}$$

where $\sigma = 5.67 \times 10^{-8}$ $W{\cdot}m^{-2}{\cdot}K^{-4}$ (the Stephan-Boltzman constant). For the purpose of analysing the phase change data it was assumed that all surfaces were perfectly black, that is $\varepsilon=\alpha=1$.

Although the samples for analysis were cylindrical, their dimensions were such that a correlation for free convection over a sphere was deemed more appropriate than correlation available for cylindrical geometries (these typically are limited to large ratios of length to diameter). The correlation used was (Churchill, 1983):

$$\bar{Nu}_D = 2 + \frac{0.589Ra_D^{1/4}}{[1 + (0.469/Pr)^{9/16}]^{4/9}} \tag{3.2}$$

where $Pr \geq 0.7$ and $Ra_D \lesssim 10^{11}$.

To compute the combined effect of the radiative and convective heat transfer two cases were considered; firstly for a sample cooling from 20°C in an environment of -30°C, and secondly heating a sample at -30°C in an environment at 20°C. The data used for the fluid properties of air was taken from Kay (1986). The combination of the two heat fluxes is shown in Figure 3.2, and with it are two lines that represent the linear regressions of the data. The linear function (of gradient m) is of the simple form:

$$q_{total} = mA\Delta T \tag{3.3}$$

where ΔT is the temperature difference between the sample and the environment and A is the surface area. For cooling of the sample $m = 9.34(\pm 0.02)W{\cdot}m^{-2}{\cdot}K^{-1}$, and for heating $m = 8.79(\pm 0.03)W{\cdot}m^{-2}{\cdot}K^{-1}$. It can be clearly seen that the linear functions represent the calculated heat flux well.

The application of these functions to the collected data consisted of first finding the mean temperature difference of the sample with that of the surroundings, and then calculating the associated heat flux. Next, the time interval between the data sets was used to calculate the heat transfer to the sample. Finally the data was normalised to give thermal data in terms of the unit mass of the sample. As a test of the validity of modifying the data a sample of water contained in a vessel of appropriate dimensions was thermally cycled, and the relevant temperatures recorded.

The data are shown below in Figure 3.3. There are three regions of interest, the first is

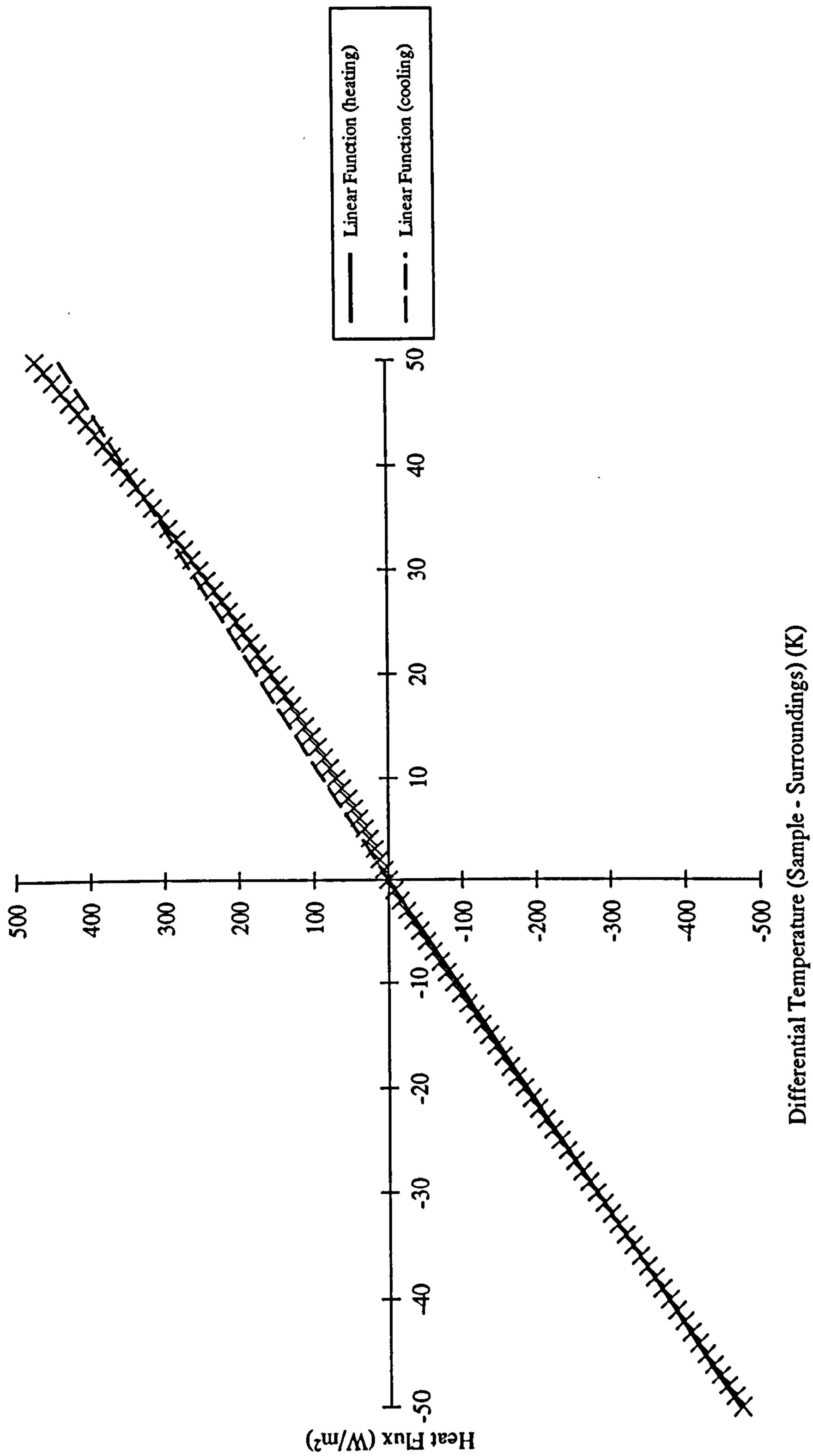

Figure 3.2: Comparison of Predicted Heat Flux with Linear Function.

the cooling of the water from 20°C to 0°C, the second the phase transition of water at 0°C, and the third the cooling of ice from 0°C to -30°C. The first region shows relatively good agreement with the predicted energy change yielding a C_p value of $4.8 kJ \cdot kg^{-1} \cdot K^{-1}$ (c.f. $C_p = 4.2 kJ \cdot kg^{-1} \cdot K^{-1}$). Similarly the known value of the heat of fusion for water is $333 kJ \cdot kg^{-1}$ (Kay, 1986 - Table 2.10.5), compared with the mean value of $300\text{-}360 kJ \cdot kg^{-1}$. However, when considering the C_p of ice, there is a major discrepancy between quoted values of $2.04 kJ \cdot kg^{-1} \cdot K^{-1}$ and those from the test of $3.5 kJ \cdot kg^{-1} \cdot K^{-1}$ up to $6.5 kJ \cdot kg^{-1} \cdot K^{-1}$.

There were several reasons for the error of the analysed data, one was the lack of distinction of where phase transition ended and sensible cooling started (Figure 3.3). This could cause the estimate of energy change in the temperature range 0°C to -30°C to be to high. To compensate for this the energy change between -10°C and -20° was used, this gave a result in favour $3.5 kJ \cdot kg^{-1} \cdot K^{-1}$ but still 75% larger than the literature data for pure ice. Another cause of this error was that the temperature differential was smaller during the sensible cooling region below 0°C. A small differential temperature would result in the calculated data being more sensitive to errors in the thermocouple signals.

Similarly Figure 3.4 shows the results for thawing the water sample. The discrepancies between the predicted thermal data and that measured are quite high during both of the sensible heat regions, although the agreement between latent heat values is acceptable. In all the freezing and thawing tests of water the latent heat values derived from this method have been within ±15% of expected values. This part of the project was primarily concerned with the phase transition behaviour of hydrophilic materials hence this method was considered acceptable. However for the rest of this section, the scale for the modified data will only be used as a comparison between very similar samples, or different tests on the same sample.

3.2.2 The Effects of Ageing

The thermally cycled samples used by Kay (1990) were made available to this project to investigate the long term stability (~3 years) of the 'normal' phase change behaviour achieved after repeated thermal cycling. For comparison purposes, a fresh set of samples were prepared from the same sources of blanks used by Kay (1990). The pre-cycled samples were still hydrated although some algae growth was present. To remove this the hydration water was flushed several times, as was the water of the new samples.

The main observation was that the original samples showed no further change during the 20 thermal cycles applied in these tests (Figure 3.5).

Furthermore comparison of the 15th thermal cycle of both the new and old samples shows that the phase transition behaviour of both is very similar (Figure 3.6). As with Figure 3.5, the small deviations between the curves shown in Figure 3.6 exist due to the errors of the thermocouples, and as a result of the slightly different conditions of each

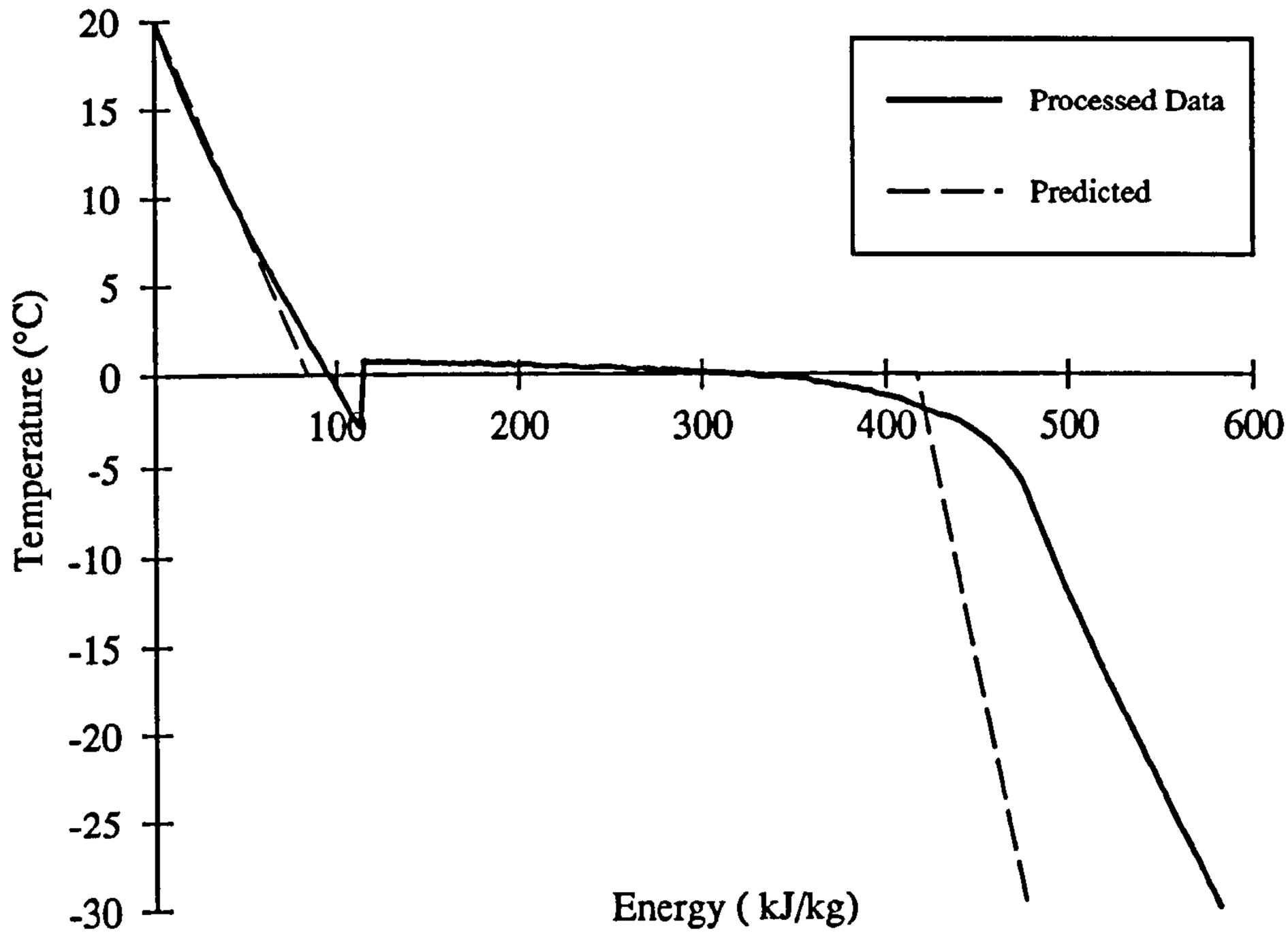

Figure 3.3: Energy Curve for Phase Transition of Water - Freezing.

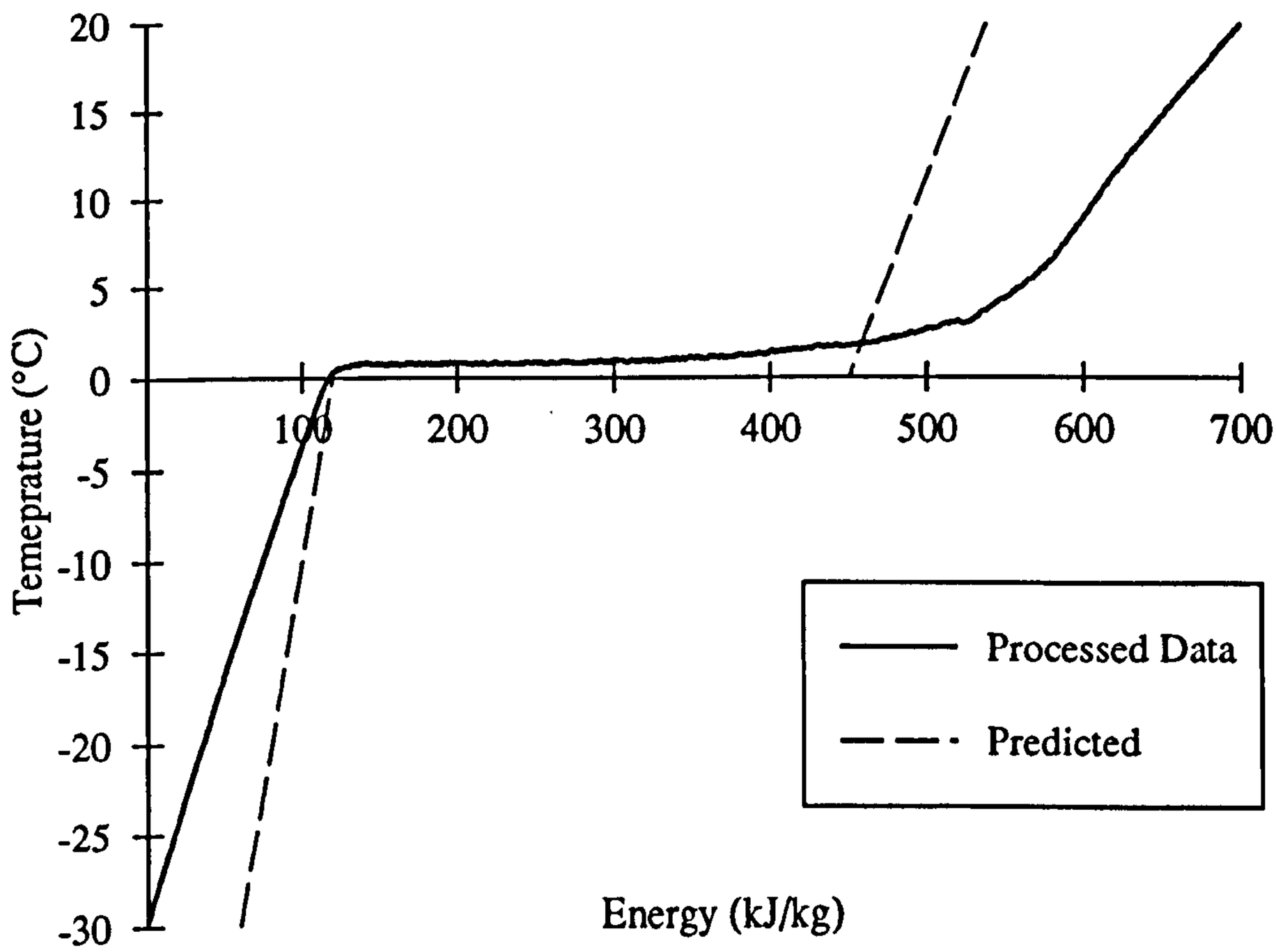

Figure 3.4: Energy Curve for Phase Transition of Water - Thawing.

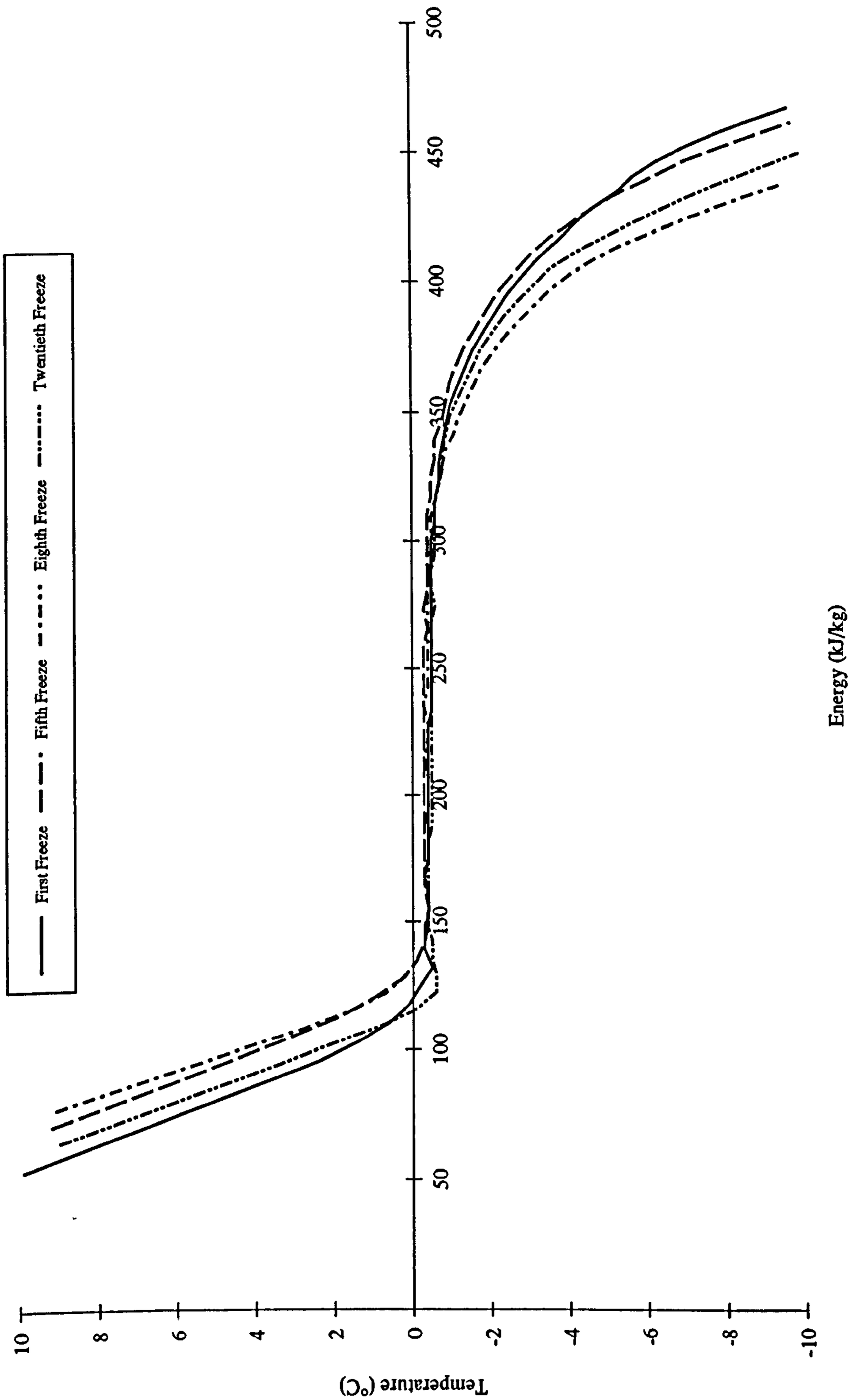

Figure 3.5: Example Energy Curves for the Freezing of Old (3 Years) Pre-Cycled Hydrophilic Samples.

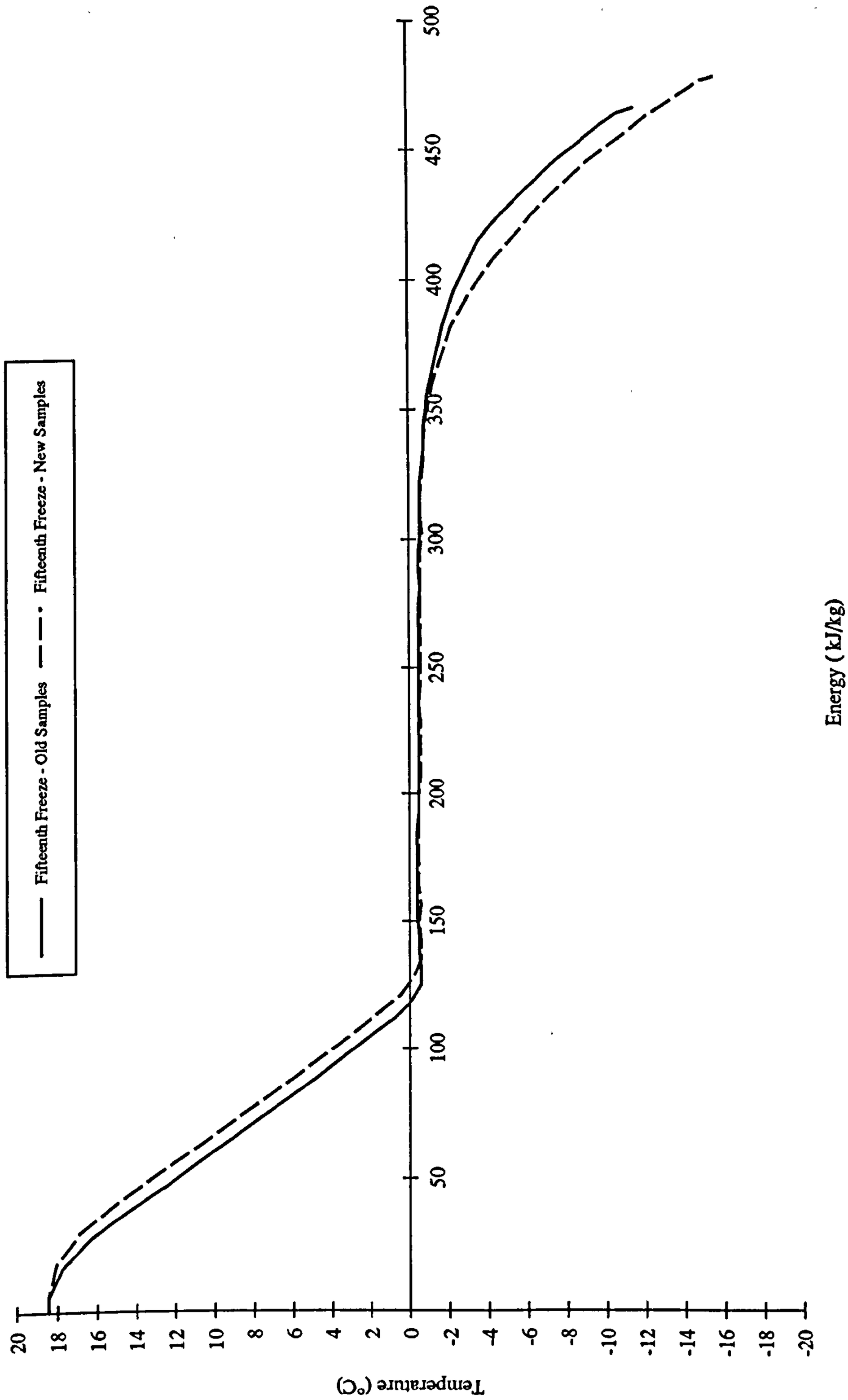

Figure 3.6: Comparison of Freezing Curves for New and Old (3 years) Hydrophilic Samples.

test (air temperatures ranged from -24°C to -27°C). From this it is possible to conclude that no significant change has occurred in the hydrophilic samples over time. Hence, from this point of view, they are stable engineering materials.

3.2.3 Alternative Hydration Fluids

The possibility of hydrating the hydrophilic materials in alternative fluids, other than water, was investigated experimentally. The object of this was to identify the potential for modifying the phase transition temperature, which would serve to extend the range of applications for hydrophilic based thermal storage and transmission systems. Phase transition fluids, suitable for application with hydrophilic materials, are limited to aqueous solutions. Two were studied in this investigation, sodium chloride (NaCl) and calcium chloride ($CaCl_2$), as they are low cost salts which are available commercially in large quantities. Their general effect upon the phase transition temperature of water is to (a) reduce the temperatures at which phase transition occurs (Table 3.1) and (b) extend the temperature range over which transition occurs. Similar effects were expected from solutions absorbed into the hydrophilic materials.

The dry hydrophilic samples chosen for this test were 75% materials as used in Section 3.2. Four solutions of each salt were made at a variety of concentrations, and the temperature at which phase transition started in each of the solutions was measured before they were used to hydrated the samples. The results (Table 3.1) showed good agreement with the published data (Carrier, 1965; ASHRAE, 1985). Three dry hydrophilic blanks were placed in each solution and hydration was allowed to occur over several days until no further mass change was observed. Pairs of the hydrated blanks from each solution were assembled with thermocouples, as described in Section 3.2, and thermally cycled.

The third sample, from each set, was used as a means of checking the concentration at which the hydration fluid was absorbed. The method used was to first evaluate the equilibrium mass of solution absorbed. The samples were then allowed to dry in air over several days, leaving the original hydrophilic and the salt. The final mass was measured and the concentration of the absorbed solution evaluated. The results, together with the thermal data of the free solutions, are shown in Table 3.1. Great care had to be taken in weighing the dried sample in order to avoid losing the fine crystals of salt that formed on its surface.

As a control sample in the phase change tests two pairs of hydrophilic blanks were hydrated in tap water. One pair was used with the sample hydrated in calcium chloride solution, the other pair with the samples hydrated in sodium chloride solution. The trends in the results for both sets of solutions were similar to each other. The initial freeze of all samples showed a suppression in the temperature at which phase change started, compared to the free hydration fluid. For example, the sample hydrated in 10% $CaCl_2$ solution started phase transition at -17.5°C (Figure 3.8) compared to -4.6°C (measured for the free fluid). As with samples hydrated in water, the start of phase

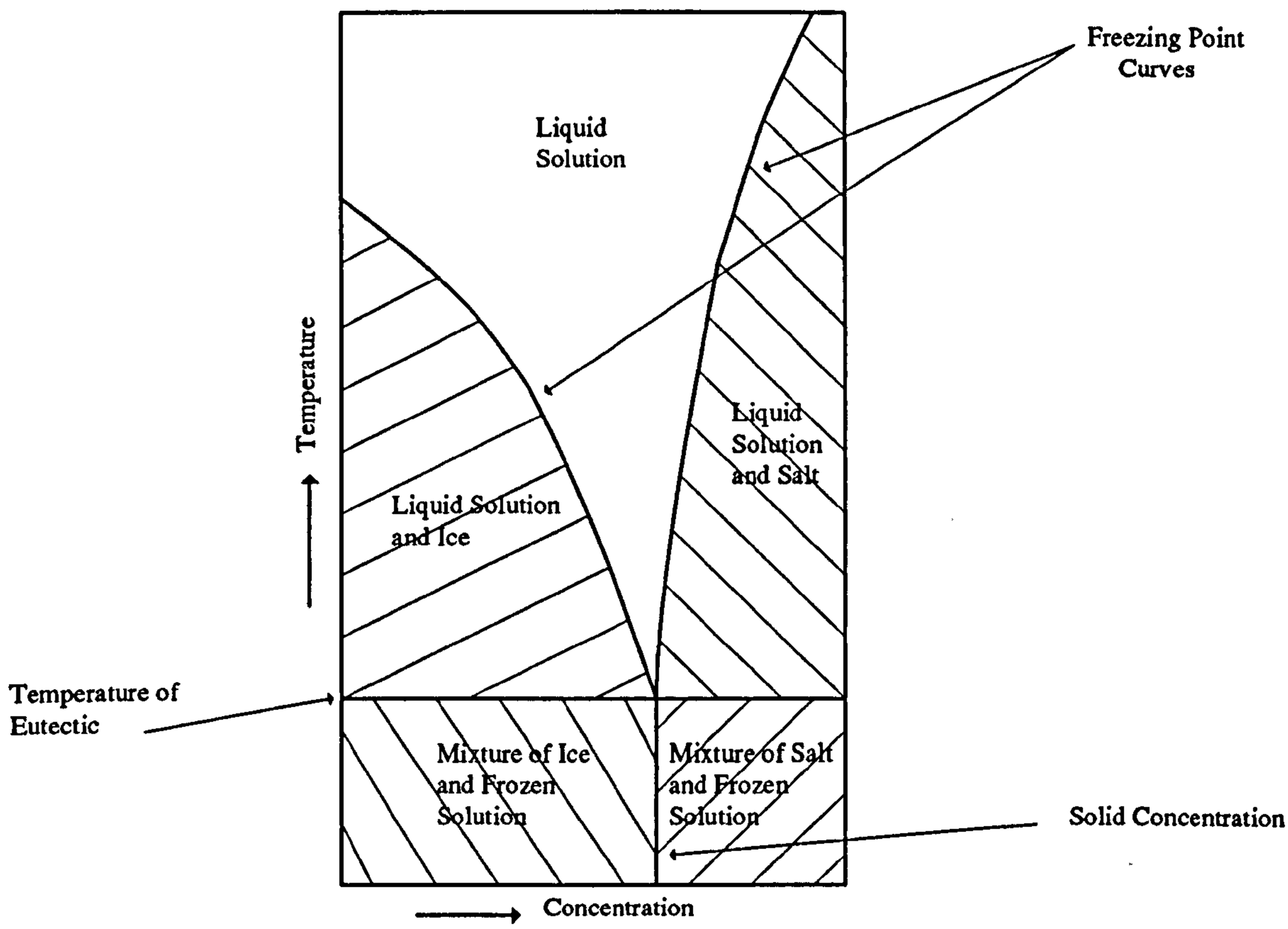

Figure 3.7: Typical Phase Diagram of a Solution.

Table 3.1: Hydration Solution Data.

Solution	Concentration (% by mass)		Start of Phase Transition / °C		Absorbed Concentration
	Nominal	Actual	Published	Measured	(% by mass)
$CaCl_2$	5	4.8	-2.3	-2.4	4.7
$CaCl_2$	10	9.1	-4.8	-4.6	9.1
$CaCl_2$	15	13.1	-8.0	-7.8	13.1
$CaCl_2$	20	16.7	-11.8	-11.7	16.5
NaCl	5	5.2	-3.0	-3.1	5.2
NaCl	10	10.1	-6.7	-6.7	10.0
NaCl	15	15.3	-11.2	-11.3	15.2
NaCl	20	19.9	-16.4	-16.2	19.9

transition moved closer to that of the free fluid as the number of thermal cycles increased, becoming constant after 5 to 10 cycles. An increase in the number of cycles beyond 10 had no further effect on the temperature at which phase transition appeared to start.

A further trend in all of the samples was that the energy transferred between two particular temperatures decreased as concentration of the hydration solution increased, this was most evident in the transition region (Figure 3.9). Also the energy transferred to a particular sample increased with the number of cycles, again clearly evident in the transition region (Figure 3.8).

Analysis of the final transition temperatures (20th freeze) showed that none of the materials hydrated in $CaCl_2$ or NaCl were starting phase transition at the value measured for the free hydration fluid (Figure 3.8, 3.9). All were below the temperatures of the free hydration solutions. The differential between the start of phase transition of the free fluid and the cycled materials was also seen to be greater with higher salt concentration (Table 3.2). On interpretation the results confirm the assumption that in the hydrophilic materials a fraction of the water is weakly bound to polar sites in the material (Highgate, 1989). In the water-only test, this results in a smaller than expected latent heat of fusion because part of the water is unavailable to freeze (Okoroafor, 1997).

A salt solution does not freeze in the same manner as pure water. As the temperature drops, a fraction of pure water will freeze out leaving the remaining solution at a higher concentration (Fukusako, 1990). This process is continuous and accounts for the temperature range over which salt solutions exhibit phase transition. The process of freezing stops at a point where the concentration of the remaining solution reaches a value known the *Solid Concentration of Eutectic* (Carrier, 1965) (Figure 3.7). The solid concentration of eutectic for sodium chloride is 25.2% by mass, and is reached at a temperature of -22.7°C. At this temperature and below, the remaining solution freezes as a solution liberating latent heat. This would result in a second transition point and would be more apparent with solutions of higher initial concentrations.

In the test described here, using salt solutions, the fraction of water bound to polar sites would not be available to freeze. This would effectively increase the concentration of the brine as it undergoes phase transition, which in turn would suppress the temperature at which the phase transition started. Figure 3.10 compares the hydration concentration with that calculated from the measured transition temperature data, for materials hydrated in the solutions. The data indicates that the sample initially hydrated with a 20% solution behaved with a concentration equivalent to ~22%. This is very close to the eutectic concentration and accounts for why only one transition was observed compared to two clear transitions for the sample hydrated in the 15% concentrations of sodium chloride solution.

The tests using sodium chloride and calcium chloride show that salt solutions can be utilised to achieve phase transition temperature in hydrophilic materials other than 0°C.

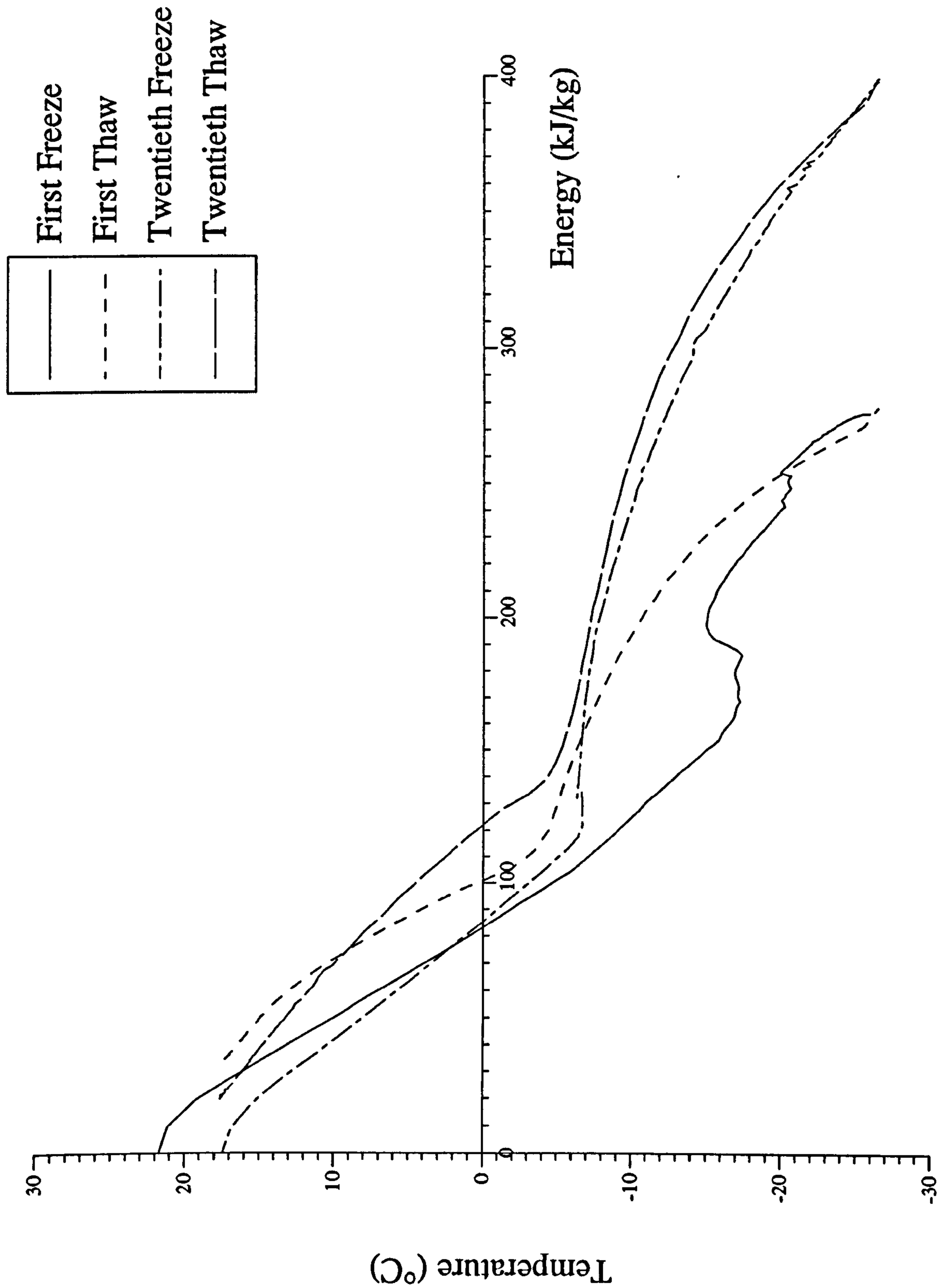

Figure 3.8: Initial and 20th Freeze-Thaw Cycle of Hydrophilic Sample Hydrated in 10% Calcium Chloride Solution.

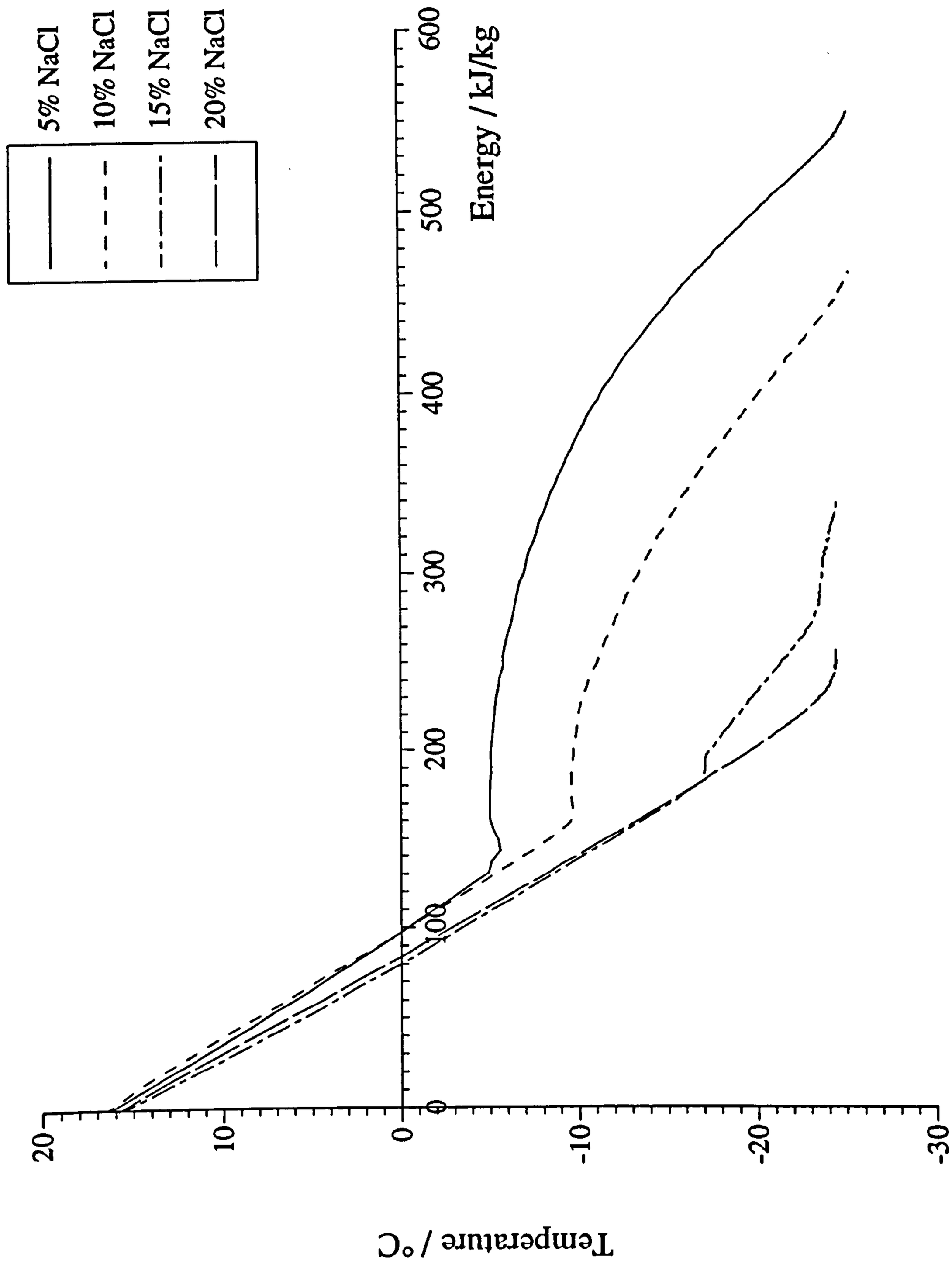

Figure 3.9: Phase Transition Curves for Hydrophilic Blanks Hydrated in NaCl Solutions - 20th Freeze.

Table 3.2: Measured and Apparent Concentrations of Hydration Fluids of Hydrophilic Samples.

Salt	Hydration Concentration	Transition Temperature / °C		Apparent Concentration
		Expected	Measured	
NaCl	5.2	-3.1	-5.3	8.7
NaCl	10.1	-6.7	-9.7	13.5
NaCl	15.3	-11.3	-16.4	20.0
NaCl	19.9	-16.2	-22.7	>25.3
CaCl	4.8	-2.4	-2.9	6.0
CaCl	9.1	-4.6	-6.7	11.7
CaCl	13.1	-7.8	-18.0	15.8
CaCl	16.7	-11.7	-20.9	18.7

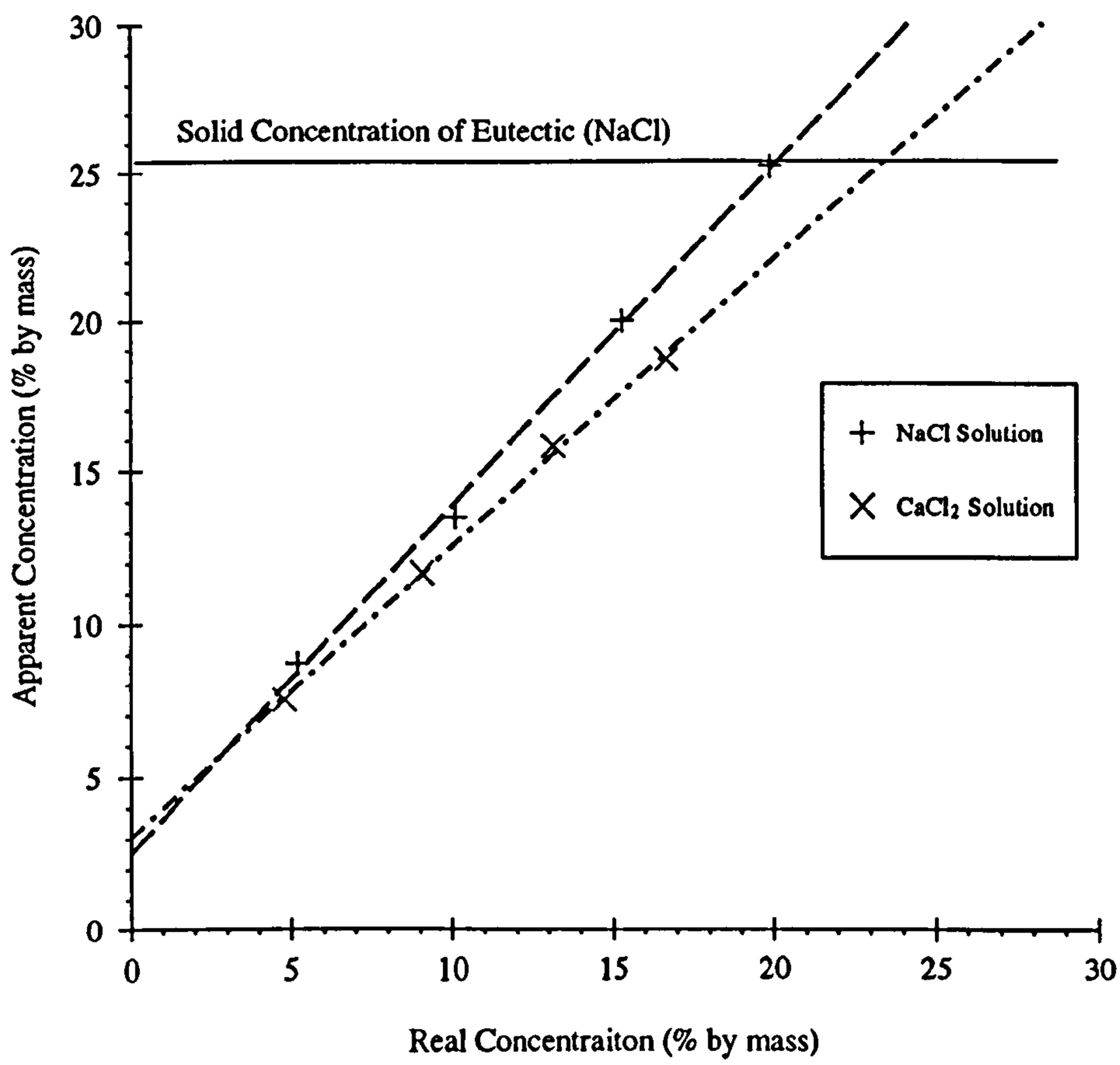

Figure 3.10: Extrapolated Data for NaCl Results.

The apparent increase in the concentration of the hydration solution will have to be accounted for to achieve the desired transitional temperatures of the application.

3.2.4 Novel Hydrophilic Materials

This chapter has looked at conventional crosslinked hydrophilic materials, of high strength and medium water uptake, normally used for biomedical applications, based on vinyl pyrollidone (VP) and methyl methacrylate (MMA). The production of crosslinked hydrophilic co-polymers is often both costly and hazardous. The main production route is (i) the purification (by vacuum distillation) of volatile monomers, (ii) mixing with chosen initiators and crosslinking agents in an inert nitrogen environment, and finally, (iii) thermal processing to polymerise the mixtures into dry polymer blocks or rods. (Such rods have been the basis of the 'blanks' used in this Chapter). To employ the materials for application as phase change slurries, further grinding in a hammer mill was required to achieve the required particle sizes before hydration.

The whole process, because of excessive production time, hazards and expense, makes this method of producing hydrophilic materials inadequate for the possible quantities required for engineering applications. For this reason alternative materials have been investigated for their suitability. These were in the form of pre-extended (pre-hydrated) high-water content materials which have a higher equilibrium water content, but lower mechanical strength, than the conventional medium-water content materials.

The basic process involved in the formation of these materials was the crosslinking of aqueous polymer solutions. This involved the use of γ radiation to crosslink a solution of a low molecular weight polymer forming a pre-hydrated hydrophilic material. This has the advantages of reducing the associated high cost by enabling the use of low cost polymers that are non-toxic and require no additional purification, and eliminating the requirement dry grinding.

For testing the potential for making pre-hydrated hydrophilic materials through radiation polymerisation, an acrylamide monomer (BDH Electran, CH_2:CH.CO.NH, molecular weight 71.08) was used. This was formed into a number of solutions of concentrations ranging from ~5% to 15% by mass of monomer, Table 3.3. Each solution was placed into polythene tubes and dispatched for radiation processing, which was through gamma rays from a Co_{60} source.

The resulting hydrophilic polymers were cut into a number of cylindrical samples (diameter $\simeq$14mm, length $\simeq$10mm) for hydration and thermal cycling tests. All of the samples were immersed in water to fully hydrate them, and all were found to be hydrolytically stable (ie they did not dissolve in excess water). The mass of a representative sample, for each of the initial acrylamide solutions, was taken before allowing it to dehydrate in air until no further change occurred. This gave a measure of the water uptake of each hydrated material and was found to be between 90% and 95%, although no trend was found relating to the initial concentration of the acrylamide

solution. It has since been shown (Leguay, 1994) that the equilibrium water content is independent of the initial concentration of the solution before crosslinking. The variability found here resulted from excess water being present on the hydrated samples when the wet mass was taken, this water resided in small cracks in the samples and could not be removed without damaging the sample.

Table 3.3: Details of Solutions Used to Form Pre-Expanded Hydrophilic Polymers Through Radiation Polymerisation.

Nominal Conc. / %	5.0	7.5	10.0	12.5	15.0
Mass of Water / g	203.8	207.7	209.5	202.3	204.3
Mass of Acrylamide / g	10.3	15.8	21.1	25.4	30.6
True Conc. (% mass)	4.8	7.1	9.1	11.2	13.0

The phase transition tests showed several key features that differed from previously tested materials. The first of these was the complete absence of any phase suppression when comparing the initial freezing cycles with subsequent ones (Figure 3.11). This may result from (a) the higher water content, (b) the nature of the crosslinking mechanisms in the high water content materials, or (c) the different ionic bonding process operating in these gels, compared to those based on MMA-VP mixtures.

The results, over a number of cycles, indicated that the latent energy change decreased slightly (5 to10%) between the first and forth cycle, remaining stable in subsequent tests (20 cycles) (Figure 3.12). The lower latent energy content is possibly due to a loss of a small amount of water as the thermal cycles progressed. This was observed to collect at the base of the material after thawing although appeared to be partially absorbed before the next freeze cycle was performed. No detailed analysis has been made of this phenomena, although it is considered that the high water content materials used here may have to be applied in a partially dehydrated state in application to thermal energy storage and transmission systems, to avoid the excess water forming ice bridges between particles. The occurrence of ice bridges has caused agglomerations of particles to form (Chapter 4, Chapter 6), which in turn have caused the failure of some of the cold storage devices under certain circumstances (Chapter 4).

Within the errors of the methods used here, it was also observed that all of the absorbed water was available to take part in the phase transition process, Figure 3.11. After many freeze-thaw cycles (20) the materials were examined and it was found that some degradation had taken place in the form of an increase in the number of cracks in the material, although unlike lower water content materials the samples had not become opaque. This suggested that the change in optical properties in lower water content materials was directly linked to the loss of freeze suppression, possibly a microscopic degradation in the polymer matrix.

Acrylamide is itself toxic both through ingestion and skin contact. However higher molecular weight polymeric forms are safe and available in industrial capacities. A sample solution of polyacrylamide was polymerised and tested in the same manner as

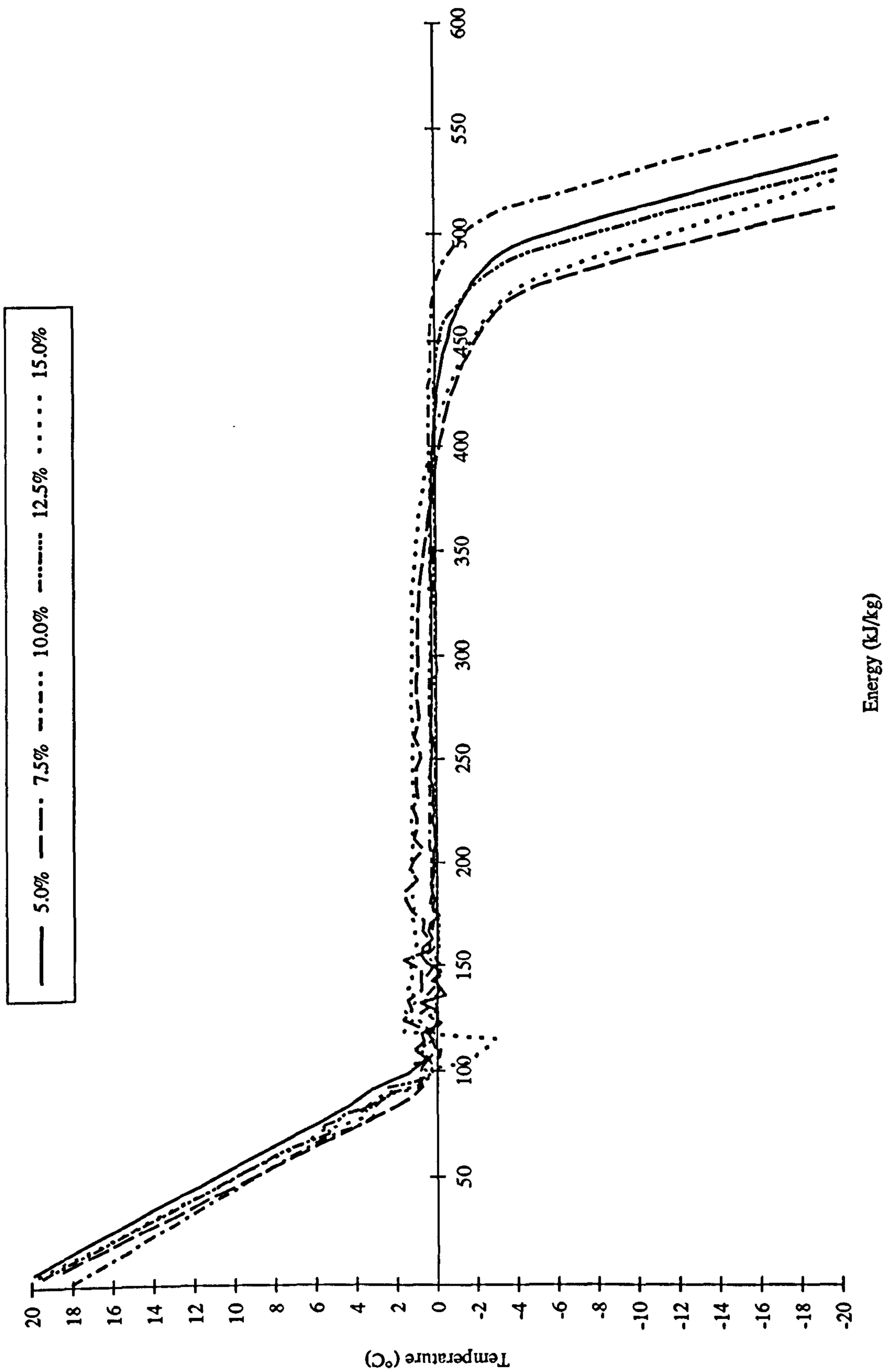

Figure 3.11: First Freeze of Hydrophilic Materials Formed from Acrylamide Solutions.

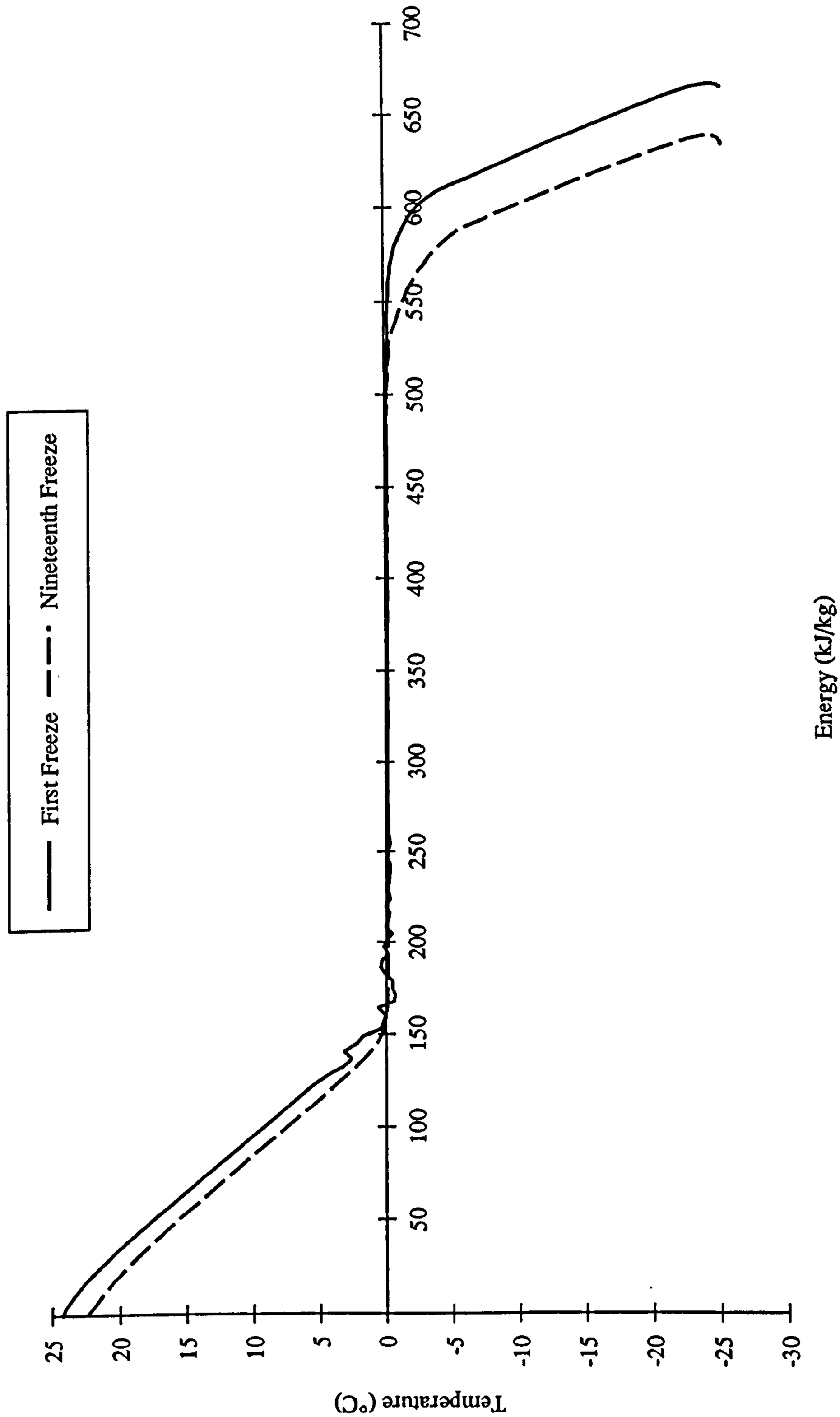

Figure 3.12: The Effect of Thermally Cycling a Hydrated Hydrophilic Polymer Produced from an Irradiated Solution of Acrylamide (10%).

above. The freeze-thaw characteristics of this sample were again found to be 'natural', or as expected, for the free water of hydration. Because of this, the use of hydrophilic polymers based on such solutions would have a lower cost (and time) for large scale production compared with commercial materials currently available. These savings would be in addition to those already described of lower material cost, cheaper handling and easy processing to achieve particulate form of the material.

Further work on these novel hydrophilic materials, and those based on poly-vinyl alcohol (PVA), has been undertaken at Cranfield since these tests (Leguay, 1994). The PVA based hydrophilic polymers were found also to have a high water uptake (~95% mass) and similarly to exhibit no freezing suppression on initial and subsequent thermal cycles. From this work and related studies (Highgate, 1996) it has been estimated that the cost of commercial scale production for high water content materials could be as little as £0.95 per kg (wet).

3.2.5 Miscellaneous Tests

The tests reported so far have been for composite cylinders in their hydrated state (diameter ≃21mm, length ≃16mm). For application as phase change slurries the hydrophilic materials would (a) have smaller sizes (~2mm) and, (b) be in contact with a support fluid (Shell Fusus oil). The effects of each on the phase change behaviour was investigated.

To investigate the effect of particle size, samples of specific particle size range were prepared. This involved washing hydrated particles through several grades of mesh to collect specific size ranges, namely 2000-1400μm, 1400-1000μm, 1000-500μm and 500-250μm. Each sample was placed on absorbent paper to remove excess surface water and then placed in sealed containers. To overcome poor thermal contact between the particles and the thermocouple, a small copper disc was used (diameter 10mm). This had the thermocouple attached to it, and was placed in the centre of the mass of particles. The results showed similar phase transition behaviour to that of the cylindrical samples. Particles prepared in the same manner were also mixed with a sufficient quantity of oil to fully immerse them. Again transitional behaviour was apparent as found with larger samples.

A thermally cycled sample pair (Section 3.2.2) was allowed to dry in air for one week. The mass of these samples were found to be the same as before initial hydration and thermal cycling (0.82(±0.01)g). These were again hydrated until saturation was completed and their final mass measured (2.97(±0.01)g). The results showed no measurable change in the quantity of water they absorbed compared to pre-thermal-cycling. Subsequent tests of the phase transition properties showed no suppression of freezing. This, and the findings of Section 3.2.2 show that the changes in the material from thermal cycling have a permanent effect. Furthermore the preservation of this effect with dehydration and re-hydration would suggest that the changes are solely a mechanical effect (Highgate, 1989). Such a change would account for the increase in

opacity of the samples after a number of thermal cycles.

3.3 The Thermal Conductivity Of Hydrophilic Materials

The thermal conductivity within the particles of a flowing slurry are the limiting factor in the rate at which the latent heat can be removed (or added), and hence limit the rate of heat transfer to and from that system. Hydrated hydrophilic materials can be considered as water trapped in a polymer matrix (therefore unable to convect) and hence the expected, and later shown, thermal conductivity would be a combination of that of the constituents. The anomalies found in the phase transition test suggested that the thermal conductivity needed to be measured, since poor thermal conductivity values in either the ambient state or the frozen state would have revealed a serious flaw in the aims of the project.

To gain data of this nature several tests were performed to determine the thermal conductivity of hydrophilic materials in their hydrated state. The technique used was a steady state method which involved comparing the known thermal conductivity of a material (reference) to that of the hydrophilic sample (test). The method adopted was to place the test sample and the reference sample in thermal contact with each other and apply different temperatures to the outer surfaces of the samples (Figure 3.13). The net effect of the different temperatures was to cause heat to flow through the samples.

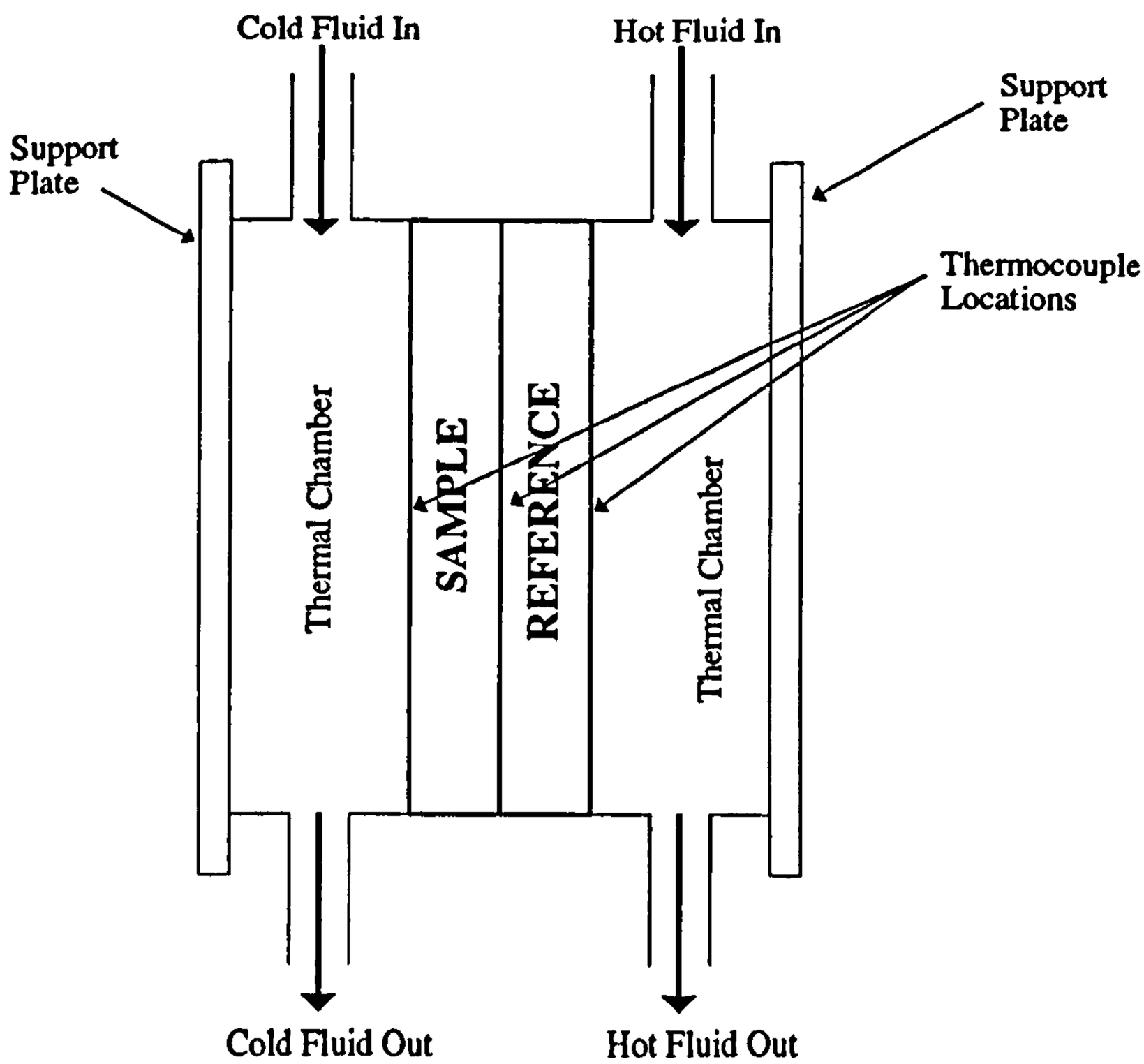

Figure 3.13: Thermal Conductivity Test Apparatus

If the geometry is correct the heat flux can be considered to flow in one dimension between the hot and cold surfaces, and hence be equal in magnitude for both samples. The general conductive heat flux equation can be written in terms of the unknown thermal conductivity of the test sample (k_{test}) and gives:

$$k_{test} = k_{ref}\frac{\Delta T_{test} x_{test}}{\Delta T_{ref} x_{ref}} \tag{3.4}$$

The reference used was a disc of plate glass, diameter 100(±1)mm, with a known thermal conductivity k_{ref}=1.0(±0.1)W·m^{-1}·K^{-1} at 300 K (Kay, 1986). The thickness of the glass disc was measured in several locations and gave a result of 3.1(±0.025)mm. Three dry hydrophilic discs were machined from the same sample, all with a dry diameter of 59.9(±0.1)mm. After hydration in several flushes of water, the final diameter of the samples was 80(±1)mm and thicknesses of 7.0mm, 7.5mm and 14.6mm, all with an error of ±0.1mm. The temperatures at the interfaces were measured with thermocouples (wire diameter 0.2mm) which were placed along the axis connecting the centre line of the discs.

The temperature gradient was produced between the contact surfaces of the thermal chambers shown in Figure 3.13. Each chamber was a copper cylinder with external dimensions of 105mm in diameter and 38mm deep. The contact faces were constructed from 5mm copper plate that had been machined to provide a good thermal contact with the samples. Heating or cooling was provided for each block via heater-chillers (Conair Churchill 02CTCV). The support plates holding the thermal blocks, samples and thermocouples together, were connected by studs so enabling sufficient contact pressure to be applied while ensuring that all surfaces remained parallel. To aid thermal contact, silicon oil was applied.

The assembled system was covered in glass fibre insulation to minimise heat transfer perpendicular to the direction of the measured temperature profiles. Initial tests performed with the system gave thermal conductivity values of 1.0 to 1.6W·m^{-1}·K^{-1}. This range was twice that expected from consideration of the constituent parts, hence the system was investigated further. The origin of the high conductivity values was found to be due to the loss of water from the exposed surfaces of the test samples, which in turn caused a high enthalpy change in the test sample. The heat required by this was drawn across the reference sample producing an excessive temperature differential, ΔT_{ref}. To solve this problem each test sample was sealed by placing it in a thin polythene wrapping (clingfilm) together with its associated thermocouples. The common thermocouple was now no longer measuring the true temperature of the references surface (due to the polythene layer) so a fourth thermocouple was added.

The results from this newly assembled system are shown in Figure 3.6. As can be seen, the measured thermal conductivities of the samples were in close agreement with that of water (Incropera, 1990), and no detrimental changes are evident. The figure does show a tendency for the measured data to be higher than that for water alone. The origin of this discrepancy might be (a) heat loss from samples, and (b) errors in the

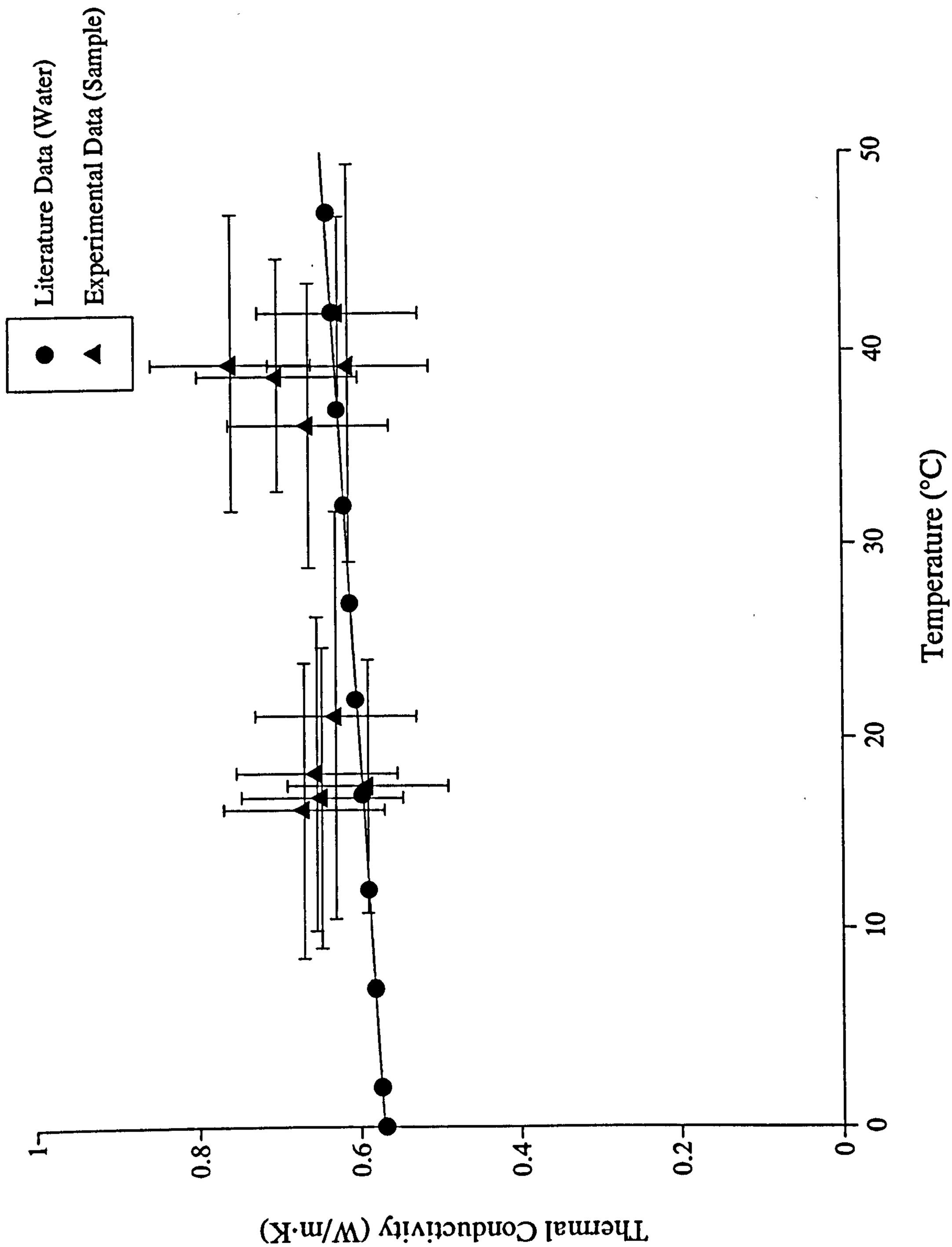

Figure 3.14: The Measured Thermal Conductivity of Hydrophilic Materials.

thermocouples used (the effect of which has been shown in Figure 3.14). To reduce errors the apparatus would require more precise temperature measurement at the interfaces, and the application of guard heaters to ensure energy flow was in one dimension. Such an enhancement to the apparatus has not been undertaken.

3.4 Discussion

The work reported in this chapter has extended the knowledge concerning the phase transition properties of hydrophilic materials hydrated in both water and salt solutions. This has provided sufficient data to establish their suitability as phase change materials for application in slurry based thermal energy storage systems operating at 0°C or below.

The 75% water uptake materials require thermal cycling 10 to 20 times before their transitional behaviour stabilises at 0°C. However once the desired behaviour has been established, it remains stable over periods of >3 years (Section 3.2.2). Moreover the results discussed in Section 3.2.5 suggest that the changes that occur through initial thermal cycling are permanent, and are related to a physical change in the hydrophilic material alone.

The investigation into using salt solutions for hydration fluids (as opposed to water) has shown that the phase transition temperature can be lowered (Section 3.2.4). A more detailed study of the effects of salt solutions on transitional behaviour is required, although the data presented in Figure 3.10 can be used as a guide accounting for the effects of the material on the transitional temperature.

The application of high water content materials (~90%), in situations where high mechanical strength is not required, could provide cost reductions to such by (a) lower initial cost of materials, (b) lower preparation time, and (c) reduced size of the thermal storage unit. Their long term stability in pumped systems needs to be established.

Chapter 4

Cold Storage Device

4.1 Introduction

In this and the following chapter, the work undertaken to design and develop a number of cold storage devices is described. All the units employed hydrophilic particles hydrated with water as the phase change element. This work has yielded a cold storage device suitable for demand side management applications (Section 4.4.6).

The first part of this chapter discusses previous work carried out at Cranfield, employing hydrophilic materials for cold storage, before this work began. Next the problem of fluidising hydrophilic particles using minimal power is readdressed, the design of a new system discussed, and its performance and limitations identified. Then the modifications made to this system to increase the energy density, are reported.

The process of fluidising the whole mass of stored solids limited the performance of the developed systems. Based on the acquired knowledge a fresh approach overcoming this problem was identified. Finally, the design, construction, and operation of this system are discussed and recommendations made.

4.2 Previous Work and Relevant Literature

The potential for using fluidised beds consisting of hydrophilic particles for thermal energy storage had previously been the theme of two MSc projects at the Department of Applied Energy at Cranfield. The first of these (Tsonis, 1989) investigated using both air and oil to fluidise the hydrophilic particles. The main focus of the air fluidisation tests were for hydrophilic particles of diameter 0.4mm (d_p) in a small bed (diameter 155mm, height 280mm). Calculations of the minimum fluidisation velocity (U_{mf}) were made using Equation 2.43. It was found that for fully-hydrated particles fluidisation did not occur at the calculated minimum velocity, and as the air flow rate was increased further severe channelling occurred. The main reason cited for failure was the tendency of the particles to adhere and form large dense agglomerations. The addition of a dry powder (callodoc) did not appear to improve the situation. However it was possible to achieve fluidisation if hydration levels were kept below 16% by weight (maximum hydration level 75% by weight). Attempts to fluidise larger particles of 1.25mm diameter were not successful due to the absence of an air supply capable of providing a sufficient flow rate across the particle bed.

The failure of air fluidisation led Tsonis (1989) to attempt fluidisation using both silicon oil and mineral oil as support fluids. The advantage of using a liquid can be seen by

inspection of Equation 2.43, where the small density differential and the increased viscosity combine to reduce considerably the minimal fluidisation velocity. The test apparatus consisted of a perspex open top cylinder of 195mm diameter and 230mm height. Cooling of the mixture was achieved via a cooling coil positioned in the oil-particle mixture in the tank. The fluid was stirred using a small turbine blade on a driven shaft. The tests proved successful for both oils and for particle concentrations from 10% to 40% by weight. The test took the mixture through the phase transition temperature down to -4°C. All materials were fully hydrated 75% hydrophilic particles.

This work was continued the following year by Kay (1990) where a focus was made on the use of oil as a support fluid. A new test apparatus, similar to Tsonis's, was designed and constructed. The major improvements were replacing the cooling coil with a cylindrical heat exchanger, construction of a close fitting turbine, and general improvements in tolerances around the device. Shown in Figure 4.1 is a cross section of the apparatus. The heat exchanger consisted of a number of turns of copper tubing enclosed between two copper cylinders, and to make good thermal contact the volume was filled with a low melting point alloy (Woods Metal). The final dimensions were OD = 124mm, ID = 96mm and height = 156mm. It was attached to the top of the tank by three studs.

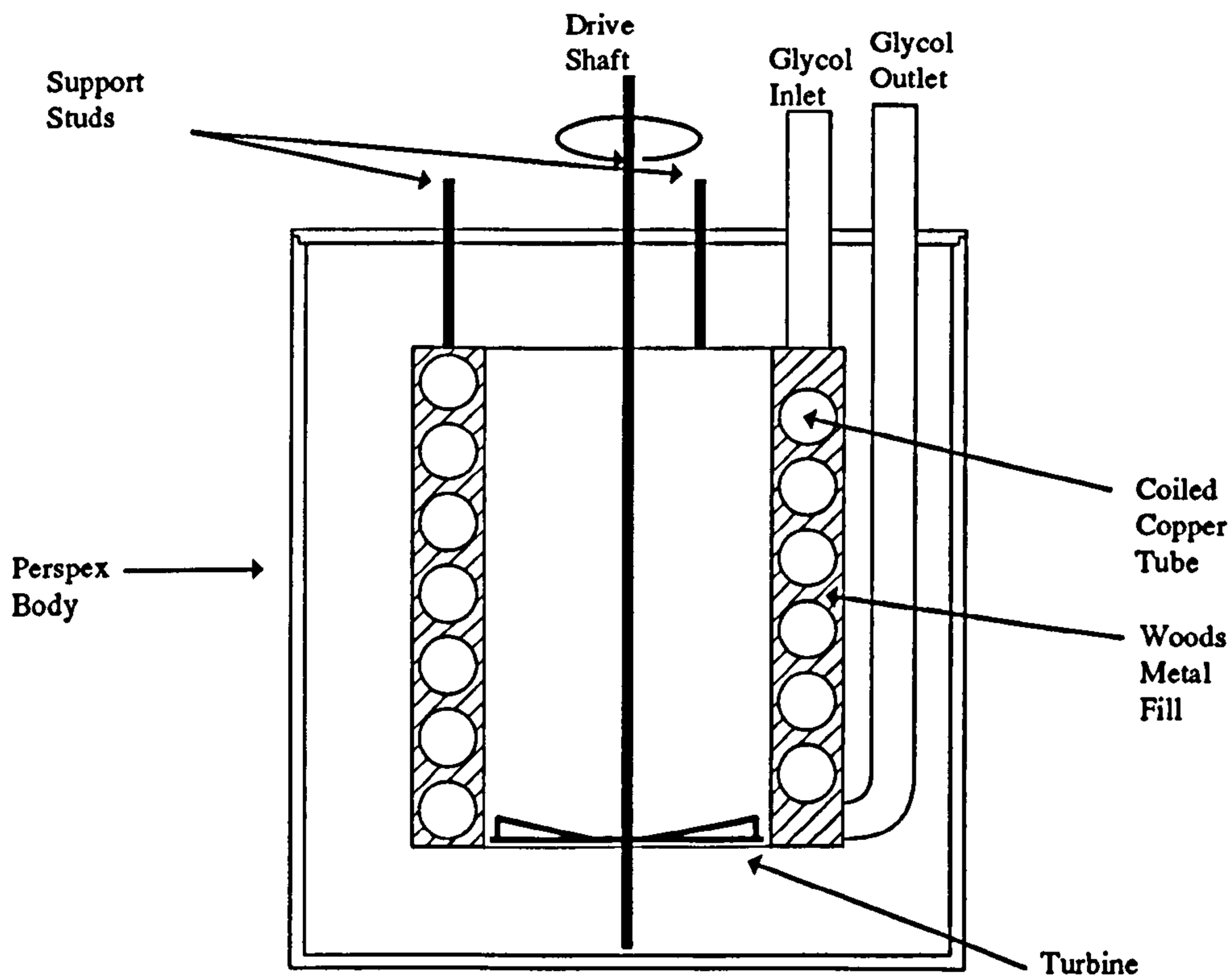

Figure 4.1: Cross Section of Cold Storage Unit Used by Kay (1990).

The main body of the device was a cylinder (190mm ID), constructed from perspex so that flow visualisation could be made. The use of perspex also benefited the design due to its relatively high thermal resistance. To further reduce the heat gains, the unit was

placed inside a box constructed of polyurethane board with a removable side for inspection and visualisation. Cooling was supplied via anti-freeze solution cooled by a chiller unit.

A number of tests were performed using this apparatus, the varied parameters were the support fluid, the solids concentration, the vertical position of the turbine, and its speed of rotation. With a 25% solids concentration in mineral oil the system was found to agglomerate and block at obstructions encountered at the top of the tank (support studs, thermocouple wires and connecting pipes to heat exchanger). The turbine was run at a rotational speed of ~600rpm, although it was found that varying the speed up to ~1000rpm for short intervals improved the flow condition temporarily. The best results were achieved with the turbine blade at the base of the heat exchanger. Similar results were obtained with a 40% solids concentration in silicone oil. The effect of varying the speed of rotation was more beneficial in this instance, although agglomerations still occurred. Below a mixture temperature of -2°C it was noted a stable (fluidised) mixture could be achieved using a constant rotational speed, furthermore this could be reduced down to ~300rpm (cf typical speed ~600rpm). In all the tests passing below the phase transition temperature, no increase in the heat transfer rate was recorded (Kay, 1990).

4.3 Preliminary Tests

Earlier discussions in this work have described the high torque requirements encountered while agitating high concentration slurries, a situation not acceptable in the context of a system aimed at demand side power reductions. Furthermore the work of Kay (1990) showed that such systems had inherent failings. The configuration chosen for this work was to use a pumped system to mobilise the hydrophilic mixture over the heat exchanger surface. To this end, a suitable pump had to be chosen and some idea of the limitations of the pump had to be found in terms of the concentration of solids that it could pump, and the rates at which the slurry could be pumped.

For simplicity and low cost, an impeller type pump was considered the most suitable unit although it had to meet certain requirements. The first of these was a geometry and construction that would not cause degradation of the particles in the slurry. This required spacings greater that the particle size (1-2mm) and elastic surfaces on the impeller that would not damage the particles on impact. Secondly it must operate in the required temperature range (30°C to -10°C) and any elastic properties of the impeller surface should not be lost at low temperatures. Finally, it must have a low power rating (<100W) both in respect of the power demand required to operate it and the amount of heat it dissipated, and possibly leaked, into the system. Many manufacturers products were investigated but most were classed as unsuitable for fluids containing particles, and hence rejected. Furthermore the power rating and operational temperatures of the pumps were unsuitable.

The only impeller pumps found that were suitable for the geometric requirements of this system were domestic/industrial washing machine pumps. These had both semi

flexible impellers, and wide spacings between the impeller and body (~5mm) (designed to cope with hard particles such as coins and buttons). They also had low nominal power ratings of 50 to 100W. It was not known if these pumps would operate at the lower temperature ranges required for this project, so after visual inspection one was bought and tested (Plaset, s.p.a., Italy, No. 94, rating 90W). The construction enabled easy disassembly and the semi-flexible impeller blades were removed and cooled down to -27°C. At these temperatures they were still found to be reasonably flexible. The pump body was made of a thermo-setting plastic. The inlet port was constricting although there was enough wall material to allow it to be machined to larger diameter (24mm). The outer diameters were suitable for attachment to 28mm copper piping using a short length of PVC hose.

Two simple tests were performed on the pump, the first was to measure the maximum achievable flow rate, and the second to check the highest concentration of solids that could be pumped. The first test used a large tank of water from which the pump inlet was connected. The outlet was returned to the tank via 3m of PVC tubing (28mm id). The flow was diverted to a bucket for a known time interval and the collected mass measured. The receptacle used to collect the sample was floated in the main tank during the collection period, this negated the change in head. The flow rate achieved was 28(±0.5)$lt \cdot min^{-1}$ (0.47(±0.01)$lt \cdot s^{-1}$). The second test used a simple closed loop of copper tubing (28mm ID) with a small heat exchanger in line. The loop was filled with a measured volume of silicone oil. Solids were added and the volumetric concentration calculated by measuring the spill from a small outlet (at ~18°C). The resulting mixture was pumped while being cooled down to -5°C. The slurry was found to be pumpable in the system at concentrations of 50% at room temperature, but blockage occurred during the phase transition temperature (0°C). The previous concentration of 40% had continued to circulate through the phase transition temperature down to -5°C. Both tests suggested that the pump was suitable for the investigations to be undertaken during this project.

4.4 The Fluidised Bed Cold Storage Device

The high rates of heat transfer achievable from fluidised systems was one of the driving factors in previous investigations (Section 4.2). The failure of air fluidisation had led to the use of oil for the supporting mixture. Such systems had been shown to work although not at a scale large enough, or a state stable enough, for practical purposes. This part of the work describes the development of a cold storage unit addressing both of these problems. As a design guide the system aimed at meeting a latent heat storage capacity which would facilitate a discharge of 1kWh (3600kJ), at a rate of 1kW.

4.4.1 Perspex Test Unit

A test unit to allow the development of a cold storage device capable of agitating a high solids concentration slurry was designed and constructed. The main body consisted of a

flanged perspex cylinder with four small ports, and a top and base constructed from aluminium (see Plate 1). The ports were tapped to accept standard 28mm pipe fittings for the connection of circulation loops. The base had a central recess to support a vertical shaft that formed the basis of agitation devices. This shaft passed out through a hole in the top plate. Perspex was used at this stage to allow the visualisation of flow and effectiveness of mixing within the unit as modifications were made.The tank had an internal diameter of 294mm and height of 430mm and without the connection of circulating loops gave a maximum volume of ~30lt. No means of cooling was added at this stage because an effective method of mobilising the slurry with low energy input was being investigated, and the thermal behaviour of hydrophilic particles at the phase transition temperature were being examined.

This diameter gave an area of 4.8×10^{-2} m^2, hence from the use of two pumped loops a maximum mean velocity of $\sim2\times10^{-2} m\cdot s^{-1}$ was expected across the area of the tank. The support fluid used to fill the tank was Shell Thermia-B (Shell, 1991). At room temperature a hydrophilic particle of 2mm diameter (fully hydrated 75% material) had a settling velocity of $\sim1\times10^{-3} m\cdot s^{-1}$ (Equation 2.43) . This velocity will be reduced even further in practice by hindered settling, due to the presence of other particles. Hence the pumps had the capacity to fluidise the material within the system. The initial test used a solids concentration of 30%.

The shaft was driven by a shunt motor (Parvalux Electric Motors Ltd., Bournemouth) rated at 190 Watts and fitted with an internal gearbox giving a maximum of 200rpm at the motor output shaft. This was further reduced to 120rpm through the use of a toothed belt and pulleys between the motor and shaft. To vary the motor speed a thyristor controller was used (M. R. Supplies Ltd. London).

Initial tests looked at the behaviour of just pumping the slurry in the device. Firstly it was found that during static periods settling of particles soon occurred. Because of this pumps had to be located in such a position that particles settling under gravity fell away from them. Secondly, severe channelling occurred in the bulk of the mixture as shown in Figure 4.2. To solve this, flat paddles were added to the agitation shaft although the torque required to rotate them at start up was excessive.

The next solution replaced the paddles with a semi-circular disc with its axis orientated to the shaft and positioned vertically, so that it was just above the lower inlet port of the perspex tank. This orientation of the disc swept a very small area through the settled solids, while rotated, and gave very little resistance during start up conditions. The combination of the rotating distributor and pump reduced channelling considerably splitting the contents of the tank into two regimes. One consisted of recently settled material the other was an evenly dispersed mixture of solids and oil. The relative proportions of these parts depended on the rate of rotation of the distributor. At the lowest rotational rates (period 10 s) the settled portion formed about 70% of the tanks volume, but periods of less than 1 second caused almost all of the volume to be evenly dispersed.

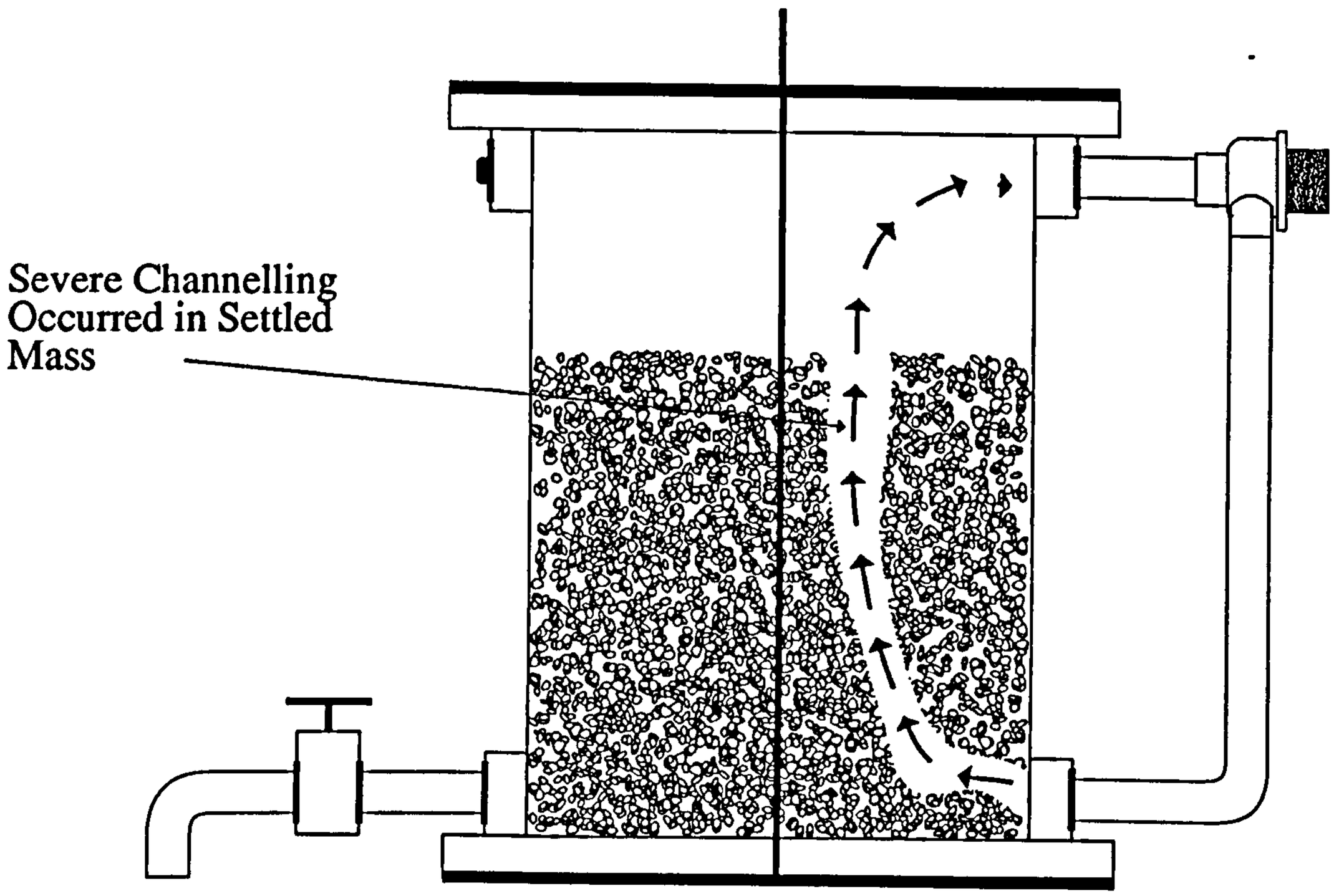

Figure 4.2: Channelling in Perspex Test Unit.

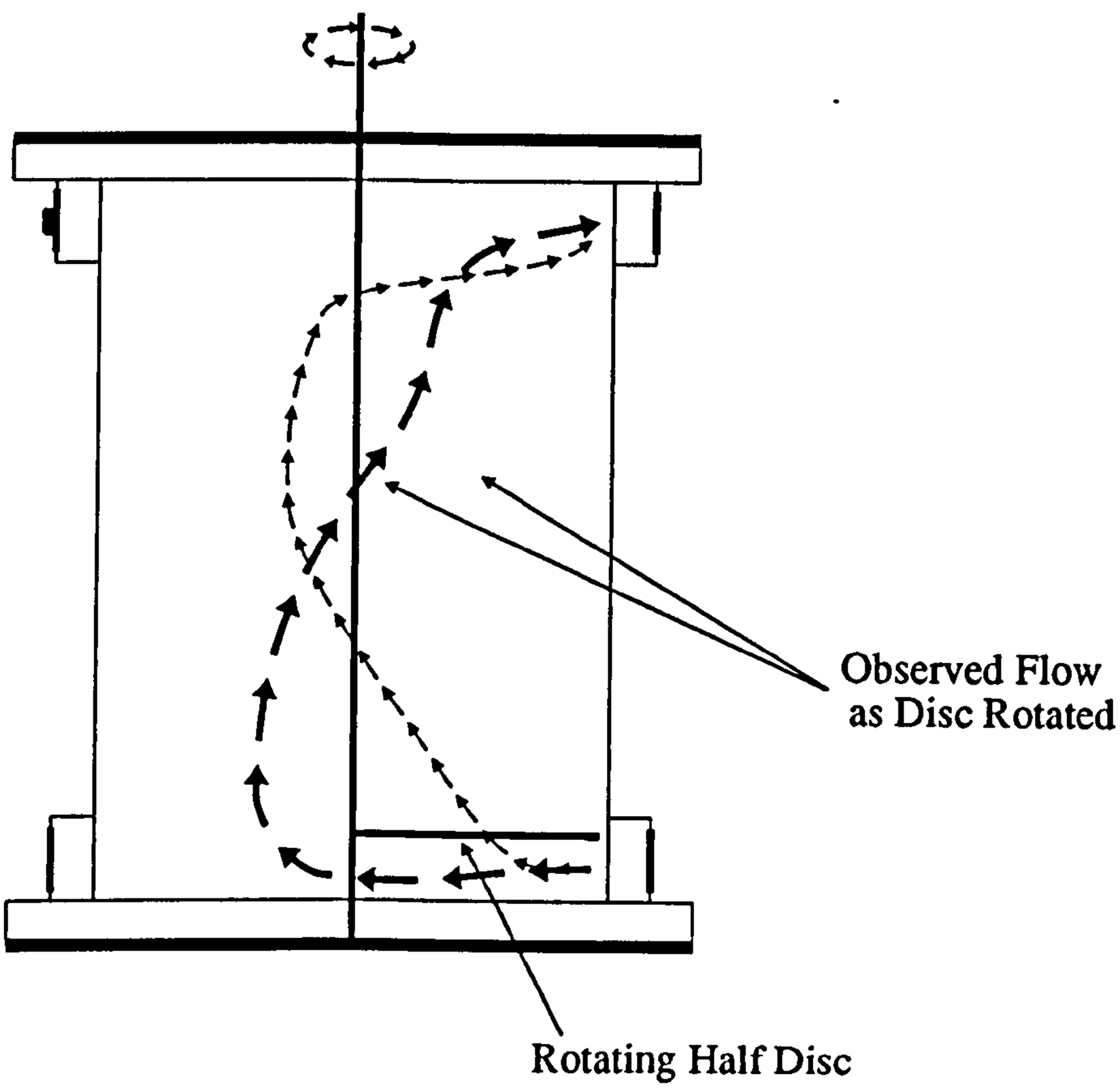

Figure 4.3: Flow Pattern for Single Plate.

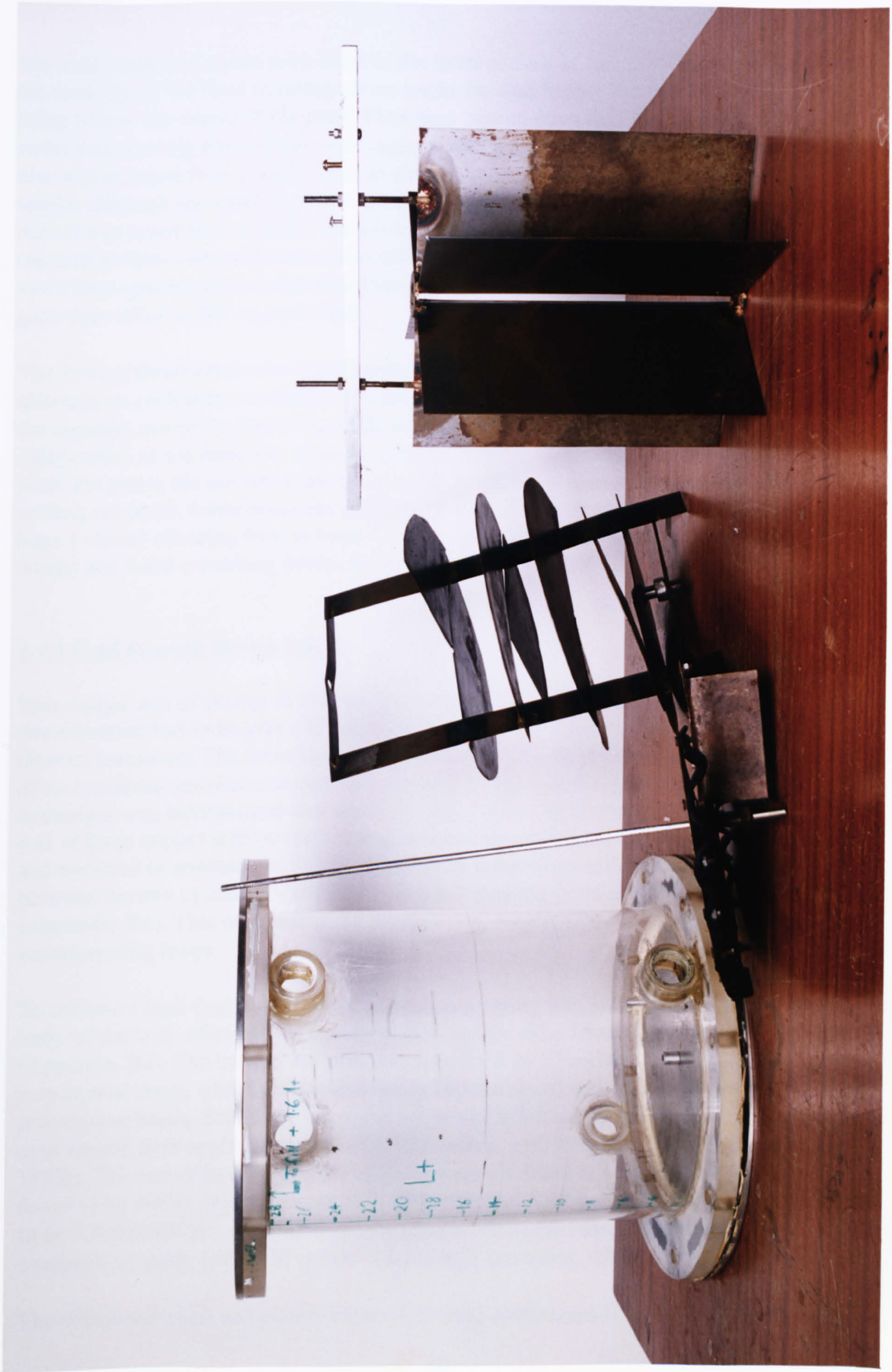

PLATE 1

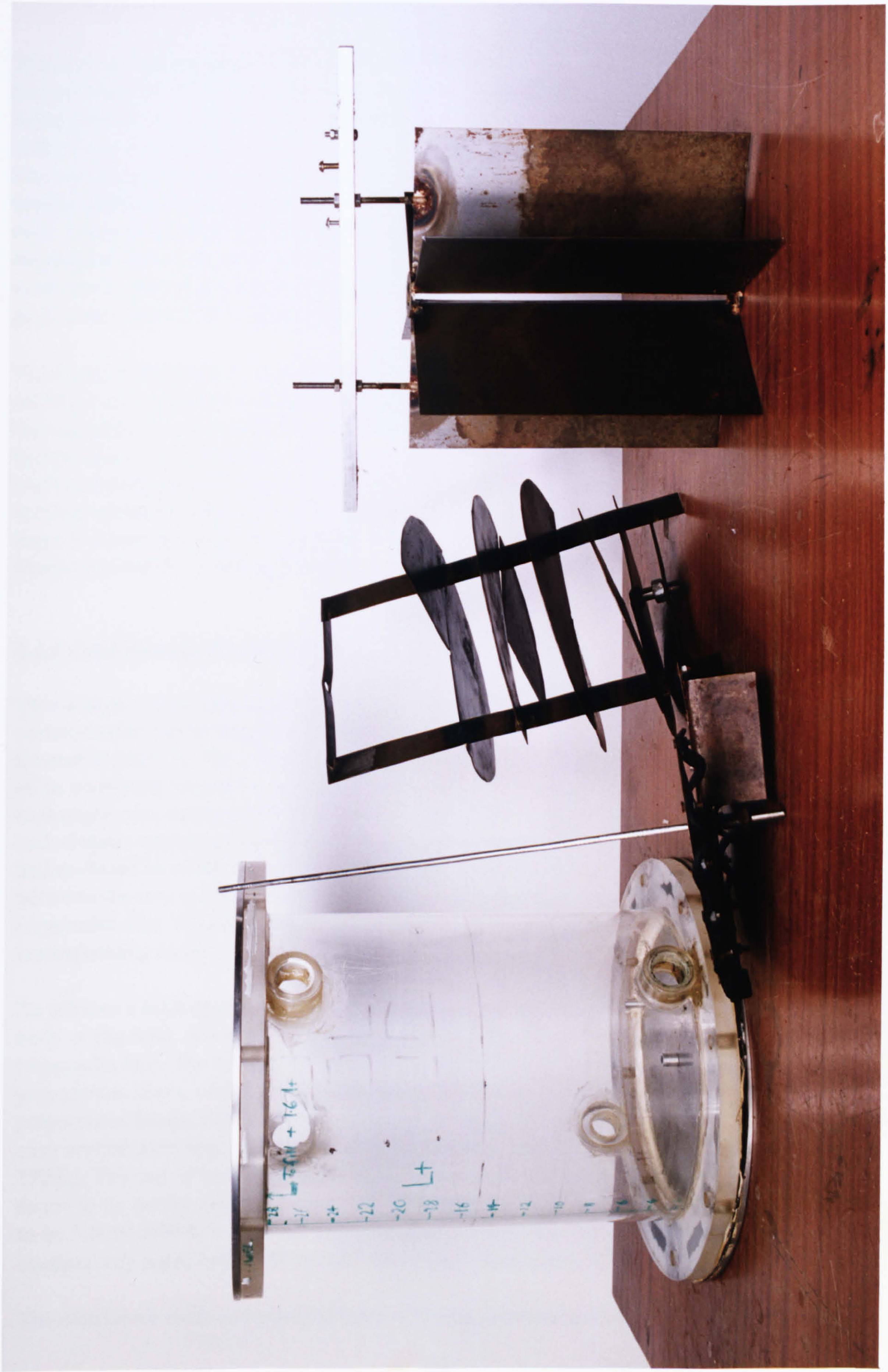

PLATE 1

The least mobilised zones were close to the outer surface of the tank (Figure 4.3) due to the tendency of the flow to emerge from under the disc to take the shortest path, this being near to the centre of the plate. Flow then moved from the edge towards the upper outlet port, leaving most of the outer regions undisturbed. To improve this further the disc was changed from a semi-circle to a three-quarter circle. The behaviour was similar although the outer regions were now disturbed as the gap in the plate swept past. Also it was noted that at 30rpm the whole contents were mobilised. The torque required at these rates of rotation was still excessive, so it was decided to add three more three-quarter discs to the distributor. These were evenly spaced vertically and the gaps were offset at 90° to each other.

The level of fluidisation was significantly improved (Figure 4.3) with this option although on each plate a volume of hydrophilic material was seen to settle. This was on the opposite quarter to that of the plate opening. This phenomena was found to be independent of the direction of rotation of the shaft. The method of construction of the shaft and plates did not allow the plates to be modified to remove the quarter where settling occurred, furthermore the gap between the tank wall and the plates' edges was large (~4mm) allowing flow to bypass them. Hence at this stage it was decided to design and build a working device for evaluation.

4.4.2 Cold Storage Device MK I

This design was of similar dimensions to the perspex test unit, although some consideration had to be given for both the integration of a heat transfer surface and thermal insulation. The main body of the tank was fabricated from aluminium, because of its combined resistance to corrosion and good heat transfer qualities. The heat exchanger was incorporated in a similar manner to that of Kay's (1990) (Figure 4.1). A coil of 8mm copper refrigeration tubing was placed around the outer cylindrical surface and enclosed in another aluminium cylinder. To achieve good thermal contact the space between the two cylinders was filled with a low melting point alloy (Wood's Metal) (Appendix B1). This unit, unlike the perspex one, employed two circulation pumps and corresponding loops.

To achieve a high degree of thermal insulation a casing was built to surround the main body of the tank, allowing for the circulation pumps to be located externally (Appendix B2). The base of the tank was supported by 55mm thick expanded polystyrene sheet, whilst the annular cavity (80mm wide) was filled with loose polystyrene beads. Sealing of the pump loops was achieved by the close fitting of the case around their applied insulation (AF/Armaflex, wall thickness 32mm (Armstrong, 1992)). The rate of heat gain to the systems was calculated at $1.9 W \cdot K^{-1}$. This was later found to be out by nearly a factor of 2, and estimated from performance measurements to be $3.6(\pm 0.8) W \cdot K^{-1}$. (The discrepancy resulted from the value of the thermal conductivity used; k=0.04 $W \cdot m^{-1} \cdot K^{-1}$ (Table A.3; Incropera, 1990)).

The distributor shaft and plates (Figure 4.5) were constructed form stainless steel. Each

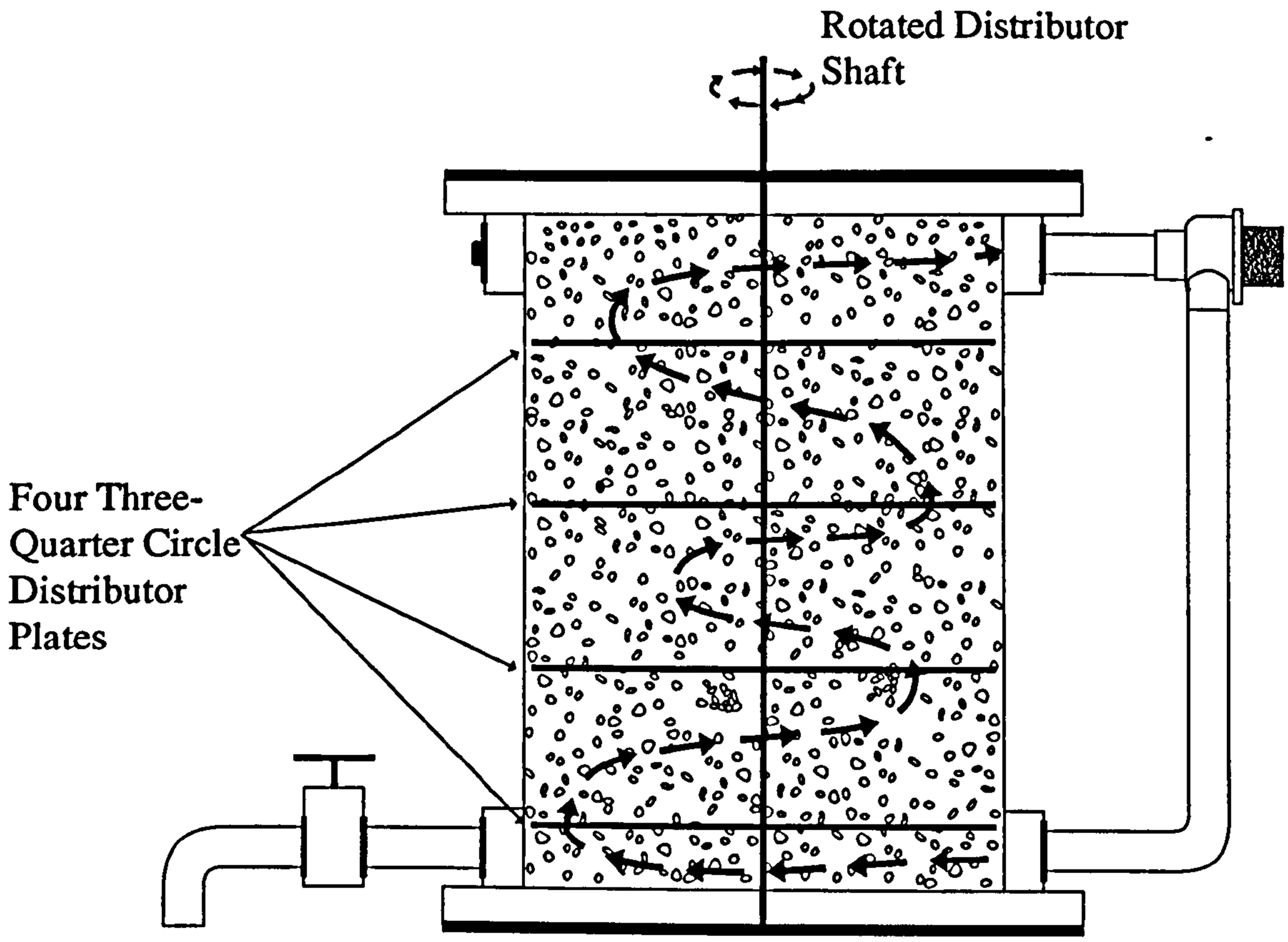

Figure 4.4: Effect of Using Four Three-Quarter Circle Distributor Plates.

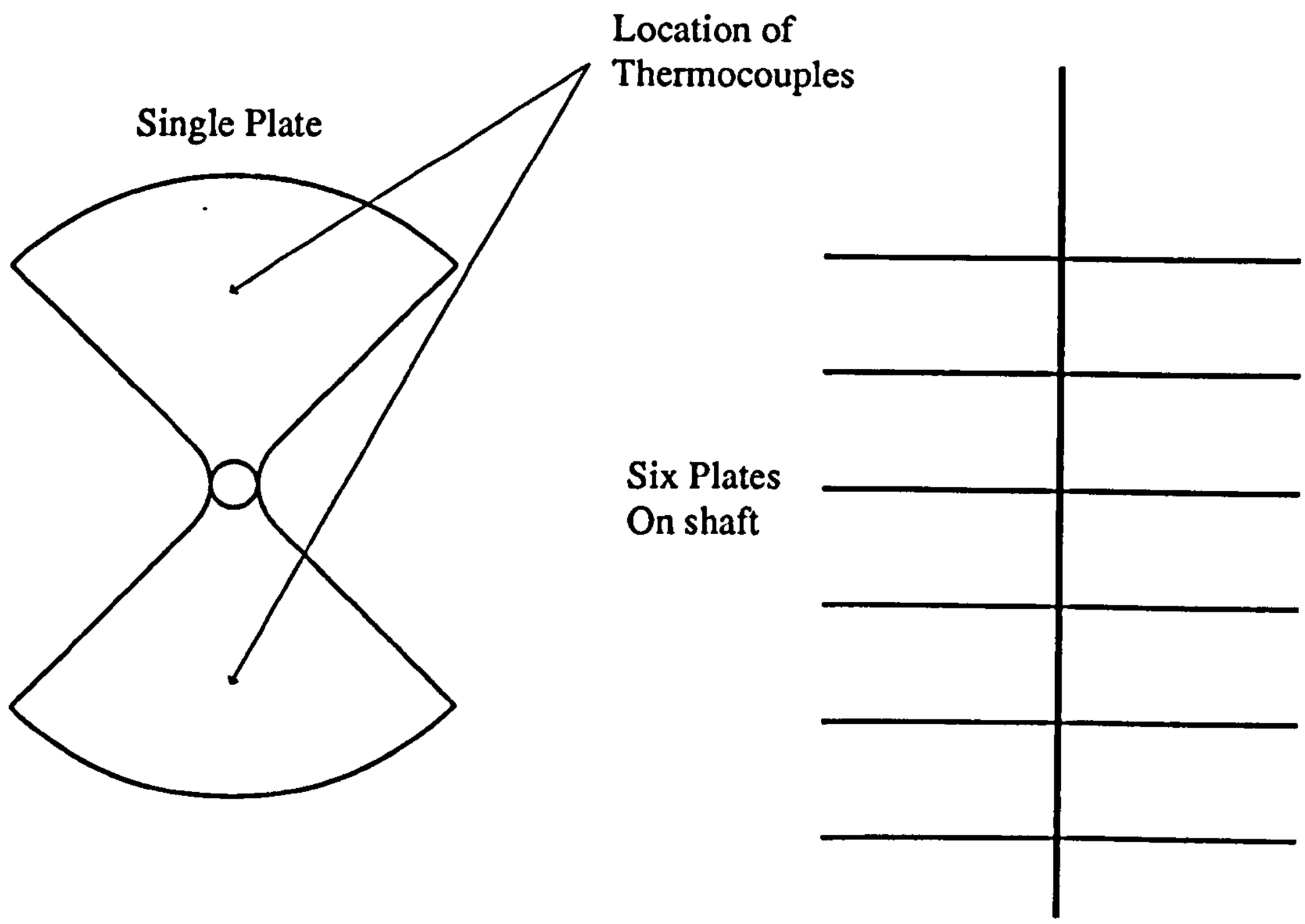

Figure 4.5: Schematic Diagram of Distributor showing Placement of Thermocouples.

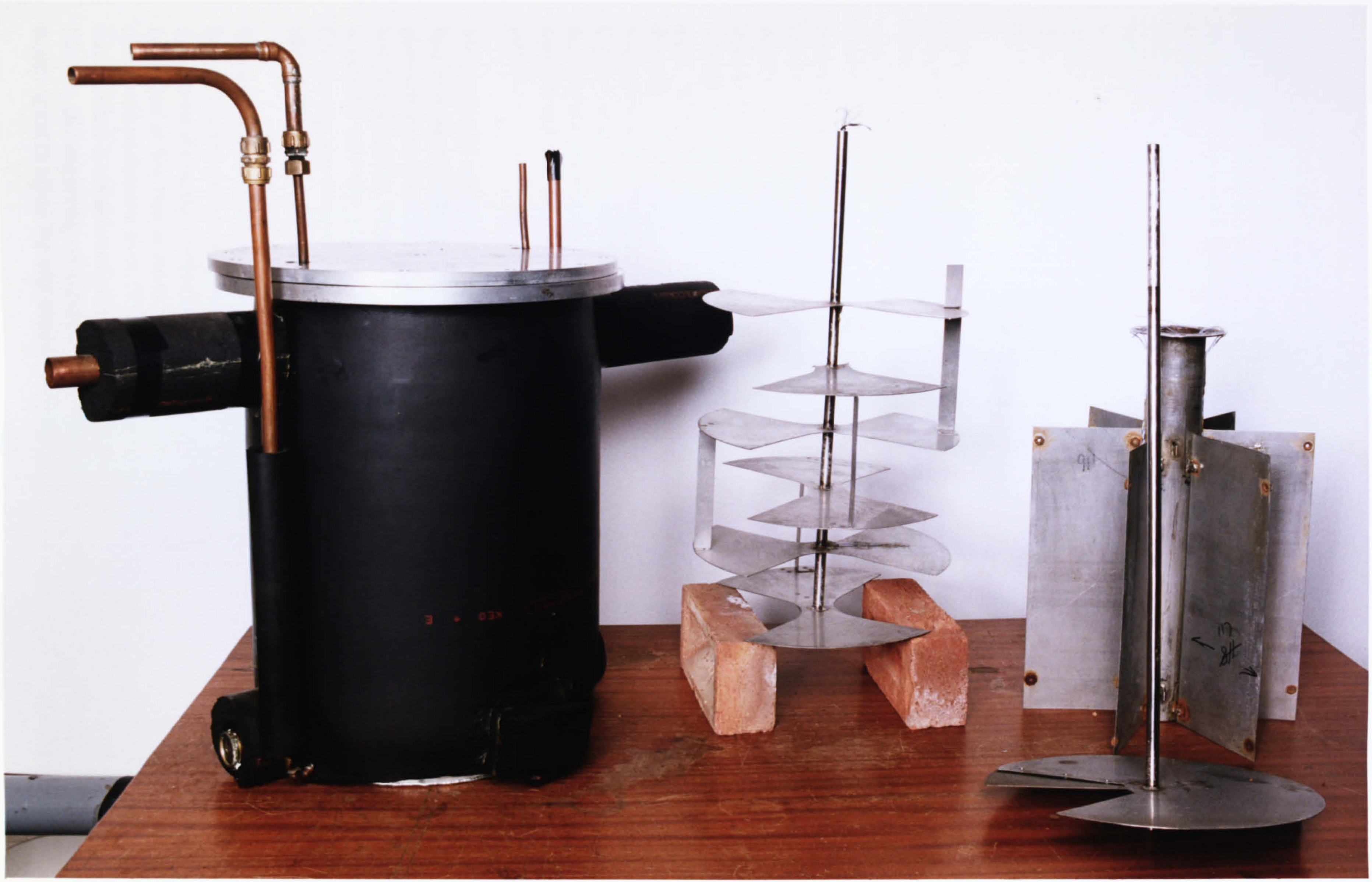

PLATE 2

plate (disc) had opposed quarters removed (Plate 2), also the shaft was hollow allowing thermocouples to be placed on the surfaces of the plates (Figure 4.5) to measure the temperature of the mixture. To accommodate the rotation of the shaft the thermocouples had to be connected to a silver slip ring device. The shaft was driven with the same unit as the perspex rig. Four thermocouples were placed in contact with the heat transfer surface. To achieve this, small areas of the outer casing were removed (10mm ×10mm) and the Wood's metal removed to expose the inner cylinder. A gas torch was then used to bond the thermocouples to the surface. The missing fill alloy was replaced by an epoxy resin loaded with aluminium powder in an attempt to ensure thermal continuity. The gap between the plates and the tank wall was reduced to <2mm, being smaller than the typical size of the particles.

Initial performance tests were conducted on the system before the phase change materials were added. The purpose of these was to determine the heat gains to the system from the pumps, the distribution device and the local environment. The tank was initially filled with a 30% (by mass) ethylene glycol solution (32.5lt). The whole system was cooled using a chiller (Conair Churchill 02CTCV) down to a specific temperature. Once this had been reached the unit was allowed to operate continuously for 24 hours while temperatures around the system were measured. The operational parameters included the number of pumps in simultaneous operation, the duty cycle of the pumps and distributor, and the speed of rotation of the distributor. From these tests, it was estimated that the pumps were injecting heat at an average rate of 7.4(±0.8)W each, whiles the agitator was dissipating heat at a rate of 10.2(±0.8)W (1 revolution per second). The mean heat transfer coefficient for this system, with both pumps operating, was estimated at h=400(±100)$W \cdot m^{-2} \cdot K^{-1}$. The inner heat transfer surface had an area of $0.15m^2$, and for a load at 8°C this would give heat transfer at a rate of 360W to 600W at the operational temperature of 0°C. This was below the desired 1kW, although the transfer rate was expected to increase when the slurry was substituted for the ethylene glycol.

This unit was operated below the phase transition temperature, although all tests to date had been at room temperature (~18°C). To compensate for this it was decided to use an alternative support fluid that had viscous properties similar to those of the Thermia-B at low temperatures. After consultation with Shell oils a fluid was chosen, Shell Fusus Oil, a paraffin normally used as a calibrating fluid (physical properties shown in Appendix C). The rig was drained of its glycol solution charge, rinsed with water and dried using absorbent paper, then filled with 32.5lt of Fusus oil.

The hydrophilic particles were prepared by hydrating, rinsing then (roughly) draining before placing then in polythene bags. Each bag contained ~1kg of hydrated material, these were thermally cycled between 18°C and -27°C by employing a domestic freezer (operated in fast freeze mode to reach the lowest possible temperature). Each part of a cycle was performed over 24 hours to ensure the materials at the centre of each batch had reached a suitable temperature. Each batch was cycled 20 times by placing in the freezer, and removing on alternate days. After cycling, the materials were placed in water again to cover for any dehydration during the thermal cycles. Following this the

materials were placed between sheets of absorbent paper to remove excess water (~1kg at a time). Finally, materials were added to the tank to the desired concentration, the first being 10% by volume.

The first test employed only one pump with the agitation device set to 15rpm. The initial temperature was 22°C and it was observed that only a few very small particles were being brought to the surface. This showed that little fluidisation was taking place. The test was allowed to continue to see if the increase in viscosity caused by reduced temperature would initiate full fluidisation. This did not occur even at -5°C. The chiller unit was switched to heating mode and the system brought back up to 22°C. The following test repeated the conditions of the first, except that the agitation rate was set at 60rpm. This gave a definite increase in the rate at which particles were rising. Plumes of material could be seen rising close to the top plate of the distributor. This increased as the temperature of the system decreased, although even at -5C° only small quantities of the material were being drawn into the circulation loop.

In the next test the rotation rate was set back to 15rpm but both pumps were operated. The effect of the second pump was dramatic. From observations full fluidisation appeared to be taking place throughout the temperature range of the test (20°C to -4°C). As the temperature dropped below 0°C small agglomerations were seen to be rising from the distributor. These were random in shape but had a characteristic size of 10mm. The structures were easily broken up with the tip of a temperature probe. Part of the insulation was removed form one of the circulation loops allowing the flow through the PVC connection on the outlet of the pump viewed. This revealed that no agglomerations were surviving passage through the pump. It was assumed that the high rate of shear in the pump was destroying the agglomerations. The cause of the noted agglomerations is associated with surface water freezing between particles to form ice bridges.

Once the cold storage unit was back to ambient temperature, the perspex inspection cover was removed and the aluminium top fitted. The system was insulated and the outer casing closed for a full analysis. The test followed the same procedure as the previous one. Data from the thermocouples indicated that the mixture was virtually isothermal and mixing was thorough. Furthermore the temperature measurements on the discs showed no deviation compared to the mean (within the error limits of the thermocouples), indicating that settling was not occurring as had been seen on the three-quarter plates of the perspex rig. After a period of two and a half hours cooling the chiller was switched to heating mode, while data collection continued, until five hours into the test. By this time the contents of the tank had passed back through the transitional temperature and were approaching the start conditions.

The mean temperature behaviour is shown in Figure 4.6, a number of points should be noted. Firstly there is a clear difference in the rate of cooling and heating above 0°C, this results from the chiller performance. Secondly, on the heating portion of the curve there is a double plateau which was unexpected. The first, starting at about 3.5h into the test (~0.4°) is believed to result from phase change in the particles. The shorter one at

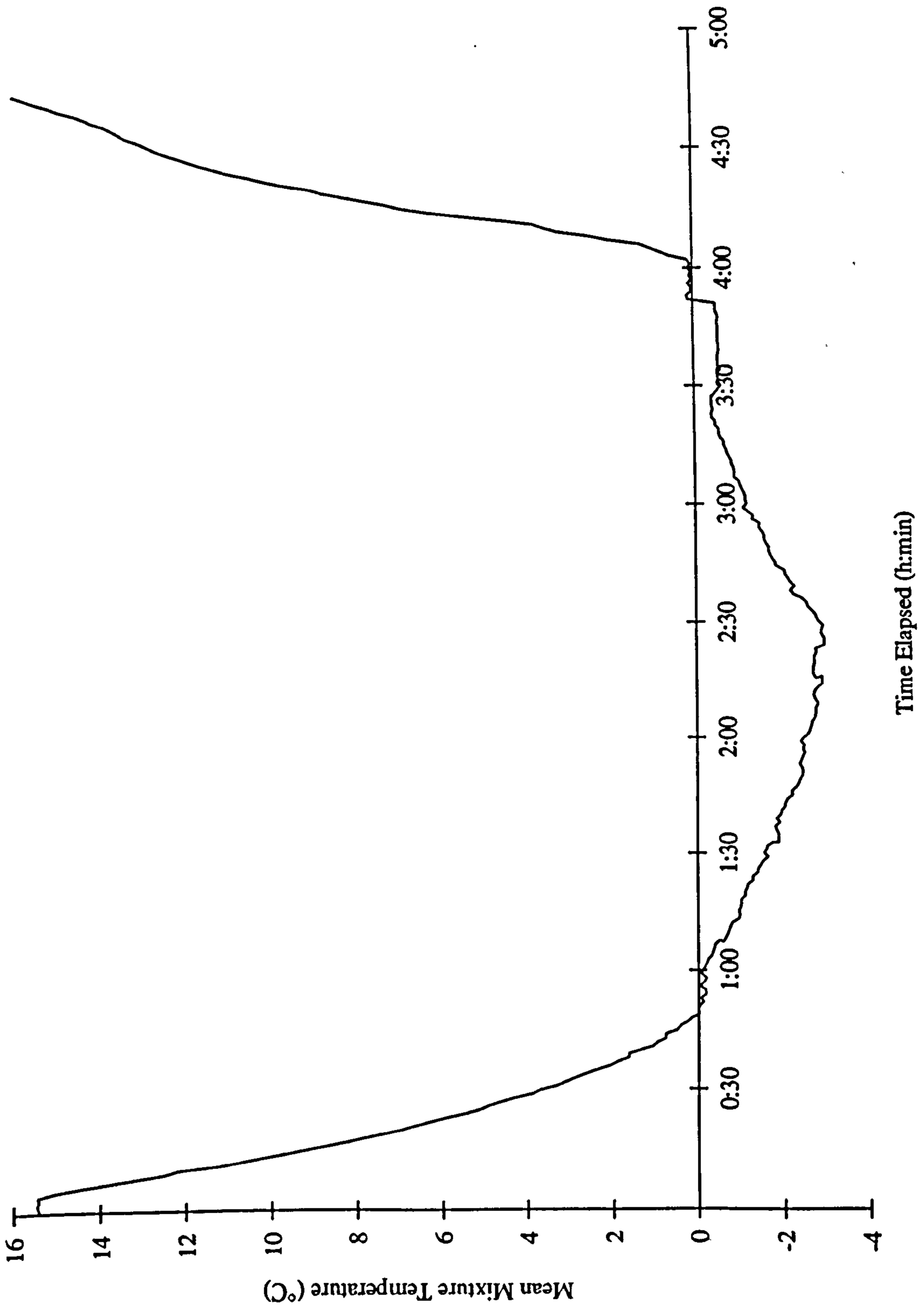

Figure 4.6: Mean Mixture Temperature of 10% Charge During Complete Cycle of Cold Storage Device (MK I).

0°C was believed to result from free water within the mixture. This water has possibly two origins. The first source may be free water remaining on the particles after preparation. The second explanation may be that the water originated from inside the particles, as their temperature decreases a slight reduction in maximum hydration level occurs resulting in free water. The heat transfer coefficients were estimated to be 800(±100)$W \cdot m^{-2} \cdot K^{-1}$ at 4°C dropping with temperature down to 400$W \cdot m^{-2} \cdot K^{-1}$ at -3°C. The decrease was associated with a viscosity increase as the fluid cooled, although the higher value relative to that of the glycol charge could be due to particle effects (no significant change was observed with wall temperature).

After disassembling the top of the cold storage rig the charge was increased to 20% and the perspex top put in place. The relative success of the tests with a 10% hydrophilic charge was not repeated with a concentration of 20%. Cooling occurred well, down to below 0°C, although the agglomerations were clearly larger than with the 10% tests (typically ~15mm opposed to ~10mm with 10% tests). Again the temperature probe could be used to break up their structures, and none were visibly surviving the pumps. As the temperature reached -2°C the agitator was noted to be juddering, and occasionally the drive belt slipped. This increased in frequency, until finally, it jammed solid, at the same time flow in one of the circulation loops stopped.

Cooling at this point was stopped and the chiller switched to heating mode. After 10 minutes the distributor could be rotated but with high resistance. Also the pump left in operation was not successfully fluidising the particles, the behaviour was similar to that in the initial test with 10%. As the temperature of the fluid reached 0°C it was noted that large particles were rising to the surface. These were much larger than those observed previously, their size close to the diameter of the outlet tube to the pump (~25mm). Initially these agglomerations were drawn into the pump, although blockage of the remaining loop soon followed due to several lumps locking together and obstructing flow. After the second loop finally became blocked the distributor came to a halt, probably due to the settled particles. The system was allowed to warm over night to ambient temperature.

Start-up of the pump loops could not be achieved the next day and the only option was to drain and strip the tank down. After clearing the loops the tank was reassembled, although provision was made for the distributor to be quickly removed for inspection. A second test of the 20% charge was started under the same conditions as the first. The behaviour was very similar except that one of the pump loops blocked before the distributor seized. The other pump was switched off while cooling was still applied, the top of the tank was dismantled to remove the distributor. This would not move at first so the chiller was set to 2°C to provide an appropriate rate of heating in the tank. After a few minutes the distributor could be moved slightly, and then came free. On removal from the system it was found that particles had bonded together and to the distributor, to form a cylinder matching the internal wall of the tank. The accretion adhered more strongly than had been observed previously with the rising agglomerations and could not be broken easily until warmed.

Analysis of this situation suggested that water was causing the particles to bond together in the low flow conditions found at the surface of the wall. The particles that rose to the surface were assumed to be formed under more turbulent, or less cold, conditions, hence their weaker structure. Attempts were made to reduce the free water in the system by the addition of some dry hydrophilic particles and operating the system at ambient temperatures for 24 hours. However, a subsequent cooling test failed in the same manner as before. It was apparent that the mixture had to be kept in a highly turbulent state during freezing conditions to inhibit, or at least reduce the production of agglomerations. This was a major problem and required a new design of the distributor.

4.4.3 Perspex Rig Modifications

The failure of the previous rig at 20% solids concentration was considered to be due to ice bonds forming between particles close to the cold surface of the tank wall. The test indicated that under highly turbulent conditions such particles were not formed (this had also been indicated by the preliminary test on the pumps, Section 4.3). The options available were (a) add more pumps in order to increasing the flow rate and hence the degree of turbulence, or (b) cause the flow to be limited a reduced cross section of the tank for short period, again increasing the turbulence of that zone but for a limited duration. The first option was rejected since it would increase the electrical demand of the system which would impair its effectiveness as a demand-side management device. Therefore it was decided to form zones within the tank by placing a number of vertical baffles in the tank with a single rotating disc at the base, to regulate the flow into the zones (Figure 4.7).

For test purposes a set of six baffles, equally spaced, were placed vertically in the perspex tank, and a disc with a single sector cut into it was fitted onto the drive shaft (Plate 1 - right). The single pump loop was replaced with two new loops containing heat exchangers. The new system was constructed and tested using the 20% mixture from the last set of tests with Fusus oils as the support fluid. Initial tests under ambient conditions were encouraging. The system was seen to force the slurry out of each of the zones as the distributor rotated. The same occurred during cooling and the system was found to be stable, no blockages occurred at a temperature of -2°C after prolonged operation (5 hours). During heating, large lumps were seen to rise to the surface as seen during the heating of the previous rig. These were large initially and fell back into their zones as the distributor moved round. The structure of the agglomerations seemed fairly weak as they could be broken easily with a probe. There was very little collection of material on the surface of the perspex tank; that which was present was thought to originate from the collection of settled material in the narrow 'V' where the baffles met. This was designed out in the new baffle system for the cold storage tank.

4.4.4 Cold Storage Device MK II

A new baffle system was designed and fabricated for the cold storage tank (Plate 2

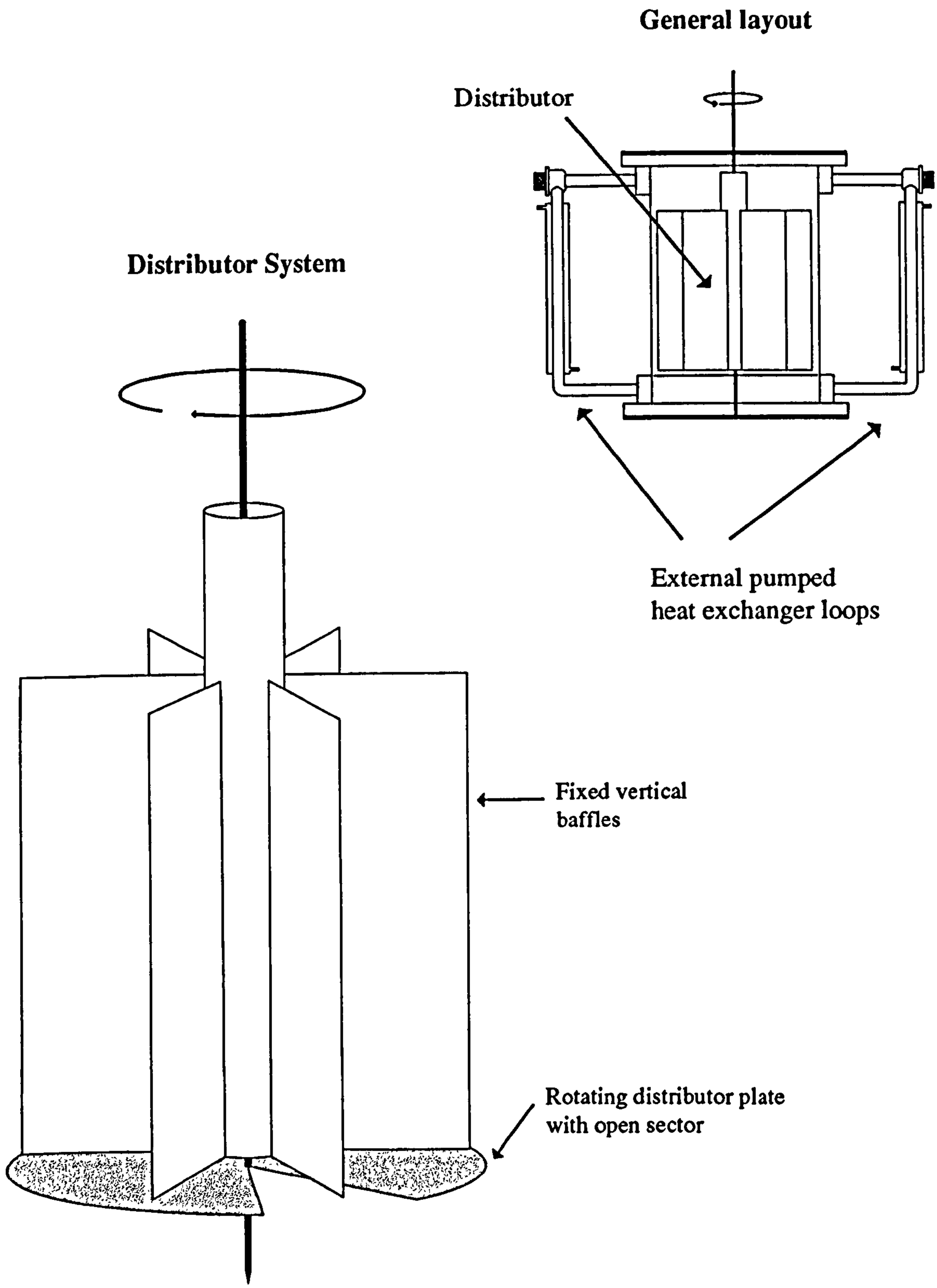

Figure 4.7: Details of the Modified Baffle System for the Cold Storage Tank.

(right), Appendix B3). The vertical blades were supported by the use of a cylindrical tube (diameter 50mm) which attached to the top plate of the tank. The relatively large diameter was used to avoid constricting geometries in the system, and only caused a reduction in volume of ~3%. The method of fitting the blades to the support tube allowed four, six or eight blades to be attached at even spacings. The distributor disc had an open sector of 70°, this could be varied by a closing plate down to 30°. An external heat exchanger was also designed for the tank that cooled both flow loops, but kept them separate. Some problems viewing the contents of the tank had been experienced during the previous test, so it was decided to run the tank in an open state. To support the baffle tube a bracket in the form of a cross was also constructed.

Thermocouples were placed at the top, middle and base of two opposing plates. Pairs of thermocouples were also placed at both the glycol inlet and outlet ports to the heat exchanger. Also still in use were the four thermocouples on the body wall. The system was filled with water for calibration, the volume was found to have increased to 34.75lt as a result of the addition of the modified pump loops and the external heat exchanger. The tank insulation was changed, instead of the loose fill of polystyrene beads, 19mm sheet AF/Armaflex was used, with a secondary layer of 50mm foil backed fibreglass sheet. Two semi-circles of 26mm thick cellular polyurethane board were used for a removable covering at the top of the tank. The insulation type was changed on account of the new heat exchanger (and resulting connections) and to simplify assembly (disassembly).

The chiller was set to just above 0°C and the tank allowed to cool. Once the system had reached 1°C the chiller was turned off and the tank allowed to warm via heat gains from the environment, the pumps and the agitation devices. A similar test was performed using a 30% ethylene glycol solution. Analysis of the data sets showed the average heat gain was 4.5(±0.7)$W \cdot K^{-1}$from the surroundings, and 23.4(±0.7)W from the pumps and agitation device. The increase in the environmental heat gains resulted from a lower thermal resistance of the applied insulation and the increased surface area of the system.

The tank was drained of its charge, dried, and filled with 24.3 lt of Fusus oil in preparation for the addition of 30% (by volume) of hydrophilic particles. These had been prepared in the same manner as those in Section 4.4.2. These were added to the oil in the tank until the level reached a previously made mark on the inner wall of the tank, indicating the total volume of the mixture was 34.75lt. The initial test of the mixture was carried out with the chiller set to -0.5°C. Flow in each of the channels was poor and as the contents approached 0°C the flow had almost stopped. There had been no large agglomerations drawn into the pump loops at this stage. It was also noticed that the flow appeared to be coming from all of the zones, even though the distributor was still rotating. A slight force was applied to raise the rotating distributor, this caused flow to take place in individual channels. The result of this sudden change in flow conditions was that the settled mass of particles in each zone rose, this surge of high density particles soon led to the pump inlet ports becoming blocked. The tank had to be drained, un-blocked and reassembled.

Before the 30% charge was re-introduced to the tank, the shaft position was adjusted to reduce the gap between the distributor disc and the base of the plates. This was done to ensure that flow only passed into one zone at a time as the distributor rotated (cf the need to raise the distributor shaft in the previous test). Flow was found to be stable, although below 0°C a build up of material was observed to occur at corners of the plates (Figure 4.8). The shape and size of the build up was independent of the zone in which it occurred. Cooling was allowed to continue down to -3°C and then the system was shut down.

A sample of the agglomerated material was collected to evaluate if free water was present. The structure was, as found before, fairly weak. As the sample warmed it became apparent that a large fraction of it was oil. This had been trapped in the macroscopic structure formed as the particles adhered to each other. No free water was seen to be present in the sample, indicating that formation of the structure resulted from surface water on the hydrophilic particles.

The tank was allowed to warm back to ambient temperature and the cooling test was performed again, down to a temperature of -5°C. Figure 4.9 shows the mean temperature of the fluid mixture in the system. The phase change commenced at just below 0°C but it is unclear as to what point it finished. The calculated change in the energy content of the mixture (Figure 4.10) shows again clear evidence of phase change occurring at 0°C. Estimates of the latent heat of the materials used in the system suggested a value between 1.8MJ to 2.2MJ. The energy-temperature curve (Figure 4.10) showed that this was not occurring at 0°C. The gradient of the curve was much higher below the transition temperature, this could only be explained if part of the latent heat was being released over a wide temperature distribution.

Once the system was below -5°C, the chiller was switched to heating mode and the data logging software started again. The flow behaviour of the system was similar to that of the cooling phase below ~0°C. Once phase transition started large agglomerations started to rise to the surface of the tank and when drawn into the pump inlets, temporary blockage soon resulted. These agglomerations were removed manually with a temperature probe, and flow continued for a while until larger lumps rose. These were pushed above the fluid surface, the effect of which was to reduce the level of the fluid at the pump ports to a point where air was entrained. This resulted in complete failure of both pumps virtually simultaneously!

The test was repeated several times under different conditions. The use of a single pump was tested but this too was found to push the large agglomerations to the surface, leading to failure. The angle of the opening in the distributor was changed but no observable benefits were found and failure occurred. The supply temperature of the heater was lowered to reduce the rate of heating, although as soon as the system reached the phase transition temperature large agglomerations rose as before and blocked the pumps. Finally the system was switched off for one hour between cooling (charge) and heating (discharge). This caused blockage almost instantly due to a high density of particles rising in each zone, although the particles appeared to be individual

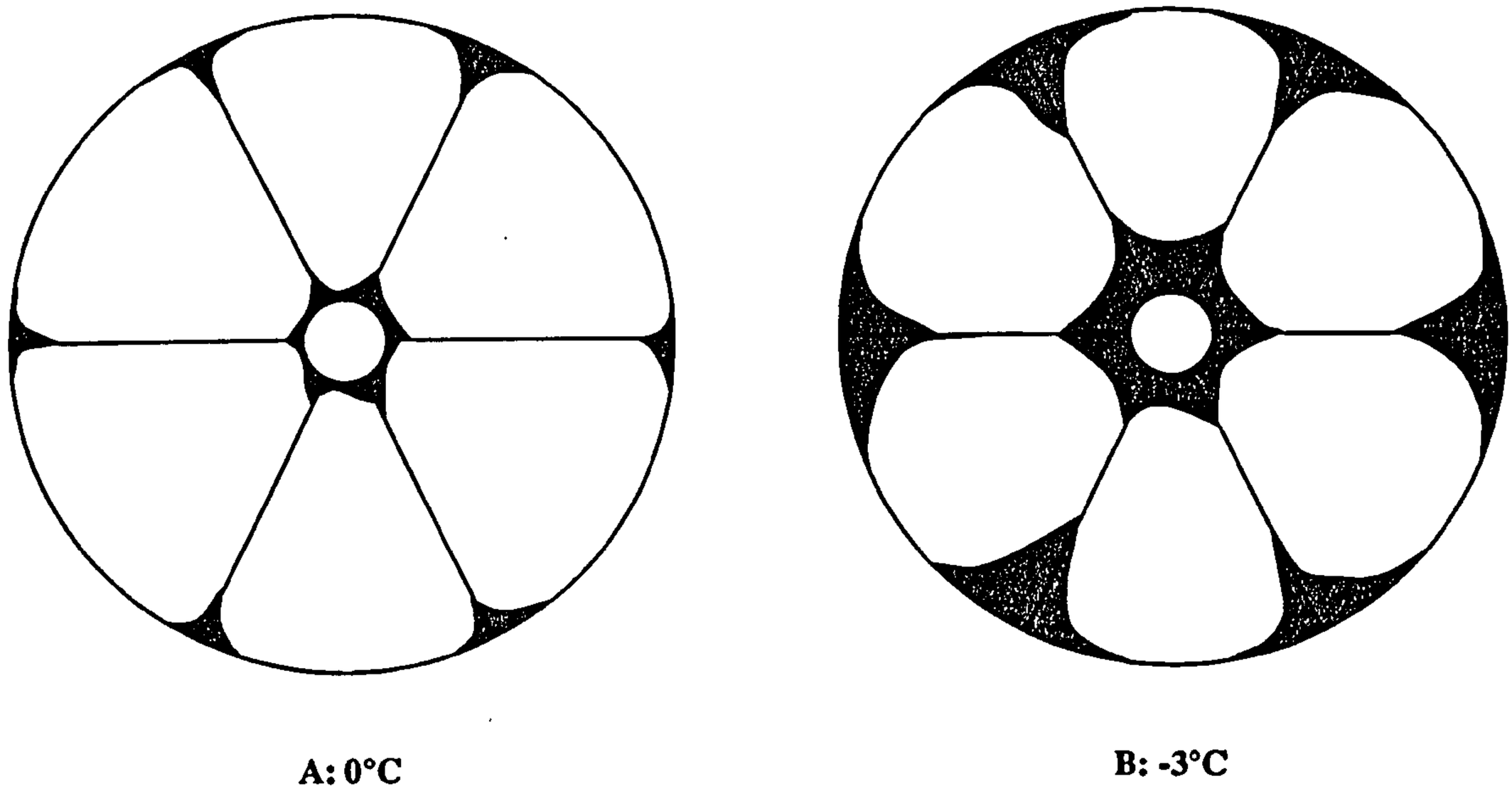

Figure 4.8: Plan View Showing Increase in Agglomerations of Baffled Zones as Temperature Decreased.

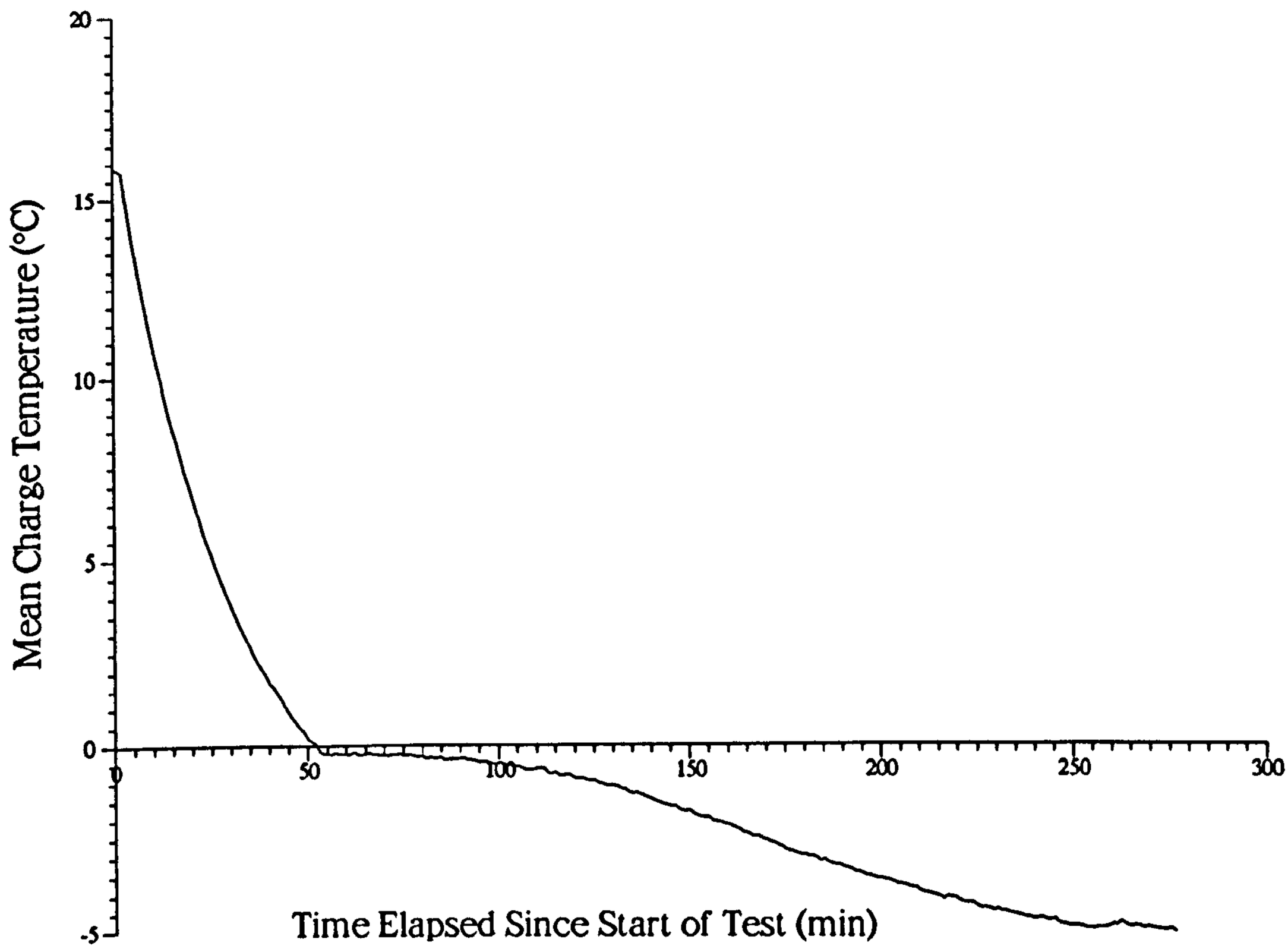

Figure 4.9: Mean Temperature of 30% Charge in the Cold Storage Device (MK II) During Cooling Period.

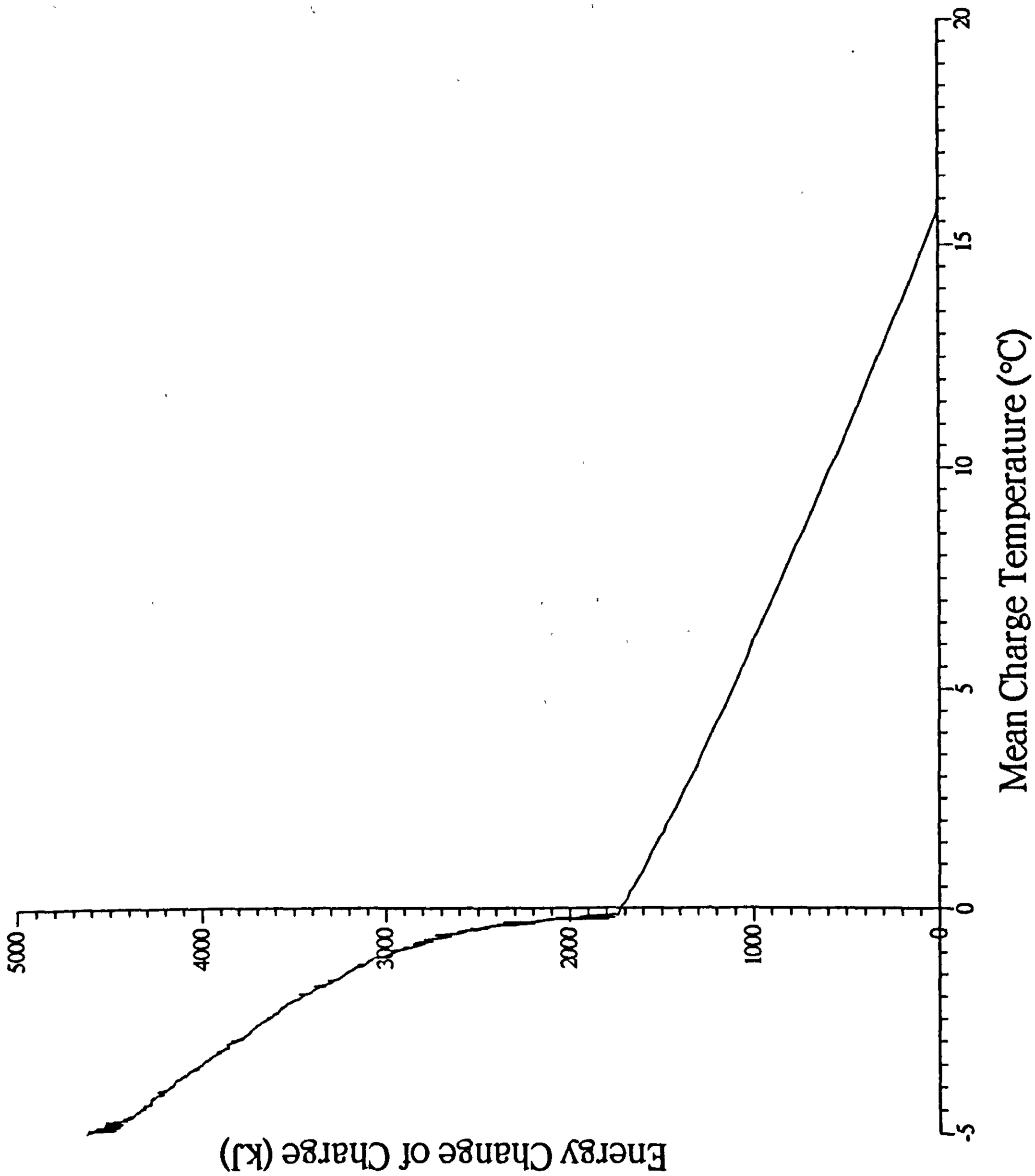

Figure 4.10: Energy Change of 30% Charge in the Cold Storage Device (MK II) During Cooling Period.

as opposed to agglomerations. The method of attempting complete fluidisation of a hydrophilic based cold store was therefore abandoned and a new approach was sought.

4.4.5 The Cold Storage Device MK III (A Feed Based System)

The limited success of the fluidising cold storage units caused a reassessment of the method used to mobilise the store. The fact that the pumps used operated well for solids concentrations up to 30% was significant. This suggested that if higher densities were required in the main store then a method of feeding the agitation/heat-transfer system, at suitable concentrations, had to be found. To achieve this the settling nature of the particles in the fluid was exploited using a method that fed settled particles into a turbulent steam of clear fluid. This passed the resulting mixture through a heat exchanger and returned it to the top of the tank (Figure 4.11). The fluid and particles were separated at this point, the particles falling on top of the remaining settled mass while the clear fluid was pumped around the system again.

This design had a number of advantages over a fully fluidising device. Firstly, the rate at which the feed device was operated would control the solids concentration passing into the heat exchanger. This could effectively regulate the rate at which the store was charged. It also meant that the feed rate could be varied as the store was cooled or heated to maintain a maximum rate of heat transfer for the existing slurry properties. Secondly, at zero feed rate the circulation system would be cleared of particles making maintenance much simpler. Thirdly, the behaviour of the transmitted slurry would be independent of the geometry of the storage part, hence the system would be relatively easy to scale up. Fourthly, the potential for pumping only in the loop containing the clear fluid would enable the use of well developed high efficiency single phase pumps. Finally, the circulation loops could be feasibly extended to any extent, allowing the slurry to be distributed over a range of distances.

A system was designed similar to that shown in Figure 4.11 (Appendix B4), although for test purposes a second pump was added onto the slurry-side of the circulation loop. The design of the feed mechanism was based upon construction considerations, which suggested a final arrangement where the outer diameter for the feed device was 80mm. The drive shaft diameter was 25mm and the pitch for the feed helix was 20mm. Hence the maximum volume displaced for each rotation of the device was ~0.9lt. Using an estimated flow rate of ~0.5lt·s^{-1} from the pumps, a concentration of 30% would require a volumetric feed rate of 0.25lt·s^{-1} of the settled mixture, hence the drive shaft had to rotate at ~15rpm.

The main part of the tubular tank had a diameter of 300mm, and a height of 970mm. The volume available for settled particle storage, including the feed section, was estimated to be 46lt. This allowed for a vertical separation between the surface of the settled particles and the clear fluid outlet of 170mm. Also the design gave a depth of 100mm of fluid above the outlet port, to avoid air being entrained as occurred in previous systems. The intention was to restrict all heat transfer to occur in the external

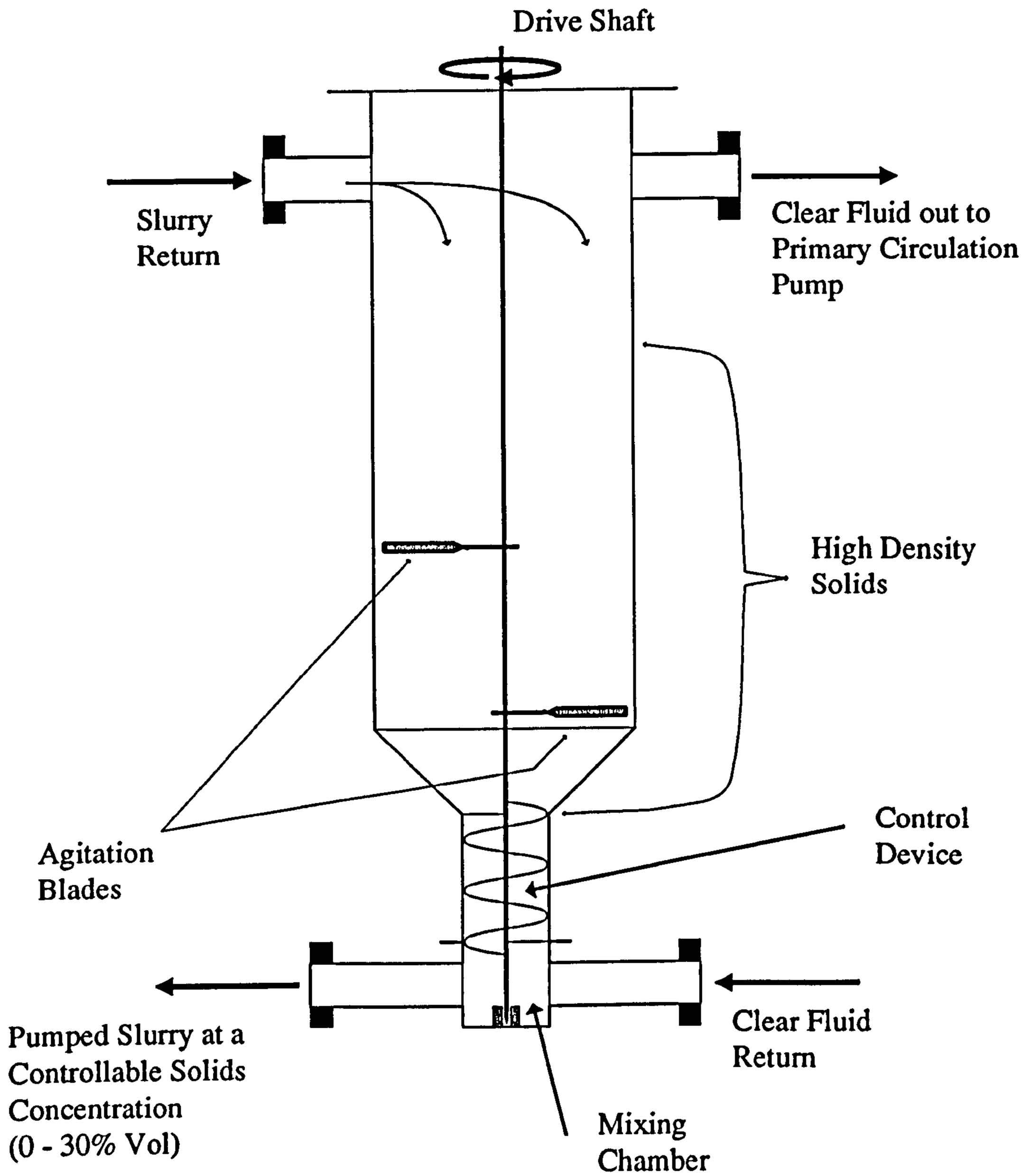

Figure 4.11: Schematic Layout of Feeder Based Cold Storage Device.

circulation loops. These consisted of 28mm copper tubing, with fittings added for the placement of thermocouple probes to measure the mid-stream fluid temperature. These were placed at the inlet and outlet of (a) the main tank, (b) the mixing chamber, and (c) the outer annuli of the heat exchangers. The heat transfer sections were of a concentric tube type, with an active length of 1.58m, giving a total heat transfer surface of ~0.14 m^2. At an estimated flow rate $0.5 lt \cdot s^{-1}$, a mean fluid temp of 0°C, and mean wall to fluid temperature differential of 5°C, values of $h \sim 500 W \cdot m^{-2} \cdot K^{-1}$ were estimated (Equation 2.39). This would give heat transfer rates of 350W at 0°C compared to estimated heat gains of ~50W. This was sufficient to cool the systems enough to check the principles of operation (the design allowed easy replacement with alternative heat exchangers, to increase performance if desired).

With the earlier cold storage systems it had been observed that the insulation had been compressed, reducing its thermal resistance. This would be more severe with this system due to the increased mass, and the reduced area of the base. Furthermore it would not be very stable. The design incorporated three brackets on the main body of the tank that would accept ½ inch diameter rods. The use of adjusting nuts on the rod ends allowed the tank to be maintained level. The rods avoided thermal bridging between the tank and the ground (Plate 3).

The device was partially assembled to test the feed rate of solids into the mixing chamber (this was left off and a bucket used to collect the solids). A mass of fully hydrated hydrophilic particles was placed in the main tank, and the motor used to turn the feed helix a few times. The material falling from the system was collected, the mass recorded, and then replaced at the top of the tank. Rates of discharge were much lower than expected at 33(±2) grams per revolution, in terms of volume this was an order of magnitude lower. The tests proceeded, as it was believed that; (a) the support oil would assist the movement of particles through the feed device, and (b) the pumps could be controlled to create a pressure differential between the main chamber and the mixing chamber to enhance the feed rate.

Once the system had been fully assembled, the re-hydrated particles were added followed by the support fluid (Fusus oil). A new method of removing the excess water from the particles employing a centrifuge was used (Section 6.3). The chiller unit was connected to the heat exchangers, and for initial test purposes the system was wrapped in foil backed fibre glass blankets. The system was run initially at ambient temperature with both pumps full on and the feed device set at a rotational speed of 60rpm. Inspection of the flow at both the top of the tank and clear connections at the pumps, suggested that the system was working as required. It was noted however, that a small fraction of the particles were not settling out between the inlet and outlet ports at the top of the tank, and were being drawn back around the system. The system was stopped and some tubular inserts were added to divert the flow and create conditions similar to those found in a cyclone (Figure 4.12).

When the tank was next started it was found that the inserts were very effective at separating the support fluid from the particles, although after several minutes of

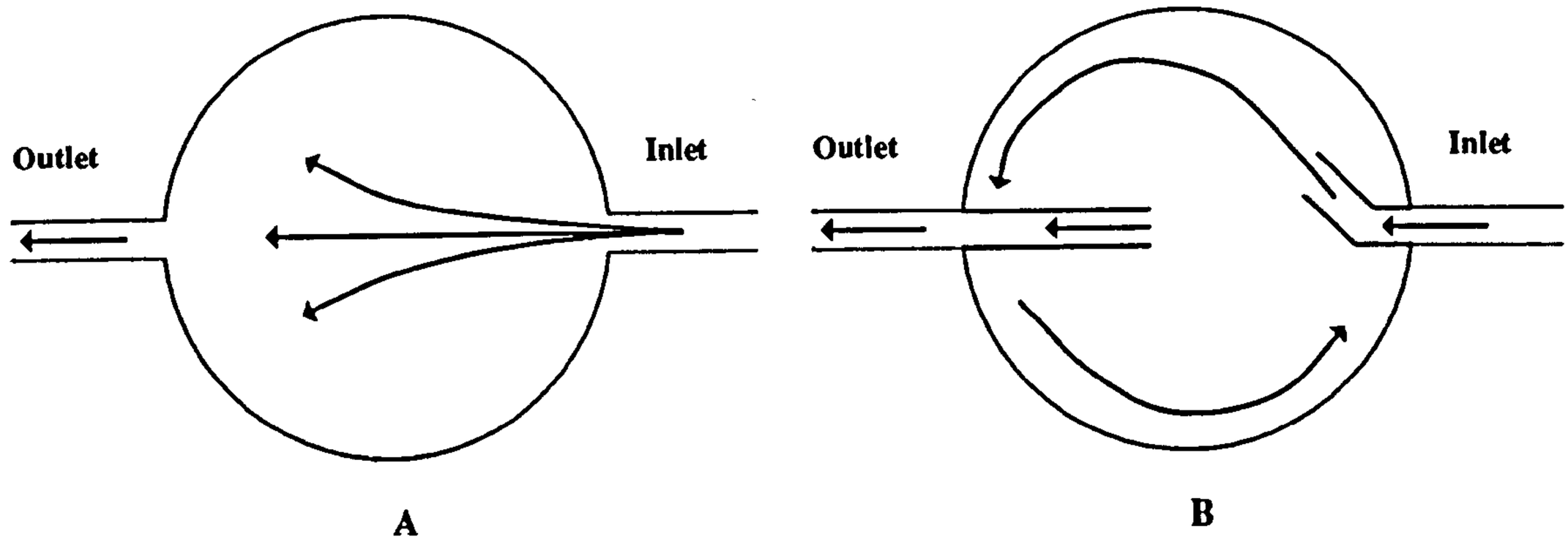

Figure 4.12: The Flow Pattern (a) Initially, (b) After the addition of Inserts.

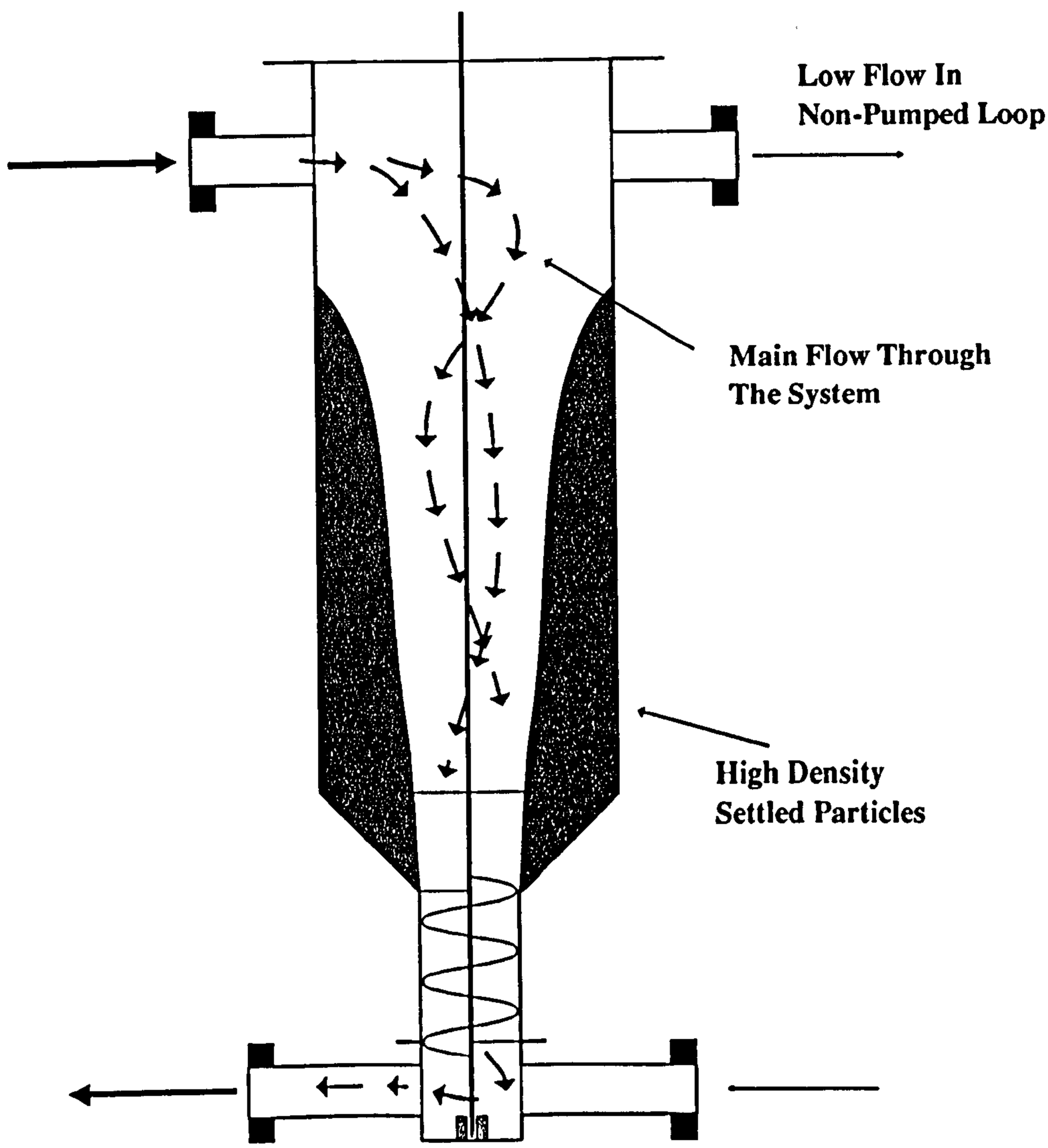

Figure 4.13: Channelling Occurring in Cold Storage Device MK III.

operation the particle concentration of the return flow was very low. The rotation rate of the distributor was increased to 120rpm, but little benefit was observed. This suggested that the discharge rate from the feed device was actually lower than that measured with out the support fluid. The ac voltage to the pump on the clear fluid side was decreased, using a variable transformer, to try and induce a pressure differential between the mixing chamber and the main chamber. The motor of the pump was a shaded pole type, this did not respond well to variation in voltage and control was not possible.

Instead the pump was simply turned off. This resulted in a drastic change in the conditions. A large burst of particles were seen to be returned to the top of the tank, although this decreased to a lower, stable state after a few minutes. The pump in the clear fluid loop was seen to be turning, which indicated that the slurry was still flowing. The system was set to cool and a thermocouple, attached to the end of a 1m long rod of PTFE, was used to measure the temperature at various depths and radii of the main tank. As the tank cooled it became clear that it was not behaving as expected. Temperature measurements indicated that the main flow of the fluid-particle mixture had formed a channel though the centre of the system (Figure 4.13). The majority of the particles appeared to have settled and formed a conical shape in the main body of the tank. This was confirmed after draining the system.

4.4.6 Modifications to MK III

Modifications were made to the rig to overcome the forementioned problems. The first of these was to replace the small diameter feed helix with one of diameter 298mm located just above the lower ridge in the main tank (Figure 4.14, Plate 3). This had a pitch of 20mm and had 1¼ turns. The lower inlet port of the tank was re-located to be just below the new feed plate. Its entrance was changed from being normal to the circumference of the tank, to entering at a tangent, so that the fluid rotation impinging on the lower plate would result in downward deflection. Similarly, the return flow to the top of the tank was at a tangent to the circumference of the tank body. This was to produce the cyclone effect that proved effective in the initial tests (A removable extension of the outlet port at the top of the tank was made to complete this). Finally two throttling valves were added to both the inlet and outlet ports at the base of the tank, to enable the inducement of a pressure differential between the volume of settled solids and the mixing flow.

On return of the modified parts the tank was partially reassembled and tests were made to determine the feed rate for the particles as previously described. The results were encouraging, giving a feed rate of 3.1(±0.2)kg per revolution. This suggested a rotational rate of ~3rpm would be required to achieve a 30% solids concentration in the flow. This was below the minimal rate achievable with the motor and pulleys, although tests with the previous rig suggested that discharge rates would be lower once the support fluid was added. After full assembly of the modified system the previously used charge (mixture) was returned to the tank. Care was taken doing this so as not to cause solids to be flushed into the narrow mixing chamber.

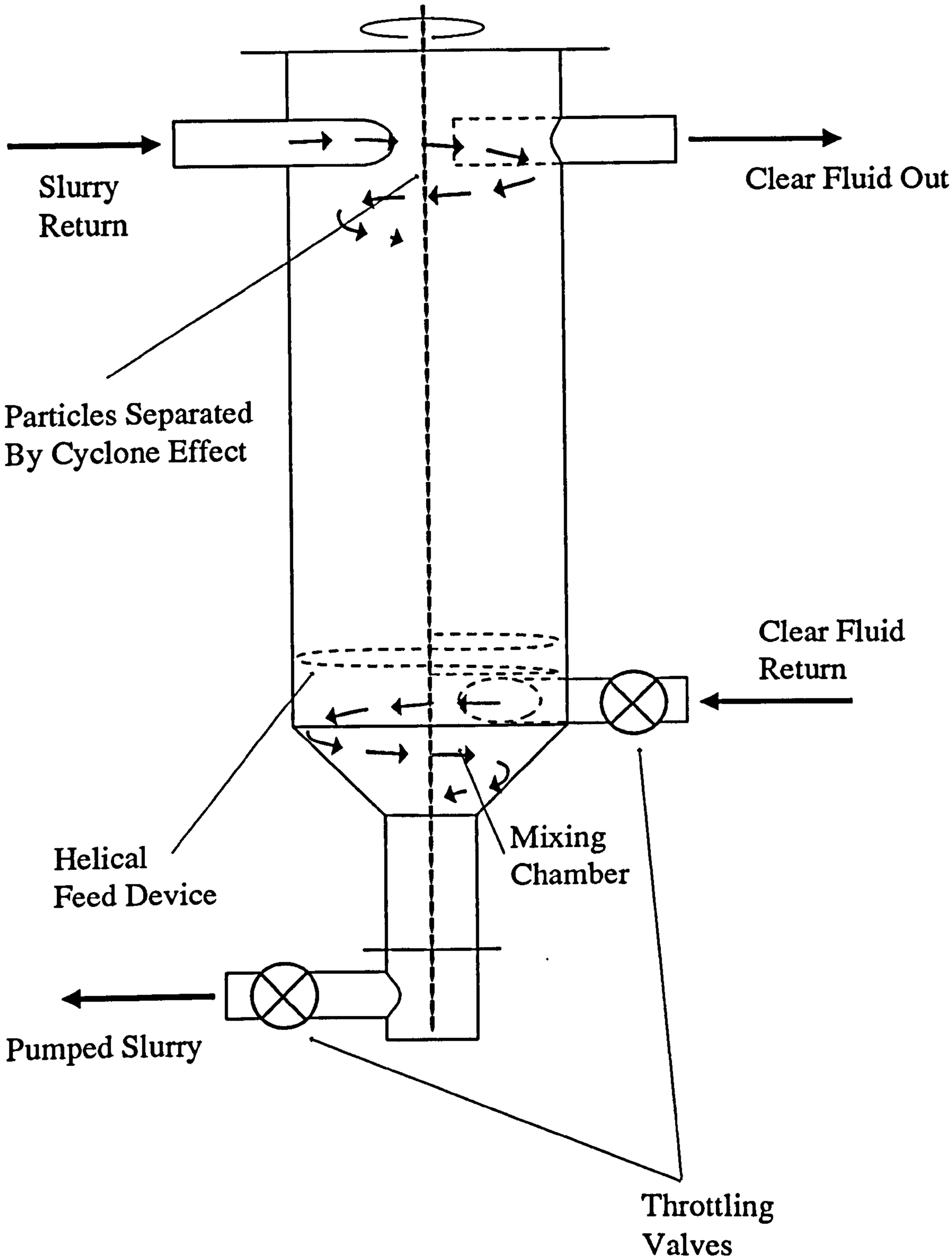

Figure 4.14: Schematic Diagram of the Final Design of the Feed-Based Cold Storage Device.

PLATE 3

The start up of the tank was performed by engaging both pumps, but with the distributor drive stationary. This was to ensure that no solids were discharged into the flow causing blockage. Both of the throttling valves were fully open. Under these conditions it was observed that a general rise in settled mass was occurring, indicating that the pressure in the mixing chamber was too high. The throttling valve on the clear fluid side was slowly closed until some particles were entrained in the flow. The rise of the settled mass had stopped and it was assumed that all particles were coming from the feed plate. The valve was opened a little until particles were no longer seen in the returned flow. The pressure differential across the plate was now assumed to be close to zero. On start up of the distributor, particles were seen to be returned to the top of the tank, indicating that the feed device was working. On shut down of the feed device particle return to the top of th tank soon stopped. This was performed with a number of rotational rates. All rates showed good start and stop behaviour, and from observation the rate of particle feed rose with rate of rotation. The system was allowed to settle overnight.

The same start up procedure was followed the next day although the valves were left in their original positions. After an initial burst of particles, solids were no longer seen in the flow around the loops. The source of these particles was either from material that had fallen from the feed plate overnight, or due to an imbalance in the differential pressure across the feed plate while the pumps started. Activation of the feed device produced a controllable feed rate of solids to the system as noted previously. The device was shut down and an insulating cover (foil backed fibreglass) was applied. The chiller unit was connected and the system started again.

The feed rate was set at a low setting (~15rpm) and the device cooled. To check the temperature of the system at different depths and diameters, a probe was used. The general trend found was; (a) initially the highest temperatures were at the outer surface, these dropped to a minimum as the probe moved towards the centre, and then up again at the centre; (b) vertically temperatures rose as the probe was lowered, indicating that warmer material was being cooled and returned to the top of the settled mass; (c) as the test progressed the highest temperatures were found at the centre of the tank, indicating that little movement was occurring in the middle of the tank.

As the system reached 0°C particles failed to completely separate at the top of the tank. The quantities involved were small and gave no problems at this stage. It was assumed that these were fine particles (<1mm diameter), their smaller size not allowing them to settle at a high enough rate to separate from the fluid. The oil level was also noted to have dropped slightly, although not enough to cause air to be entrained into the inlet port. When the temperature of the fluid had reached -3°C the settling rate appeared lower and more particles were drawn into the outlet port at the top of the tank. The motor to the feed unit was stopped. The concentration of particles returned to the top of the tank reduced but did not stop. The cause of this was seen to be the stirring of the settled mass, which appeared to have risen to a higher level than the start of the test. This was considered to be due to a general decrease in the settling rate of the particles because of an increase in viscosity of the oil, increased density of the oil, and a

reduction in the density of the particles due to freezing, or the formation of lose agglomerations. The pumps were shut down and the system allowed to settle for an hour.

The temperature probe was used to determine the temperature distribution throughout the system before it was restarted. The measurements showed that the bulk of settled particles were at 0°C, the outer regions were above this due to the flow of heat from the outer surface. All material was found to have settled and the height of the surface decreased. Only the pumps were started at first, and after an initial flow of particles decreasing over a few minutes, none were seen to be entrained. The top surface of the the settled particles was agitated by the flow, although not to a degree that caused particles to be drawn into the outlet. The agitator was switched on and particles were again fed into the system. These separated well at the top of the tank. The chiller unit was switched back on in heating mode and the system allowed to heat. The temperature of the return flow was taken up to 8°C, by which time all probe measurements indicated that the solids in the system were above 4°C. The system was shut down.

To overcome the problem of excess agitation at the top of the settled particles several iterations were performed to reduce the flow rate of the fluid. To achieve this the throttling valve on the outlet of the mixing chamber was closed slightly. After this operation the other throttling valve was adjusted to balance the pressure differential as described above. After a degree of adjustment the distributor system was switched back on and found to be stable. The chiller unit was used to cool the contents again. During this cooling test the problem of the surface material being excessively agitated was significantly reduced, and although not fully cured, did not cause a failure of the system. The test was continued until the particle bulk contained in the system had dropped below -2°C. The system was again stopped and allowed to relax for an hour. Start up of the unit was successful and again no problems were encountered during the discharge phase. The test has been repeated since and no problems have been encountered.

4.5 Discussion

The work reported in this chapter was undertaken to investigate methods of mobilising phase change particles forming the active medium of a thermal energy store device. The initial approach was to fluidise the entire contents of a storage unit with a suitable supporting fluid. This found a degree of success although the achievable concentration of solids was limited. This in turn prohibits the maximum energy densities of such a system, making them unsuitable for thermal energy storage applications.

The second approach adopted was to continually feed a high density particle bed into a turbulent stream. This provided a slurry with a controlled solids concentration. This slurry could be pumped to external heat exchangers allowing the contents of the system to be cooled. The solids were returned to the high density particle bed after passing through a cyclone, this allowed the clear fluid to be passed on and reused at the feed

device. This system proved stable at all of the temperatures tested.

The system can be considered of consisting of three components, (i) the main storage vessel, (ii) the distribution unit (feeder) and, (iii) the separator (cyclone) unit. The maximum energy density of the entire system is limited only by the packing density of the solids within the storage vessel, this is a function of the particle size distribution used. Another advantage of this system over the first approach is that the phase change slurry can be pumped to the point of application.

All heat transfer to the storage medium is external to this device which enables the choice of heat exchanger units to be made to achieve the desired performance (charge/ discharge time) of the system. For thermal engineering applications it is recommended that further investigations are made regarding the distribution unit and the separator, to increase performance and produce design data (See Chapter 7).

Chapter 5

The Heat Transfer Test Rig

5.1 Introduction

This chapter describes the design, construction and calibration of the components used to construct the heat transfer test rig. The main purpose of this device was to collect detailed heat transfer data on a number of phase-change slurries with hydrated hydrophilic solids as the phase change component.

The review of the literature in Chapter 2, concerning the heat transfer to and from slurries, concluded that very few works to date had experimentally investigated the heat transfer coefficients of phase change slurries while phase change occurred. The few that did showed an enhancement in heat transfer coefficients, at the transition temperature, above that found for the single phase support fluid alone. None provided any analysis that would allow the performance of hydrophilic base slurries to be predicted. To this end, the design of the heat transfer test rig aimed to achieve a sensitivity great enough to allow the measurement of the heat transfer coefficients to the single phase support fluid. Design considerations supported the use of tubular geometry for ease of construction, and for comparison with existing single phase correlations.

The experimental method adopted was to find the solution for $\bar{h}$ in the standard convective heat transfer equation

$$q_{conv} = A\bar{h}\Delta T \tag{5.1}$$

where A is the area of the heat transfer surface and ΔT is the temperature difference between the fluid and heat transfer surface. This temperature difference is not constant for a tube geometry; it changes along the axis (direction of flow) because of the energy that is transferred between the surface and the fluid. One method of accounting for this variation is to use what is called the *log mean temperature difference*, ΔT_{lm} (Incorpera, 1990). This is derived through the integration of the changes in energy along the tube and is given by:-

$$\Delta T_{lm} \equiv \frac{\Delta T_o - \Delta T_i}{\ln(\Delta T_o/\Delta T_i)} \tag{5.2}$$

Here T_o and T_i represent the surface to fluid inlet and surface to fluid outlet temperature differences respectively. The derivation of this equality makes the assumption that the surface temperature is constant, and that there are no discontinuities in the physical properties of the fluid (Incorpera, 1990).

Inspection of equations 5.1 and 5.2 shows that to calculate the mean heat transfer coefficient requires a measurement of the rate of energy flow across the surface, the surface temperature, and the inlet and outlet temperatures of the fluid. Furthermore to relate h to other data the flow rate must be known. The two heat transfer correlations used for comparison were that of Sieder (1936) (Equation 2.36) and Petukhov (1970) (Equation 2.37). It is stated (Incorpera, 1990) that use of Equation 2.36 can lead to errors of ±25% in the predicted value of h compared to ±10% for Equation 2.37, so the data measured on the rig had to allow the calculation of h to within these errors. The ability of this rig to achieve this is discussed in Section 5.3.

5.2 Total System Design

To measure the heat transfer coefficients of the hydrophilic based slurries, various parameters were measured around a circuit, part of which included a heat transfer test section as described in Section 5.2.1. Cooling energy was supplied to the heat transfer test section by a pumped brine circuit, which was continually cooled by a chiller unit (Conair Churchill TCW9). The slurry started in a stirred bulk holding tank, this tank provided a thermal mass to the slurry circuit and enabled mass flow rate measurements to be taken with (a) minimal change to the slurry head, and (b) minimal thermal impact upon measured data from the returned slurry sample (see Figure 6.1, Plate 4). From this tank the slurry was pumped by four identical pumps (Section 4.3), connected in series, to the heat transfer test section via a throttling valve. By selecting the number of pumps in operation and adjusting the valve the mass flow rate through the test section could be varied.

The inlet and outlet temperatures of the slurry were measured at the centre of the tube with thermocouple probes (Type E). The inlet temperature of the slurry was measured at one point, just before entry to the heat transfer test section, although the outlet temperature was measured at two places, after exit form the heat exchanger and 2m down stream. The second outlet temperature measurement was made to check that the fluid and solid particles were in thermal equilibrium at exit from the heat exchanger. The slurry then continued around the loop and passed through a 2m rheological test section, the first 1m of which was designed to allow flow conditions to stabilise prior to measurement of the pressure drop in the second 1m section. The slurry next passed through a 2.5kW electric in-line heater that acted as thermal balance load, when steady-state conditions were required. Before returning to the bulk tank, the slurry passed through a chute mechanism which allowed it to be drawn off for a selected period so the mass flow rate could be measured.

5.2.1 The Heat Exchanger Test Section (HETS)

This was designed to measure the heat transfer coefficients of various phase change slurries. As stated in Section 5.1, little published research was found concerning experimental investigations of active phase-change slurries, so the work undertaken

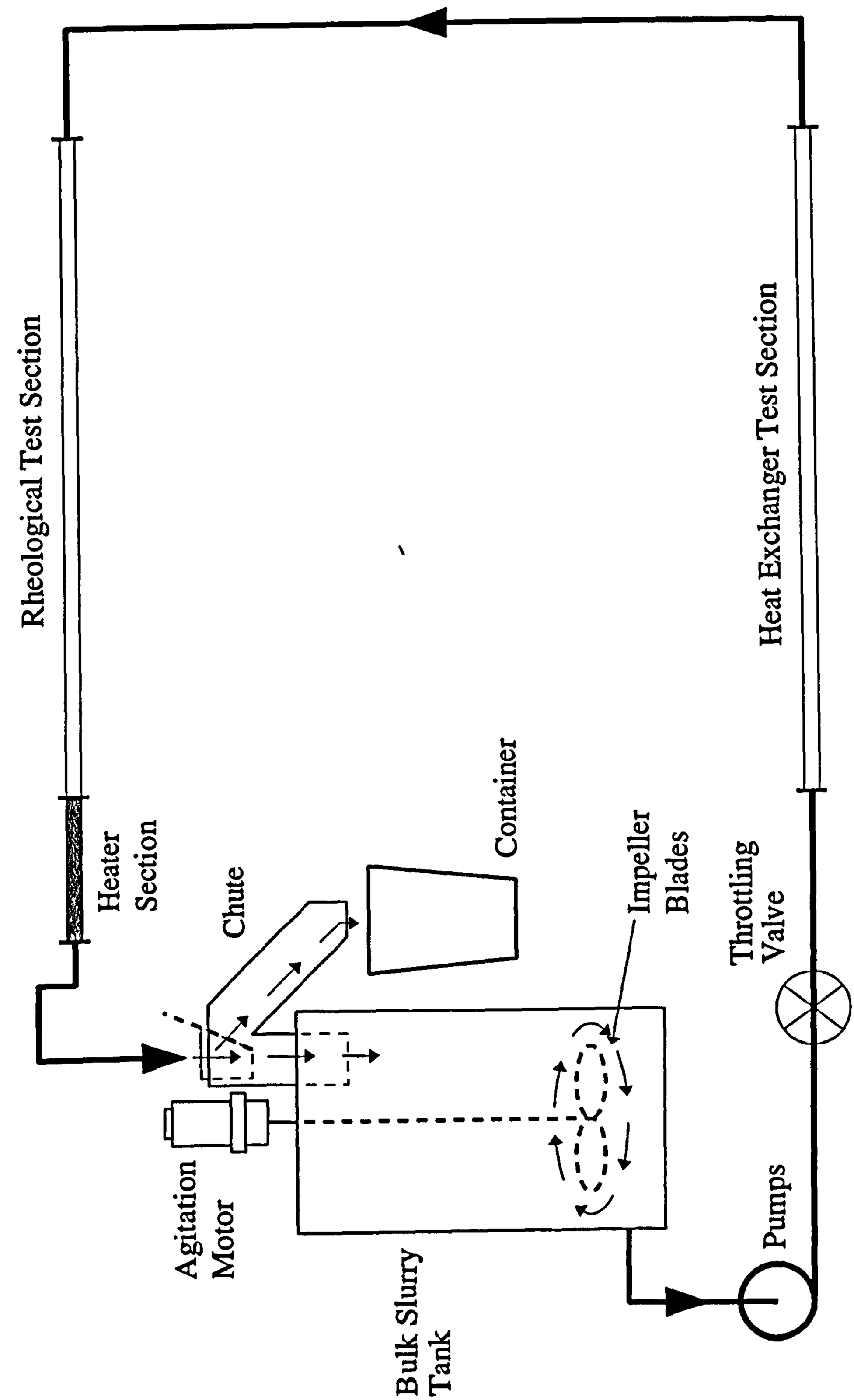

Figure 5.1. Schematic Layout of Slurry Flow in Thermo-Rheological Test Rig.

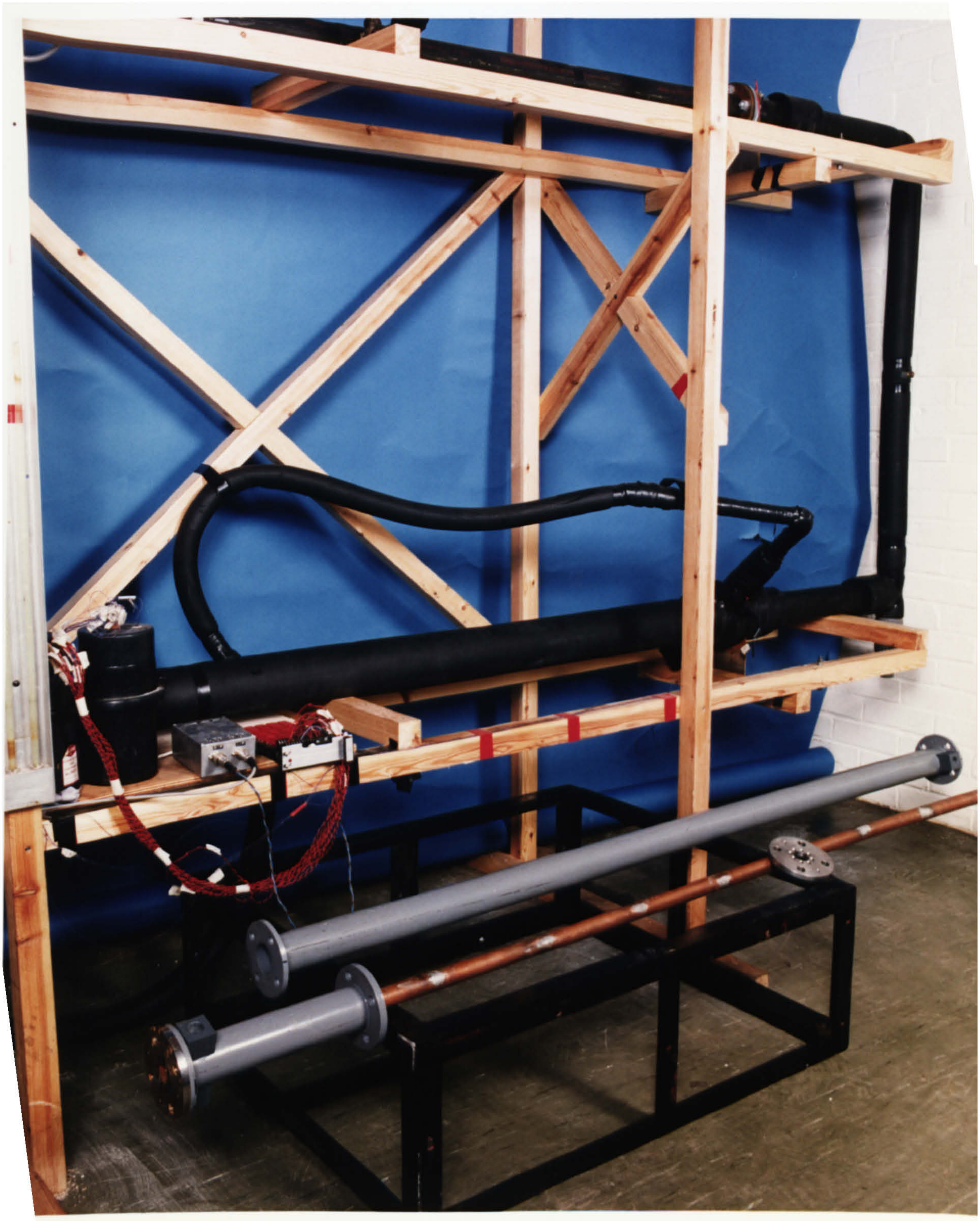

PLATE 4

here was of a fundamental nature. To enable the findings to be compared with the heat transfer coefficients of single phase systems, the test programme was focused on the behaviour of the slurries in long tubes. The type of heat exchange test section chosen was concentric circular annulus, with the slurry flowing on the inside. This required (a) a length-to-diameter ratio of >60, (b) either a constant T_w(wall temperature) or a constant rate of energy transfer to be achieved, and (c) knowing the temperature variation of the heat transfer surface (T_w).

The high thermal conductivity and relative low cost of drawn copper tubing made it the first choice as the core of the heat transfer test section. As a maximum limit in the design procedure the standard pipe diameter of 28mm was chosen, leading to a test section length of two meters (criterion (a) above). For the measurement of temperatures around the system, type E thermocouples were employed (see Section 5.2.2). Accurate measurement of the temperature of the heat transfer surface is critical to knowing the heat transfer coefficient. The greatest practical design problem was how to attach the thermocouples and yet ensure the outer annulus remained closed and sealed.

The final design consisted of six main parts (a) the inner tube (heat transfer surface), (b) the short outer casing, (c) the long outer casing, (d) the closing plates, (e) diameter reducing inserts and (f) the thermocouple plate. A cross section of the assembled heat exchanger is shown in Figure 5.2 and engineering drawings are provided in Appendix B5.

In addition to permitting the calibrated thermocouples to be positioned along the length of the heat transfer surface, this design had a number of other benefits. The first was its ability to use a range of inner tube diameters, of which three were built 28mm, 21mm and 16mm. Secondly by using a selection of diameter-reducing inserts, the ratio of the outer to inner diameters of the annulus could be kept reasonably close whatever inner tube diameter was chosen. By doing this the heat transfer coefficient, on the glycol side of the inner tube, was kept consistent. Finally two operational modes existed, counter flow and parallel flow. The second of these modes was used because of its tendency to produce an even wall temperature (criterion (c) above).

Assembly of the heat exchanger had to be performed in a specific order. This is summarised below and is also provided to emphasize the flexibility of the test section design:-

i) The short outer casing was placed over the inner tube after tinning a small area of the outer surface of this heat transfer tube (at the location for each of the thermocouples). (To avoid distorting the inner tube, all soldering must be performed using the lowest heat possible). The thermocouples were passed through the access hole on the short outer casing, and the thermocouple plate sealed in place. The ends of the thermocouples were soldered onto the inner tube at their correct location. Care was taken not to damage/burn the short outer casing.

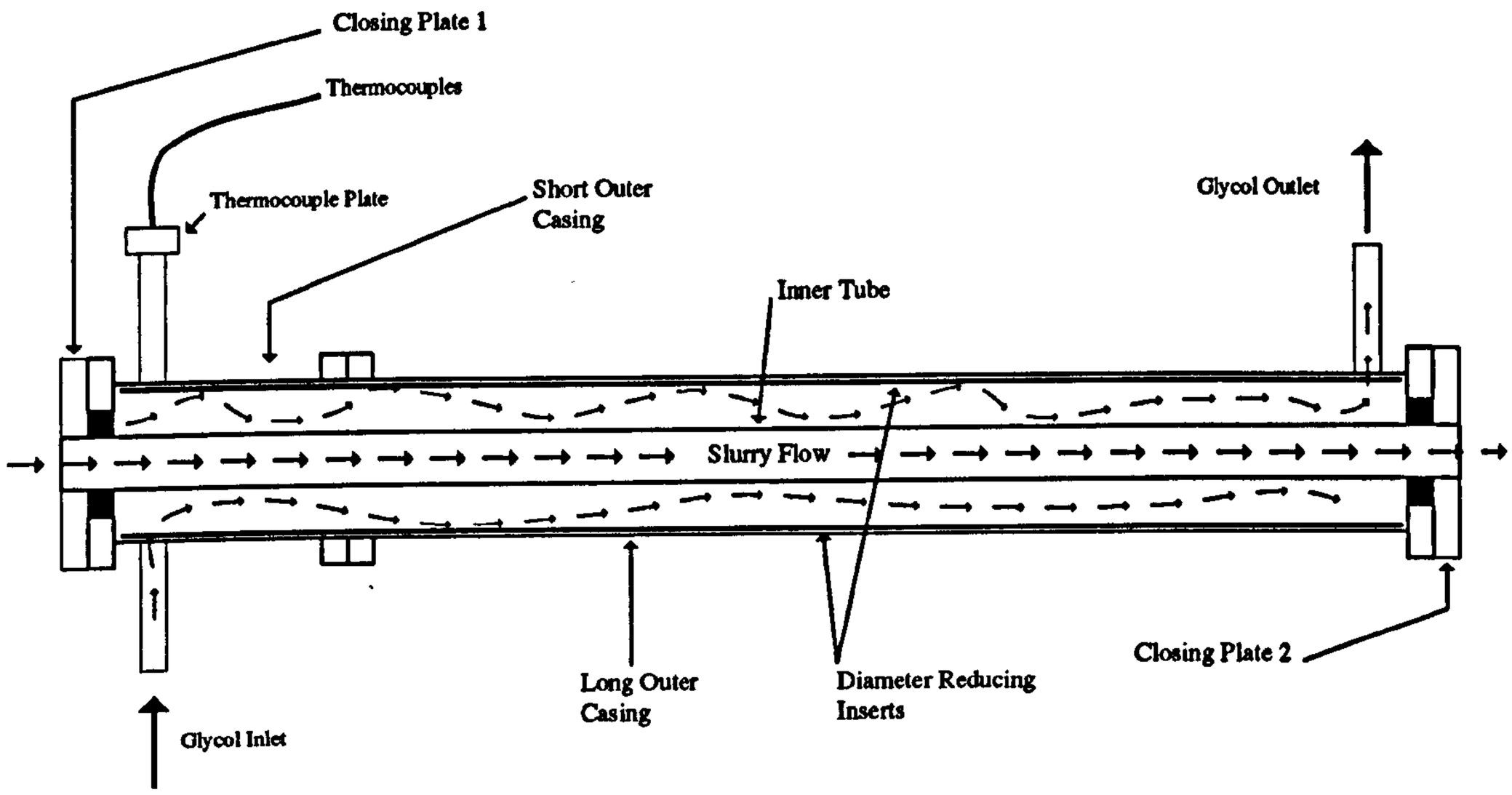

Figure 5.2 Schematic Cross Section of the Assembled Heat Exchanger.

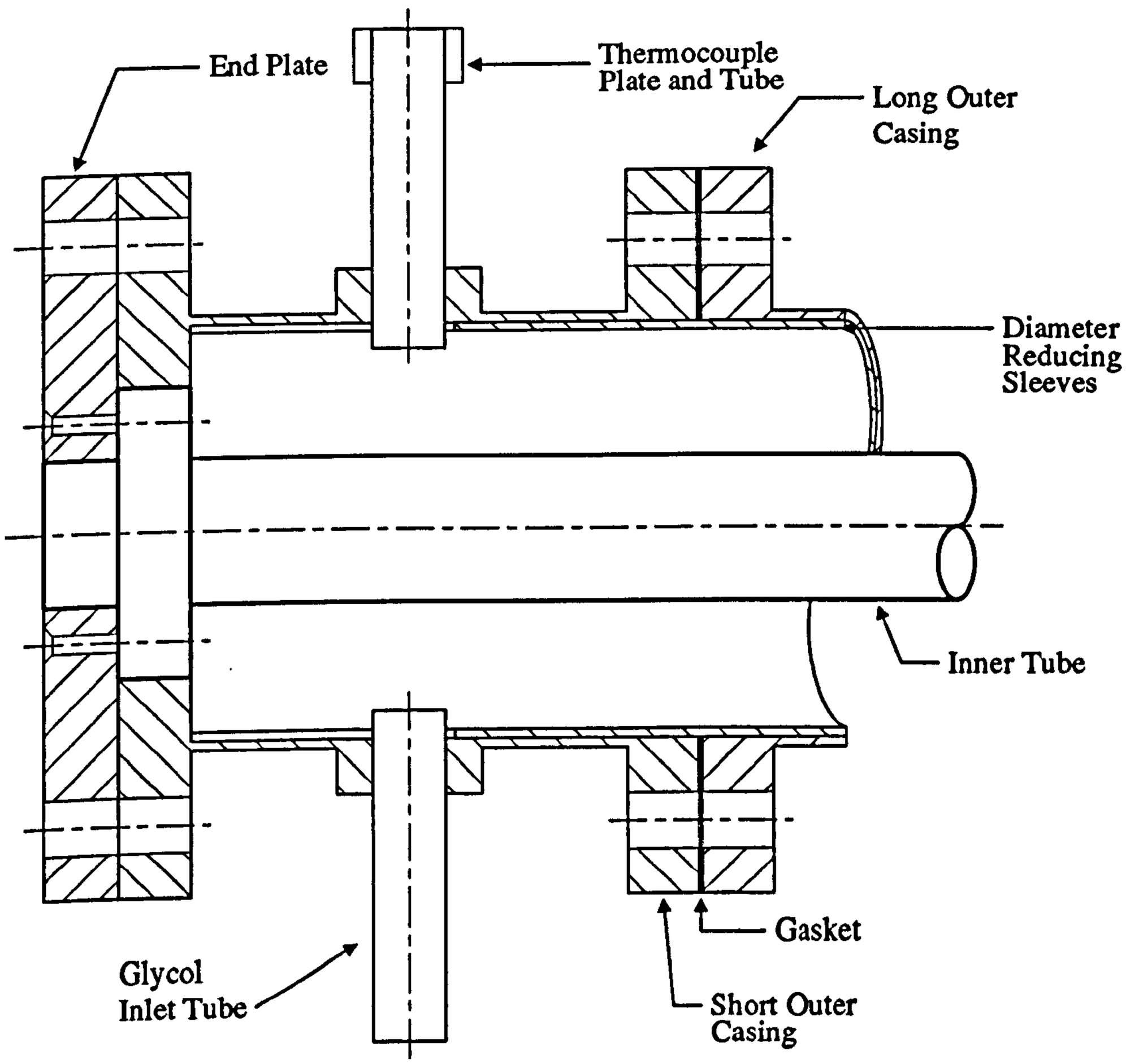

Figure 5.3 Detailed Cross Section of End of Assembled Heat Exchanger.

ii) Once the soldering was complete the inner tube and the short outer tube was connected using one of the closing plates. To ensure no leakage from the cooling circuit, silicone sealer was used between connecting surfaces. Figure 5.3 shows a detail of the assembly at this stage.

iii) Any reducing sleeves required were added at this point making sure that one of the recesses in one of the sleeves was aligned with the supply hole in the short outer casing. Great care was used so that none of the thermocouples was trapped or damaged.

v) After placing the central gasket in position the long outer casing was added. Finally the second end plate was fixed in position. Before placing the completed heat exchanger into the slurry circuit, the glycol circuit was connected and checked for leaks.

5.2.2 Thermocouple Selection and Calibration

The choice of temperature transducer for the heat transfer surface was limited, as discussed earlier, to thermocouples. There are a range of thermocouple pairings available, each with its particular use. Their application to this system required that they provided maximum accuracy and resolution in the temperature range 30°C to -20°C, and that their output was as high as possible (ie in μV/°C). Initial inspection of thermocouple tables (TCL Ltd, 1988) showed that the best selection was type E (Nickel-Chromium/Copper-Nickel). This was also confirmed via ESDU 82035 (1983). This work contains a selection flow chart and following this to its conclusion gave Type E as the most suitable pair.

The type E thermocouple pair had both the desired operational temperature range (-200 to 900 although this range is limited further by insulation material used) and the highest output per unit temperature (at 0°C ~ 60μV/°C). There were two problems associated with their use (a) BS1041 (1992) stated that the tolerance of output against standard published tables was ±1°C, and (b) the Microlink data logging system had no internal conversion code for this thermocouple type. The deviation of the output from standard tables was inherent with all thermocouple types, and had to be calibrated for whichever type was selected. Furthermore calibration would render all the internal conversion codes of the Microlink redundant anyway. Hence it was decided to manually calibrate 16 type E thermocouples.

A junction was made by spot welding one end of each 4m wire pair (0.2mm, single strand) in an inert gas environment (all pairs were taken from the same batch). The thermo-junctions were connected to a low thermal noise 32 channel switching block, with all contacts immersed in oil (Shell Thermia-B) to minimise any deviation in temperature at the contact points. For the cold junction, a Type-E emulating box was initially used for all channels and was connected so that it was active for only one of the thermo-junctions at a time (this is shown schematically in Figure 5.4 below). To

measure the *e.m.f.* (electromotive force) produced by each thermocouple a Schlumberger *Solartron 7055* Microprocessor Voltmeter was used. The operation of this unit used a 10mV range that gave a reading with a resolution to the nearest 1μV. Each reading had an integration time of 160ms and achieved an accuracy of ±[0.002% of reading + 4 digits] (Schlumberger, 1978) (which meant that a typical reading of 2000μV would have an error of ±4μV). The system is shown in Figure 5.4.

Each thermo-junction was attached to a high precision platinum resistance thermometer. These were placed in a large tank of glycol brine (large thermal mass) which was connected to a chiller and heater, so that the temperature could be varied. The tank was gently stirred, to achieve an even temperature throughout the system, and then for each thermocouple a temperature and corresponding voltage was recorded. The platinum resistance thermometer was a Systemteknik S1220 series; it consisted of a 100Ω platinum resistor probe connected to a conversion and display box. The accuracy of this unit was quoted as 0.04°C in the range -100°C to 400°C (Systemteknik, 1980).

Because of the thermal lag of the thermometer, data collection was repeated with the system cooling and heating. Considerable deviations were found between these sets of readings. A detailed inspection showed that even at ambient temperatures, where thermal lag would have no effect, the deviations were significant. It was suspected that either the micro-voltmeter or the cold junction simulator were unstable. To check the stability of the micro-voltmeter a standard cell was employed. The recorded voltage of the cell on the meter deviated by less than 2μV over a 24 hour period. This suggested that the cold junction simulator (Isotech Frosty, Type-E) was unstable. This was confirmed when one of the thermocouples was placed in an ice water bath, deviations over a two hour test period gave a swing in range of ±30μV. Replacement of the batteries did not improve the stability, and a second unit was found to behave in the same way. The long term stability was checked across ~24 hours to see if the original problem was due to 'warm up' of the device. This merely confirmed that the device itself was unsuitable for the stability and accuracy required for this part of the project.

The only choice of cold junction was to use a thermocouple pair holding one junction at a constant temperature. Typically an ice-water bath is used for this purpose because of the high latent heat and very narrow phase transition temperature, which provides a very stable reference at +0.01°C deviating by ±0.01°C (Barber, 1971). The system consisted of a vacuum flask filled with crushed ice and water, inside this was a test tube filled with oil (to act as a thermal buffer) in which the reference thermo-junctions were placed. Calibration of the thermocouple systems was performed as previously, and results were obtained with no deviation between the heating and cooling data sets. Computer analysis was performed to derive cubic equations for the temperature-voltage characteristics of each of the thermo-junctions. The cubic coefficients for each of the type E thermocouple is shown in Table 5.1, according to the following notation:

$$T = aV^3 + bV^2 + cV + d \qquad (5.3)$$

Where T is the temperature in °C and V is the voltage in μV.

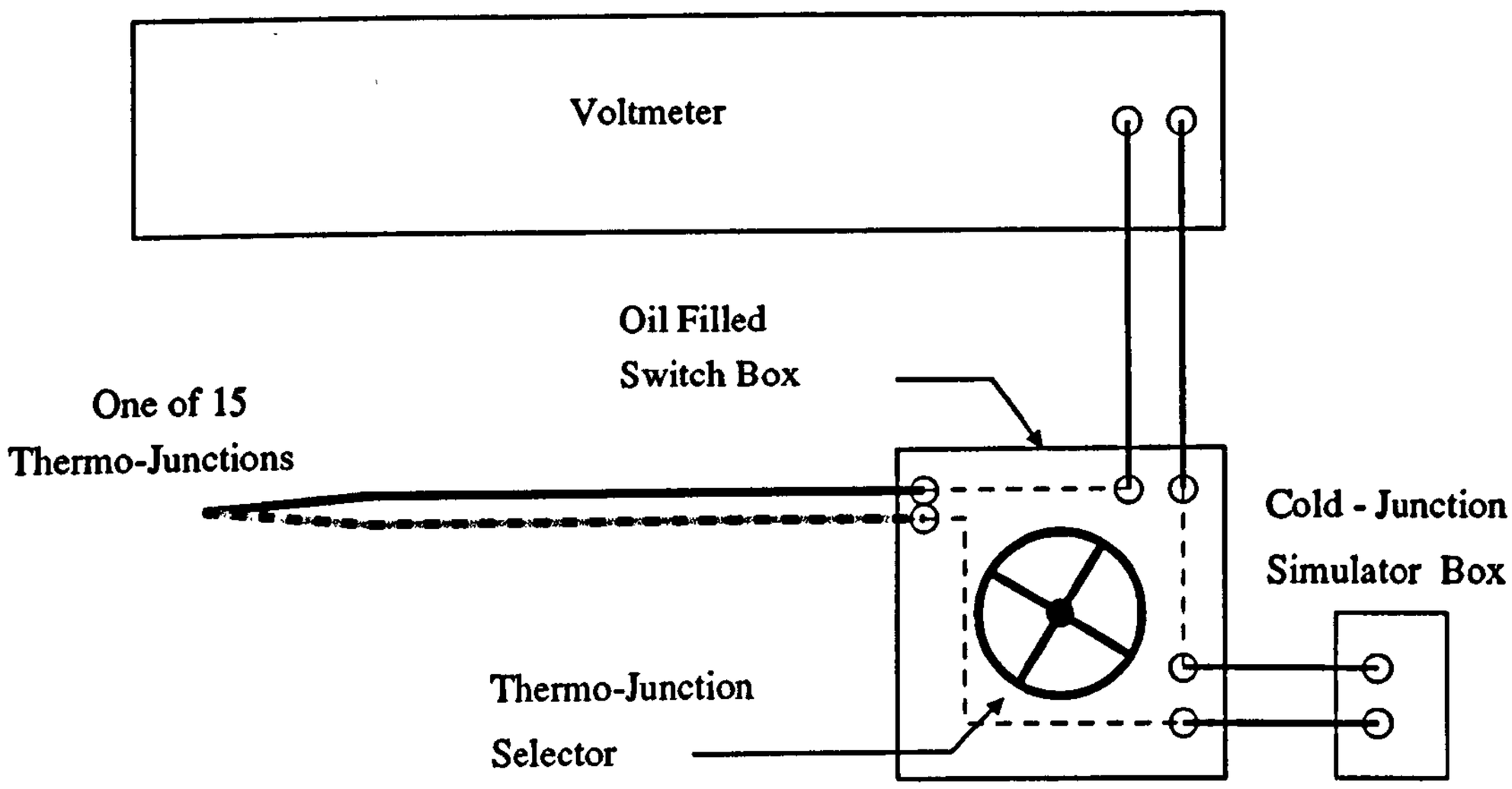

Figure 5.4 Schematic Layout of Thermo-couple Measuring System (Manual).

Table 5.1: Cubic Coefficients for Calibrated Thermocouples.

T-C No.	a	b	c ($\times 10^{-7}$)	d ($\times 10^{-11}$)
1[a]	-0.0806465	0.0169655	-2.92655	1.45886
2[b]	-0.077018	0.0169527	-2.80195	1.12168
2[c]a	-0.077018	0.0169527	-2.80195	1.12168
3[d]	-0.106288	0.0169772	-2.83111	1.22076
4[e]	-0.111797	0.0169667	-2.45103	1.00404
5[f]	-0.074731	0.0169712	-2.88147	1.40228
6[f]	-0.0862787	0.016978	-2.85109	1.2825
7[f]	-0.0834278	0.0169826	-2.86838	1.25056
8[f]	-0.0944199	0.01699555	-2.80761	1.01038
9[f]	-0.067512	0.0169797	-2.84536	1.09277
10[f]	-0.0851188	0.0169828	-2.81164	1.03709
11[f]	-0.0661144	0.0169783	-2.94797	1.35239
12[f]	-0.08722	0.0169829	-2.85085	1.11998
13[f]	-0.134738	0.0170303	-2.99709	1.4726
14[f]	-0.084742	0.0169874	-2.93472	1.36438
15[f]	-0.106038	0.0170038	-2.91672	1.22667

Notes on thermo-couple locations.

a - water, oil or slurry inlet temperature to heat exchanger

b - water, oil or slurry exit temperature from heat exchanger

c - water, oil or slurry 2m down stream of outlet temperature to heat exchanger

d - glycol inlet temperature

e - glycol exit temperature

f - equally spaced wall temperature

No numerical method exists to provide the errors in the cubic coefficients found above, although generally over short temperature ranges the behaviour of thermocouples is best describe by a cubic function. To analyse the limits of errors from using these coefficients, a regression analysis was performed on each of the thermocouple's data sets and a range of errors were found in the temperature range 30°C to -20°C using the equation (Squires, 1985):

$$\delta T = \left\{ m^2 V^2 \left[\left(\frac{\delta m}{m} \right)^2 + \left(\frac{\delta V}{V} \right)^2 \right] + (\delta c)^2 \right\}^{1/2} \tag{5.4}$$

The results for all thermocouples gave errors of ±0.1°C at 30°C down to a lowest value of ±0.04°C at 0°C rising again up to ±0.08°C at -20°C. These values represent the worst case and it was thought reasonable to use the lower value (±0.04°C) as the error for the cubic functions. Figure 5.5 shows the calibration data points for thermocouple 1 with the calibration errors, the line is for the cubic function.

5.2.3 Mass Flow Rate Measurement of the Slurry

Knowledge of the flow rate of the slurry was required to (a) investigate trends in heat transfer coefficients and (b) study the thermal capacity of the flowing mixture. A review of flow rate measurement methods was undertaken to investigate the options available (Scott, 1982; Spitzer, 1984; Beck, 1987; Baker, 1988). The only device suitable for application to slurries of the particle size and solids concentration used in this project was a Coriollis flow meter. Such a device gave a true mass flow rate measurement with an accuracy of ±1%. Several suppliers of these devices were contacted and although all units were found to be suitable, the cost of such a device was prohibitively expensive. Hence another method had to be used.

After much consideration it was decided to use a timed discharge method where, for a known period of time the flow was diverted into a container and the mass collected was measured; the sample subsequently being returned to the system manually. All standards of flow meter calibration can be traced back to such methods. For this project it had the following advantages: (a) very low cost, (b) high accuracy, and (c) it provided a sample to analyse. The design of the system had to take account of this method (although it allowed for the addition of a coriollis flow meter at a later date - see Chapter 6). However, this method of measuring mass flow rate had several disadvantages: (a) thermal shock to the system at any temperatures but ambient, (b) it caused a change in "head" of the system, (c) an open system, and (d) a non-continuous measurement method. These are discussed in the next few paragraphs.

Every time a sample was taken from the system a thermal shock was introduced, and as lower temperatures were tested, the effect of this was potentially more significant. To overcome this problem a large bulk tank was employed (see Figure 5.1 above). This increased the volume of the system and hence the cost of materials for the charge (ie the support fluid and hydrophilic materials). This also increased the time required to

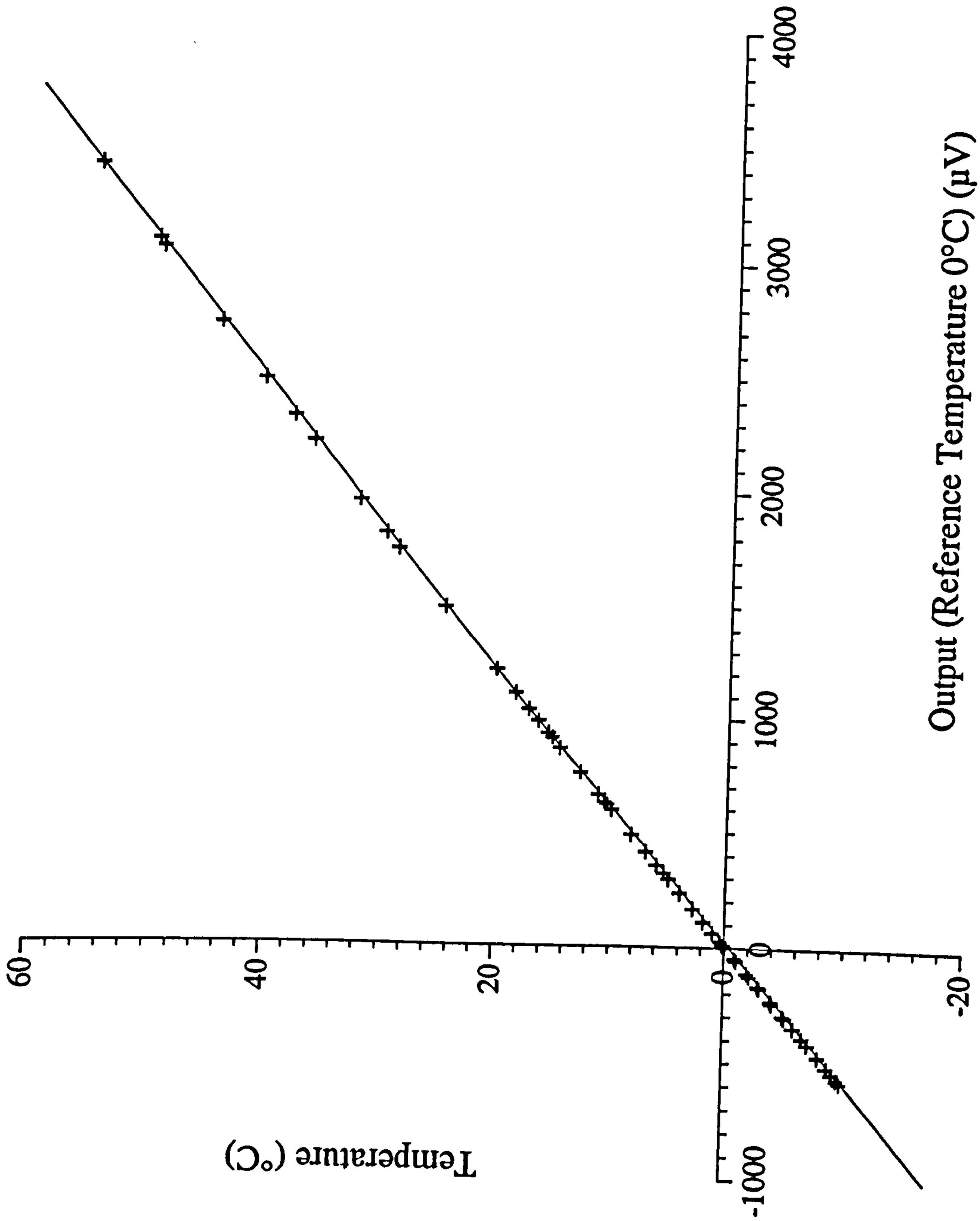

Figure 5.5: Type E Thermocouple 1 - Calibration Results.

prepare the hydrophilic samples, which for these tests, were thermally cycled twenty times.

The discharge of a sample for mass measurement caused a change in level within the bulk tank, which effectively perturbed the flow rate. Effectively the flow rate at the end of the discharge was lower than the actual flow rate at the start of the sampling period. This problem could be minimised by using a bulk tank with a geometry that ensured that any change in volume caused a small change in depth. For a particular volume this gives a preference for a wide shallow tank. Again to overcome this problem a large bulk tank was the solution with the same associated problems.

Having an open system caused an inherent loss of head to the system, which effectively reduced the maximum flow rate available with a particular pump/charge combination. Design of the system tried to minimise this loss so the vertical distances between the system outlet to the discharge device (Figure 5.6), and the surface of the fluid in the tank, was minimised. The final design had an open vertical length of 35cm at the start of the discharge, extending to 37cm at the end of a large discharge. This caused a maximum increase in free head loss of 6%. The effects of this depended on the available head produced by the pump(s), which in turn depended on the solids concentration, and the temperature of the flowing charge. The magnitude of the errors caused by this effect were checked by taking two samples (not returning the first) and comparing their masses. Only at low temperatures and high concentrations was any deviation detected, although these deviations seemed to be more a function of the slurry state within the bulk tank (see Section 6.4.3).

The potential for water vapour in the air to condense on the inner surface of the system and be absorbed or mixed with the slurry was another problem with the open system. The addition of free water to the slurry, would have effectively changed the thermal mass of the flowing mixture and its rheology (excess water in the developed cold storage devices had been known to cause ice bridging and lead to blockages). To avoid this close, fitting sections of thermal insulation were used to enclose the slurry chute and the top of the bulk tank. Furthermore the open system had a tendency to entrain air into the slurry as it returned to the bulk tank, both from the chute and during the return of samples to the tank. The depth of the charge in the tank, combined with the addition of baffles in the chute, served to reduce this problem to the point where no air was drawn into the circulation loop.

Finally using the method of time discharge meant that the mass flow rate measurement had to be achieved manually, and apart from causing thermal impact to the system and perturbations in the flow rate, gave only a few readings per cooling run. This method was suitable for checking the overall performance of the system during the steady-state tests involving single-phase fluids, and sufficed for flow rate measurement employing tests made to the phase change slurries.

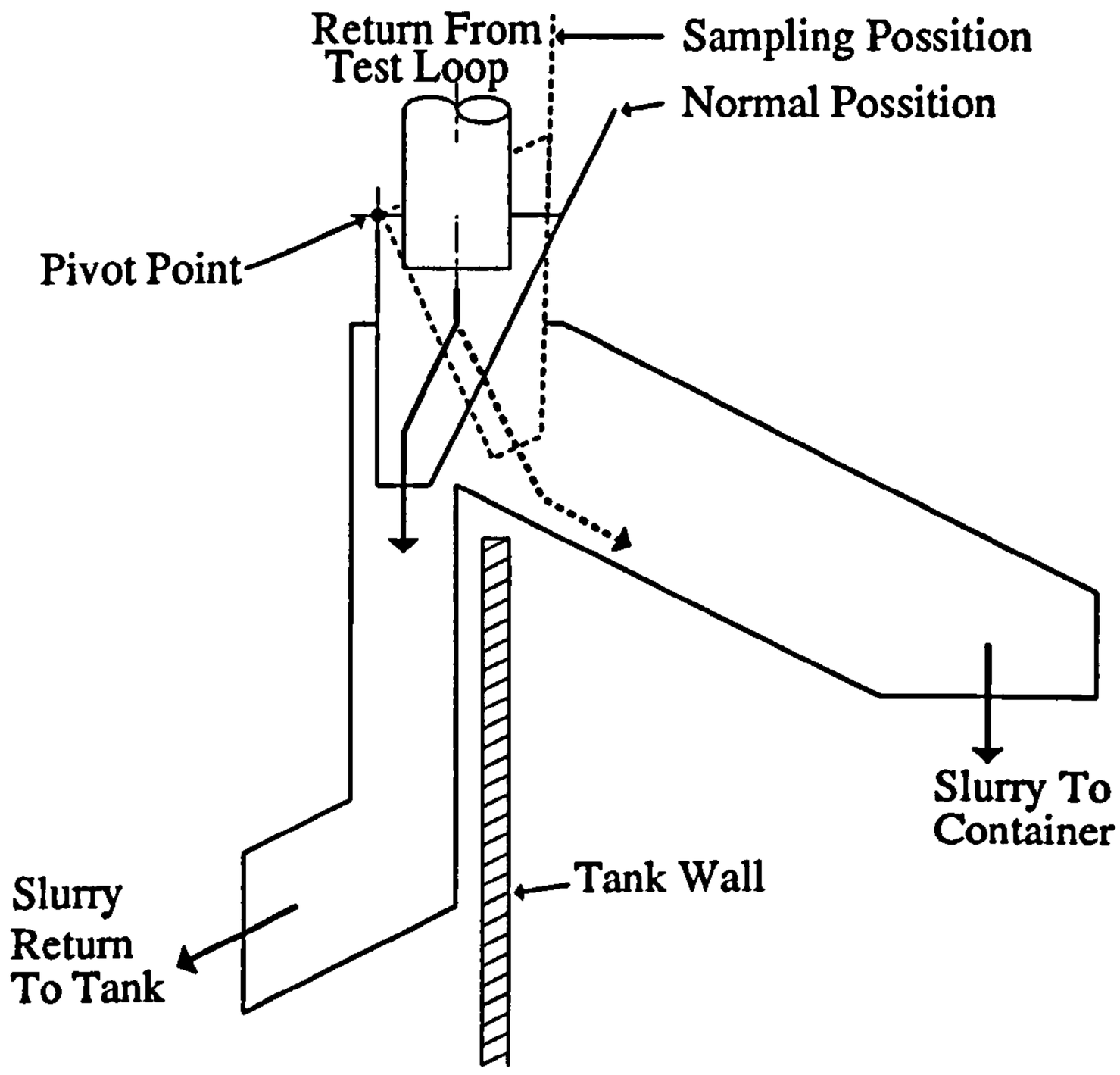

Figure 5.6: Detail of Slurry Discharge Chute.

Table 5.2 Heat Gains Around the Slurry Circuit (W).

Slurry Temperature (°C)	10	0	-10
Tank - walls	8.9	20.1	31.3
Tank - top and base	1.8	4.0	6.3
Tank to Pumps	0.7	1.6	2.3
Pumps	7.1	16.0	24.9
Pumps to Heat Exchanger	2.7	6.0	8.8
Heat Exchanger to Rheological Section	5.0	11.0	16.2
Rheological Section	4.1	9.0	13.1
Chute	2.5	5.5	8.0
Total	32.9	73.2	110.8

5.2.4 General Components of the Slurry Circuit

Pipes around the slurry circulation loop were Durapipe Supaflo ABS pipes of 1 inch nominal bore, having an internal diameter of 25mm. This gave a network of piping stable between -40°C and 80°C (Durapipe, 1990). Connection to both the heat transfer test section, and the rheological test section, were made using ABS flanges (drilled to BS 4504 - table 16/3 (10/3)). The use of ABS piping was adopted because of the relative ease with which it could be connected and modified. Thermocouples 1, 2 and 2a (Table 5.1) were fitted by the means of appropriately drilled and tapped (1/4 inch BSP) ABS blocks, that were located on the pipe network in the correct positions.

The bulk tank used in the system was an open topped domestic hot water tank measuring 760mm high and 460mm in diameter. It was known that particles would settle in the tank so an agitation unit was fitted. This consisted of a Brook Crompton D80AD-K153217 three phase motor and matching electrical control unit. The motor had an in-built support bearing allowing it, and the impeller used, to be supported at the motor end only. Because of the tendency of the charge in the bulk tank to rotate, six side-baffles were fitted inside the tank. These were each 400mm long, equally spaced around the tank's circumference, and projecting into the tank radially by 65mm. They were extremely effective at reducing the rotation of the stirred charge in the bulk tank. The direction of agitation was such that flow generally move downward in the centre and rose on the outside of the tank.

Insulation around the slurry circuit consisted of a mixture of foil coated 50mm fibreglass (tank walls), 40mm of expanded polystyrene sheet (tank base and cover) and AF/Armaflex, a closed cell elastomeric foam (Armstrong, 1992). The Armaflex insulation had an internal diameter of 28mm and a wall thickness of 19mm. Table 6.2 shows the calculated steady state thermal energy gain to various parts of the slurry circuit. This is for an ambient temperature of 18°C and assumes that the slurry is isothermal throughout the system.

5.2.5 The Primary Cooling System

The cooling power requirements for the thermo-rheological test rig were estimated to be a minimum of 1.5kW at -10°C, in order to sustain a minimal wall-to-fluid temperature difference of 2°C. The mode of operation also required an accurate method of measuring the energy supply, or removal from the test system. The most practical method of achieving this was to employ a chiller unit using a brine that would not freeze at the required operational temperature. Only one chiller (Conair Churchill TCW9) with the correct thermal capacity existed in the laboratory, although initially this was unavailable. Another chiller of lower capacity was available (Conair Churchill MCW5) which had a capacity sufficient for the heat transfer test employing water, so this was used to verify the rigs ability to reproduce standard heat transfer correlations. Connection of the chillers was the same, so that replacement of the lower capacity chiller could be easily performed at a later stage.

Temperature control for either chiller was performed by on/off switching with a definable time lag before restart (minimum 1 minute). This switching would have caused relatively large and rapid changes in temperature in the supply to the cooling circuit. This in turn would cause errors when measuring energy flow across the heat exchanger, because the duration of fluid in the heat transfer test section was longer than the time of supply from the chiller. To overcome this problem a large tank (190 lt) was used as a thermal buffer. This was connected directly to the chiller unit and agitated constantly. From this tank the brine was pumped through the heat exchanger circuit, and upon its return it passed through a chute to enable mass flow rate measurements to be made, Figure 5.7 shows the layout of the system.

Insulation around the tank consisted of expanded polystyrene sheet, 40mm thick over the bulk tank and 19mm thick (internal diameter 22mm) closed cell elastomeric pipe insulation around the rest of the system. Table 5.3 shows the heat gain to the cooling circuit and indicates that the worst gains to system would be ~330 W (for ambient temperature of 18°C).

5.3 Performance Verification

Once constructed the performance of the heat transfer test rig had to be verified, that is its ability to reproduce heat transfer coefficients within the errors of standard correlations. Equation 5.1 can be re-written in terms of the errors as:-

$$\delta\bar{h} = \bar{h}\left\{\left(\frac{\delta A}{A}\right)^2 + \left(\frac{\delta q}{q}\right)^2 + \left(\frac{\delta \Delta T_{lm}}{\Delta T_{lm}}\right)^2\right\}^{1/2} \qquad (5.5)$$

The measurement of the area of the heat transfer surface was a static measurement, hence a reduction of the error to <1% was feasible. For example when the 21mm inner tube of the heat transfer test section was measured with an accurate steel rule, it yielded a length of 2.04(±0.002)m. The tube's internal diameter was measured with vernier calipers to give a result of 20.4(±0.05)mm. Combining these results gave an area of $6.67(\pm0.02)\times10^{-4}m^2$, and an error of ≈0.4%. The two other parameters q and ΔT_{lm} were measured in real time, hence their errors tended to be larger.

The value of q relied on measurements of both the mass flow rate and temperature differential across the inlet and outlet of the heat exchanger. The mass flow rate itself required the measurement of the mass of discharge glycol, and the time of discharge. In the range 1 to 12kg the scales used had an accuracy of ±10g, while the time could be measured to ±0.1second. For a typical discharge of 6kg in 20 seconds this gave errors of ±0.5%. Temperature differentials between the glycol inlet and outlet ranged from 4°C down to 1°C, hence the errors (Section 5.2.2) were at worst 5%. This gave a final accuracy in q of ±5%. A similar analysis was undertaken for ΔT_{lm} to give errors ranging from 2% up to 8%. By combining these in Equation 5.5 the accuracy ranged from 9% at worst, down to 3%, being within the errors quoted for standard heat transfer correlations.

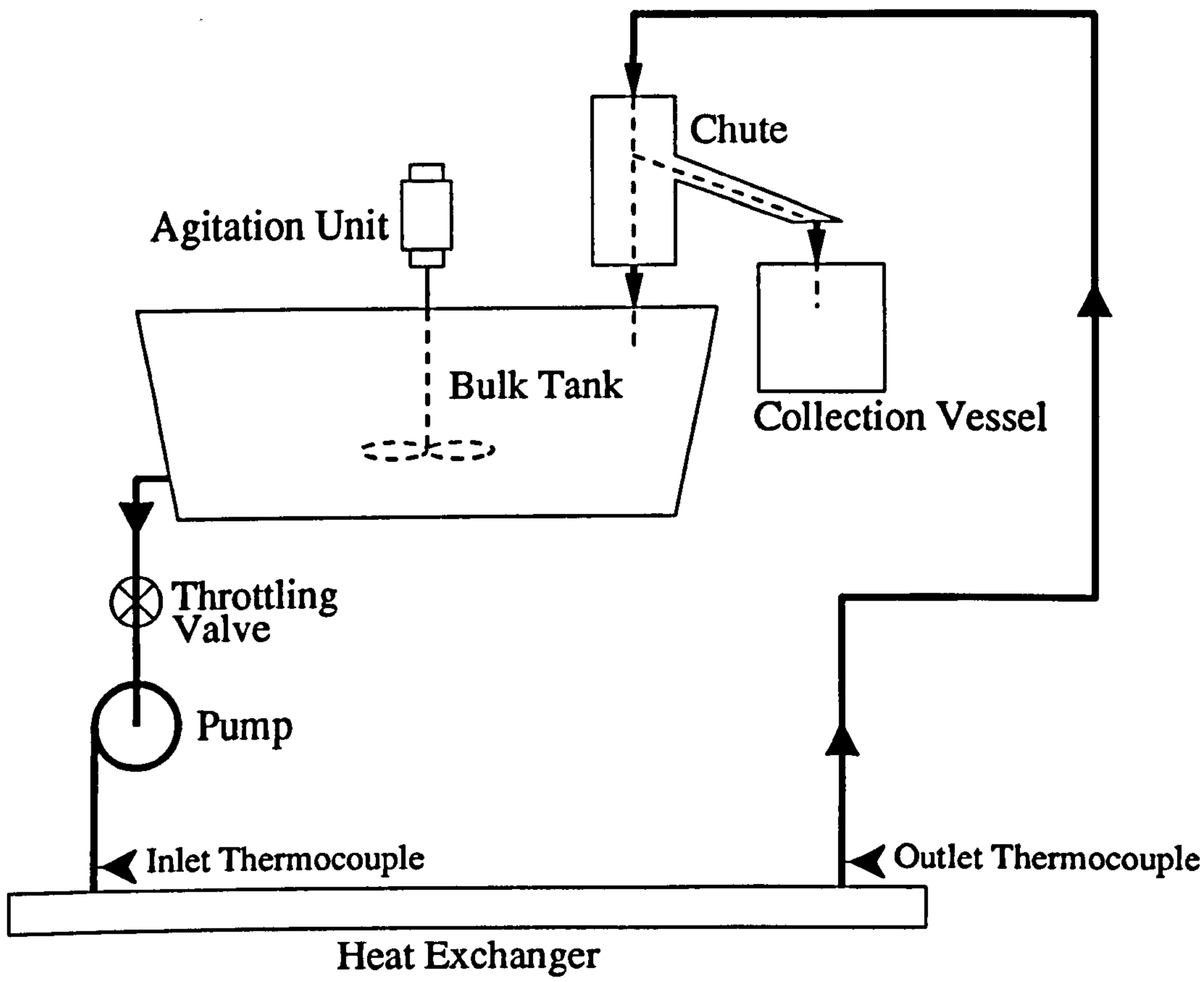

Figure 5.7: Layout of Glycol Cooling Circuit.

Table 5.3: Heat Gains to the Cooling Circuit at Various Glycol Coolant Temperatures (W).

Glycol Temperature (°C)	10	0	-10	-20
Tank	10.9	24.6	38.2	51.9
Tank to Pump	4.3	9.4	13.8	18.2
Pump	12.0	27.0	42.0	57.0
Pump to Heat Exchanger	11.1	24.2	35.5	46.7
Heat Exchanger	7.3	24.5	35.9	47.2
Heat Exchanger to Chute	27.7	60.6	88.7	116.6
Total	73.4	170.4	254.2	337.6

5.3.1 Water Heat Transfer Tests

A number of tests were performed with the apparatus (Figure 5.1) to measure the heat transfer coefficients. The procedure was to set up steady-state conditions around the test circuit. This involved selecting a flow rate for the fluid (water and oil), setting the heating rate for the balance load and the set point temperature of the chiller unit. Once these parameters were set, the system was allowed to achieve steady state conditions. Measurements were made of thermocouple 1 at regular time intervals of 15 minutes. The system was considered close enough to steady state once the rate of change of this reading was below one microvolt per minute (<0.02°C/min).

The data for heat transfer calculations was now collected, this consisted of taking three complete sets of thermocouple readings. At the end of each set a repeat reading was made of thermocouple 1 to see if any major changes had occurred; and if so, the readings were discarded and the existence of steady state was re-checked. After three sets of readings, the mass flow rate of the test fluid was measured. This consisted of mass and time measurements for five discharges of the fluid. Next another three sets of thermocouple measurements were taken, applying the same checks as in the first three. On completion of the data collection, the conditions around the system were changed and the process was repeated. These tests were performed for both the 28mm and 21mm diameter heat transfer tubes. The results are shown in Figures 5.8 and 5.9. It is evident from the data presented in these figures, that the heat transfer test rig can reproduce the standard heat transfer correlation for turbulent heat transfer in tubes (Equations 2.36 and 2.37).

5.4 Computer Data Acquisition

The analysed data from the rig gave heat transfer coefficients that fell within the quoted errors of the two standard heat transfer correlations. At this stage, it was decided to add a computerised data acquisition system, which had not been employed initially. It was important to prove that the method of measuring the heat transfer coefficients was correct, without the additional complication of incorporating an automated data collection system. Data logging systems are prone to electrical noise at the voltage levels required for temperature measurements from thermocouples. The availability of a low thermal noise card for the Microlink data logger (Biodata, 1994), and the need to monitor not only absolute heat transfer data but also trends at and through the phase transition temperature, necessitated continuous data acquisition.

5.4.1 Addition and Calibration of Glycol Brine Flow Meter

The heat transfer tests performed on the single phase oil charges required the temperatures of the glycol brine to go down to -10°C. The viscosity of the brine at this temperature was high enough to cause air entrained through the chute to build up in the bulk tank. After a period of prolonged operation, it was observed that the suspended air

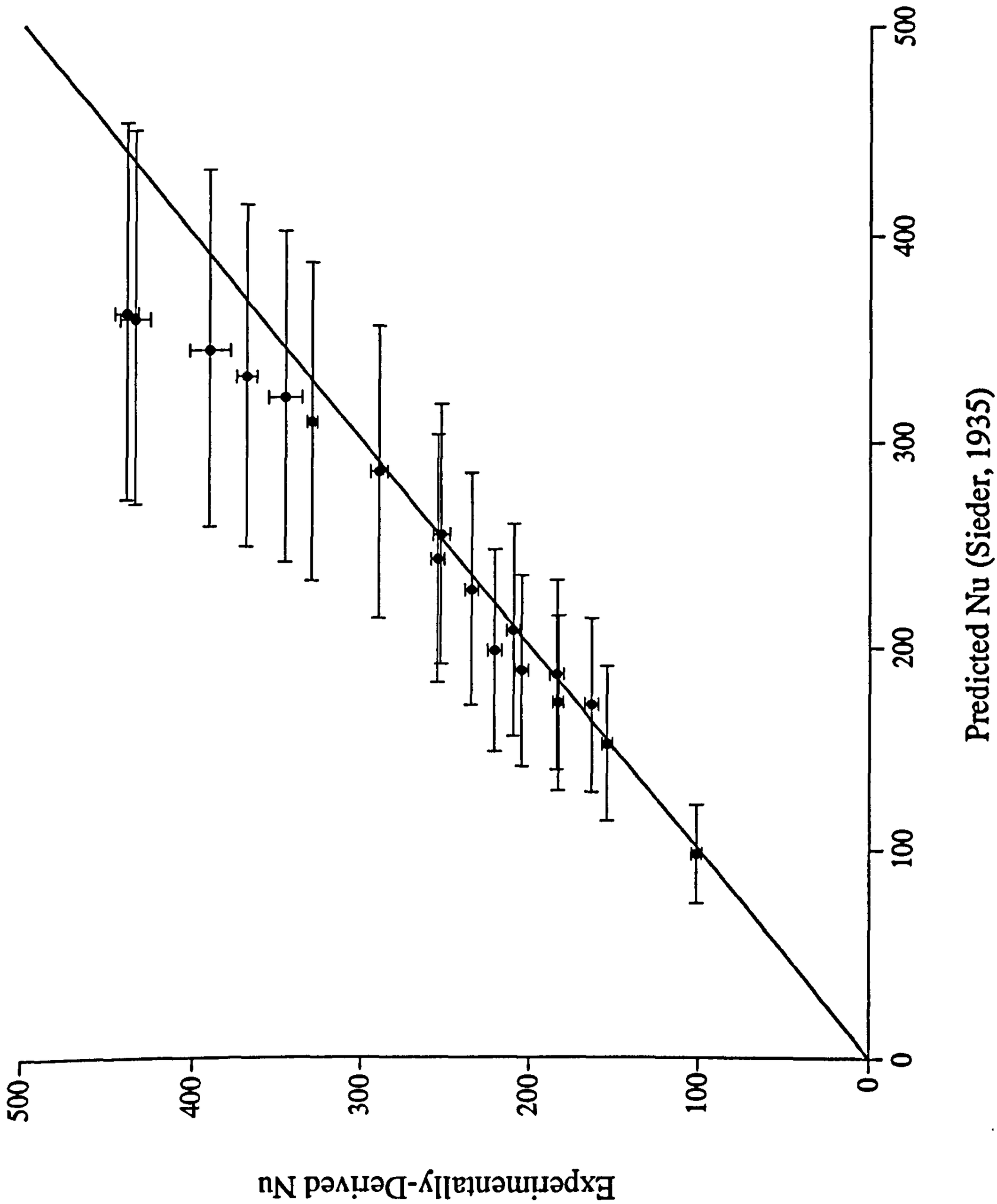

Figure 5.7: Comparison of Predicted Values of The Nusselt Number (Nu) from Equation 2.36 (Sieder, 1935) with that Derived from Measured Data.

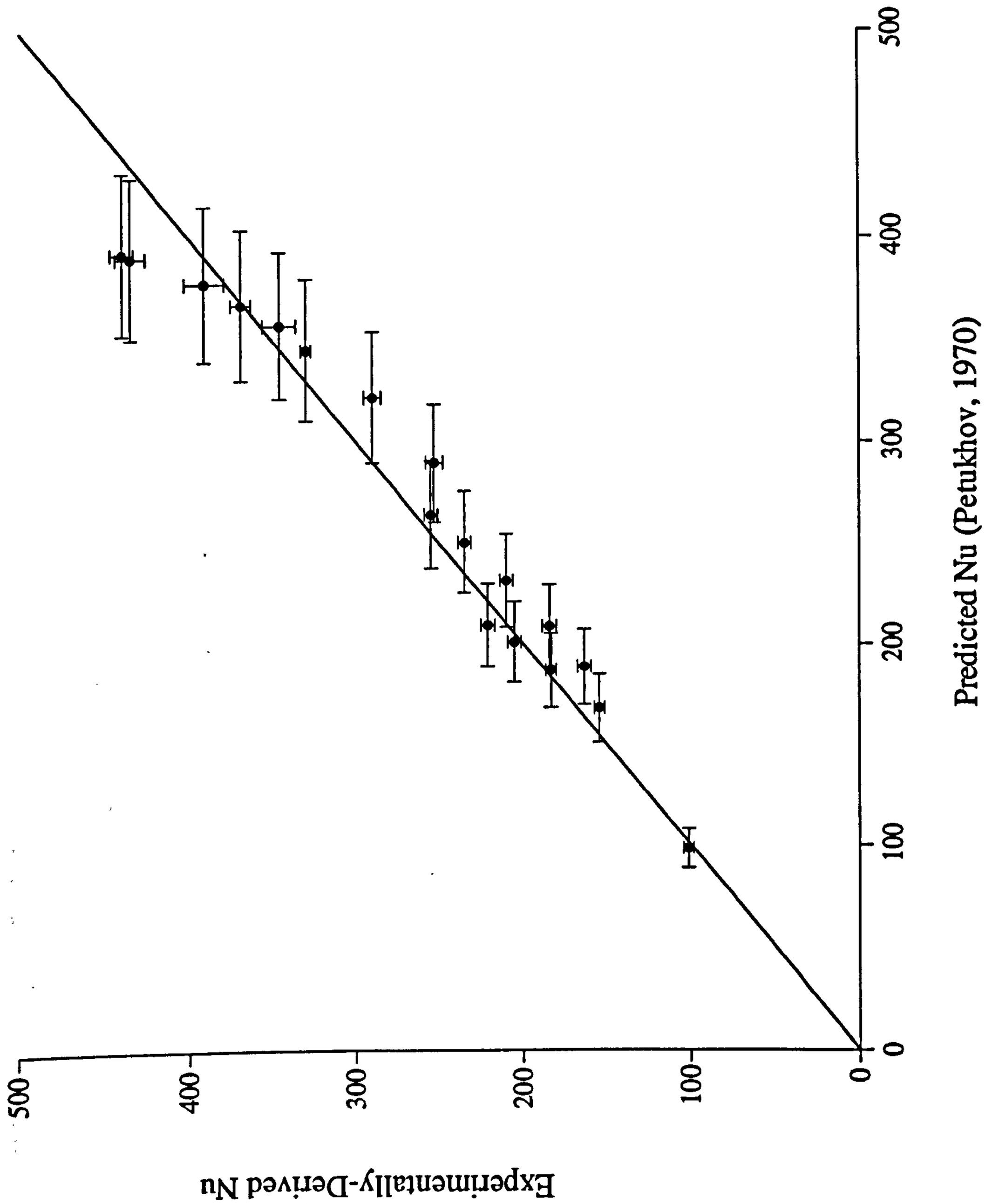

Figure 5.8: Comparison of Predicted Values of The Nusselt Number (Nu) from Equation 2.37 (Petukhov, 1970) with that Derived from Measured Data.

bubbles had reached the outlet of the tank and were being drawn into the heat exchanger circuit. This effected the performance of the pump and, more significantly, added an unknown thermal capacity into the calculations of energy transfer across the heat exchanger wall, hence $\bar{h}$. Baffles were added to the chute in order to reduce the velocity of the fluid as it returned to the tank but the benefits gained were insufficient.

During the tests involving single-phase fluids, the air could be eliminated by bypassing the chute for a period, but this would not be possible while testing the slurries where a continuous measurement of the energy transfer rate was required. Furthermore it was known that the viscosity of the glycol brine would be much higher while testing the slurries, due both to a lower temperature (~ -20°C), and the need to increased glycol concentration for safe operation of the chiller unit (recommended to be >42% by mass at -20°C). This elevated viscosity would be high enough to cause air bubbles to stay suspended for many hours (this was verified when the glycol concentration of the charge was increased). Also since the energy flow was to be continuously logged, an accurate flow meter was required.

To measure the energy transfer rate it is preferable to measure the mass flow rate, as opposed to a volumetric flow rate, hence a turbine flow transducer was chosen to produce a flow signal. Such devices can produce an accuracy as high as ±1% of the measured rate (Miller, 1989). The unit used was a Kent Pottermeter TB/½/4/LT which employed an inductance coil to produce an output signal (Kent, 1967). The output produced was an ac signal with both peak to peak voltage, and frequency, dependent on the flow rate. This signal required conditioning before the Microlink system was able to read the signal. To perform this task a frequency to voltage (dc) converter was used, this method was more resistant to electrical noise than voltage (ac) to voltage (dc) conversion at the level of signal output produced. A phase lock amplifier was available, although this had been built for operation at higher frequencies than those from this system. This limited the sensitivity of the system, because of the signal to noise ratio, so it was decided to adjust the unit for operation at this systems frequency. The glycol brine circuit containing the test heat exchanger was set up, and the system was allowed to flow at its maximum rate (all valves opened). A CRO was used to analyse the signal, and the period was found to be 3.1ms (frequency of 322Hz). The phase lock amplifier was adjusted to provide a maximum output of 5V at 400 Hz.

Additionally, while the flow meter was being added to the circuit, a two way valve was incorporated so that glycol returned to the tank could either go through the chute, or pass directly back to the tank beneath the fluids surface (hence avoid entraining air). Figure 5.10 shows the layout of the modified glycol circuit and the transducer.

Calibration of the system was required, and it was not clear initially if the glycol brine at the high concentration would behave in a Newtonian manner. So the calibration method adopted was to set the glycol system at a particular temperature, adjust the flow rate until a voltage was obtained, then take a set of mass flow rate measurements. The data was logged with a developed program that took 100 consecutive voltage and temperature readings from the Microlink, then calculated the average readings. Ten sets

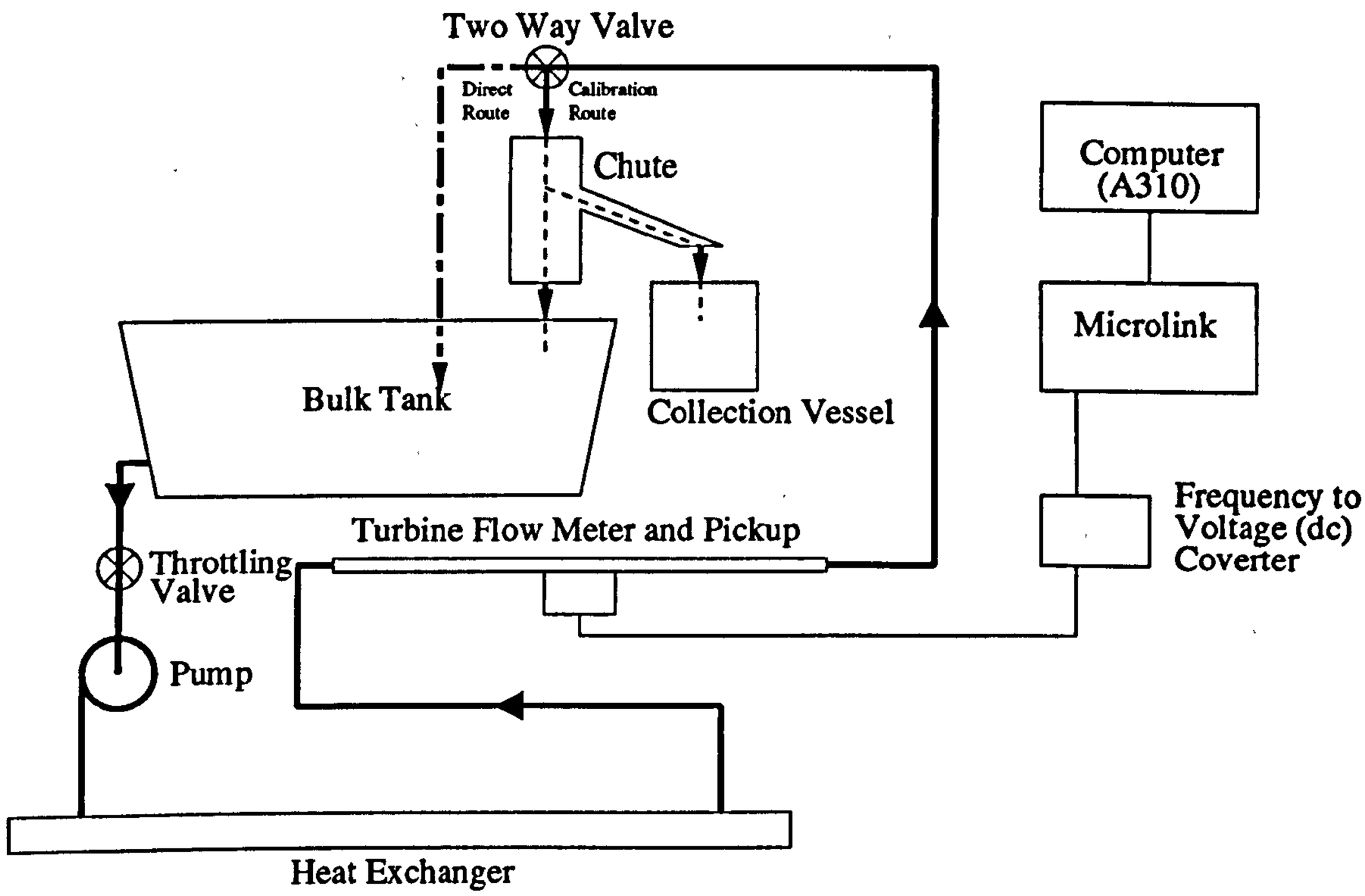

Figure 5.10: Schematic Layout of Modified Glycol Circuit Including Turbine Flow Meter, Frequency to Voltage Converted and Data Logger.

Table 5.4. Summary of Flow Meter Coefficients.

Temperature (°C)		Coefficients of Equation 5.6			
Nominal	Actual	***a***	error ***a***	***b***	error ***b***
30	31.4	0.1844	0.0017	-0.1016	0.0029
15	16.5	0.1884	0.0027	-0.1026	0.0027
0	1.6	0.1842	0.0015	-0.1026	0.0027
-5	-3.4	0.1861	0.002	-0.1043	0.0034
-10	-8.5	0.1339	0.009	-0.0116	0.0136
-15	-13.4	0.1425	0.012	-0.028	0.0184
Used		0.17	0.005	-0.075	0.018

were taken and displayed on the screen, with an eleventh set showing a continuous output. This allowed for a hard record to be made, and real time monitoring while adjustments were made for a new state. After a set was recorded the mass flow rate was measured in the same way as for the calibration of the whole system. If after the mass flow rate was taken, there was a change of more than ± 0.1°C in the inlet glycol temperature (TC 3), another set of voltage and temperature readings were taken. These were averaged with the initial readings. This only occurred during readings below -10°C where a rise of 0.2°C was observed, due to warming of the brine by the measuring equipment.

Within the limits of the temperature and flow used, the brine gave a linear output allowing a function to be used rather than interpolating from a data set. The Figure 5.11 indicates that the behaviour of the system was linear. The change in glycol concentration (43% by mass (±0.5%)) during calibration, which was recorded over a one month period, was small, so the flow rate system appeared to be stable; this was later found to be true throughout subsequent testing. The temperature range of calibration was 31.4°C to -13.7 °C and the investigated mass flow rate ranged from 0.08 $kg \cdot s^{-1}$ to 0.33 $kg \cdot s^{-1}$.

The results of linear interpolation of the data are summarised in Table 6.4 and where coefficients are for the function:

$$\dot{m} = aV + b \tag{5.6}$$

When it came to combining these results the mean coefficient was used. For the error value there were too few values to perform any form of statistical analysis, and the maximum error of that coefficient was used (as the system was operated mainly at similar temperatures, to where these maximum errors occurred this assertion was considered valid).

5.4.2 Thermocouple Voltage Measurement Using Data Logger

To permit the continuous recording of temperatures around the heat transfer test rig, a Microlink data logger was employed (Biodata, 1995). This simplified the measurement process and allowed many more readings to be taken than could have been achieved manually. This was critical, since the mode of testing the phase change slurries during cooling was a transient method, and trends had to be recorded as contents of the system passed through the transition temperature.

The data logging system employed a low-thermal-noise module (Series 3055). This module gave a thermal noise of <1μV (Biodata, 1995) and combined with a 16 bit analogue-to-digital converter in the Microlink frame, was capable of resolving to the nearest μV. This in turn allowed the same resolution in temperature, compared to the manual method, to be achieved (Section 5.2.2). This was verified by employing a standard cell (Weston, Type 1149, No. 188998) and comparing the voltages recorded by

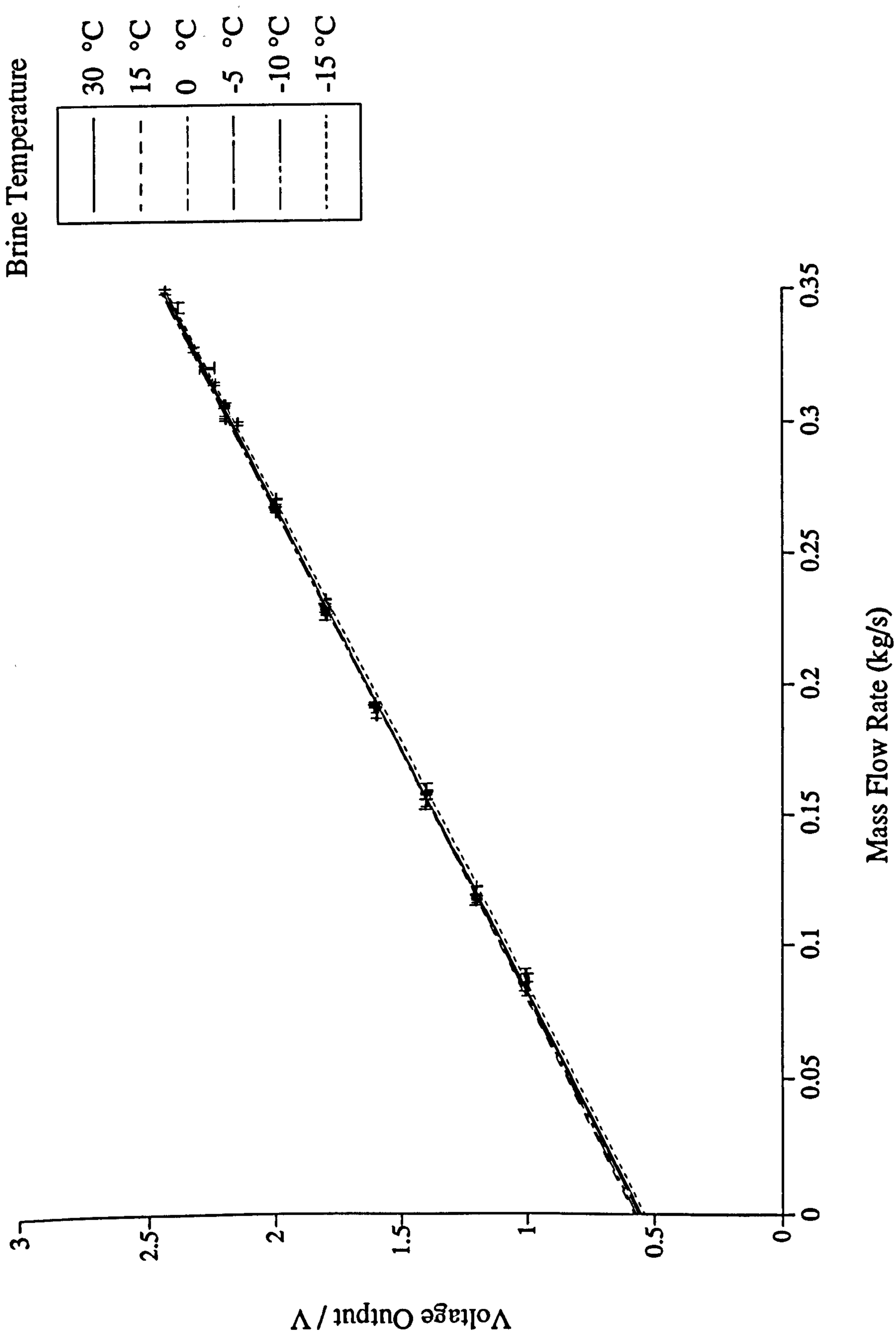

Figure 5.11: Flow Meter System Output (with error bars).

both the Microlink system, and the Solartron 7055 voltage meter (Section 5.2.2). The voltage of the cell was nominated as 1.01859V at 20°C, this allowed a comparison to be made to ±10μV.

The Microlink data logger was controlled by an Acorn computer (Acorn, 1987). Communication was via an IEEE 488 bus and standard protocols for the exchange of data were employed (Intelligent Interfaces, 1988). All computer code was written in BBC BASIC V (Acorn, 1987) for both communication across the IEEE 488 bus, and employment of the Microlink control commands (Biodata, 1995). Measured data was recorded in data files, the format of which was CSV (Comma Separated Variable) allowing easy inspection and subsequent processing.

5.5 Summary

This chapter has described the design used to develop a test apparatus for the investigation of the heat transfer properties of phase change slurries. The performance of the system has been verified by comparing the measured heat transfer coefficients of water with those predicted from standard correlations. Agreement was found to be good. In the following Chapter results from tests using a range of phase change slurries are presented and examined.

The design of the rig has allowed for the addition or modification of components to be made with relative ease. It is believed that both the accuracy and the range of data collected (with respect to phase change slurries) could be enhanced with some additional components. A discussion of this is made in Chapter 7.

Chapter 6

The Slurry Heat Transfer Tests

6.1 Introduction

This chapter describes the heat transfer tests performed on a number of phase change slurries during cooling. Significant enhancements to the heat transfer coefficient (h), compared to that of the single phase support fluid, were identified; their degree being dependent on the temperature, solids concentration and flow rate of the slurry. Analysis of this data indicated three categories for consideration; (i) all temperatures above 0°C, (ii) heat transfer surfaces below 0°C but mean fluid temperatures above 0°C (transitional) and, (iii) all temperatures below 0°C.

All of the class (i) systems, in which the slurries had solids concentrations below 10%, behaved in a predictable manner, if flow rates were sufficient to overcome the settling of particles within the test section. Agreement between measured data, and a standard heat transfer correlation, was found to be close, provided that the physical properties used accounted for the presence of the particles. At concentrations of 10% or higher this agreement was not preserved.

At system temperatures low enough for phase change to occur at the heat transfer surface (class (ii) transitional), all concentrations showed a significant change in their heat transfer coefficient, compared to the single phase fluid. This was found to increase with solids concentration and flow rate. Analysis of the data has revealed that particle interaction at the heat transfer surface was occurring, and that this was a major influence on the heat transfer coefficient in this case (ii). Qualitative arguments are presented for this. These indicate that under low flow conditions particle bonding at the surface can occur, reducing the heat transfer rate.

The end of the transitional phase occurred when the inlet temperature reached 0°C. Heat transfer coefficients were found to increase above those for a single phase fluid. All data showed two peaks in the measured heat transfer coefficient, these have been associated with the particle size distributions of the materials used.

6.2 Data Acquisition and Analysis

This section discusses the development of two software programs developed to monitor and analyse data from the heat transfer test rig. The first, the data acquisition software, was developed for the purpose of collecting and recording temperature data from the calibrated thermocouples around the heat transfer test section. The analysis software

was designed to retrieve this data for processing with the manually recorded data (mass flow rate measurements), and output the results in a format that made it suitable for importing into existing graphical computer packages, for graphical plotting and further analysis.

The addition of a low thermal-noise voltage module to the Microlink system was discussed in Section 5.4.2, together with the interfacing protocols and basic control coding. The operation of the data acquisition software was to read, and record, the raw thermocouple voltages from this module, and simultaneously display the system temperatures in real time on the computer screen. The software also permitted pausing during recording to allow for both refreshing the cold-junction ice bath or measuring the intermediate mass flow rate of the slurry. The first version of this software recorded a single voltage from each thermocouple at regular intervals. To accompany this, a preliminary version of the analysis software was written to calculate both the heat transferred in the heat exchanger, and the associated heat transfer coefficient, from the collected data.

Trial runs of the heat transfer rig and the software initially gave very poor results. The typical magnitude of $\bar{h}$ calculated from the recorded data deviated from estimates, based upon Equation 2.37, by ~200%. Furthermore the recorded data appeared chaotic in nature, and swings of the order ±100% were seen between consecutive readings. A process of elimination was undertaken, analysing both the methodology and the system, in order to identify the causes. It was found that the problem originated from random fluctuations in the recorded thermocouple voltages due to electrical noise. This noise had a magnitude of up to 30μV, this could generate a swing of ±0.5°C in the calculated temperatures. Such a temperature fluctuation was most significant in the calculation of the energy transferred in the heat exchanger. Here the differential glycol temperature was used, this being typically 0.5°C or less.

To overcome the noise, the electrical grounding of the rig was checked, also screening was applied to the thermocouple wires. Also a check was made for the existence of any earth loops in the thermocouple/data-logging system. A repeat of the initial test was made but there were no improvements in the results. There were many local sources of electrical noise, the three most significant being the chiller unit, the agitation motors, and the air pump (used to agitate the cold junction ice bath). The contribution of each was checked by repeating the initial test several times but with alternate devices turned off.

It was found that the worst offender was the motor (and control unit) driving the agitator for the bulk tank. To overcome this, the control unit and the connecting cables were surrounded by an earthed screen. A repeat test showed that no improvement had been gained, although during the test the motor was turned off several times at the control box. This revealed that the actual control unit was responsible for the noise, and not the operation of the motor directly. The use of this motor could not be avoided during system operation.

In addition to local devices causing noise, it was observed that fluctuations in the recorded data increased between 5:00pm and 6:00pm! This suggested that fluctuations in the 240V ac mains was responsible for the errors in the recorded data from the Microlink. To overcome this an electrical filter was added to the mains supply; this yielded a small improvement, although at this stage the fluctuations were still of the order of 15μV. Some form of averaging, therefore, had to be applied to reduce the effects of the electrical noise being recorded.

Because the system was operated in a transient mode, errors would occur if the data averaging was taken over a long period. It was decided that a deviation not exceeding 0.1°C, during the data collecting period would be an acceptable limit. Based on typical rates of temperature change in the system (Figure 6.1) a limit of ~30s was feasible. It was found that for >100 readings, the error in the average results was to <3% (cf ~100%). Each channel of the Microlink could be read in 8×10^{-2}s, hence taking 100 readings from each channel would take about 13 seconds.

The actual mode of data collection was to read each channel sequentially once, and then repeat this process 100 times. This method ensured that all data, from each channel, were recorded over the entire integration period. The processing time for the statistical analysis of this number of readings was about 30s. This allowed the system to record data sets every minute during operation of the heat transfer test rig. The remaining time in the 1 minute interval allowed interaction with the user, so a pause in data logging could be initiated (this allowed samples for mass flow rates and analysis to be taken). The statistical analysis used the standard deviation method (Squires, 1985) in calculating the error in the reading. As a check, the median voltage value was measured for each thermocouple and recorded in a separate data file.

The original deviation of the predicted heat transfer coefficient was found to be a result of the use of Equation 2.37. This is limited to fully developed turbulent flow (Re>10,000), but from the results of the initial clear oil tests the maximum value obtainable in practice was Re=8,630. This resulted in the fluid having transitional flow conditions, hence Equation 2.39 was more appropriate. The analysis software was modified to produce values of $\overline{h}$ based upon this correlation. To interpolate tabulated data values of viscosity, heat capacity, density and thermal conductivity, the mean temperature of the fluid was used. The mean fluid velocity, required for calculations, was based upon a linear interpolation of the mass flow rate measurements. (The software prompted for these at the start of the program.) Comparison of experimental heat transfer coefficients with those produced by both Equations 2.37 and 2.39 (Figure 6.2, Figure 6.3), show that Equation 2.39 (Gnielinski, 1979) for transitional flow conditions gave good agreement in the range 0.4 to 0.8 $kW\cdot m^{-2}\cdot K^{-1}$.

The discrepancy between the predicted and measured data shown in both Figures 6.2 and 6.3 (at high temperatures in Figure 6.2, and high values of $\overline{h}$ in Figure 6.3) originated from the high rates of temperature change in the system at the start of the test run. It is for this reason that all following discussions will be limited to temperatures

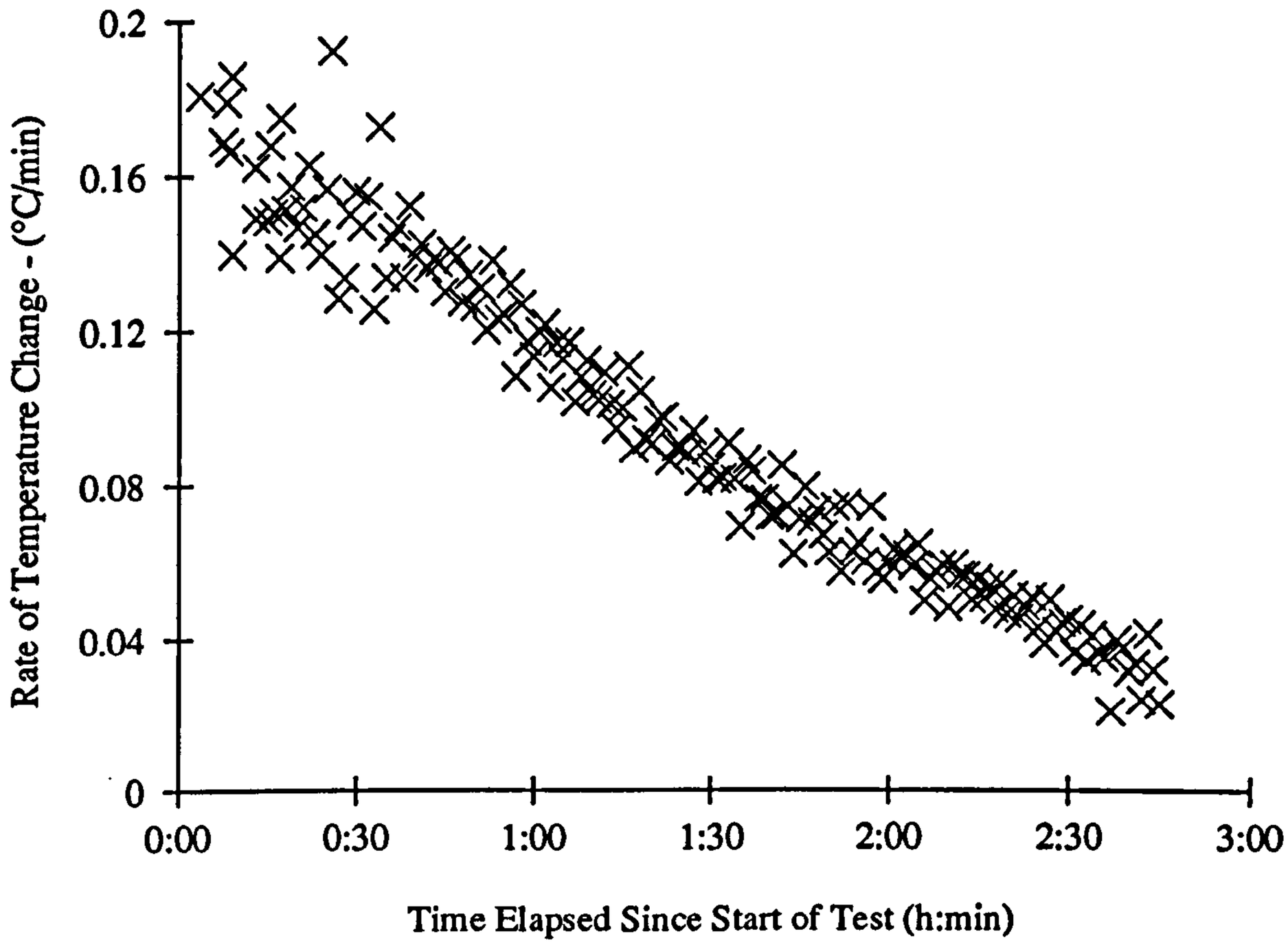

Figure 6.1: Rate of Change of the Test Fluid Temperature at the Heat Exchanger Inlet.

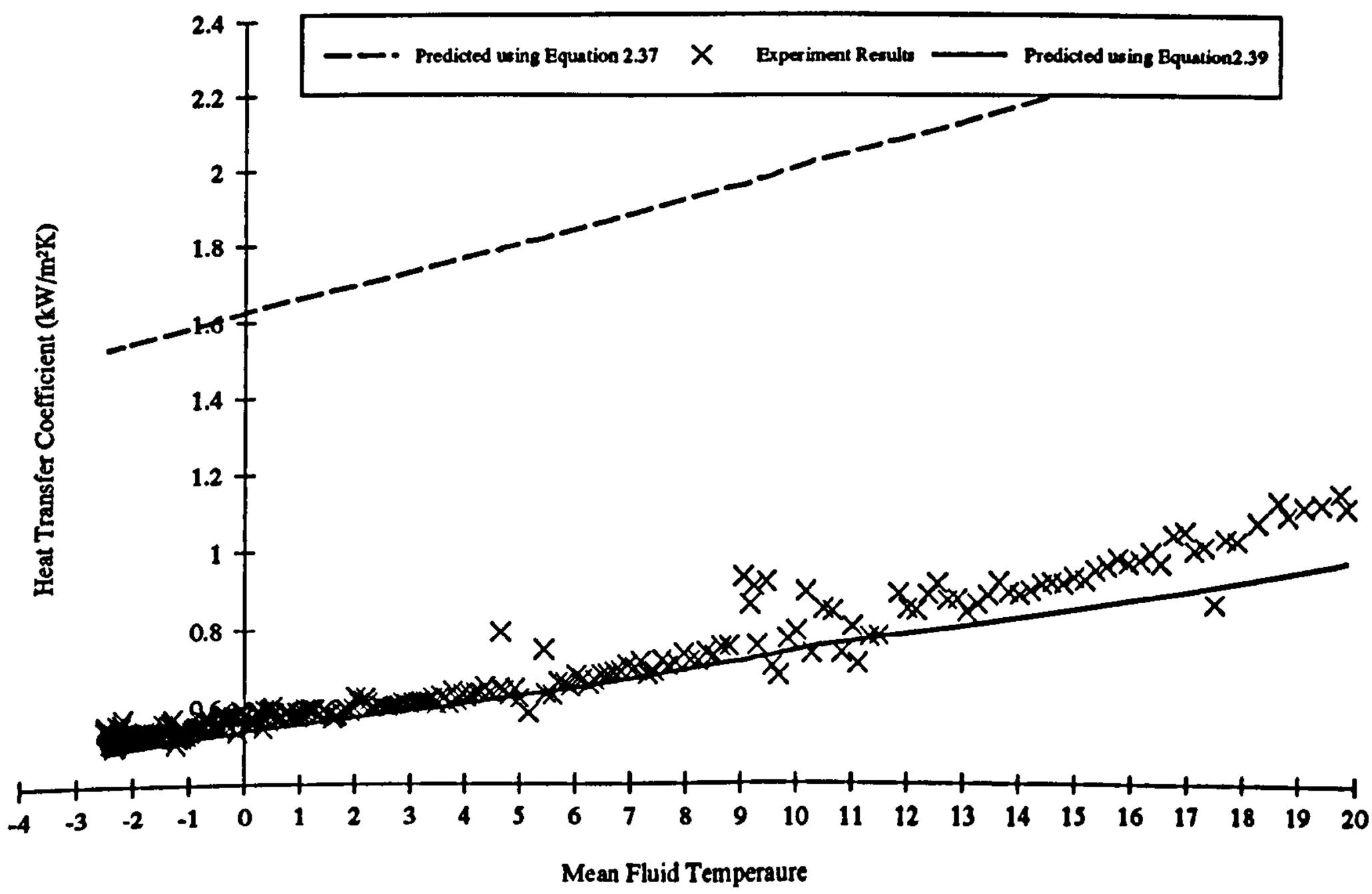

Figure 6.2: Measured and Predicted Heat Transfer Coefficients for Fusus Oil.

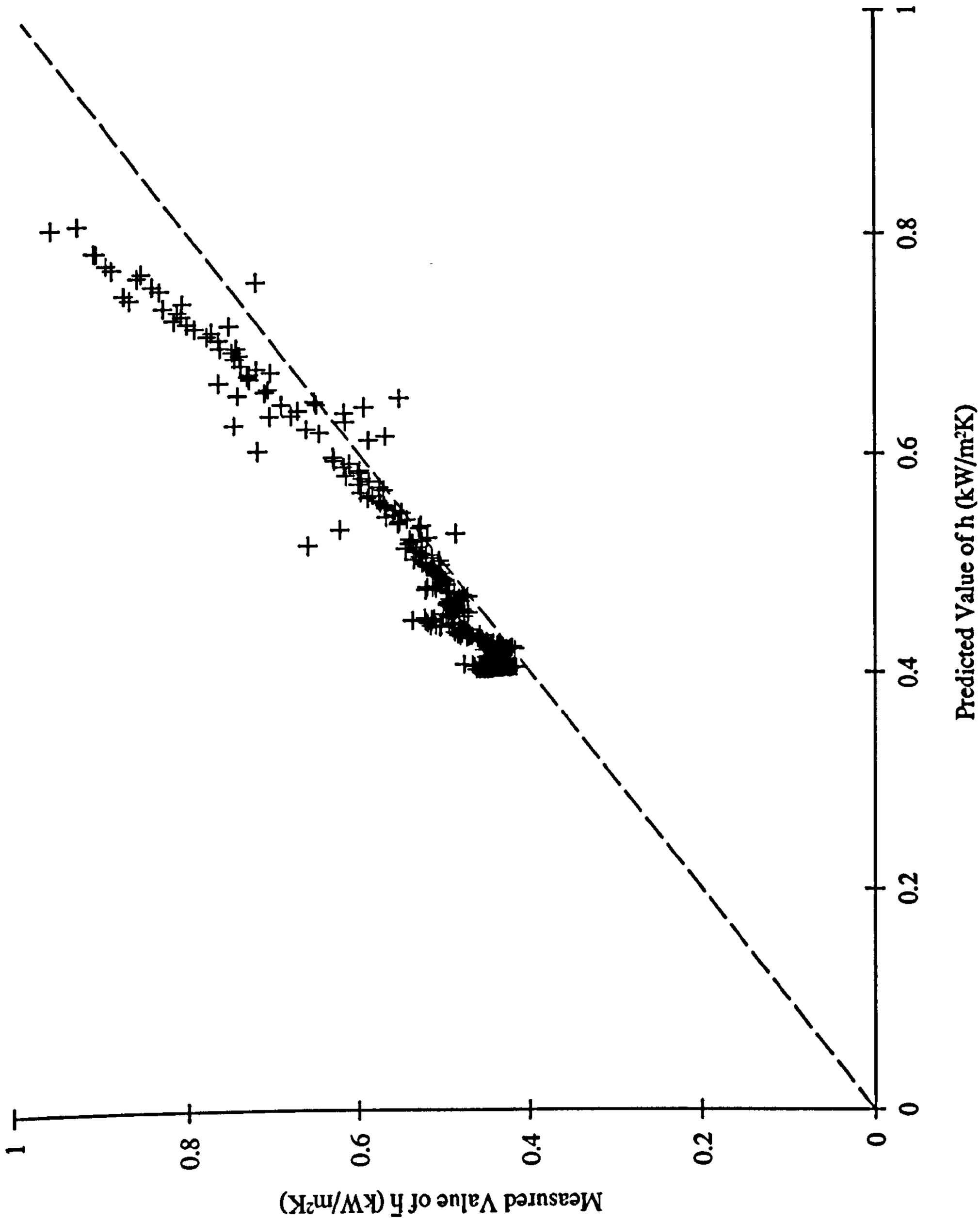

Figure 6.3: Comparison of the Measure Heat Transfer Coefficient for Fusus Oil with that Predicted by Gnielinski (1979).

below 14°C. There was also a bias in the measured heat transfer coefficients, the average value of this is 7(±5)%. A possible source of the bias might originate from a deviation between the true values of the physical properties of the oil, to those actually used in the calculations (based on *typical* data supplied by Shell). It is also evident that occasional large deviations occurred, eg at ~5°C in Figure 6.2. The source of these is again thought to be due to errors, due to electrical noise, in the recorded thermocouple voltages.

6.3.2 Modelling of the Effects of Particles

To account for the addition of solids to the system, the analysis software calculated the principal fluid properties, density, viscosity, thermal capacity and thermal conductivity, based on correlations presented in Chapter 2. The first, and simplest of these, was to account for the change in the mean density of the fluid, this employed Equation 2.53. Before this could be calculated the solids concentration, initially set at 18°C, had to be adjusted to account for the change in the oil density as the mixture cooled. Analysis showed that the new density was:-

$$\phi_{new} = \frac{\phi_{set}}{(1-\phi)\left(\frac{\rho_{set}}{\rho_{new}}\right)+\phi} \tag{6.1}$$

The modified solids concentration was used in calculating the other mixture properties. The thermal capacity used was calculated using Equation 2.54.

The size of particles used during charging of the system were in the range of 1mm to 2mm. The rheological behaviour, at low concentrations (<10%), is Newtonian (Section 2.4.3). To account for the increase in viscosity due to the presence of particles Equation 2.57 was employed. The choice of this was made because it applied to a wide range of concentrations, and its deviation from other, more complex, correlations was small. The effects on the apparent thermal conductivity, due to the presence of solid particles, was accounted for by Maxwell's equation (Equation 2.58).

Again the physical properties of the fluid employed in these calculations, were for the mean fluid temperature during a particular interval. The physical properties of the solid particles were those for a 75% hydrophilic material. All data were appropriate above 0°C, it was anticipated that below 0°C the effect of latent heat during phase change would make the correlation (Equation 2.39) for *Nu* invalid. The density of the hydrophilic particles was taken as $1040 kg \cdot m^{-3}$, and the thermal capacity $3.75 kJ \cdot kg^{-1}$. The thermal conductivity used was $0.6(\pm 0.1) W \cdot m \cdot K^{-1}$ (0°C to 10°C) as measured experimentally (Section 3.3).

The calculated physical properties were saved in the processed data file together with a number of non-dimensional numbers (the Reynolds number, Prandtl number and the Nusselt number again based on Equation 2.39), which were exploited to analyse the data.

6.3 Phase-Change Slurry Heat Transfer Test

A number of solids concentrations were investigated, namely 1%, 5%, 10% and 25% (by volume). The materials used for the tests were all medium-strength 75% water-content material. These were thermally cycled 20 times in the same manner as described in Section 4.2.2. To remove excess water from the materials, before placing in the heat transfer test rig, a centrifugal device was employed. After processing with this device, samples were taken to check their water content. Comparison of their initial mass, with that after drying gave a water content of 75(±2)% indicating that excess water had been removed. Particles were added to the system to achieve the desired concentration.

The test procedure adopted was to set the flow conditions for the rig (ie number of pumps in use, and the position of the control valve) and allow the slurry to circulate for one hour. At the same time the glycol circuit was circulated with the compressor of the chiller unit switched off. This allowed both systems to reach very similar temperatures, before the cooling and data logging were started.

After the start of the test, the system was allowed to cool to below 0°C. A number of samples were taken to (i) measure the mass flow rate and (ii) check the solids concentration of the flow mixture. For heat transfer analysis, samples were only taken at the start and end of the test, to avoid errors in the recorded data. All measurements showed a virtually linear flow rate with temperature. Measurements of solids concentrations were made, to check that the agitation device was fully mixing the contents of the bulk tank. Only for concentrations originally mixed at 25% solids, and at temperatures below 0°C, was any deviation found (Section 6.3.4).

Chapter 2 presented a number of correlations for the physical properties of solid-liquid mixtures. Generally these are considered to fail at a point where the mean particle separation is similar to the characteristic size of the particles. For systems of mono sized particles, this occurs at concentrations >10%. For this reason attention was given to concentrations of 5% and 10%.

6.3.1 Overview of Heat Transfer Results

General consideration of the behaviour of the slurry during cooling suggests a three stage process. The first is while all components of the slurry are above the phase change temperature. The second stage of consideration is a transitional phase, during which the heat-exchanger surface is at, or below, a temperature where phase change occurs, while the inlet temperature is above this. The third, and final stage, being when the inlet temperature also drops below the phase change temperature.

The behaviour in the first stage would show only the effects of the solid particles on the behaviour of the slurry's heat transfer coefficient. Figure 6.4 illustrates the measured heat transfer coefficients for concentrations of 1%, 5% and 10% under very similar

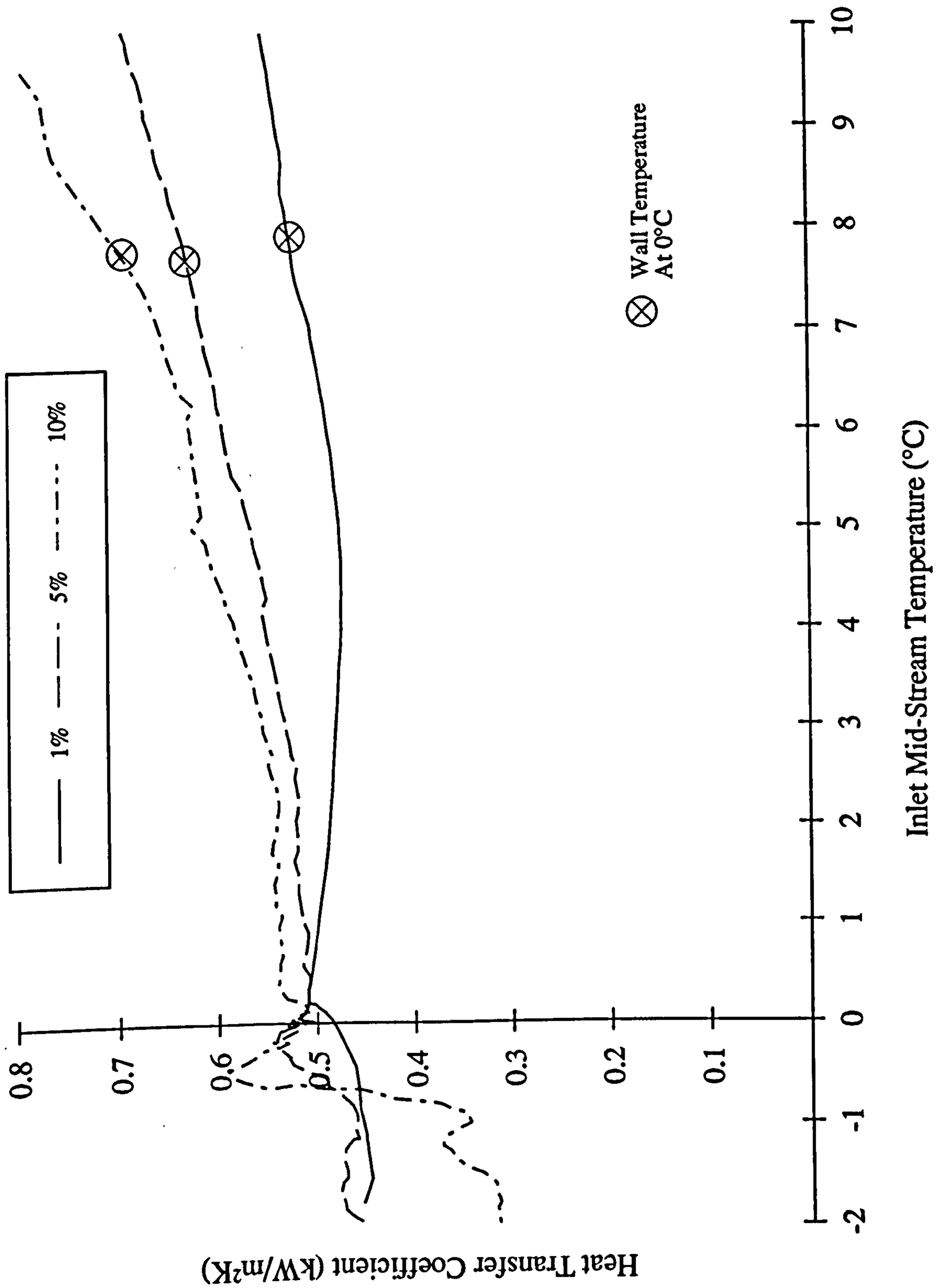

Figure 6.4: The Effect of Solids Concentration on the Heat Transfer Coefficient.

flow conditions (mass flow rate of 0.52(±0.02) $kg \cdot s^{-1}$ at 10°C). (The point at which the wall temperature reached 0°C is marked). It can be seen that no significant change in the gradient of $\bar{h}$ occurs, at this point, for the 1% and 5% slurries, although there is a change for the 10% slurry. Furthermore as the the inlet fluid temperature drops below 0°C, the gradient of $\bar{h}$ for the 1% fluid shows increase.

For inlet temperatures below 0°C there is a distinct change in behaviour with concentration. The 1% curve shows a smooth profile, indicating that phase change had occurred over a very restricted temperature range. However the 5% and 10% curves show a significant increase, reflecting the high thermal capacity of the mixtures due to phase change in the materials.

The effect of the flow rate was, as with a single phase fluid, to increase the overall value of $\bar{h}$.

6.3.2 The Heat Transfer Model

In this section the heat transfer data is compared with that of both a single phase fluid, and that predicted by applying the revised physical properties accounting for particles. As discussed in Section 6.2.1, these are limited to temperatures above 0°C. Attention focussed on concentrations of 5% and 10%.

With 5% solids in the system it was found that the predicted and measured values were in close agreement to those measured (Figures 6.5, 6.6, 6.7) if high mass flow rate conditions were used (at 10°C these were 0.59$kg \cdot s^{-1}$, 0.58$kg \cdot s^{-1}$ and 0.57$kg \cdot s^{-1}$ respectively). As flow conditions were reduced, a rapid decrease in values of $\bar{h}$ was observed (Figures 6.8 and 6.9 - at 10°C these were 0.51$kg \cdot s^{-1}$ and 0.48$kg \cdot s^{-1}$ respectively). This deviation occurred over a very narrow range of flow rates. At 10°C for all of the tests the value of $\bar{h}$ decreased from 0.65$kW \cdot m^{-2} \cdot K$ at 0.59$kg \cdot s^{-1}$ down to 0.37$kW \cdot m^{-2} \cdot K$ at 0.48$kg \cdot s^{-1}$. This was a decrease of nearly 50% in $\bar{h}$ over a change in the flow rate of 20%.

This suggested that at the lower flow rates the degree of turbulence was insufficient to overcome settling. Under these conditions the particles were believed to have formed a moving bed on the lower surface of the heat transfer tube. If this was the case, heat transfer would be reduced due to the increase in thermal resistance resulting from the particle bed (cf Harada (1985), Section 2.5). To illustrate this, dimensional analysis was applied (see Figure 6.10) using an apparent Reynolds number based on the mass flow rate of the mixture. The failure of *Run05a07* and *Run05a08* (Appendix D) to correlate with the other data (Run05a04, Run05a05, and Run05a06) shows that such an analysis is insufficient where phase separation has occurred and further terms must be considered.

Analysis of the heat transfer tests for 10% mixtures, revealed that the use of the standard heat transfer equation fails to give any correlation at the flow rates tested. This

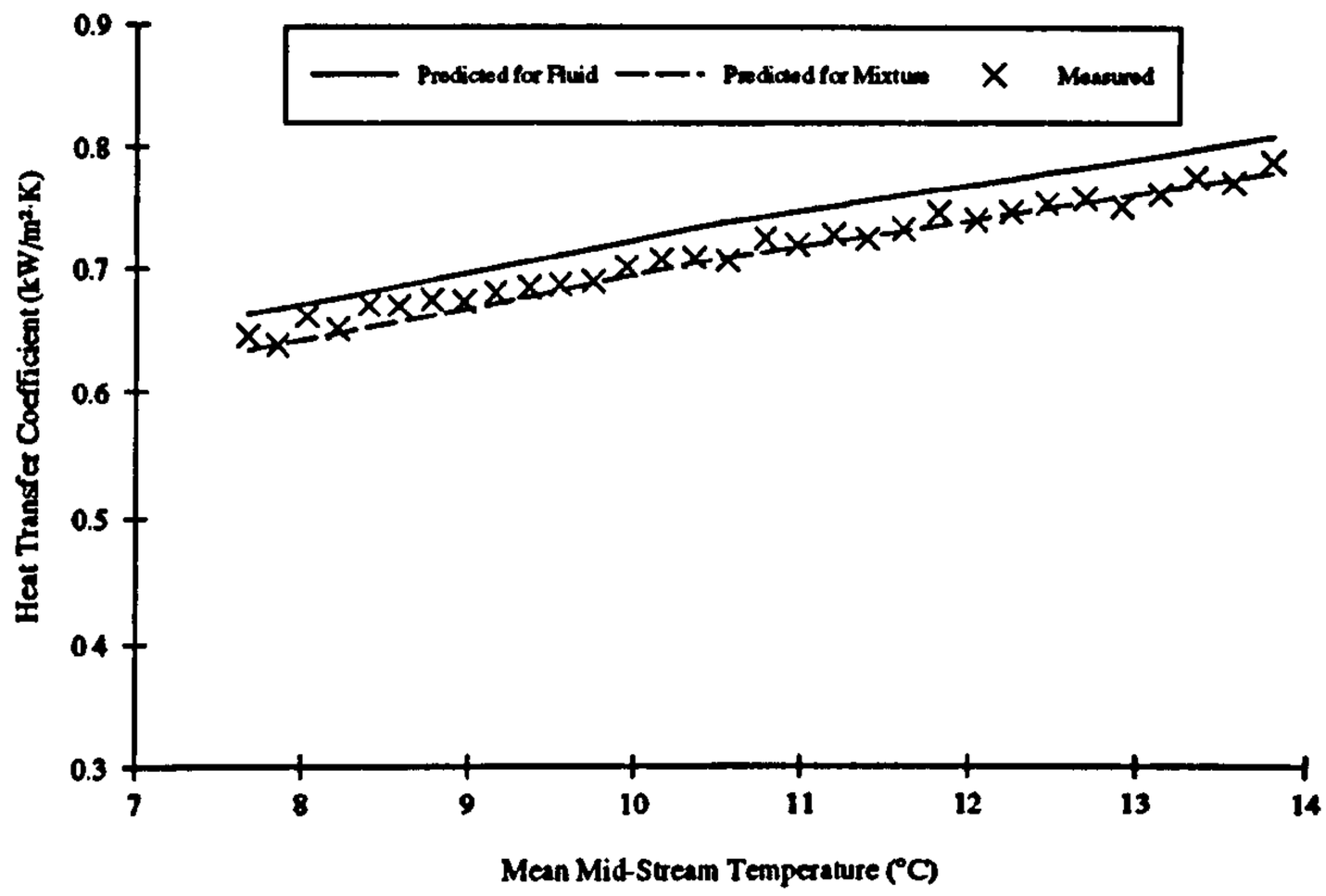

Figure 6.5: Comparison of Heat Transfer Coefficients for test Run05a04.

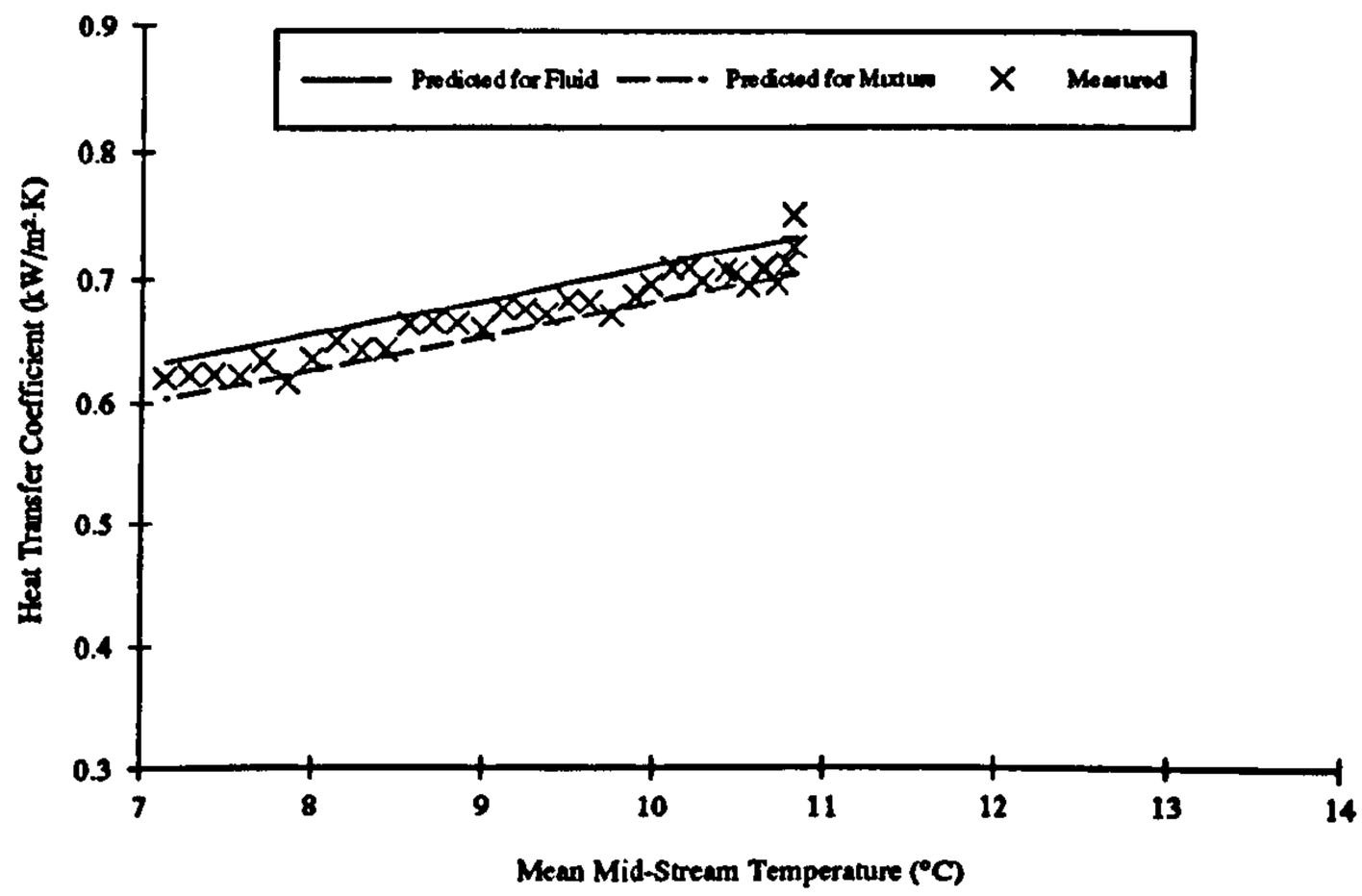

Figure 6.6: Comparison of Heat Transfer Coefficients for test Run05a05.

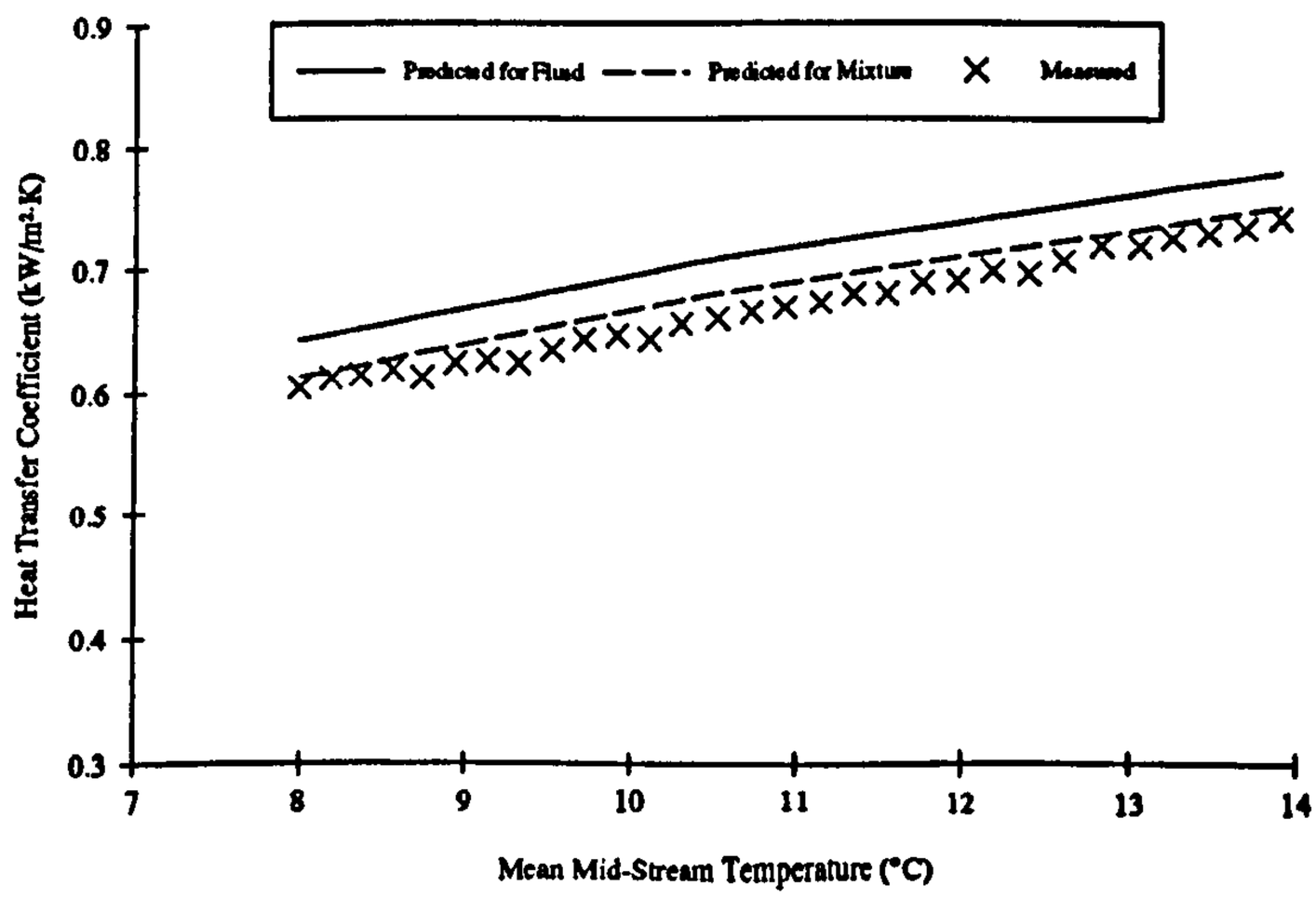

Figure 6.7: Comparison of Heat Transfer Coefficients for test Run05a06.

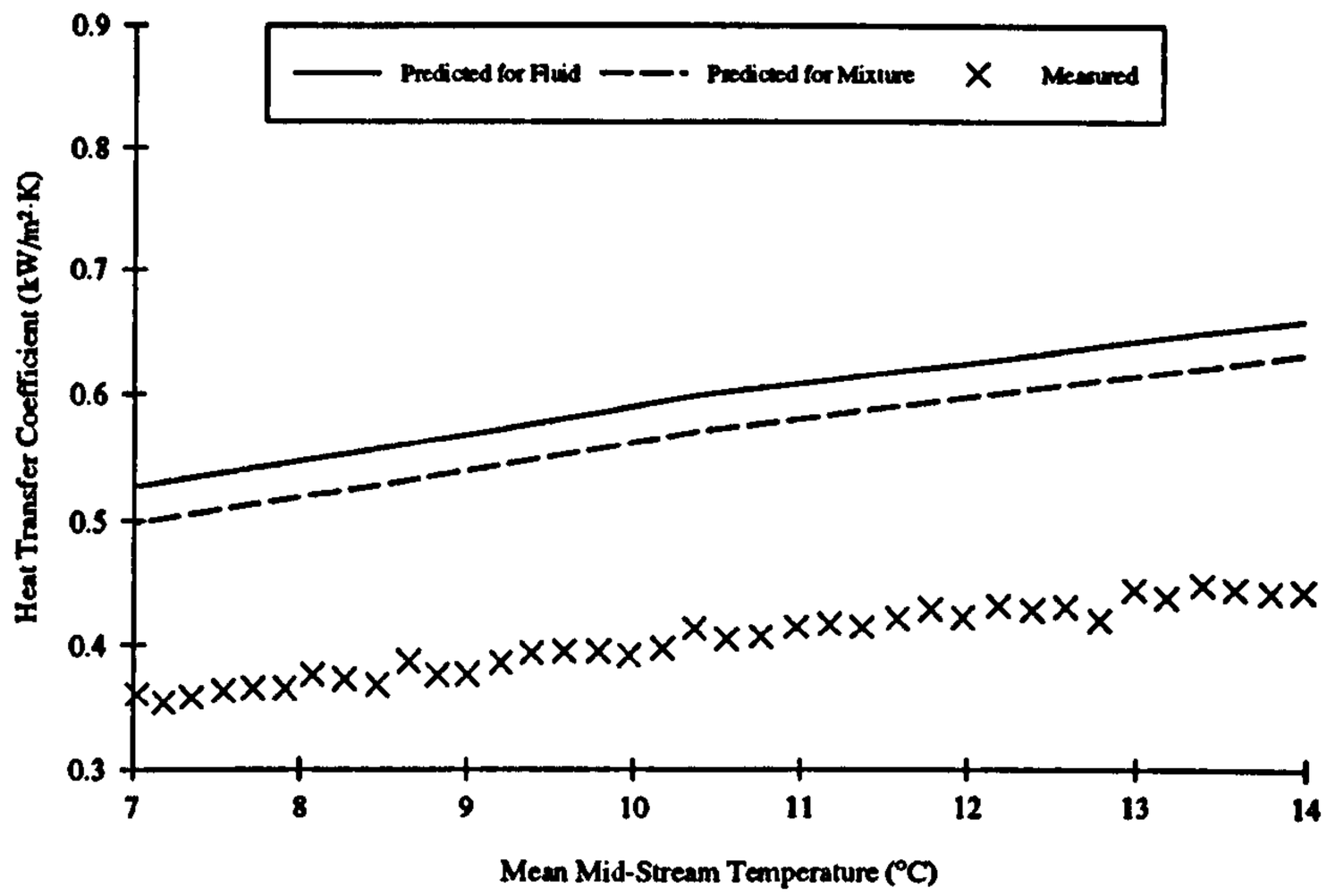

Figure 6.8: Comparison of Heat Transfer Coefficients for test Run05a08.

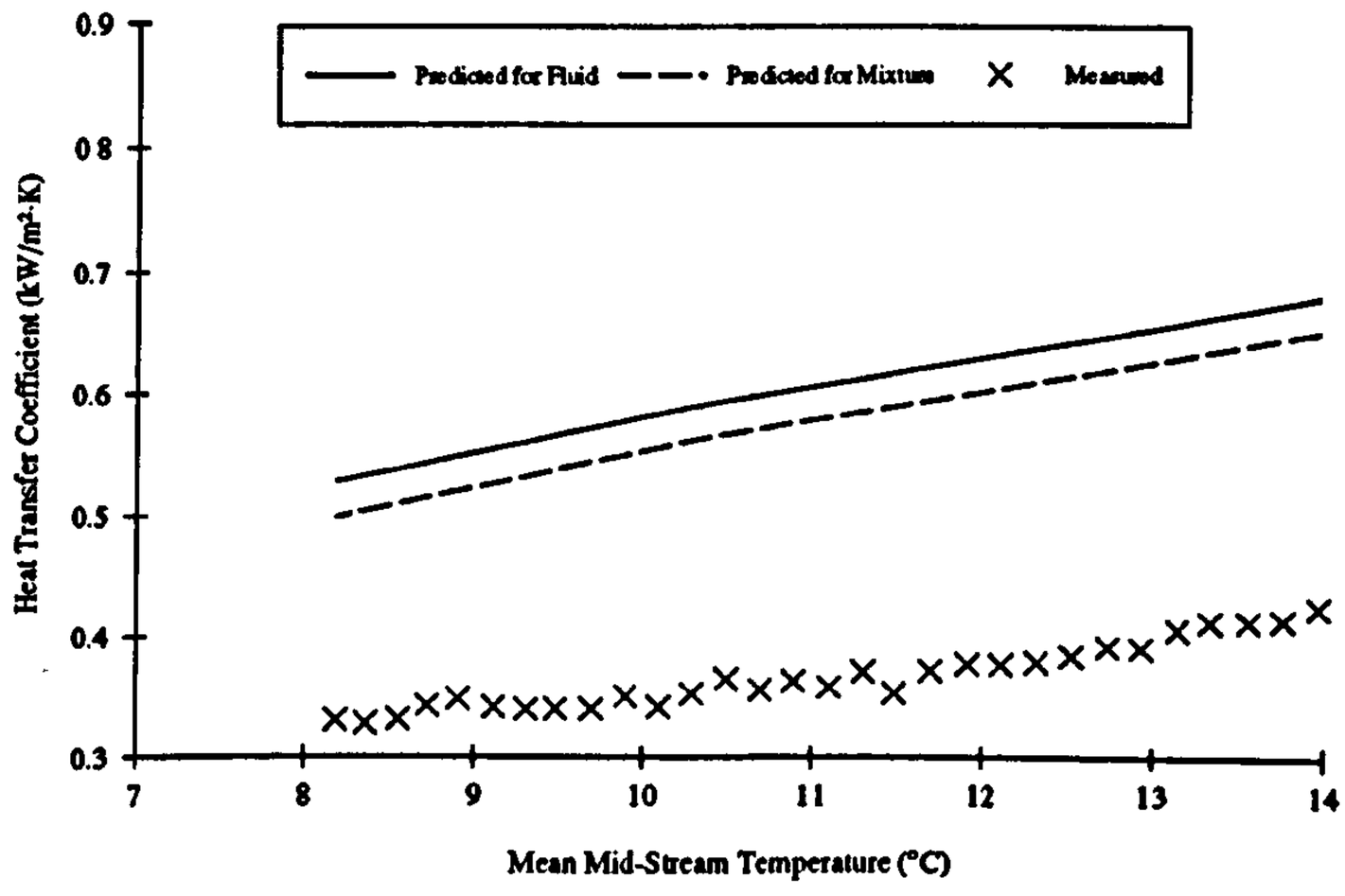

Figure 6.9: Comparison of Heat Transfer Coefficients for test Run05a07.

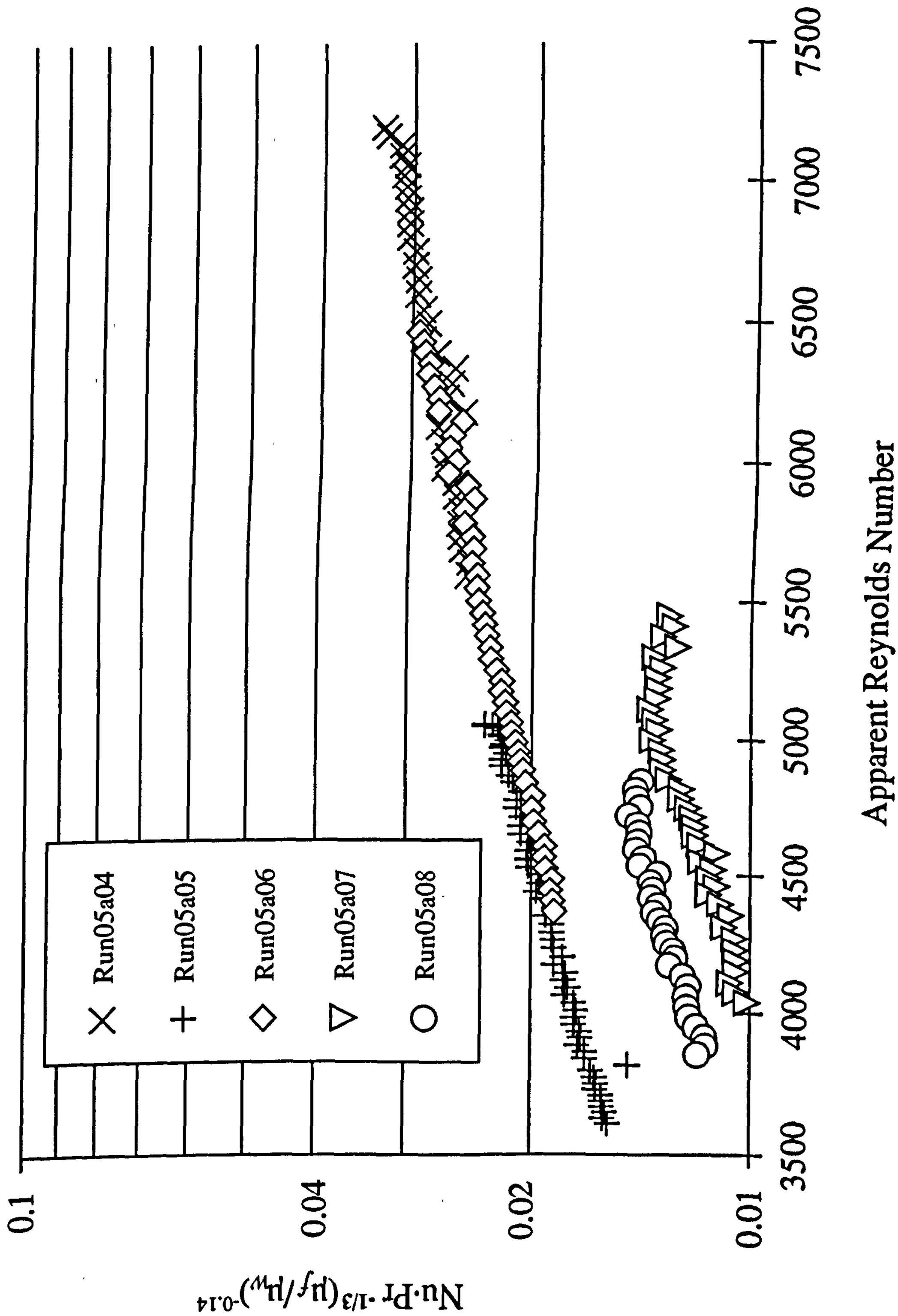

Figure 6.10: Comparison of Re against $Nu \cdot Pr^{-1/3}(\mu_f/\mu_w)^{-0.14}$ for Different Flow Conditions of 5% Slurry Heat Transfer Tests.

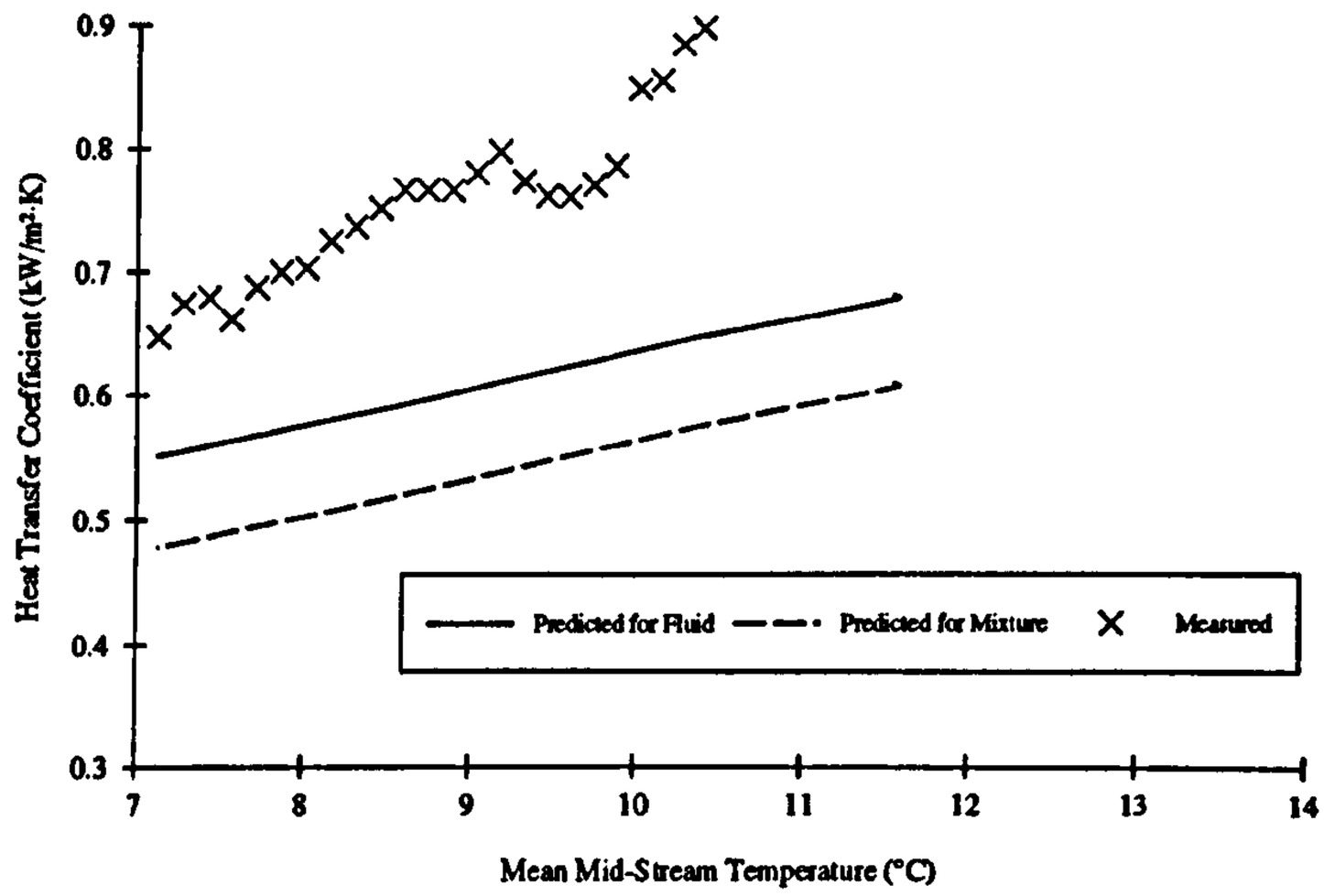

Figure 6.11: Comparison of Heat Transfer Coefficients for test Run10a04.

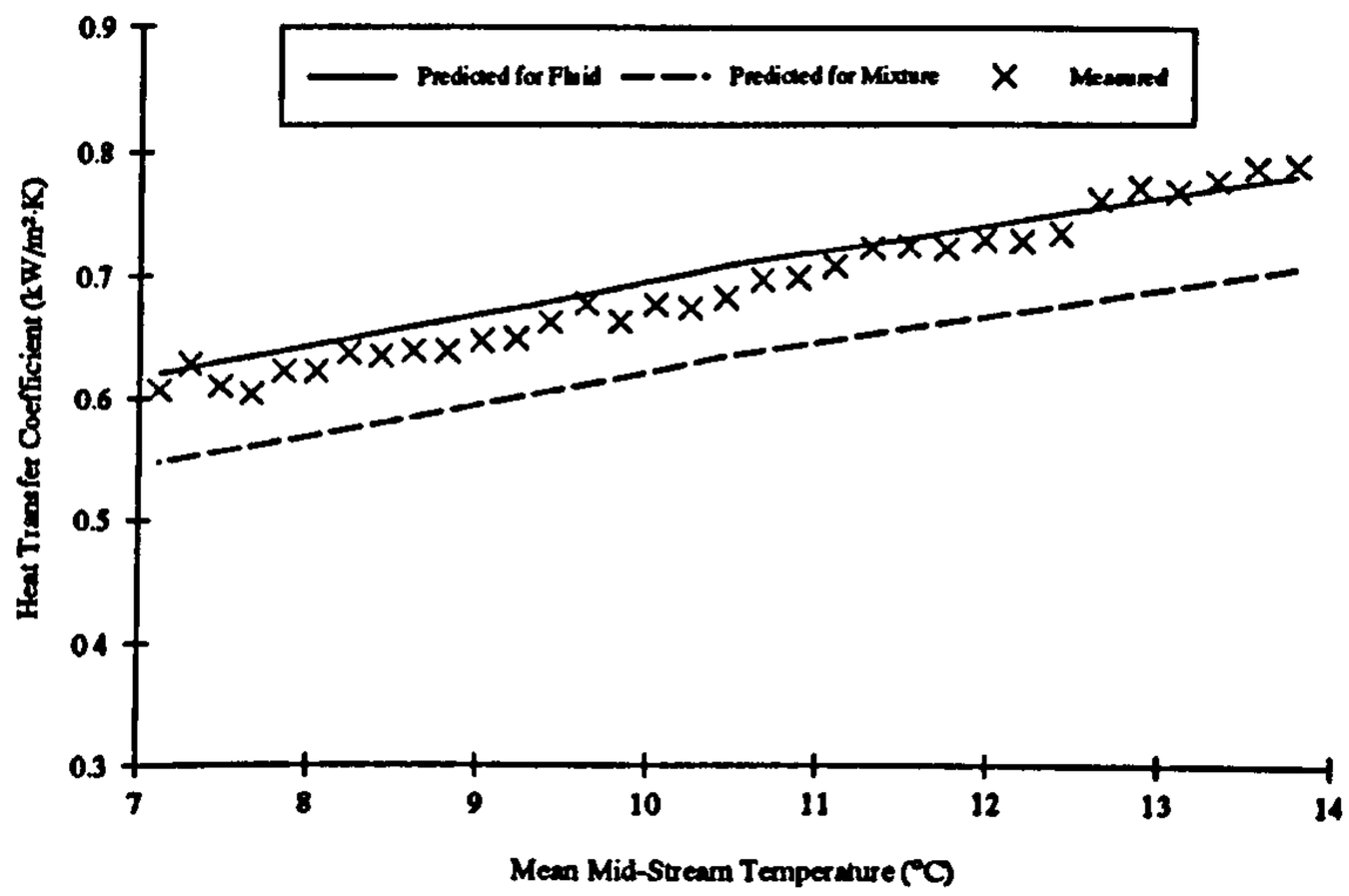

Figure 6.12: Comparison of Heat Transfer Coefficients for test Run10a05.

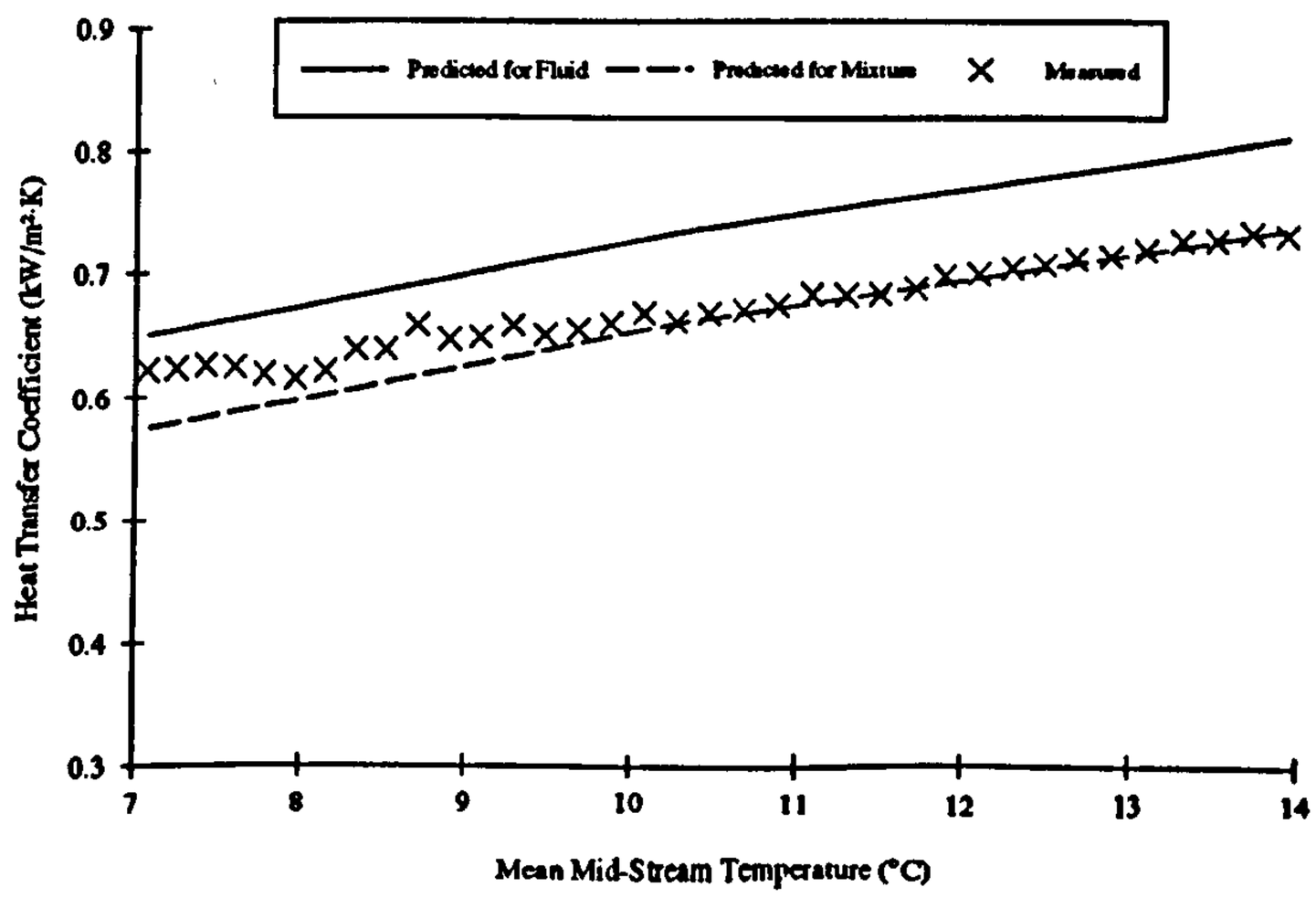

Figure 6.13: Comparison of Heat Transfer Coefficients for test Run10a06.

is illustrated in Figure 6.11. At the higher flow rates (Figures 2.12 and 2.13), $\bar{h}$ was found to be significantly enhanced above predictions for both a single phase fluid, and when applying modifications to account for solid particles. This was further illustrated by dimensional analysis for the test of 10% slurries (Figure 6.14). The results obtained for 10% solids concentrations clearly indicate that the correlations used for single phase fluids no longer apply, and some other form of analysis is required. As this work was primarily concerned with applying actively phase changing slurries to thermal storage systems, no further analysis will be presented for temperatures above the phase transition.

Results are not presented for the 10% mixture at low flow rates since the system was found to fail due to blockage at the control valve. This required the rig to be drained and dismantled to clear the blockages.

6.3.3 The Effects of Phase Change

In Section 6.3.1 typical curves for the behaviour of the phase change slurries were presented (Figure 6.4). It is evident that the 10% mixture gave a significant enhancement at transitional temperatures. This section details the data from further investigations made at these concentrations. Particular attention is given to the higher flow conditions, on account of the higher heat transfer rates previously observed.

The limitations imposed on the lowest temperatures of the glycol circuit of the test rig, due to chiller performance, caused the differential temperatures used in calculating $\bar{h}$ to become small as the system cooled. This resulted in the electrical noise to having a significant effect on the final value of $\bar{h}$ measured close to the phase change temperature. Furthermore particles were believed to be adhering to the temperature probes in the mixture for small periods, causing additional fluctuations. To negate these effects tests were repeated under the same system flow condition and the resulting data averaged to reduce the errors. The controlling parameter used was the number of pumps operated, and is referred to as; High flow rates (all four pumps), Medium flow rates (three pumps), and Low flow rates (two pumps). As with the previous tests, the low flow rates were not always stable. Taking mass flow rate measurements often disturbed the conditions in the system enough to lead to blockages. The equivalence of the flow rates for the repeated tests is illustrated in Figure 6.15.

The heat transfer coefficient at high flow rates, averaged for 5 test runs, is shown in Figure 6.16. The results again show that around the phase transition temperature, the heat transfer coefficients are enhanced by 10% to 20%. More significant is the enhancement below 0°C; it is typically 60% although at -2.5°C it peaked at 70%. This general increase in $\bar{h}$ results from the effective thermal capacity of the fluid having increased, due to the latent heat exhibited by the particles. Of interest are the dual peaks evident during the phase transition (see Figure 6.16). There is no definite explanation for this phenomena, although two possibilities are (a) the materials used had two phase transition temperatures (originating form incomplete thermal cycling), and (b) the

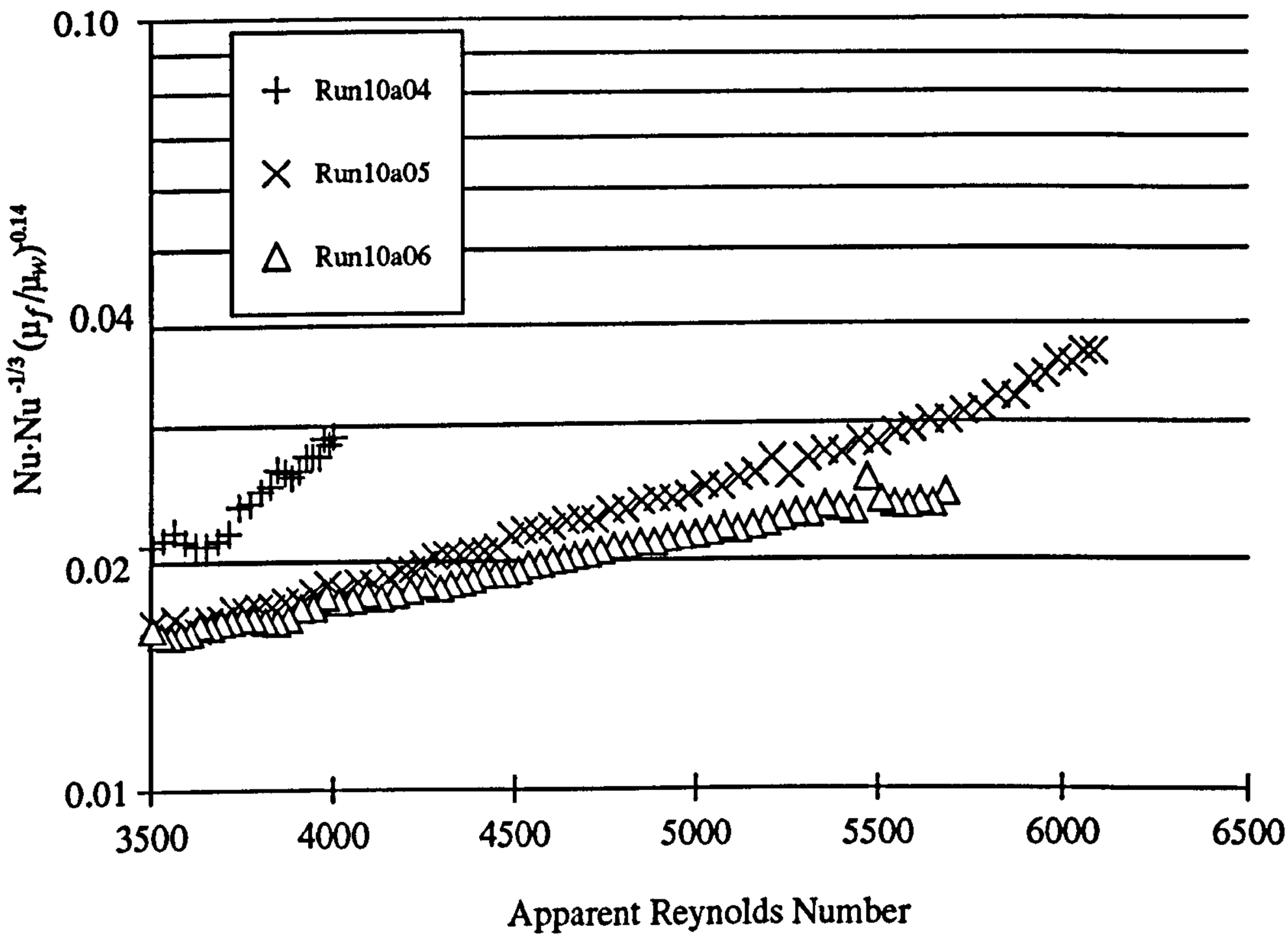

Figure 6.14: Comparison of Re against $Nu \cdot Pr^{-1/3}(\mu_f/\mu_w)^{-0.14}$ for Different Flow Conditions of 10% Slurry Heat Transfer Tests.

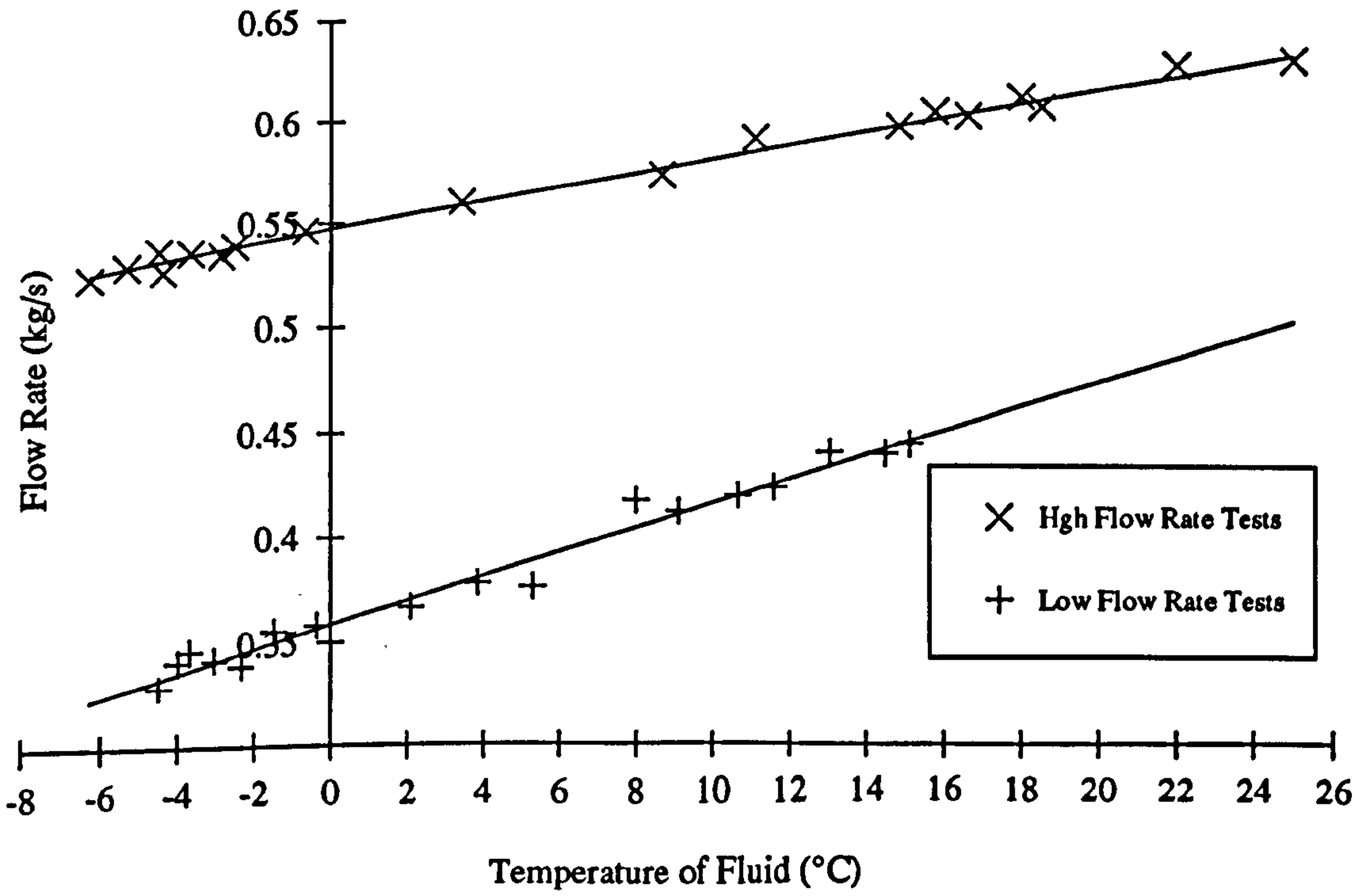

Figure 6.15: Distribution Of flow Rates during Equivalent Flow Conditions.

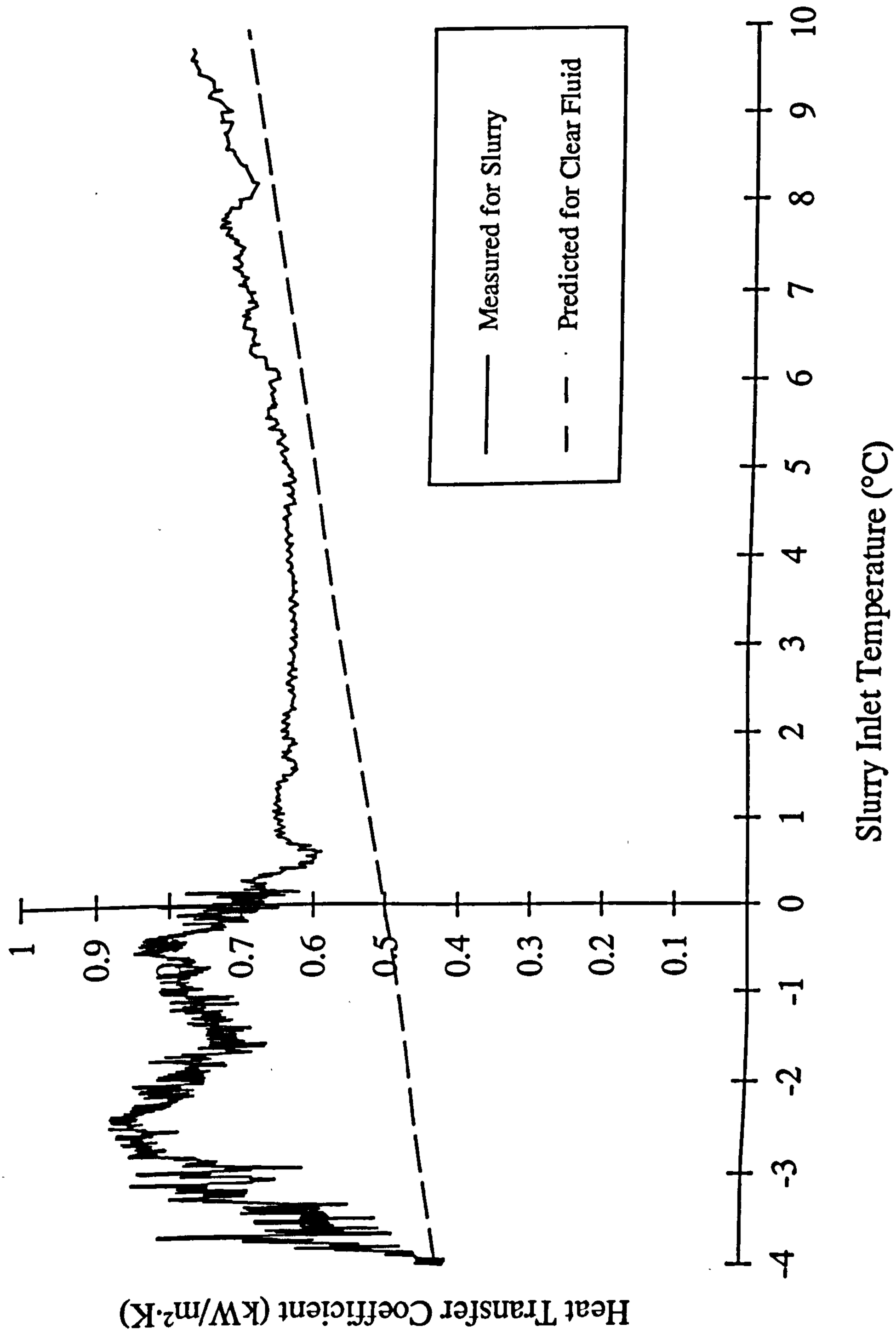

Figure 6.16: Measured Heat Transfer Coefficient for High Flow Rates at Concentrations of 10%.

particle size distribution.The second possibility would require the particles to have two peaks in the particle size distribution. The small particles would complete their phase transition more rapidly than the larger particles. This aspect is a topic recommended for further research (see Chapter 7). The time limitations of this project have not allowed this to be investigated.

Below -2.5°C a very sharp decrease in $\overline{h}$ was measured. This is indicated that phase transition had been completed.

A similar increase in the heat transfer coefficient above 0°C was seen for both the medium flow rates, and the low flow rates. For both, the increase was more significant than that recorded for the high flow rates, being of the order of ~20%. The behaviour of $\overline{h}$ below the transition temperature differed from those of the high flow rate test. For the medium flow rates an increase of <30% was observed. There was also evidence of peaks in the enhancement of $\overline{h}$ at similar temperatures, although these occurred at slightly lower temperatures than for the high flow rates (-0.8°C and -2.7°C). This trend was seen to follow, in the low flow rate tests, where the two peaks occurred at -1.2°C and -3°C, compared to -0.5°C and -2.4°C at the high flow rates. This would further suggest the existence of two particle sizes in the mixture, as opposed to different phase change temperatures.

The low flow rate test showed a significant drop in the heat transfer coefficient between 0°C and -1°C (Figure 6.17). There is no explanation for this process although checks were made on a repeat test of the flow rate across this region. This showed a virtually linear variation in the flow rate with temperature. It is possible that at these flow conditions small agglomerations were forming due to ice bridging (Section 4.4.2). This would cause a plug-like flow. Such agglomerations would have been subjected to high rates of shear, in the pumps and the agitated bulk tank, causing them to break down. At lower temperatures the surface of the particles would have completed phase transition and no further formation of ice bridges would have occurred.

6.3.4 High Concentration Slurry Tests

Only two tests were successfully conducted at concentrations of 25% with a single flow rate. The reason for this was failure at the open part of the bulk tank at temperatures below 0°C. This occurred in the chute where particle agglomerations formed causing blockage of the system. In practice near-continuous manual probing of the area had to be performed to overcome the problem. Furthermore, the slurry returning to the bulk tank formed agglomerations that floated. These were not sufficiently broken up by the agitation device and rapidly formed a complete floating mass on the surface. This is thought to result from the particles adhering together due to ice bridging. These groups of particles trapped air, resulting in their attaining a density below that of the oil. Samples taken during the test had a fraction of material floating, which could be diminished by gentle stirring. These samples also showed that the solids concentration had dropped from 25% at the start of the tests to 19% at -4°C. This was assumed to be a

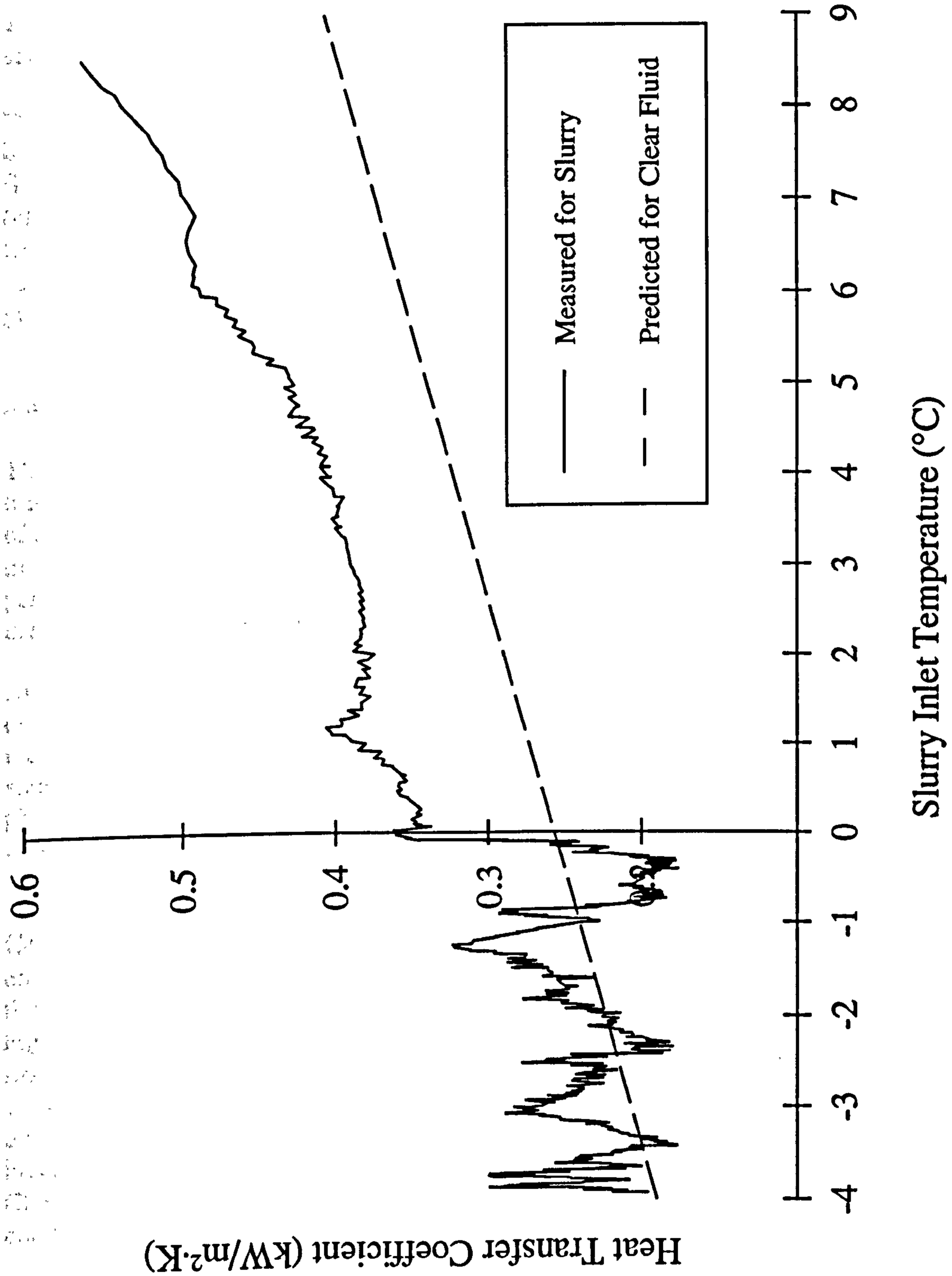

Figure 6.17: Measured Heat Transfer Coefficient for Low Flow Rates at Concentrations of 10%.

result of the materials floating and forming a solid mass in the bulk tank.

The measured heat transfer coefficient at a concentration of 25% (Figure 6.18) showed some similarity to those of the tests for 10%. There was a general enhancement in $\overline{h}$ above that of the clear fluid down to ~2°C, at which point a sudden decrease was seen to occur. The cause of this is again believed to be related to ice bridges occurring between particles, causing agglomerations to form in the heat transfer test section. The flow rates of this test were similar to those of the low flow conditions for the 10% tests (cf 0.43 $kg \cdot s^{-1}$ at 12.3 °C), although due to the higher solids concentration the turbulence was reduced. This caused particles to remain closer to the heat transfer surface for longer periods, allowing the conditions for ice bridging to occur sooner at a given inlet temperature.

6.4 Conclusions

The tests reported in this chapter have extended the published range of data for the heat transfer properties of solid-liquid mixtures. The first is that the heat transfer behaviour of a solid-liquid mixture at low concentrations (<10%), without phase change, can be modelled by applying appropriate modifications accounting for the presence of particles. This fails when turbulence is not sufficient to overcome settling, and under these conditions a reduction occurs in the heat transfer coefficient.

At solids concentrations ≥10% the heat transfer coefficient shows a significant increase over that modelled for a single phase fluid, with or without particle modifications included. This suggests that the particle interaction with the boundary layer is becoming significant. This was further confirmed once conditions at the boundary layer allowed phase change to occur. The scale of the effect was found to be very dependent on the flow conditions, and it is believed that ice bridging between particles is a controlling factor.

Generally the data collected indicates that the use of phase change slurries in thermal energy storage systems can be used at the temperatures required for storage. To improve the performance of these mixtures requires a support fluid with a lower viscosity, and a higher thermal capacity/conductivity, than the oil used. This in turn will require higher flow rates to be applied to maintain homogeneity within the flow. Flow rates tested were not sufficient for fully developed turbulence to be established. It is believed that under such conditions particle interaction with the boundary layer will increase, thereby increasing the heat transfer rate. Modifications required to the rig are discussed in Chapter 7 together with recommendations for improving performance with high solids concentrations.

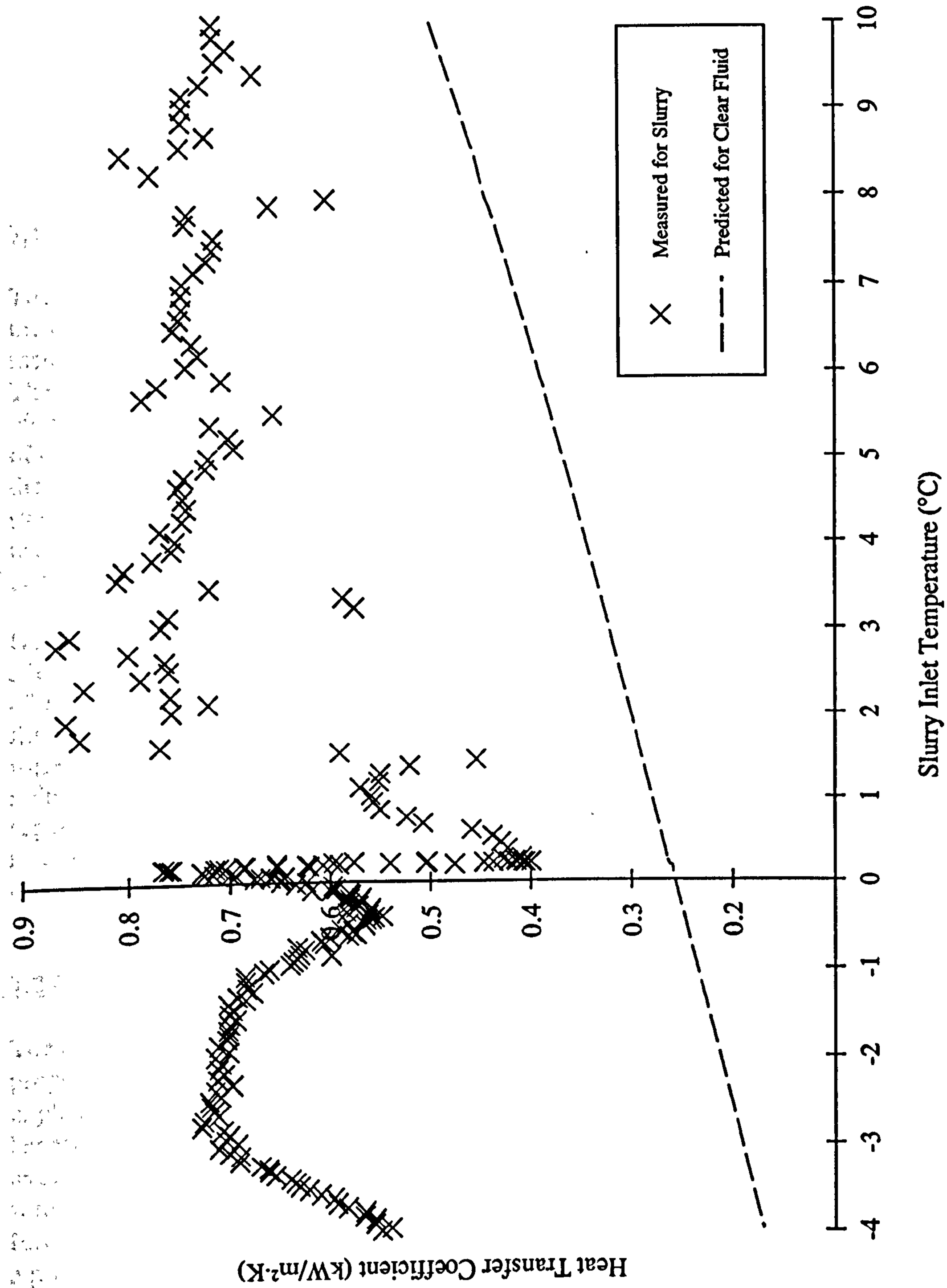

Figure 6.18: Heat Transfer Coefficient Measured for 25% Concentration.

Chapter 7

Discussion and Recommendations

7.1 General Discussion

The research presented in this thesis has demonstrated that hydrated hydrophilic materials supported in a suitable non-freezing fluid, can produce a phase change medium for application in thermal energy storage systems operating at or below 0°C. The resulting phase change slurry can be pumped, thus providing a thermal fluid of high effective thermal capacity. Such pumpable thermal fluids are desirable as a means of overcoming the thermal capacity limitations of conventional cold storage systems that employ a secondary refrigerant, such as glycol brines. The storage temperatures (the transition temperature of the hydrated hydrophilic material) can be reduced by the use of salt solutions to hydrate the materials, thus providing a further gain over conventional ice storage systems by extending the range of application temperatures.

Using these materials an effective storage system has been constructed, which in addition to a heat transfer test rig, has been designed and used to measure the properties of a range of hydrophilic slurries. There are two conflicting demands upon the support fluid. For the final design of the cold storage device high rates of particle separation were desired, whereas for high rates of heat transfer any settlement of material caused a reduction in the value of $\bar{h}$. This could be overcome by (i) improving the design of the separation device in the cold storage system; and (ii) applying higher flow rates in the heat transfer loop to increase turbulence, thus avoiding settling. A extensive review of possible support fluids is required.

7.2 Materials Tests

The material tests, undertaken during this project, have shown that the thermal properties of currently available hydrophilic materials are suitable for cold storage applications. The novel high water content materials investigated (>90%) have certain benefits over conventional materials (75%), namely their higher water content, and avoidance of the need for thermal cycling (Chapter 3). These are however mechanically weak, compared with the 75% materials used in this study. It is recommended that further tests are undertaken to establish their mechanical strength while forming part of a pumped phase change slurry which undergoes repeated thermal cycling, to assess degradation of the particles.

The phase transition temperature can be reduced by using salt solutions for hydration, successful trials in the range 0 → -10°C have been carried out. Although the principal

interest in this project has been energy storage at temperatures below ambient, the requirements of good heat transfer apply to storage at any small ΔT. There are a number of aqueous solutions that show non-freezing transitions above 0°C (eg sodium sulfide at concentrations >13% by mass). The application of these may provide a means of extending the range of thermal storage applications for hydrophilic materials, investigation is recommended.

7.3 Cold Storage Device

The final design of the cold storage device described in Chapter 4, achieved a solution to the problem of mobilising a high solids concentration store, while separately controlling the properties of an associated circulation system. The method employed was to feed the particles into a turbulent stream at a controlled rate. After passing through a heat exchanger, the solids were returned to the main storage volume, allowing the clear fluid to be recirculated, hence allowing the process to continue.

The design of both the feeder device, and the separation device, requires more investigation to provide engineering design data. It is recommended that the feeder system used is replaced with some form of sealed conveyor operating at the base of a tank (Figure 7.1). This would eliminate the need for a central shaft, giving a device that could be attached to the base of a rectangular vessel.

The separator requires more detailed analysis, although again this could be considered independent of the geometry of the bulk storage tank used. Further investigations should study the cyclone design in relation to the particle size, the solids concentration, the flow rate and the supporting fluid used.

7.4 Heat Transfer Test

The results from the heat transfer tests of active phase change slurries, have extended the range of studied concentrations into regions where non Newtonian behaviour occurs. The developed rig is sensitive enough to be useful to a further research programme. This section discusses some of the improvements that could be made to the system to increase its ability to collect more detailed heat transfer data, and other parameters requiring investigation (eg pressure drops).

Most crucial is the addition of a Coriollis flow meter (or some other device to give accurate flow rate data from a closed system). In conjunction with this, the pumps should be replaced with a controllable lobe pump to achieve higher flow rates (×2). The combined application of these two devices will yield a number of benefits. Firstly, the feed back of the flow rate within the system will allow a constant value to be maintained throughout the temperature range investigated. Secondly, the total volume of the system will be reduced by an estimated 80%. This will reduce the cost of the materials used, the processing time required during preparation, and the response time

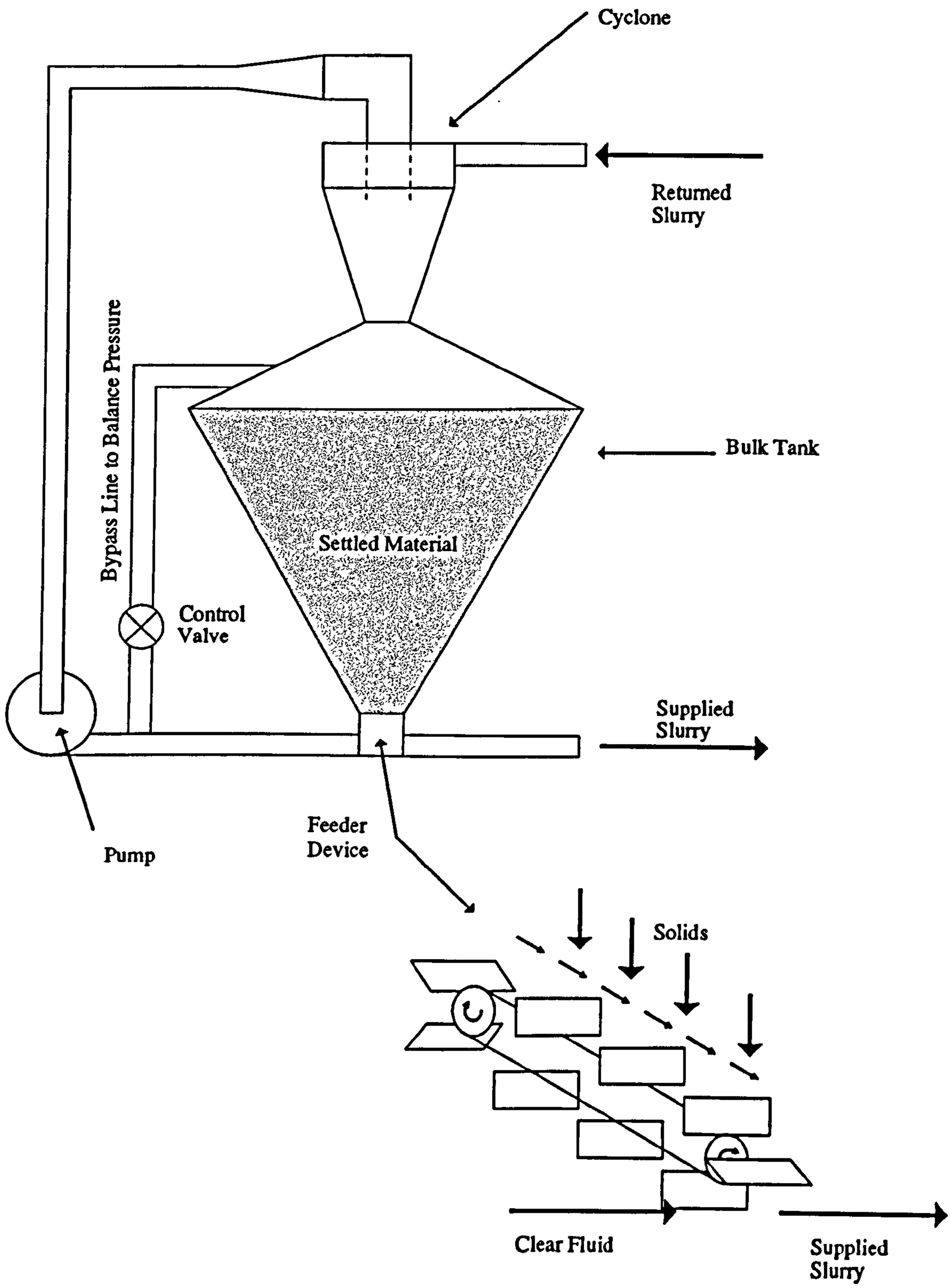

Figure 7.1: Typical Layout of Cold Storage System

of the system. Thirdly, with feedback of flow rate to the system, critical points can be investigated under more controlled conditions, (eg constant inlet mixture temperatures with changing heat transfer surface temperatures). Next the closed nature of the test apparatus may overcome the problems encountered with the high solids concentrations and stop excess water from gaining access to the system. Finally a closed system combined with an improved pump, will increase the flow rate into the range where fully developed turbulence exists. In fact, with appropriate control software, such a system could be designed to collect a full range of data for a particular charge (mixture) with minimal intervention.

By making these modifications the range of mixtures investigated could be greatly increased. The parameters of most interest are (i) the support fluid, (ii) the particle size and size distribution, (iii) the hydration fluid, and (iv) the materials used. All are believed to have significant effects on the heat transfer properties of the slurry.

References

Acorn — Acorn Computers Ltd, User Guide, Cambridge, UK,1987.

Ames — Ames, D. A., The Past, Present and Future of Eutectic Salt Storage Systems. ASHRAE Journal, May 1989, pp. 26-27.

Armstrong — Armstrong, Armstrong Insulation, Armstrong World Industries Limited, Middlesex, 1992.

ASHRAE — American Society of Heating, Refrigerating and Air-Conditioning Engineers, ASHRAE handbook: 1985 Fundamentals, ASHRAE Atlanta, GA, 1085.

Bael — Bael, J. V., Flo-Ice as a Carrier for Cold, CADDET Newsletter, No. 4, 1996.

Baker — Baker, R.C., An introductory guide to flow measurement, Mechanical Engineering, London, 1988.

Barber — Barber, C. R., The Calibration of Thermometers, HMSO, London 1971.

Barnes — Barnes, H. A.. Shear-Thickening ("Dilatancy") in Suspensions of Nonaggregating Solid Particles Dispersed in Newtonian Liquids. Journal of Rheology, Vol. 33, No. 2, pp. 329-366, 1989.

Beck — Beck, M.S. and A. Plaskowski., Cross correlation flowmeters : their design and application, Hilger, Bristol, 1987.

Bennett — Bennet, C. O., and Myers J. E., Momentum, heat and Mass transfer, 3rd ed, Mc Graw Hill Inc, USA, p18-20, 1992.

Biodata — Biodata Ltd., Hardware Users Manual, Manchester, UK, March 1995.

Bolin — Bolin, B., Döös, B., Jäger, J., and Warrick, R., The Greenhouse Effect, Climate Change, and Ecosystems, Wiley, Chichester, 1986.

BS1041 — British Standard: Temperature Measurement Part 4: Guide to the selection and use of thermocouples. BS 1041 : Part 4 : 1992.

Carrier 1965 — Carrier Air Conditioning Company, Handbook of air conditioning system design, McGraw-Hill, New York, 1965.

Charunkyakorn Charunkyakorn, P., Sengupta, S. and Roy, S. K., "Forced Convective Heat Transfer in Microencapsulated Phase Change Material Slurries: Flow in Circular ducts." Int. J. Heat Mass Transfer. Vol. 34, No. 3, pp. 819-833, 1991.

Choi Choi, E., Cho, Y. I. and Lorsch, H. G., Forced Convective Heat Transfer with Phase-Change-Material slurries: Turbulent Flow in a Circular Tube, Int. J. Heat Mass Transfer. Vol. 17, No. 2, pp. 207-215, 1994.

Churchill 1983 Churchill, S. W., "Free Convection Around Immersed Bodies," in E. U. Schlünder, Ed.-in-Chief, Heat Exchanger Design Handbook, Section 2.5.7, Hemisphere Publishing Corp., New York, 1983.

Coulson Coulson, J. M., and Richardson, J. V., Chemical Engineering, Vol. 1, McGraw-Hill, Ney York, 1954.

Colburn Colburn, A. P., Mean Temperature Difference and Heat Transfer Coefficient in Liquid Heat Exchangers, Industrial and Engineering Chemistry, Vol. 25, No. 8, pp. 873-876, 1933.

Dittus Dittus, F. W., and L. M. Boelter, University of California Publications on Engineering, Vol. 2, p. 443, Berkley, 1930.

Dodge Dodge, D. W., and Metzer, A. B., Turbulent Flow of Non-Newtonian Systems, A.I.Ch.E. Journal, Vol. 5, No. 2, pp. 189-204, 1959.

ESDU 82035 Engineering Science Data Unit, Temperature measurement: thermocouples, EDSU 82035, April 1983, Engineering Science Data Unit, 251-259 Regent Street London W1R 7AD.

ESDU Forced Convection Heat Transfer in Straight Tubes. Part1: Fully-developed turbulent flow. Data Item No. 92003, Engineering Sciences Data Unit, London, May 1992.

Einstein Einstein, A., Ann. Physik, Vol. 17, p.459, 1905.

Frivik Frivik, P., CADDET Newsletter, No. 4, 1996.

Fukusako Fukusako, S., Thermophysical Properties of Ice, Snow, and Sea Ice, International Journal of Thremophysics, Vol. 11, No. 2, 1990.

Goel Goel, M., Roy, S. K., and Sengupta, S., Laminar Forced Convective Heat Transfer in Microcapsulated Phase Change Material Suspensions, Int. J. Heat Mass Transfer, Vol. 37, No. 4, pp. 593-604, 1994.

Govier — Govier, G. W., The Flow of Complex Mixtures in Pipes, Robert E. Krieger Publishing Co., Inc., New York 1977.

Green — Green, R. G., and Griskey, R. G., Rheological Behaviour of Dilatant (Shear-Thickening) Fluids. Part 1. Experimental Data. Transactions of the Society of Rheology, Vol. 12, No. 1, pp. 13-25, 1968.

Gribbin — Gribbin, J., The Hole In The Sky, Corgi Books, London, 1990.

Gribbin — Gribbin, J., Hothouse Earth: The Greenhouse Effect and Gaia, Black Swan, Reading, 1990.

Griskey — Griskey, R. G., and Green, R. G., Flow of Dilatant (Shear-Thickening) Fluids, A.I.Ch.E. Journal, Vol. 17, No. 3, pp. 725-728, May 1971.

Grumman — Grumman, D. L., and Butkus, A. S., The Ice Storage Option, ASHRAE Journal, pp. 20-27, May 1988.

Guyer — Guyer, E. C., and Brownell, D. L. (Eds), Applied Thermal Design, McGraw-Hill, New York, 6-3, 1988.

Harada — Harada, E., Toda, M., Kuriyama, M. and Konno, H., Heat Transfer Between Wall and Solid-water Suspension Flow in Horizontal Pipes, Journal of Chemical Engineering, Vol. 18, No. 1, pp. 33-38, 1985.

Harada — Harada, E., M., Kuriyama, M. and Konno, H., Heat Transfer Between the Wall and a Solid-Liquid Suspension Flowing Through a Horizontal, Rectangular Duct, International Chemical Engineering, Vol. 29, No. 4, pp. 671-678, October 1989.

Harris — Harris, J., Rheology and Non-Newtonian Flow, Longman, London, 1977.

Hetsroni — Hetsroni, G., Particle-Turbulence in a Boundary Layer, Proc. 10th International Heat Transfer Confrence, Vol. 1, pp. 81-92, Brighton, 14-18 August 1994.

Hibberd — Hibberd, D. G., Alternatives to CFCs in Refrigeration, in - Power Generation, Energy Management and Environmental Sources Book, Fairmont Press Inc., GA, USA, 1992.

Highgate — Highgate, D., C. Knight and S. D. Probert, Anomalous 'Freezing' of Water in Hydrophilic Polymeric Structures, Applied Energy, 34, pp 243-259, 1989.

Highgate — Highgate D. J., A Fluidised Bed Energy Storage System using Hydrophilic Materials, (DTI/Link programme DTI ref: EW5/049, SERC ref: GR/H87087), 1996.

Houghton — Houghton, j. T., Jenkins, G. J., and Ephraums, J. J. (Eds), Climate Change - the IPCC Scientific assessment, Cambridge, 1990.

Hsu — Hsu, F., Turian, R. M., and Ma, T., Flow of Noncolloidal Slurries in Pipelines, A.I.Ch.E. Journal, Vol. 35, No. 3, pp. 429-442, March 1989.

Incropera — Incropera, F. P., and David P. De Witt, "Fundamentals of Heat and Mass Transfer", 3rd ed., John Wiley & Sons, 1990.

Intelligent Interfaces — Intelligent Interfaces Ltd., IEEE Interface Expansion Card for Acorn Archimedes Computer Systems: User Guide, Eastleigh, UK, 1988.

IPCC — Climate change: the 1990 and 1992 IPCC assessments, IPCC, WMO and UNEP, 1992.

Itoh — Itoh, M., First Applied Energy Lecture on Artificial Intelligence and Energy: New Industrial Challenge for Electric Supply Aided by Information Technology, Cranfield, UK, 1990.

Jensen — Jensen, J., and Sørensen, B., Fundamentals of Energy Storage, John Wiley and Sons, New York, 1984.

Kármán — von Kármán, T., The Analogy Between Fluid Friction and Heat Transfer, Trans. ASME, Vol. 61, pp. 705-711, 1939.

Kasza — Kasza, K. E., Chen, M. M., Development of Enhanced Heat Transfer/ Transport/Storage Slurries for Thermal Systems Improvement, Argonne National Laboratory, ANL-82-50, June 1982.

Kasza — Kasza, K. E., and Chen, M. M., Improvement of the Performance of Solar Energy or Waste Heat Utilization Systems by Using Phase-Change slurry as an Enhanced Heat-Transfer Storage Fluid, Journal of Solar Energy Engineering, Vol. 107, pp. 229-236, August 1985.

Kawase — Kawase, Y., and Moo-Young, M., Heat Transfer in Bioreactors with Dense Suspension Broths, The Chemical Engineering Journal, Vol. 41, pp. B17-B26, 1989.

Kay — Kay, G. W. C., and Laby, T. H., *Table of Physical and Chemical Constants*, 15th Edition, Longman, London, 1986.

Kay — Kay, D., Thermal Storage at Low Temperatures Using Fluidised Hydrophilic Particles, MSc Thesis, Cranfield Institute of Technology, 1989-90.

Kemp — Kemp, D., An Analysis of Cost and Savings Utilizing Thermal Storage, Energy Engineering, Vol. 87, No. 6, pp. 68-78, 1990.

Kent — Operators' Handbook for Kent Pottermeter Type 252, Kent Industrial Instruments Limited, Gloucester, T.P 13 Issue 2, February 1967.

Kostyum — Kostyum, F. P. E., and Ames, D. A., Arizona Utility Adds Eutectic Storage Unit, ASHRAE Journal, may 1987, pp. 28-32.

Krieger — Krieger, I. M., Rheology of Monodisperse Latices, Advances Colloid Interface Sci., Vol. 3, pp. 111-136, 1972.

Kunii — Kunii, D., and Smith, J. M., Heat Transfer Characteristics of Porous Rocks, A.I.Ch.E. Journal, Vol. 6, No. 1, March 1960.

Leal — Leal, L.G.,"On the Effective Thermal Conductivity of Dilute Suspensions of Spherical Drops in the Limit of Low Particle Peclet Number." Chem. Engng. Commun. Vol.1, pp. 21-31, 1973.

Leguay — Leguay, C., Hydrophilic Materials for Use in a Fluidised Bed Energy Storage System, MSc Thesis, Cranfield Institute of Technology, 1993-94.

Lizardos — Lizardos, E. J., and Pavone, D. J., Refrigeration CFC's Recovery, Reuse, Alternatives and New Legislation, in - Power Generation, Energy Management and Environmental Sources Book, Fairmont Press Inc., GA, USA, 1992.

Lovelock — Lovelock, J., The Ages Of Gaia. Oxford University Press, Oxford, 1988, pp. 164-170.

Lui — Lui K.V., Choi U.S., and Kasza K.E., 'Pressure Drop And Heat Transfer Characteristics Of Nearly Neutrally Bouyant Particulate Slurry For Advanced Energy Transmission Fluids', ASME FED, Vol. 75, pp. 107-113, 1988.

Massey — Massey, B. S., Mechanics of Fluids, 5th Edition, an Nostrand Reinhold, UK, 1983.

Maxwell — Maxwell, J. C., A Treatise on Electricity and Magnetism. Vol 1, 3rd ed., Dover Publications, Inc., New York, 1954, pp. 440-441.

McCullough — McCullough, J. M., Ice Thermal Storage: System Selection and Design, Consulting-Specifying Engineer, pp. 70-77, January 1988.

Metzner — Metzner, A. B., and Reed, J. C., Flow of Non-Newtonian Fluids-Correlation of the Laminar, Transition, and Turbulent-flow Regions, A.I.Ch.E. Journal, Vol. 1, No. 4, pp. 434-444, December 1955.

Miller — Miller, R. W., Flow measurement Engineers Handbook, (Table 6.1 Flowmeter Selection Table), McGraw-Hill, Second edition, 1989.

Natgun — Natgun Corporation, Thermal Storage Tanks Save Hundreds of Thousands of Dollars, ASHRAE Journal, August 1991, pp. 56-57.

Nir — Nir, A. and Acrivos, A., "The Effective Thermal Conductivity of Sheared Suspensions." J. Fluid Mechanics. Vol78(1), pp. 33-48, 1976.

Okoroafor — Okoroafor, E. U., Newborough, M., Highgate, D., and Augood, P., Thermal Behaviour of Water in Crosslinked Hydro-Active Polymeric Structures: Water Crystallization, Journal of Material Science, In Press.

Paul — Paul, J., Binary Ice - Technologies for the Production of Pumpable Ice-Slurries, Proc. Inst. Refrigeration, Adavnced Proof: Session 1992-1993, 5-1 to 5-10.

Peters — Peters, D. C. J., Thermal Storage in Air Conditioning Systems, in Air Conditioning-Impact on the Built Environment, pp. 37-55, CIBSE, March 1986.

Petukhov — Petukhov, B. S., in T. F. Irvine and J. P. Harnett, Eds., Advances in Heat Transfer, Vol. 6, Academic Press, New York, 1970.

Pitts — Pitts, D. R., and Sissom, L. E., Heat Transfer, Theory and Problems of., Schaum's Outline Series, McGraw-Hill Inc, New York, 1977.

Quader — Quader, A. K. M., and Wilkinson, W. L., Turbulent Heat Transfer To Dilute Aqueous Suspensions of Titanium Dioxide in Pipes, Int. J. Multiphase Flow, Vol. 7, No. 5. pp. 545-554, 1981.

Reiner — Reiner, G., and Wietlisbach, K., Supermarket deep-freeze Using CO_2 Coolant, CADDET Newsletter, No. 4, pp. 11-13.

Rohsenow — Rohsenow, W. M., Hartnett, J. P., and Ganic', E. N., (Eds.), Handbook of Heat Transfer Fundamentals, Second Edition, McGraw-Hill Book, New York, 1985.

Roscoe — Roscoe, R., Suspensions, in Hermans, J. J., Flow Properties of Disperse Systems, North-Holland Publishing Company, Amsterdam, 1953.

Rutgers — Rutgers, I. R., Relative Viscosity of Suspensions of Rigid Spheres in Newtonian Liquids, Rheologica Acta, Vol. 2, pp. 305-348, 1962.

Salomone — Salamone, J. J. and Newman, M., "Heat Transfer Design Characteristics; Water Suspensions of Solids," Industrial and Engineering Chemistry, Vol. 47, No. 2, pp. 283-288, 1955.

Schlumberger — Solatron Instrumentation Group, Microprocessor Voltmeters 7055 and 7065 Operating Manual: Part1 Measurement, Schlimberger, Farnborough, 1978.

Scott — Developments in flow measurement, Edited by R.W.W. Scott. Applied Science Publishers, London, 1982.

Sieder — Sieder, E. N. and Tate, G. E., "Heat Transfer and Pressure Drop of Liquids in Tubes," Industrial and Engineering Chemistry, Vol. 28, No. 12, pp. 1429-1435, 1936.

Shell — Shell Oils, Shell Thermia Oil B, Data sheet LPDS/80, Shell Oils, Chesshire, England, 1991.

Shook — Shook, C. A. and Roco, M. C., Slurry Flow: Principles and Practice. Butterworth-Heinemann, Boston, USA. 1991, pp.259-262.

Sohn — Sohn, C.W. and Chen, M.M., "Microconvective Thermal Conductivity in Dispersed Two-phase Mixtures as Observed in Velocity Couette Flow Experiment." J. Heat Transfer. Vol. 103, pp. 47-51, 1981.

Spitzer — Spitzer, D. W., Industrial flow measurment, Instrument Society of America, USA, 1984.

Squires — Squires, G. L., Practical Physics, Cambridge University Press, Cambridge, England, Third Edition, 1985.

Systemteknik — Systemteknik A B, High Precision Temperature Meters, Systemteknik, Vasavägen, Sweden, 1980.

Tanner — Tanner, R. I., Engineering Rheology, Oxford Science Publication (OUP), Oxford, 1985.

TCL Ltd — Thermocouple and Resistance Thermometry Data Book, pp 2-3, TCL Ltd., Chesterfield, 1988.

Timm — Timm, M. I., Cool Storage fo Industrial Applications, Energy Engineering, Vol. 87, No. 6, pp. 23-33, 1990.

Thomas — Thomas, D. G., A.I.Ch.E. Journal, Vol. 9, p. 310, 1963.

Tsonis 1989 — Tsonis, G., Fluidised Bed Cold Storage, MSc Thesis, Cranfield Institute of Technology, 1988-89.

Turiel — Turiel, I., and Levine, M. D., Energy-Efficient Refrigeration and the Reduction of Chlorofluorocarbon Use, Annu. Rev. Energy, Vol. 14, 173-204, 1989.

Vand — Vand, V., Theory of Viscosity of Concentrated Suspensions, Nature, Vol. 155, pp. 364-364, 1945.

Wellburn — Wellburn, A., *Air Pollution and Climate Change: The Biological Impact*, Longman Scientific & Technical, Harlow, Second edition, 1994.

Wendland — Wendland, R. D., Storage to Become Rule, Not Exception, ASHRAE Journal, May 1989, pp. 22-23.

Wilkinson — Wilkinson, W. L., Non-Newtonian Fluids: Fluid Mechanics, Mixing and Heat Transfer, Pergamon Press, 1960.

Zhang — Zhang, Y., and Faghri, A., Analysis of Forced Convective Heat Transfer in Microencapsulated Phase Change Materials, Journal of Thermophysics and Heat Transfer, Vol. 9, No. 4, pp. 727-732, 1995.

Appendix A

Dimesionless Groups Used

Group	Symbol	Physical Significance
Coefficient of Friction	c_f	Dimensionless surface shear stress
Nusselt Number	Nu	Basic dimensionless convective heat transfer coefficient - ration of convection heat transfer to conduction in a fluid slab.
Peclet Number	Pe	Dimensionless heat transfer coefficient: ratio of forced convective heat transfer to conduction.
Prandtl Number	Pr	Ratio of molecular momentum and thermal diffusivities.
Reynolds Number	Re	Ratio of inertial to viscous forces.
Stanton Number	St	Dimensionless heat transfer coefficient: ratio of heat transferred at the surface to that transferred by fluid in its thermal capacity.
Stephan Number	Ste	Ratio of sensible heat capacity to latent heat capacity.

Appendix B

Engineering Drawings

Reference	Drawing Code	Title and Description
Appendix B1	PC22408 PC22409	*Hydrophilic Slurry 1kWh Cold Storage Tank* *1kWh Cold Storage Tank Stirring Blade* These were employed as parts of the MK I Cold Storage Device discussed in Section 4.4.2.
Appendix B2	PC22411	*Insulation Sleeve For 1kWh Cold Storage Tank* This was employed with the above to enable the tank to be insulated with lose fill insulation.
Appendix B3	PC26300	*Assembly of Cold Storage Tank* This is an assembly drawing of the MK II Cold Storage Device (Section 4.4.4).
Appendix B4	PC26308	*Cold Storage Tank III - General Assembly* This assembly drawing details the feed based cold storage device (MK III) discussed in Section 4.4.5.
Appendix B5	PC26313	*Assembly of TEST heat Exchanger with 28mm Tube Fitted* This is an assembly drawing of the heat transfer test section discussed in Chapter 5 and 6.

MODIFICATION

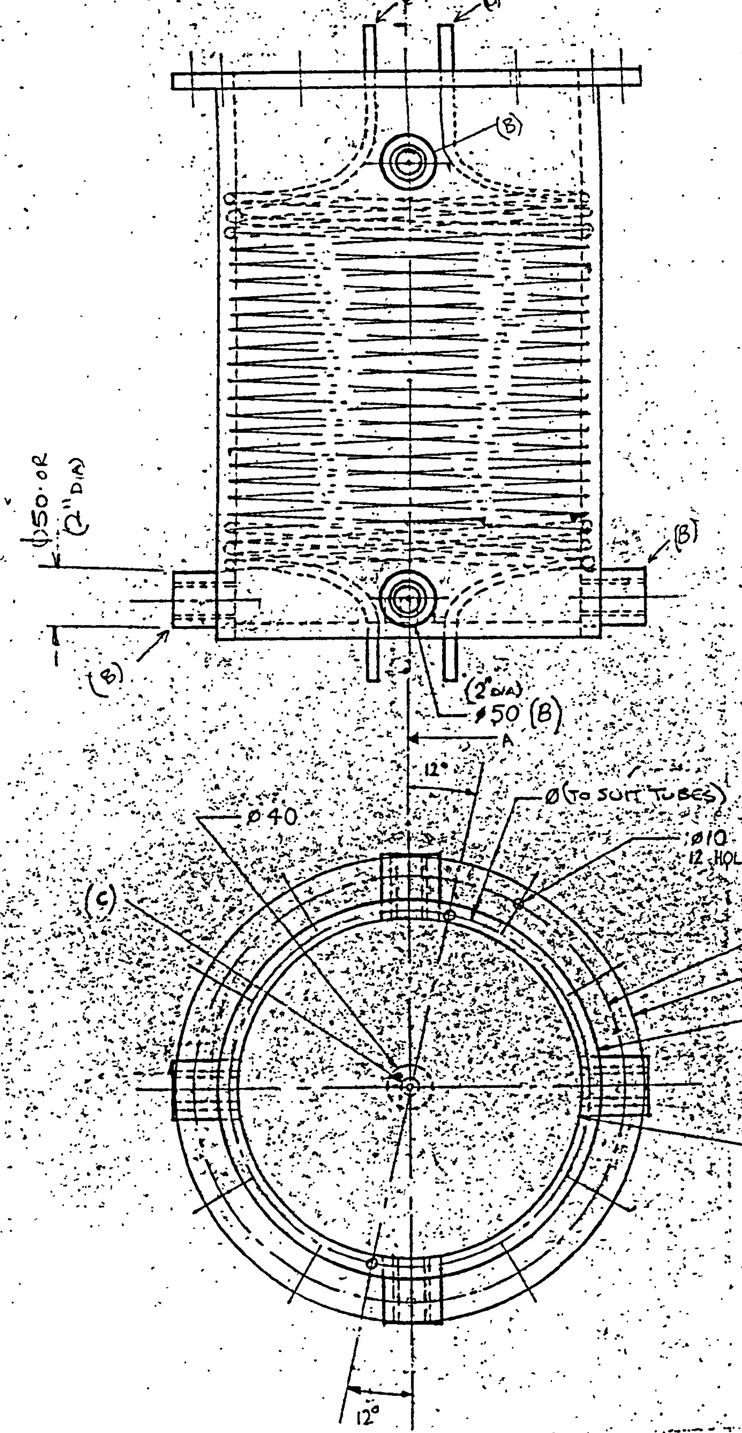

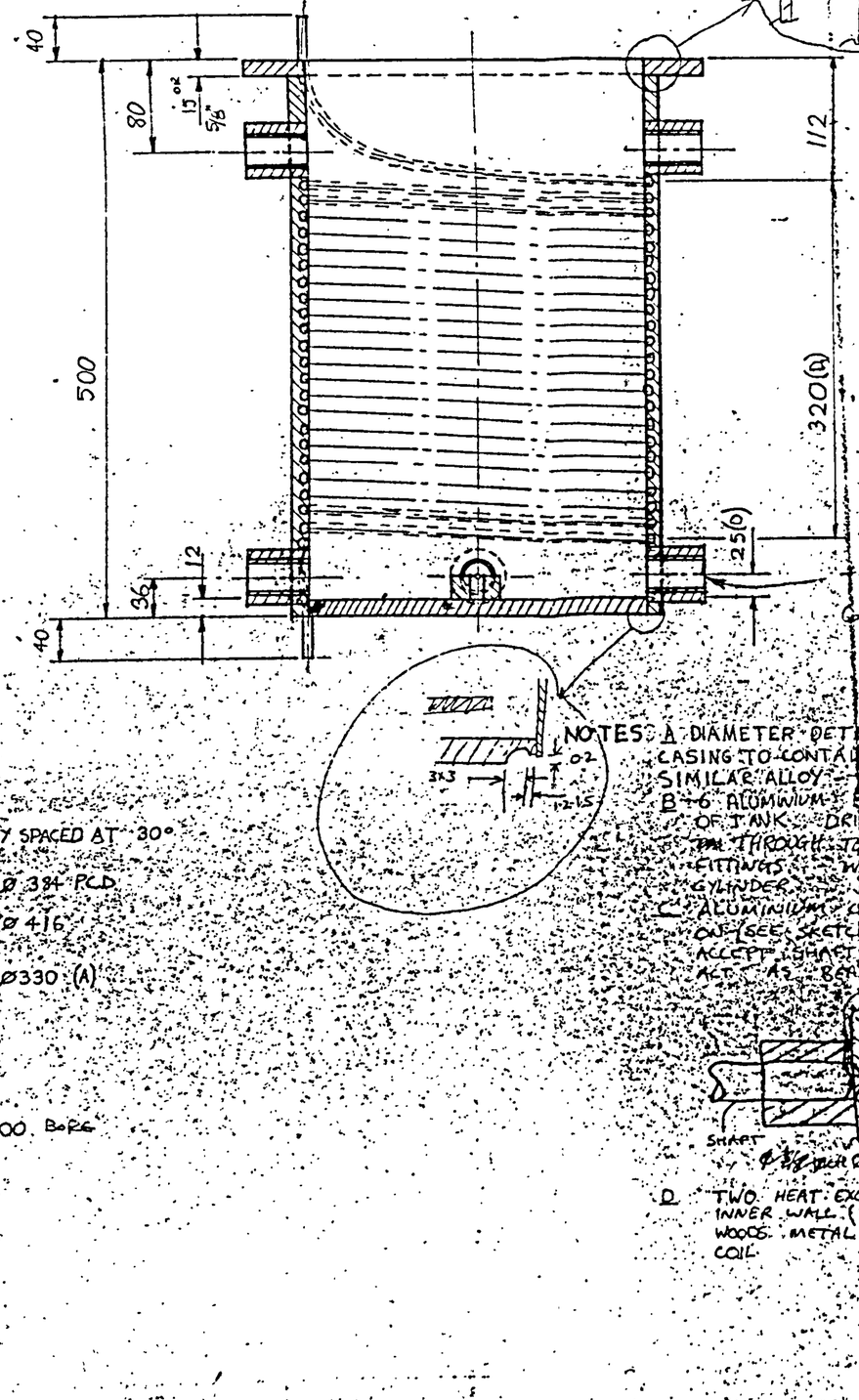

MACHINE FLANGE O/Ds & BORES ONLY
REMOVE SHARP EDGES.
LID ½" TK. 416 O/D WITH 12 HOLES FOR BOLTING & RELIEF HOLES FOR TUBES.

THIRD ANGLE PROJECTION			SHEET SIZE	ITEM	PART No.	DESCRIPTION	No. OFF	MAT'L	SPEC.	REMARKS
			A 2	1	PC 22408	TANK	1	ALUM ALLOY & COPPER		—

GENERAL TOLERANCE ON DIMENSIONS	JOB No.	No. OF SETS REQ'D	SCALE	DRAWN	CHK'D	APPV'D	STRESS APPVD.	TITLE :- HYDROPHILIC SLURRY I.R.W.H. COLD STORAGE TANK BODY No1
MACHINED ±0.2			1:4	P AUGOOD				
UNMACHINED ±1	29106	1			21.1.92			
OTHER DIMENSIONS AS STATED			FINISH	ISSUED BY SME				DRAWING No.
WELD WHERE SHOWN THUS			SELF	CRANFIELD INSTITUTE OF TECHNOLOGY CRANFIELD.				PC 22408
MACHINE WHERE SHOWN THUS ✓	USED ON DRG.	—						SHT. 1 OF 1 SHEETS

DRAWING No.	
PC 22408	
ISSUE	MODIFICATION
	—

ALL DIMENSIONS IN MILLIMETRES UNLESS OTHERWISE STATED.

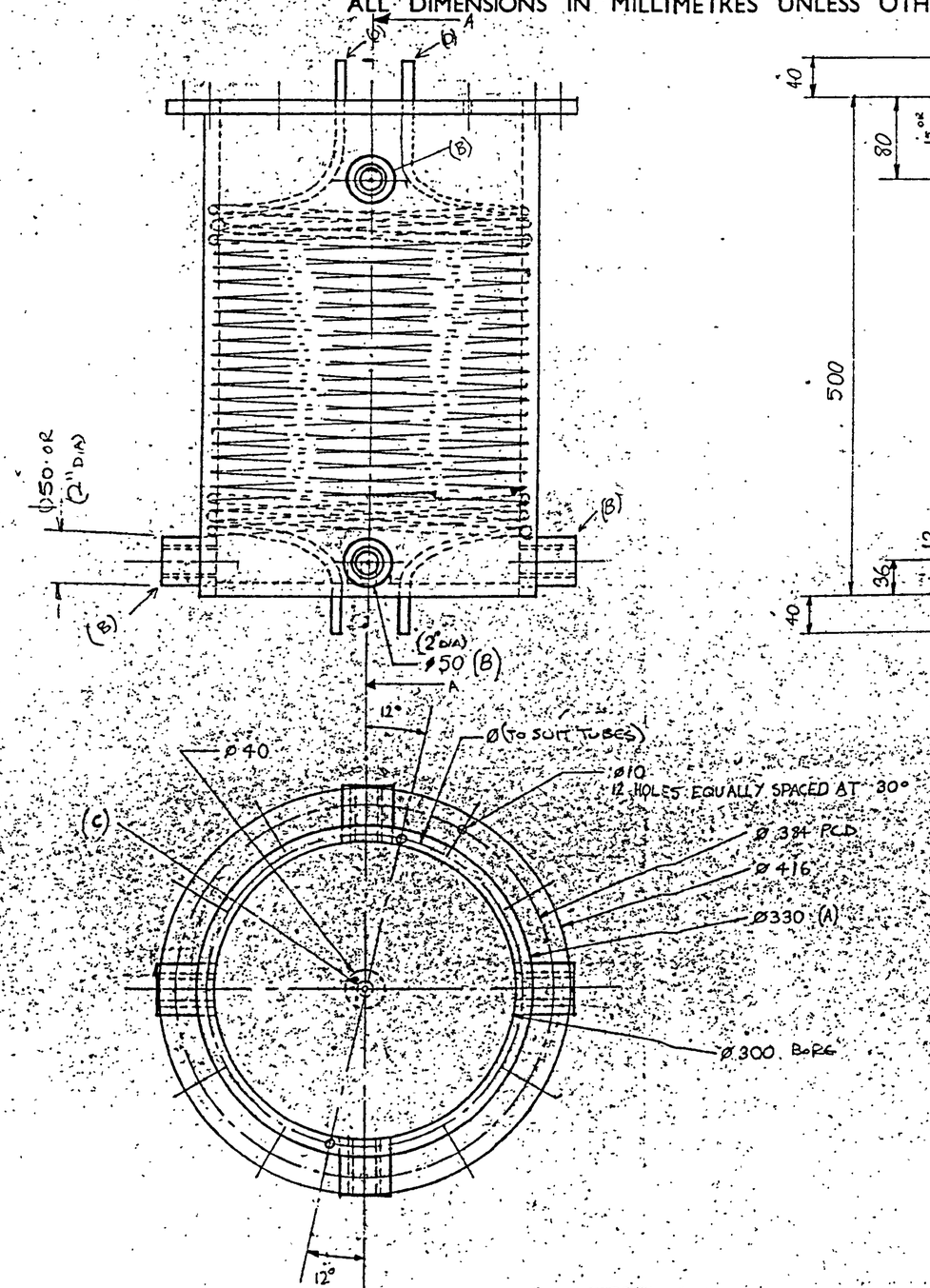

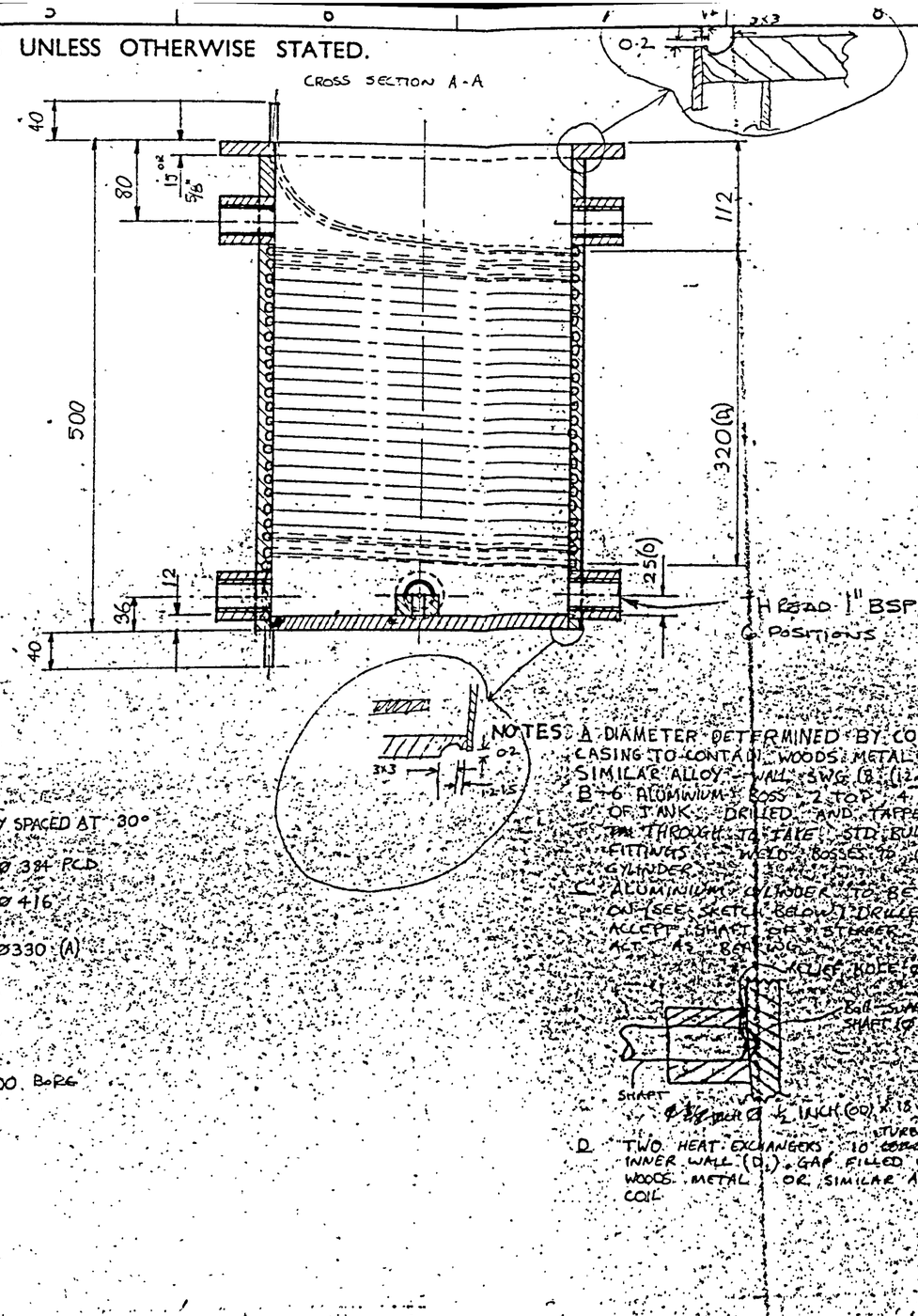

NOTES

1. MACHINE FLANGE O/Ds & BORES ONLY
2. REMOVE SHARP EDGES.
3. LID ½" TK. & 16 O/D WITH 12 HOLES FOR BOLTING & RELIEF HOLES FOR TUBES.

THIRD ANGLE PROJECTION			SHEET SIZE	ITEM	PART No.	DESCRIPTION	No. OFF	MAT.	SPEC.	REMARKS
			A 2	1	PC 22408	TANK	1	ALUM ALLOY & COPPER		—
GENERAL TOLERANCE ON DIMENSIONS MACHINED ± 0.2 UNMACHINED ± 1 OTHER DIMENSIONS AS STATED	JOB No. 29106	No. OF SETS REQD 1	SCALE 1:4	DRAWN P AUGOOD	CHKD KHD 21/9/92	APPVD	STRESS APPVD	TITLE:- HYDROPHILIC SLURRY I.R.W.H. COLD STORAGE TANK BODY No 1		
WELD WHERE SHOWN THUS			FINISH SELF	ISSUED BY SME						
MACHINE WHERE SHOWN THUS ✓	USED ON DRG. —			CRANFIELD INSTITUTE OF TECHNOLOGY CRANFIELD.				DRAWING No. PC 22408		
								SHT. 1 OF 1 SHEETS		

DRAWING No.	
PC 22408	
JE	MODIFICATION
	—

ALL DIMENSIONS IN MILLIMETRES UNLESS OTHERWISE STATED.

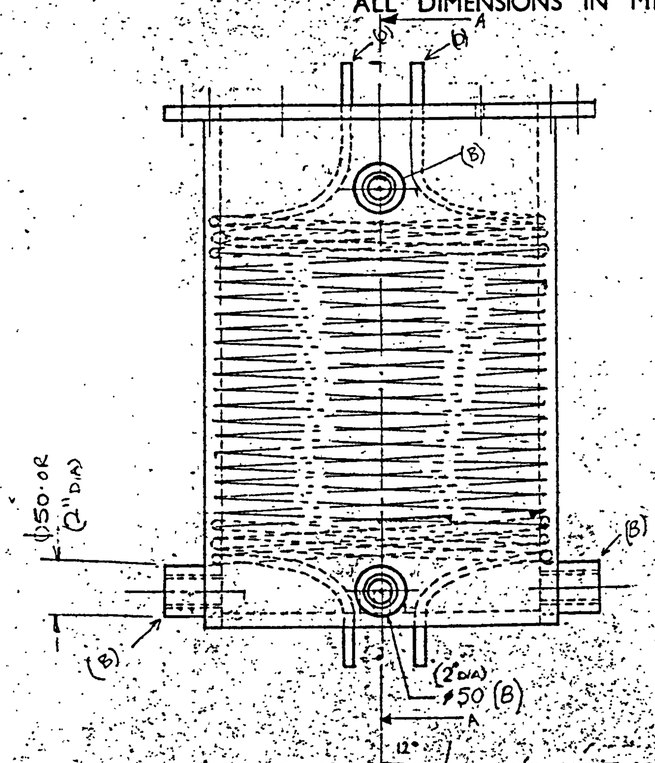

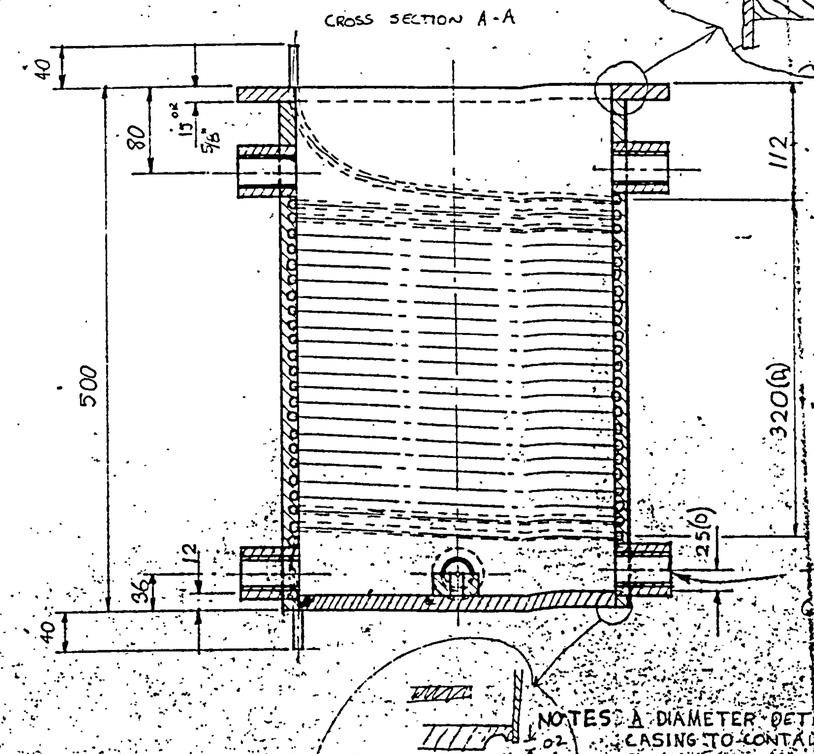

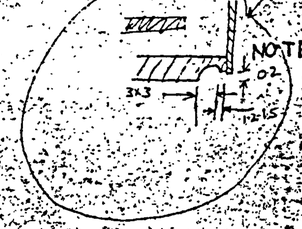

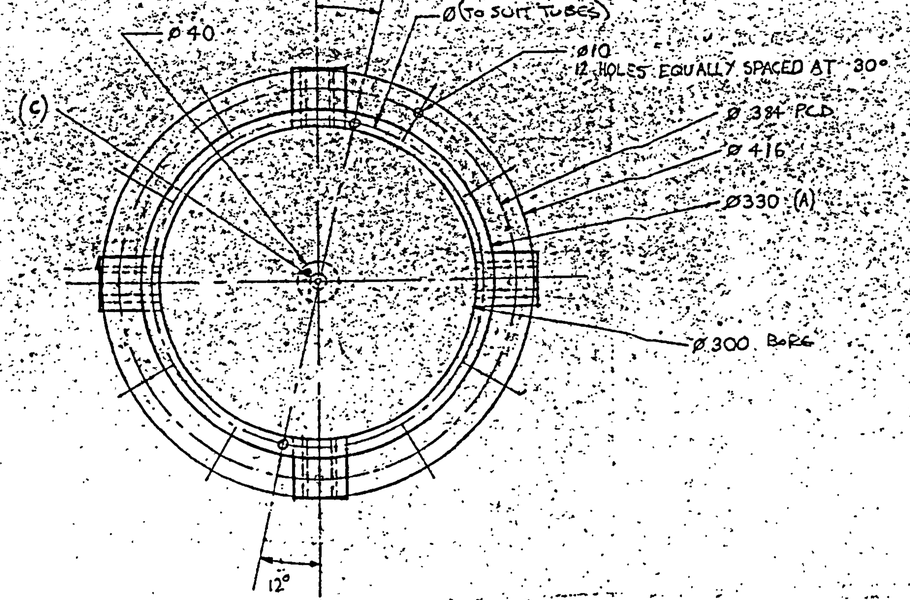

NOTES: A DIAMETER DETERMINED BY COILS (D).
CASING TO CONTAIN WOODS METAL FOR SIMILAR ALLOY — WALL 3WG (3 (12mm) ALUMINIUM)
B 6 ALUMINIUM BOSS 2 TOP 4 BOTTOM OF TANK DRILLED AND TAPPED ~~TO~~ THROUGH TO TAKE STD BUCKSHEAD FITTINGS — WELD BOSSES TO INNER CYLINDER
C ALUMINIUM CYLINDER TO BE WELDED ON (SEE SKETCH BELOW) DRILLED TO ACCEPT SHAFT OF STIRRER AND ACT AS BEARING
CLOSE HOLE φ4mm
Ball shaft for shaft (φ4 or 2)
SHAFT
φ½ inch (φ) ½ INCH (φ) x 18 SWG TUBES EACH
D TWO HEAT EXCHANGERS 10 COILS AROUND INNER WALL (D.) GAP FILLED WITH WOODS METAL OR SIMILAR ALLOY COIL

Notes

1. Machine flange o/ds & bores only
2. Remove sharp edges.
3. Lid ½" tk. & 16 o/d with 12 holes for bolting & relief holes for tubes.

THIRD ANGLE PROJECTION			SHEET SIZE A 2	ITEM	PART No.	DESCRIPTION	No. OFF	MAT.	SPEC.	REMARKS
GENERAL TOLERANCE ON DIMENSIONS MACHINED ±0·2 UNMACHINED ±1 OTHER DIMENSIONS AS STATED	JOB No. 29106	No. OF SETS REQ'D 1	SCALE 1:4	1	PC 22408	TANK	1	ALUM ALLOY & CASTING		—
				DRAWN P AUGOOD	CHK'D KHD 21/9/92	APPV'D	STRESS APPVD.	TITLE :- HYDROPHILIC SLURRY I.R.W.H. COLD STORAGE TANK BODY No 1		
WELD WHERE SHOWN THUS			FINISH SELF	ISSUED BY SME				DRAWING No. PC 22408		
MACHINE WHERE SHOWN THUS ✓	USED ON DRG. —			CRANFIELD INSTITUTE OF TECHNOLOGY CRANFIELD.				SHT. 1 OF 1 SHEETS		

67

DRAWING No
PC22409

MODIFICATION

ALL DIMENSIONS IN MILLIMETRES UNLESS OTHERWISE STATED.

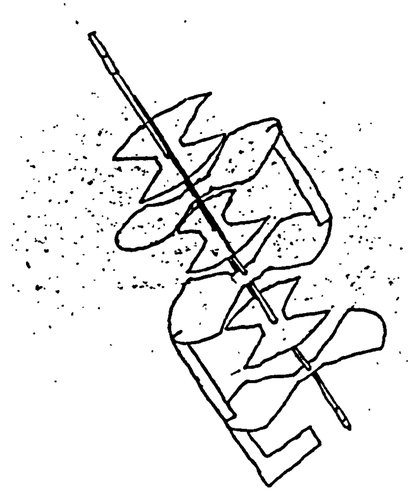

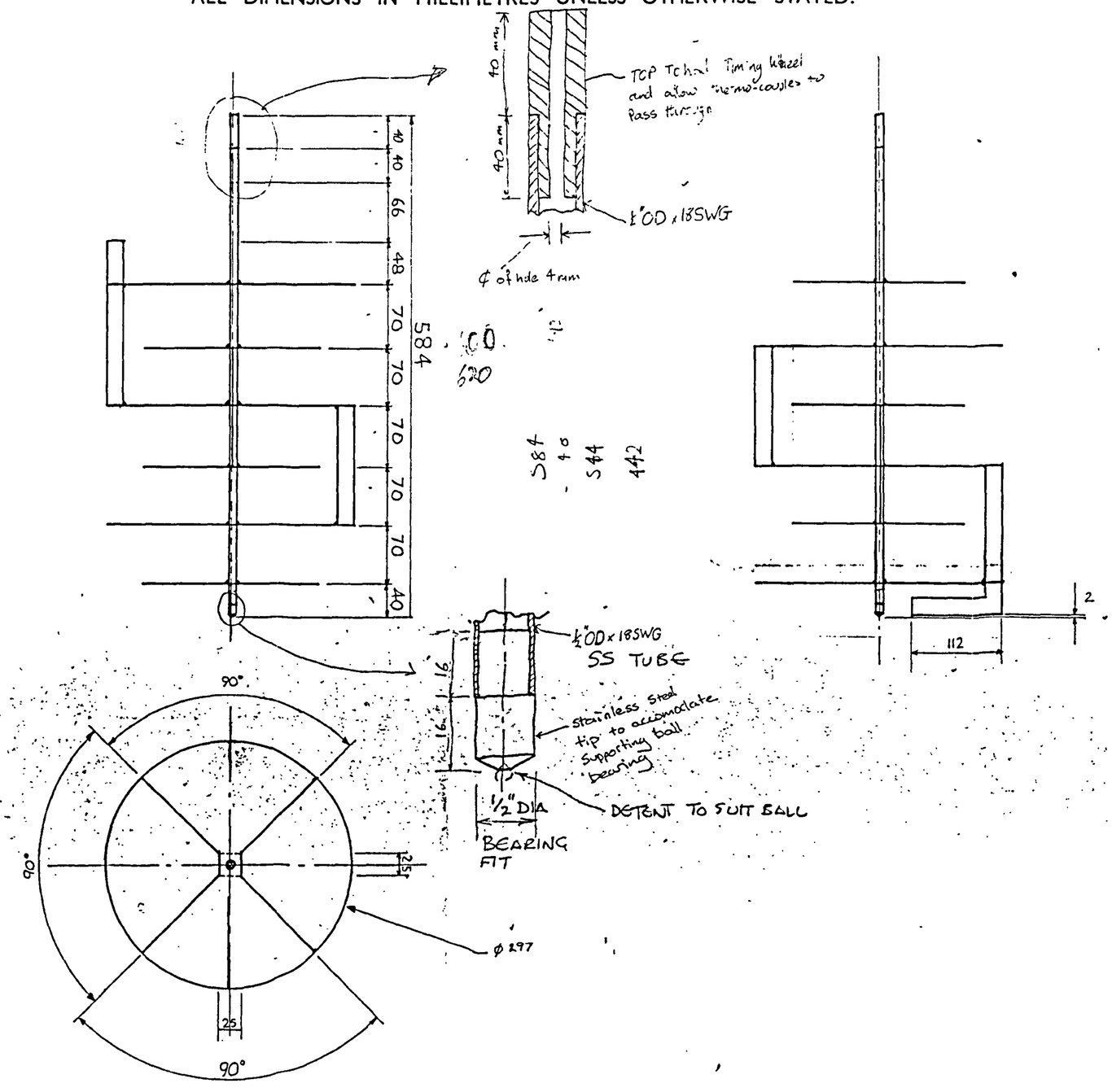

THIRD ANGLE PROJECTION			SHEET SIZE A 2	ITEM	PART No.	DESCRIPTION	No. OFF	MAT'L	SPEC.	REMARKS
				1	PC22409	ST. REQ'D	1			
GENERAL TOLERANCE ON DIMENSIONS MACHINED ·2mm UNMACHINED 1mm OTHER DIMENSIONS AS STATED	JOB No. 23106	No. OF SETS REQ'D 1	SCALE 1:4	DRAWN P AUGOOD	CHK'D RAD 22/9/72	APPV'D	STRESS APPV'D.	TITLE:- 1KWH COLD STORAGE TANK STIRRING BLADE		
WELD WHERE SHOWN THUS			FINISH Sci.	ISSUED BY SME				DRAWING No. PC22409		
MACHINE WHERE SHOWN THUS ✓	USED ON DRG. —			CRANFIELD INSTITUTE OF TECHNOLOGY CRANFIELD.				SHT. 1 OF 1 SHEETS		

168

ALL DIMENSIONS IN MILLIMETRES UNLESS OTHERWISE STATED.

DRAWING No.	
ISSUE	MODIFICATION

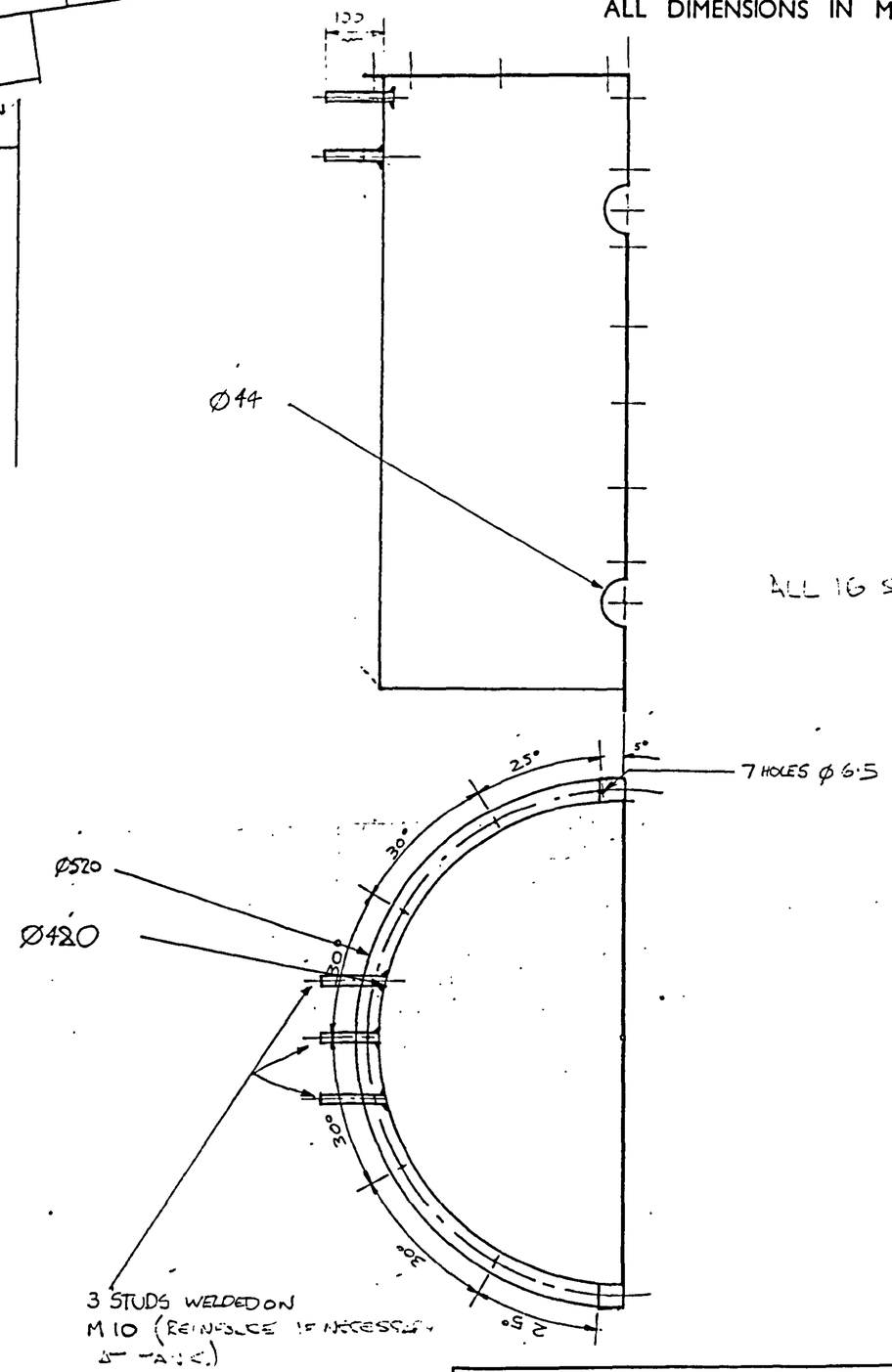

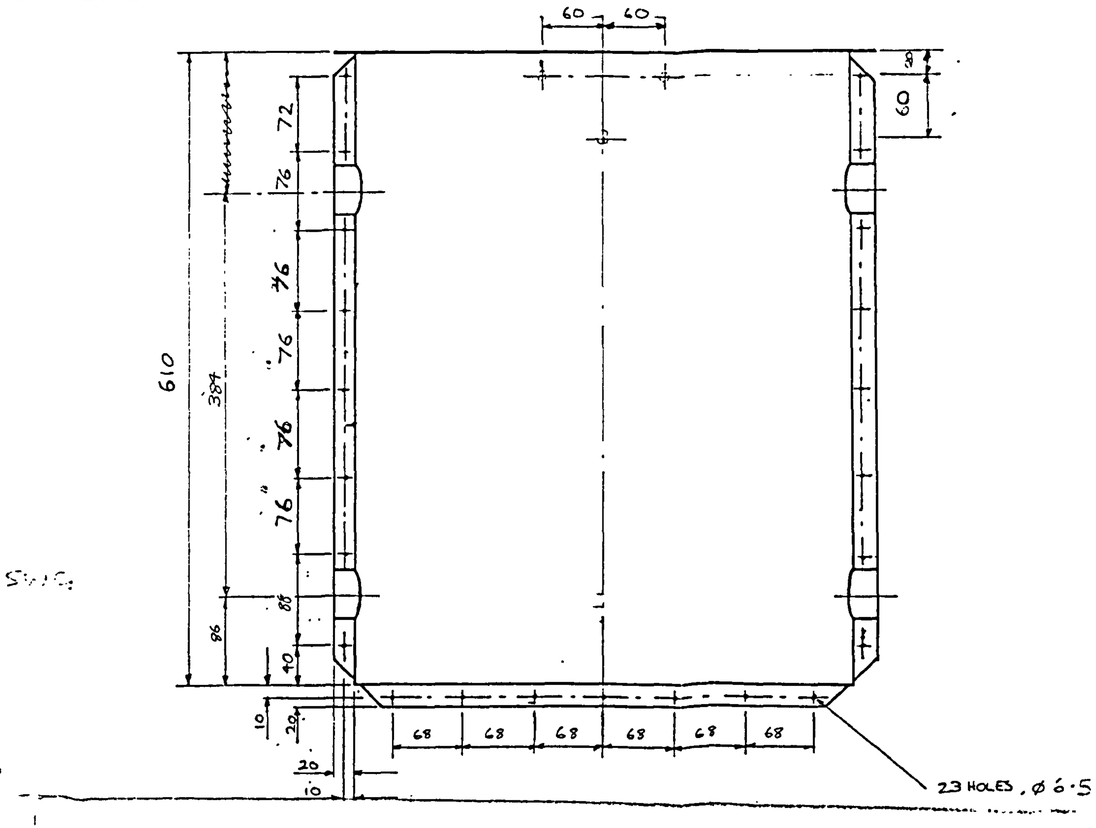

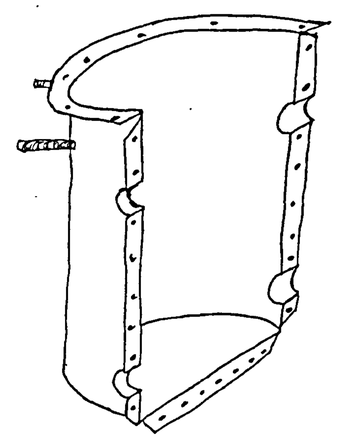

NOTES.

1. ALSO SUPPLY TOP PLATE Ø 520 DRILLED TO MATCH FLANGE + ONE HOLE Ø 20 IN CENTRE
2. SUPPLY WITH 37 off M6 NUT, BOLT, & WASHERS
3. REMOVE SHARP EDGES

THIRD ANGLE PROJECTION			SHEET SIZE A 2	ITEM 1	PART No. [illegible]	DESCRIPTION OUTER SLEEVE	No. OFF 2	MAT'L MS	SPEC.	REMARKS 16 SWG
GENERAL TOLERANCE ON DIMENSIONS MACHINED ±0·2 UNMACHINED ±1 OTHER DIMENSIONS AS STATED	JOB No. 29106	No. OF SETS REQ'D 1	SCALE ½	DRAWN P. AUGOOD	CHK'D RHD 23/11/92	APPV'D	STRESS APPV'D	TITLE :- INSULATION SLEEVE FOR 1KWH COLD STORAGE TANK		
WELD WHERE SHOWN THUS			FINISH SCALE	ISSUED BY SAME					DRAWING No. PC 2241	
MACHINE WHERE SHOWN THUS	USED ON DRG. —			CRANFIELD INSTITUTE OF TECHNOLOGY CRANFIELD.					SHT. 1 OF 1 SHEETS	

169

G No. PC26300

MODIFICATION

—

ALL DIMENSIONS IN MILLIMETRES UNLESS OTHERWISE STATED.

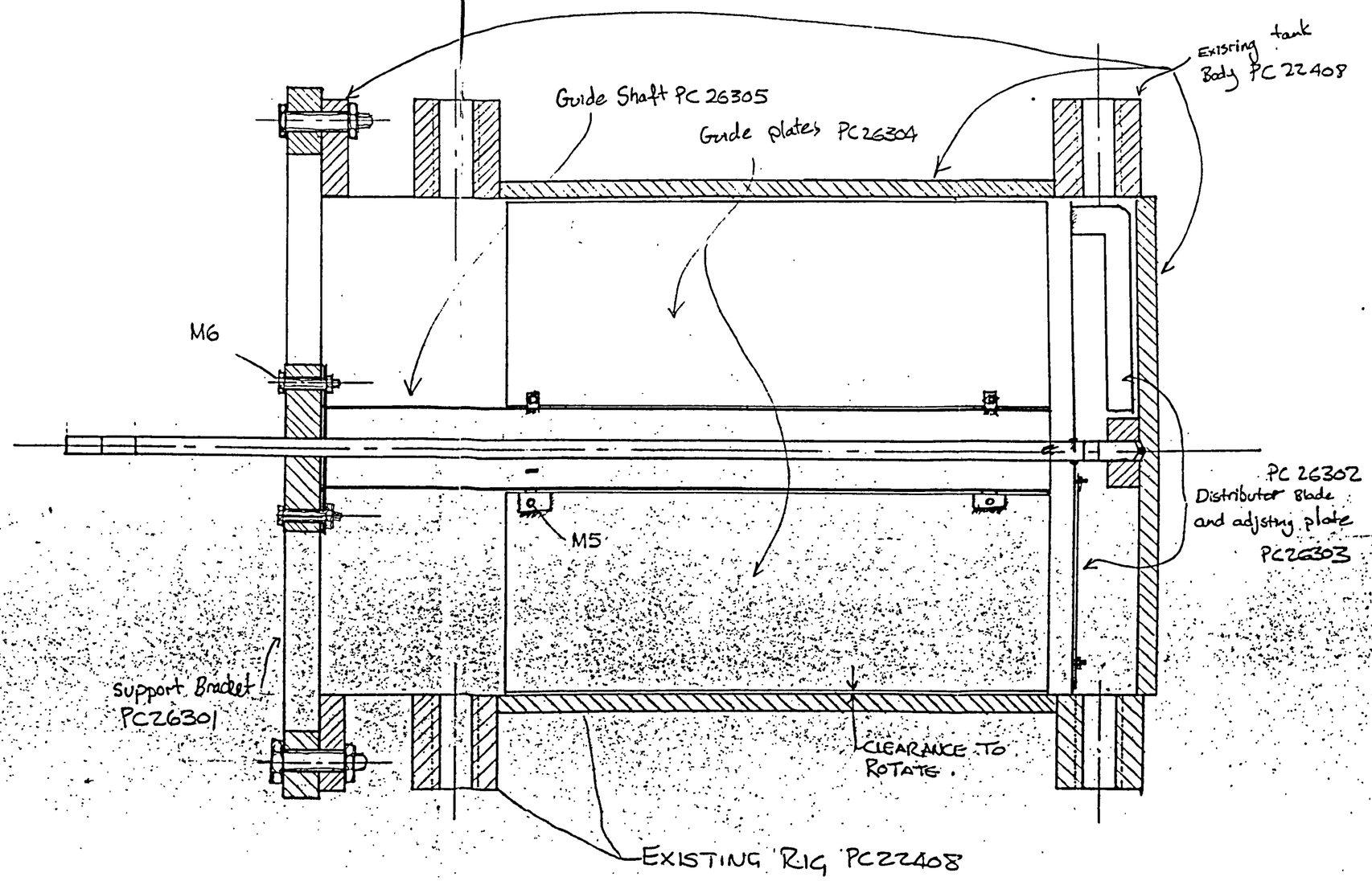

NOTES

ASSEMBLE PARTS AS SHOWN TO EXISTING HYDROPHILIC SLURRY TANK IN APPLIED ENERGY LABORATORY

ITEM	PART No.	DESCRIPTION	No. OFF	MAT.	SPEC.	REMARKS
1	PC26300	ASSEMBLY of TANK	1	-	-	-

THIRD ANGLE PROJECTION

SHEET SIZE A2

SCALE 1:2

FINISH SELF

	DRAWN	CHK	DATE	STRESS APPVD
	P.C. Augood	RHD		
	4-10-93	4/10/93		

TITLE:- Assembly OF COLD STORAGE TANK

GENERAL TOLERANCE ON DIMENSIONS
MACHINED —
UNMACHINED —
OTHER DIMENSIONS AS STATED

WELD WHERE SHOWN THUS

MACHINE WHERE SHOWN THUS

JOB No.	No. OF SETS REQ.
29106	1

USED ON DRG.

SCHOOL OF MECHANICAL ENGINEERING
CRANFIELD INSTITUTE OF TECHNOLOGY

DRAWING No. PC26300

SHT. 1 OF 1 SHEETS

MY 320836 E

DRAWING No. PC26308

	MODIFICATION
	—

ALL DIMENSIONS IN MILLIMETRES UNLESS OTHERWISE STATED.

CROSS SECTION X-X — NUTS, BOLTS & WASHERS NOT SHOWN
— CENTRAL FEED SHAFT COMPLETE

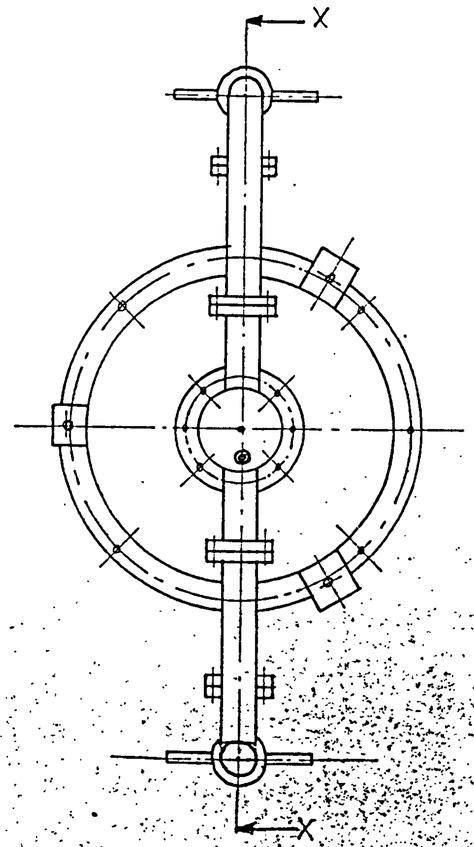

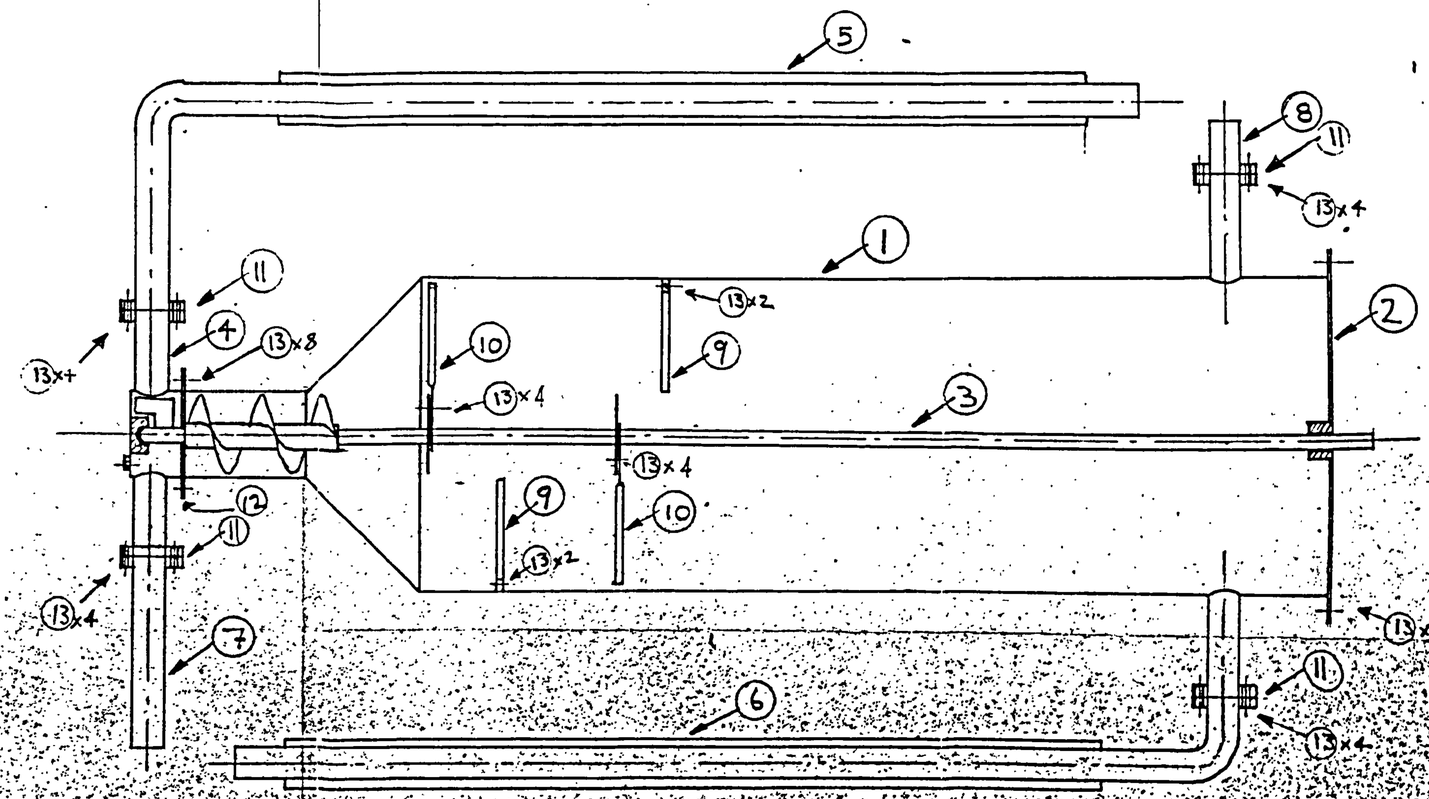

ITEM	PART No.	DESCRIPTION	No. OFF	MAT.	SPEC.	REMARKS
13		M6 NUTS, BOLTS + WASHERS	42			
12	SK587	LOWER GASKET	1			
11	SK587	FLANGE GASKETS	4			
10 (TO BE DRAWN)		DRIVE SHAFT BLADES	2			
9		TANK BLADES	2			
8	SK 588	SHORT FLANGED TUBE	1			
7	SK 588	LONG FLANGED TUBE	1			
6	PC26312/2	LHD HEAT EXCHANGER	1			
5	PC26312/1	RHD HEAT EXCHANGER	1			
4	PC26311	MIXING CHAMBER	1			
3	PC26310	FEED DRIVE SHAFT	1			
2	SK 586	TANK LID	1			
1	PC26309	TANK BODY	1			

PRINT No.	342151
ISSUED TO	B PHILLIPS
ISSUED FOR	MANUFACTURE / ~~QUOTATION~~ / ~~INFORMATION~~
DATE	15.2.94

THIRD ANGLE PROJECTION

SHEET SIZE A2

SCALE 1:4

FINISH SELF

GENERAL TOLERANCE ON DIMENSIONS
MACHINED —
UNMACHINED —
OTHER DIMENSIONS AS STATED

WELD WHERE SHOWN THUS

MACHINE WHERE SHOWN THUS

JOB No.	No. OF SETS REQ.
29106	1

USED ON DRG. —

DRAWN	CHK	DATE	STRESS APPVD
P AUGOOD	RHD		
11/2/94	14/2/94		

TITLE:- COLD STORAGE TANK III
GENERAL ASSEMBLY

SCHOOL OF MECHANICAL ENGINEERING
CRANFIELD INSTITUTE OF TECHNOLOGY

DRAWING No. PC26308

SHT. 1 OF 1 SHEETS

MT 270836 B

DRAWING No. PC26313

MODIFICATION
—

ALL DIMENSIONS IN MILLIMETRES UNLESS OTHERWISE STATED.

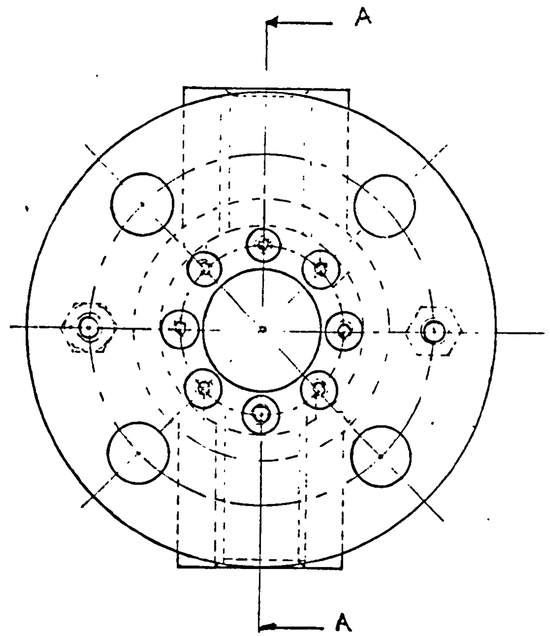

CROSS SECTION ON A-A

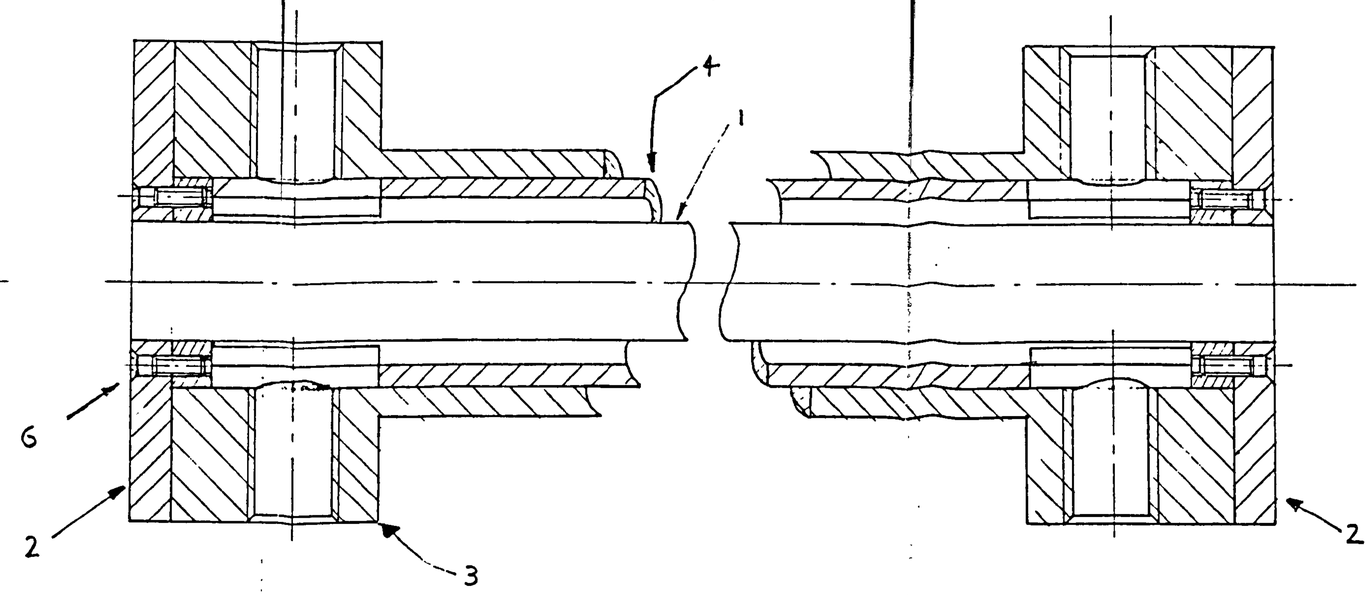

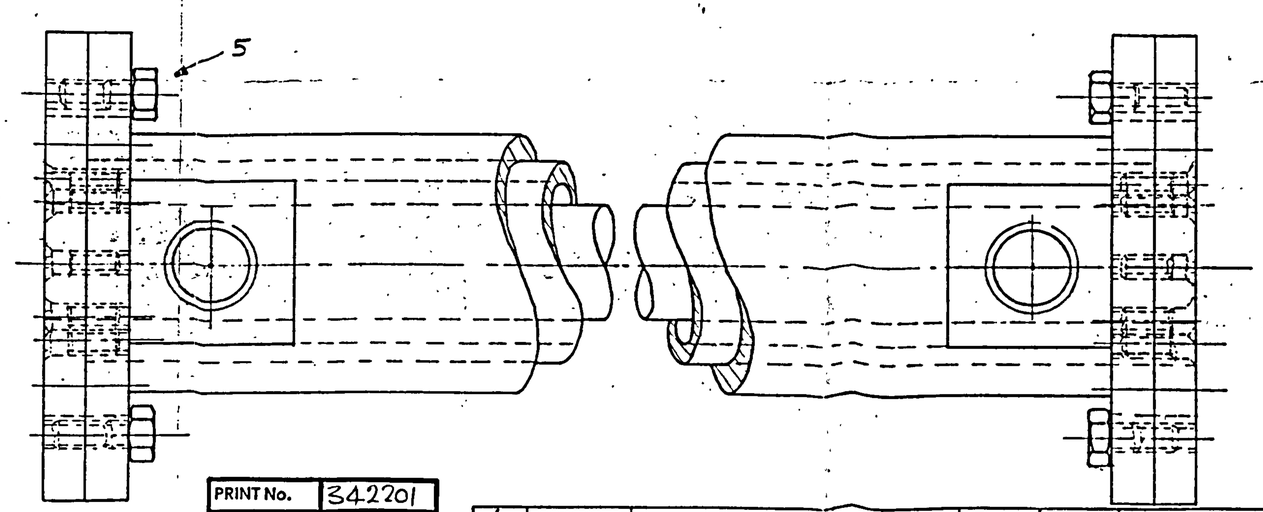

PRINT No.	342201
ISSUED TO	B. PHILLIPS
ISSUED FOR	MANUFACTURE ~~QUOTATION~~ ~~INFORMATION~~
DATE	16/3/94

ITEM	PART No.	DESCRIPTION	No. OFF	MAT.	SPEC.	REMARKS
6			16			
5		M6 BOLTS	2			
4	PC26317	REDUCTION TUBES	2			
3	PC26316	OUTER TUBE	1	✓		
2	PC26315	END FLANGE	2	✓		
1	PC26314	HEAT TRANSFER TUBE				

THIRD ANGLE PROJECTION

SHEET SIZE A2

GENERAL TOLERANCE ON DIMENSIONS
MACHINED —
UNMACHINED —
OTHER DIMENSIONS AS STATED

WELD WHERE SHOWN THUS

MACHINE WHERE SHOWN THUS ✓

JOB No.	No. OF SETS REQ.
29106	1
USED ON DRG. —	

SCALE 1:1

FINISH SELF

DRAWN	CHK	DATE	STRESS APPVD
P AUGOOD	RHD		
15-3-94	15-3-94		

TITLE:- ASSEMBLY OF TEST HEAT EXCHANGER WITH 28 MM TUBE FITED

SCHOOL OF MECHANICAL ENGINEERING
CRANFIELD INSTITUTE OF TECHNOLOGY

DRAWING No. PC26313

SHT. 1 OF 1 SHEETS

MT 320836 R

172

Appendix C

Physical Properties of Fusus Oil

Temperature T (°C)	Density ρ (kg/m^3)	Heat Capacity C_p (kJ/kg·K)	Thermal Conductivity k (W/m·K)	Viscosity ν (m^2·s × 10^6)
-20	859	1.748	0.1376	25.2
-12	854	1.782	0.1380	17.1
-5	849	1.816	0.1383	12.3
0	846	1.833	0.1386	10.4
10	840	1.879	0.1390	7.3
20	834	1.920	0.1395	5.4
30	827	1.966	0.1400	4.2

Appendix D

Experimental Codes as referred to in Chapter 6

		Initial conditions		Final conditions	
Code	Conc. (%)	m ($kg \cdot s^{-1}$)	Temperature (°C)	m ($kg \cdot s^{-1}$)	Temperature (°C)
Run05a04	5	0.623	18.6	0.523	-5.1
Run05a05	5	0.577	10.6	0.496	-6.6
Run05a06	5	0.599	18.0	0.492	-7.0
Run05a07	5	0.538	17.7	0.454	-6.8
Run05a08	5	0.500	17.9	0.450	-6.6
Run10a04	10	0.537	13.6	0.465	-0.4
Run10a05	10	0.520	8.1	0.395	-3.8
Run10a06	10	0.614	17.62	0.523	-4.9